POLITECNICO DI TORINO

Master of science program in

AUTOMOTIVE ENGINEERING

Master's degree thesis

Low alloy steels with ultimate tensile strength greater than 2000 Mpa

Supervisor:

Prof. Paolo Matteis

Candidate:

Hang Chen

Academic year 2021/2022

Index:

Introduction …….....4

1. Melting and casting practice…….6

2. High-carbon bearing steels……...8
2.1. Ball bearing forming processing…….....9
2.2. Spheroidization of 100Cr6 bearing steel……..9
2.3. Heat treatments and microstructures of 100Cr6 bearing steel……11
2.3.1. Martensitic quenching and tempering process…….11
2.3.2. Bainite isothermal quenching process……...14
2.3.3. Martensite and bainite duplex structure quenching process……...18
2.3.4. Bainite temperature varying quenching process…….....19
2.3.5. Analysis of retained austenite and dimensional stability…….21
2.4. Mechanical properties of 100Cr6 bearing steel……..22
2.4.1. Hardness…….....22
2.4.2. Strength vs. ductility……....24
2.4.3. Fracture toughness ……..……....25
2.4.4. Fatigue …….....29
2.5. Discussion……..……36

3. Medium-carbon engineering steels……...…….37
3.1. Machining processing of engineering steels……38
3.2. Heat treatment and microstructures of engineering steels……..….39
3.2.1. Annealing(spheroidization) of engineering steels……..39
3.2.2. Normalizing of engineering steels…….....39
3.2.3. Quenching and tempering of engineering steels……...40
3.2.3.1. Structure of the as-quenched martensite of AISI 4340 steel…….40
3.2.3.2. The effect of austenitizing temperature on the structure of AISI 4340 steel……41
3.2.3.3. The effect of tempering temperature on the structure of AISI 4340 steel……42
3.2.3.4. The effect of austenitizing temperature on the structure of 300M steel……44
3.2.3.5. The effect of tempering temperature on the structure of 300M steel……46
3.3. Mechanical properties of engineering steels……..47
3.3.1. Hardness…….....47
3.3.2. Strength vs. ductility……..48
3.3.2.1. The effect of alloying elements and smelting processes on strength and ductility…….48
3.3.2.2. The effect of heat treatment on strength and ductility……..49

3.3.3. Fracture toughness and impact toughness…….....52
3.3.3.1. The effect of heat treatment on toughness……..52
3.3.3.2. The effect of smelting methods and rolling on toughness…….57
3.3.4. Fatigue…….....58
3.3.4.1. The effect of heat treatment on fatigue……..58
3.3.4.2. The effect of cryogenic treatment on fatigue……..63
3.3.4.3. The effect of smelting methods on fatigue……..64
3.4. Improvement of heat treatment process of engineering steels……..64
3.5. Discussion……..67

4. Low-carbon high strength hot-stamped steels……...68
4.1. Hot stamping processing……..70
4.2. Heat treatment and microstructure of hot-stamped steels…….....73
4.2.1. Annealing(spheroidization) of hot-stamped steels……73
4.2.2. Quenching and tempering of hot-stamped steels…….....74
4.2.2.1. Structure of the as-quenched martensite of 22MnB5 steel……75
4.2.2.2. The effect of austenitisation on the structure of 22MnB5 steel…….77
4.2.2.3. The effect of tempering temperature on the structure of 22MnB5 steel……79
4.3. Mechanical properties of hot-stamped steels……..81
4.3.1. Hardness…….....81
4.3.2. Strength vs. ductility……....83
4.3.3. Fracture toughness…….....87
4.3.4. Cold bending properties……90
4.4. Recent advances in hot-stamped steels……91
4.4.1. New steels by adjusting the C content……91
4.4.2. New steels adding micro-alloying elements……...92
4.5. Material Surface Protection–AlSi coating and Zinc-based coating of hot-stamped steel……95
4.5.1. AlSi coating……..96
4.5.2. Zinc-based coating…….....96
4.6. Discussion……..97

5. Armor and wear resistant steels……..98
5.1. Armor steels……..98
5.1.1. Series and chemical composition of Armor steels……98
5.1.2. Processing of Armor steels……..99
5.1.3. Microstructure of Armor steels……100
5.1.4. Mechanical properties of Armor steels……101
5.1.5. Strengthen of the armor……104
5.1.6. Discussion……..106

5.2. Wear resistant steels ……..……..106
5.2.1. Series and chemical composition of wear resistant steels……..106

5.2.2. Microstructure of wear resistant steels……..……..107
5.2.3. Mechanical properties of wear resistant steels……108
5.2.4. Optimizing the choice of wear materials…….……....111
5.2.5. Discussion……..113

6. Nanobainitic steels…….114
6.1. Alloy design of nanobainitic steels……115
6.2. Microstructure of nanobainitic steels……118
6.2.1. Effect of prior austenite grains…….119
6.2.2. Effect of heat treatment process to nanobainitic steels……..121
6.2.3. Other effecting factors……..124
6.3. Mechanical properties of nanobainitic steels……124
6.3.1. Strength vs. ductility…….124
6.3.2. Toughness……..126
6.3.3. Fatigue……...126
6.4. Discussion……128

7. Cold drawn pearlitic wire……..130
7.1. Processing of pearlitic wire……130
7.1.1. Quenching process of wire rod…….131
7.1.2. Cold drawing process of steel wire……..134
7.2. Microstructure of cold drawn pearlitic wire…….136
7.3. Mechanical properties of cold drawn pearlitic wire……143
7.4. Strengthening mechanism…….148
7.4.1. Solid solution strengthening…….148
7.4.2. Precipitation strengthening……..148
7.4.3. High angle grain boundary strengthening……..149
7.4.4. Dislocation strengthening…….150
7.5. Discussion……150

8. Quenching and Partitioning steel…….....151
8.1. Q&P processing……..151
8.2. Chemical composition of Q&P steel……..154
8.3. Microstructure and properties of Q&P steel…….....155
8.4. Q&P attempt in hot stamping steel……156
8.5. Quenching and flash-partitioning (Q&FP)……..161
8.6. Discussion……162

9. Conclusion……..163

Acknowledge…….165

References…….166

Introduction

In the process of industrialization development, the development of steel materials has become an important indicator to evaluate the level of national economic development. Most steel usage is carbon structural steel and alloy structural steel. Although widely used, their strength is low, generally not more than 1000MPa, especially the strength of carbon structural steel is only 400MPa. Therefore, they cannot be widely used in special fields such as vehicle load-bearing components, military and aerospace. If the strength of commonly used steel is increased to more than 2000MPa, the annual output of steel will be greatly reduced which will have a very important impact on the world's environment, resources and energy. Therefore, high performance is not only the inevitable trend of market economy and technological progress, but also the only way for the development of steel materials.

At present, it is accustomed to refer to the structural steel with ultimate tensile strength exceeding 1500MPa as ultra-high strength steel. The most significant advantage of the low alloy ultra-high strength steel is the relatively low alloying elements content, which the total amount is generally not more than 5%. With the development of the steel industries, low alloy ultra-high strength steel has been widely used in some applications with excellent comprehensive properties, simple processing technology and low cost.

In this paper, the current status and latest achievements of ultra-high strength low alloy steels with ultimate tensile strength exceeding 2000Mpa are studied from the aspects of composition, processing, microstructure and mechanical properties by analyzing the literature.

The most conventional heat treatment process for low alloy ultra-high strength steel is quenching and low temperature tempering to obtain lath martensite structure.

High carbon chromium bearing steel 100Cr6 is the bearing steel with the largest production volume in the world. Since its birth in 1901, the main composition has basically remained unchanged for more than 100 years. It takes more than 80% of the world's total bearing steel production as the quality continues to improve in time. So that if there is no special description for bearing steel, it refers to 100Cr6. Although tempered martensite has high tensile strength, its low toughness can lead to brittle fracture of the material thus reduce service life. On the basis of the conventional heat treatment, the process can be improved e.g., by introducing isothermal transformation which the steels with lower bainite could be developed.

As a typical representative of medium carbon low alloy ultra-high strength steel, AISI4340 steel was developed in 1950 and successfully applied to aircraft landing gear in 1955. The successful development of AISI4340 steel provides new ideas and directions for the subsequent development of ultra-high strength steel. On the basis of AISI4340 steel, AISI4130, AISI4140, AISI4330 and other modified steels have been successfully developed. In order to increase the tempering temperature range of this type of steel, improve the fracture resistance, and at the same time suppress low temperature tempering brittleness, the chemical composition of the steel can be improved, on the basis of AISI 4340 steel, 300M alloys and D6CA steel, etc. with different alloying elements content are developed.

The use of ultra-high strength steel in automobiles allows to achieve lightweight and safety at the same time. Boron steel and hot stamping process are currently the most trustworthy materials and process technologies for lightweight of body. Hot-stamped low carbon steels include from

conventional 22MnB5 steel to the latest steel grades with ultimate tensile strengths exceeding 2000MPa and higher elongation by changing alloy designs or coupling different processes such as Q&P. Advances in materials and processes allow cars to meet increasingly stringent emissions and safety regulations. The hot stamping process of boron steel is the most important piece of the puzzle.

Protecting the vehicle with armor steel over 2000Mpa can achieve protection without making the vehicle too heavy, so that it looks and rides like a normal vehicle. In addition, as a special vehicle steel, the wear resistant steels also have extremely high strength under wear conditions.

Developing since the 21st century, in addition to tempered martensitic steels listed above, new advanced ultra-high strength steels such as nanobainitic steels and Q&P steels with mixed microstructure have also emerged with considerable ductility and toughness. The tensile strength of cold drawn pearlite steel wire could even grow up to 7000Mpa in recent years.

The research and development of these steels widely used in automobile parts with excellent performance greatly reduces the production cost, providing a broad application forecast and direction for the development of new high-performance materials.

1. Melting and casting practice

Nowadays, steel is produced using two main production routes (see Figure 1): the ore-based production route and the scrap-based production route.

The ore-based production route is based on Blast Furnace (BF) and Basic Oxygen Furnace (BOF) and uses different raw materials such as iron ore, metallurgical coal, limestone and recycled steel (representing about 30% of the total charge materials). The process is generally: BF and BOF →ladle refining (LF) → vacuum degassing (VD)/ Ruhrstahl Heraeus (RH) degassing → continuous casting.

The scrap-based production route is based on the electric arc furnace (EAF) and uses recycled steels (up to 100% of the total charge materials) and direct reduced iron (DRI) or hot metal, and electricity. The general process flow includes: EAF → LF → VD / RH degassing → continuous casting.

In 2020, about 70.2% (about 1320 million tons) of the total world steel production is produced by the ore-based production route and 29.8% (558 million tons) is produced by the scrap-based production route. [2]

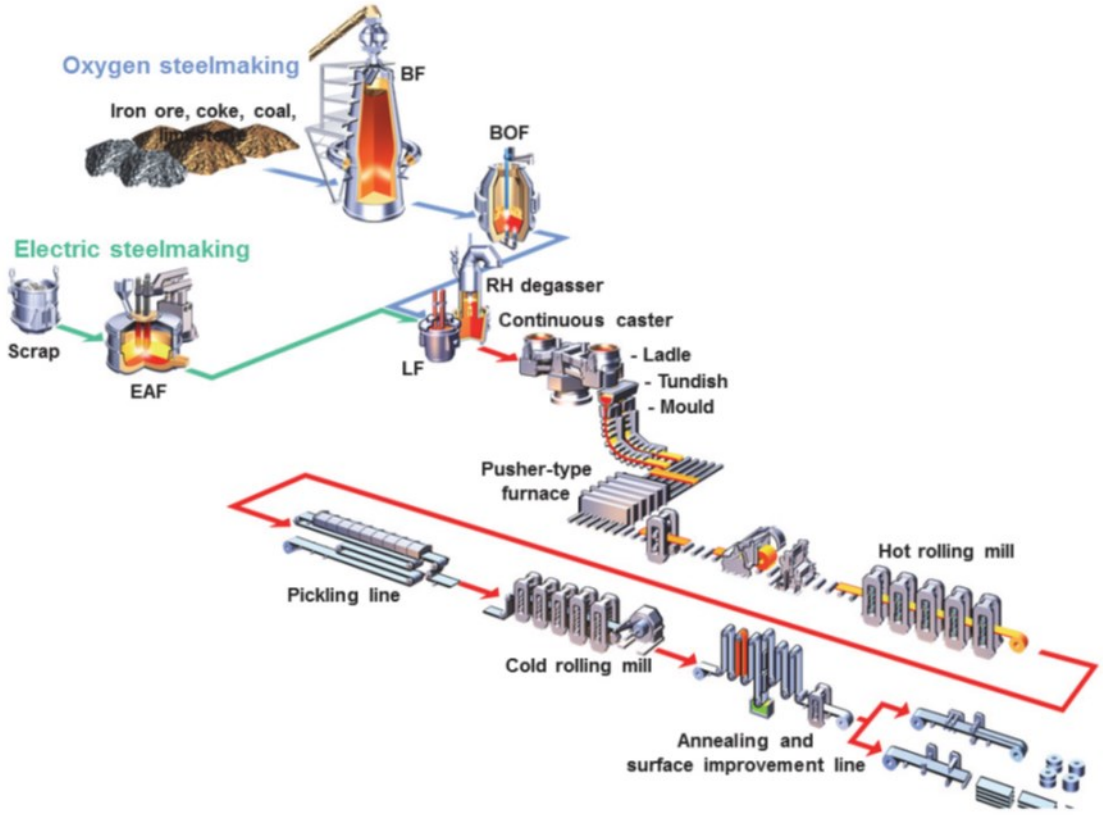

Figure 1. Steel production routes: (a) Oxygen steelmaking along BF and BOF converter. (b) Electric steelmaking in EAF. [1]

The casting process also plays a crucial role in controlling the composition distribution of the steel and improving the uniformity of the structure. Although steel produced by traditional die casting has certain advantages over continuous casting in terms of mechanical properties and

internal quality, its production cost is relatively high. Therefore, at present, the continuous casting method is mainly used for production. Due to the different distribution ratios of solute elements in solid and liquid during solidification, macro-segregation and micro-segregation will occur in continuous casting slabs. In order to improve the segregation state, methods such as soft reduction, electromagnetic stirring and electric pulse nucleation can be used simultaneously in the continuous casting process.

In addition, for some steels with high quality requirements, general refining methods are difficult to meet the requirements. Therefore, technologies such as vacuum induction melting (VIM), electroslag remelting (ESR) and vacuum arc melting (VAR) are used. It is worth noting that most special materials such as high-quality superalloys and corrosion-resistant alloys do not use a single process, but a double or triple method. That is, through a vacuum induction furnace + electroslag remelting furnace (VIM+ ESR) as shown in Figure 2 or vacuum induction furnace + vacuum consumable furnace (VIM + VAR) for production. There are also a small number of harsh industries such as military supplies taking VIM + ESR + VAR for production.

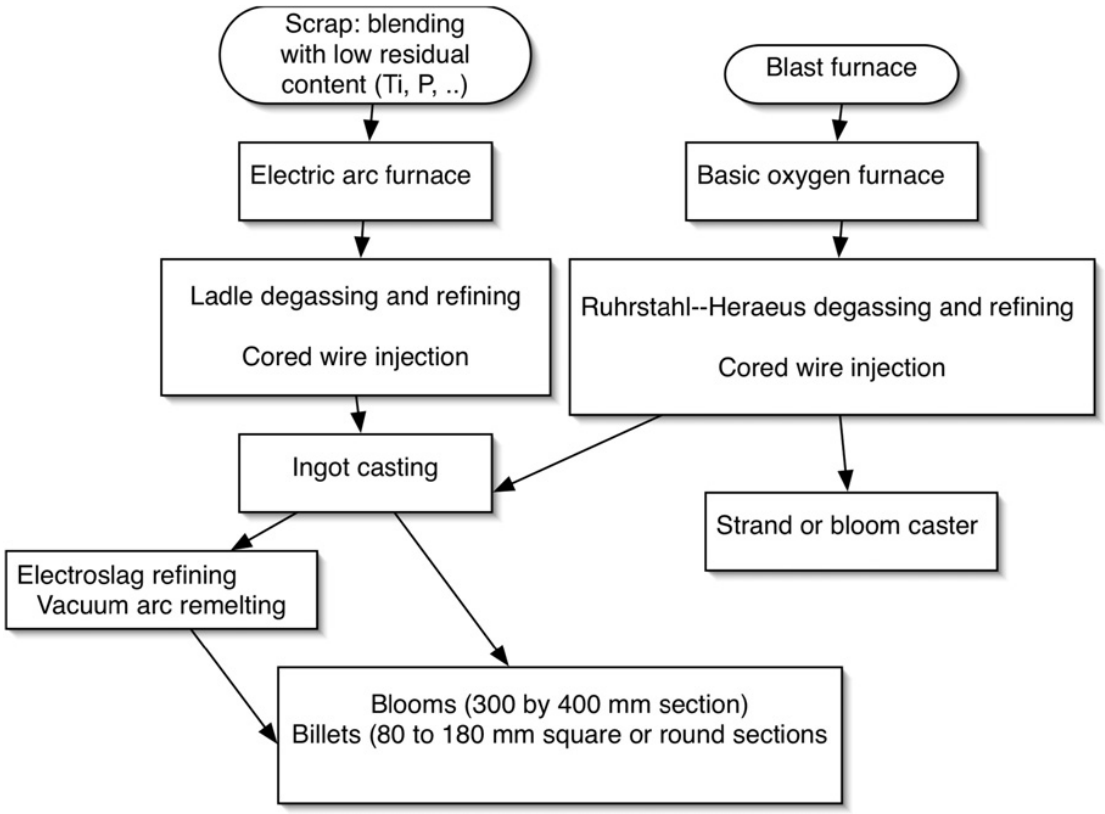

Figure 2. Simplified chart illustrating the processing paths from EAF and BF sourced metal. In some case a part of the load of an EAF may in fact be liquid steel from the BF. Tank degassing is an alternative to the RH process, but is regarded as less effective in removing impurities such as hydrogen. [3]

2. High-carbon bearing steels

The Oxford English Dictionary defines a bearing as follows: a part that reduces friction as much as possible during the relative rotation or movement of two parts in contact with each other in mechanical equipment. Bearings are basic mechanical equipment parts with a long history. They are widely used in various machines, equipment, instruments, and meters, and are vividly called "mechanical joints". Bearings have penetrated into all areas of human production and life, no matter it is automobiles, ships, airplanes, radars, motors, rolling stock, textiles, mining, metallurgy, petrochemicals, agriculture, household appliances, IT and other fields, you can find the trail of the bearings. The quality of the bearing directly determines the reliability, precision, performance, and service life of mechanical equipment. Currently, a large number of materials used to manufacture bearings are bearing steel. Since the Swedish SKF company invented high carbon chromium bearing steel with 1% C and 1.5% Cr in 1905, in order to adapt to the requirements of different environments, the bearing steel family has been expanding. So far, there are about 35 kinds of bearing steels with different compositions in the world. Because high carbon chromium bearing steel has high fatigue resistance, high ductility, good wear resistance, suitable elasticity and toughness, a certain anti-rust ability, and good cold and hot processing performance, the simple heat treatment method, and other advantages such as low content of alloying elements and low price. It has been widely used in the world. High carbon chromium bearing steel accounts for more than 80% of the total output of bearing steel in various countries in the world, and 7 steel grades for rolling bearing are included in the international standard ISO683-17:2014 as shown in Table 1.

Steel designation	% [mass fraction] [a, b]									
Name	C	Si	Mn	P	S	Cr	Mo	Ni	V	W	Others
Through-hardening bearing steels											
100Cr6	0,93 to 1,05[c]	0,15 to 0,35[d]	0,25 to 0,45	0,025	0,015[e]	1,35 to 1,60	0,10	–	–	–	Al: 0,050 Ca: [f] Cu: 0,30 O: 0,0015[g] Ti: [h]
100CrMnSi4-4	0,93 to 1,05[c]	0,45 to 0,75	0,90 to 1,20	0,025	0,015[e]	0,90 to 1,20	0,10	–	–	–	
100CrMnSi6-4	0,93 to 1,05[c]	0,45 to 0,75	1,00 to 1,20	0,025	0,015[e]	1,40 to 1,65	0,10	–	–	–	
100CrMnSi6-6	0,93 to 1,05[c]	0,45 to 0,75	1,40 to 1,70	0,025	0,015[e]	1,40 to 1,65	0,10	–	–	–	
100CrMo7	0,93 to 1,05[c]	0,15 to 0,45	0,25 to 0,45	0,025	0,015[e]	1,65 to 1,95	0,15 to 0,30	–	–	–	
100CrMo7-3	0,93 to 1,05[c]	0,15 to 0,45	0,60 to 0,80	0,025	0,015[e]	1,65 to 1,95	0,20 to 0,35	–	–	–	
100CrMo7-4	0,93 to 1,05[c]	0,15 to 0,35	0,60 to 0,80	0,025	0,015[e]	1,65 to 1,95	0,40 to 0,50	–	–	–	
100CrMnMoSi8-4-6	0,93 to 1,05[c]	0,40 to 0,60	0,80 to 1,10	0,025	0,015[e]	1,80 to 2,05	0,50 to 0,60	–	–	–	

Table 1. Steel grades and chemical composition (cast analysis). [4]

The main components of the 100Cr6 bearing steel studied in this subject are shown at first in the table. The steel is a high carbon steel and also contains a certain amount of Cr and Mn, among them, the content of Cr is relatively large, which is a typical low alloy steel.

In addition to the basic components listed in the table, it also contains trace elements such as Ni, V, and W. The higher C content makes the bearing steel have higher strength and hardness, and it is easier to spheroidize annealing. Containing a certain concentration of Cr element, it has better hardenability. At the same time, Cr element can also increase the stability of carbides and prolong the service life of the bearing. Mn element can also improve hardenability, but does not form carbides that are difficult to decompose. Other alloying elements also have a certain effect on improving the performance of bearing steel. For example, the Si element can enhance the tempering resistance and thus the fatigue life, and the Ni element can improve the toughness and plasticity.

The working conditions of the bearings are extremely harsh. The contact area between the rolling element and the raceway of the ring is very small, so that the contact pressure stress could

be as high as 3000~5000Mpa, and the number of cycles of force can reach tens of thousands of times per minute. The ball is also subject to additional load caused by centrifugal force when rotating, which increases with the number of revolutions increasing. Meanwhile, there will be sliding friction between the bearing balls and the inner and outer rings. As a material for manufacturing bearings, the mechanical properties of bearing steel must also reach a very high level in order to meet the requirements of industrial manufacturing. Because the bearing will be subjected to high contact compressive stress during use, the bearing steel should have extremely high contact fatigue strength and high hardness after proper heat treatment. The additional load caused by centrifugal force and the frequent cyclic loading process require the bearing steel to have a high elastic limit, good impact and fracture toughness, and good dimensional stability. The friction between the bearing components requires the bearing steel to have high wear resistance and low friction coefficient. Because engineering requires very high machining accuracy of bearing components, bearing steel must also have good hot and cold processing properties.

2.1. Ball bearing forming processing:

The entire process flow is shown in the Figure 3. First, the rod is heated on a continuous line of induction heating which consists of several induction coils. The material flow rate and induction parameters are adjusted to insure homogeneous temperature distribution in the rod prior to the forging operation. The hot rod is then precisely sheared into short rods. The rolling ring preforms of both inner and outer rings are hot forged from the shear bars in the same die set using a crank press. After cooling to room temperature, the forged rings are batch spheroidized in a continuous spheroidization furnace. The preforms are then sandblasted in preparing for the subsequent cold ring rolling operation. Then the rings are machined to their final geometry and dimensions before the heat treatment by turning operation. Finally, the specimens are fully hardened and tempered in a continuous batch heat treatment line. The rest of the process-chain includes hard grinding, superfinishing and assembly operations.

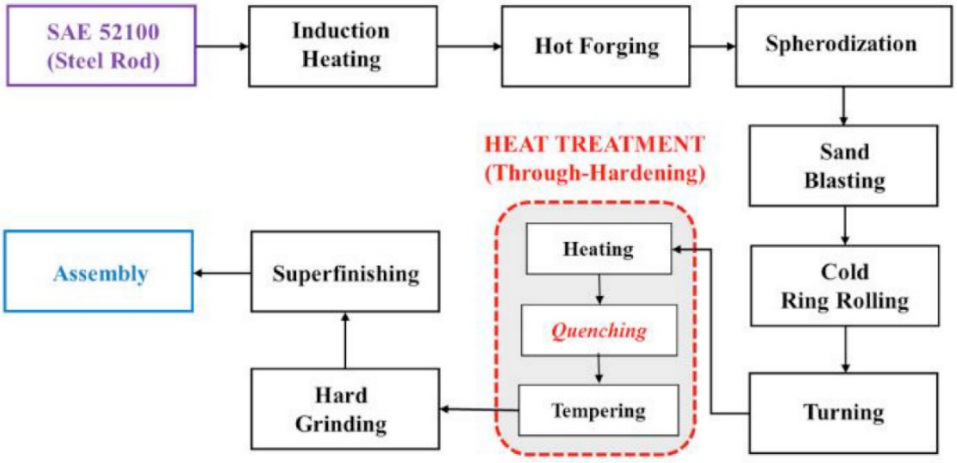

Figure 3. Manufacturing process-chain of 100Cr6 steel ball bearings. [5]

2.2. Spheroidization of 100Cr6 bearing steel:

The initial structure of bearing steel is usually hot rolled, and its microstructure is lamellar pearlite, as shown in Figure 4(a). The actual production process and a large number of studies have shown that the bearing steel after hot rolling with lamellar pearlite is easy to crack and is not easy to be machined. Therefore, it is generally necessary for lamellar pearlite to undergo spheroidizing annealing treatment to obtain a granular pearlite structure of bearing steel.

The purpose of spheroidizing annealing of bearing steel is to reduce the hardness to facilitate cutting; the other is to obtain a structure of fine, small, uniform and round carbide particles uniformly distributed on the ferrite matrix, so as to prepare the structure for the final heat treatment. The shape, size, quantity and distribution of carbides have a great influence on the final performance. The structure of carbides is difficult to change by the most quenching and tempering, because a considerable part of the carbides cannot be dissolved during quenching. The morphology is basically determined by spheroidizing annealing, hence spheroidizing annealing should be strictly controlled. As shown in the Figure 4(b), the microstructure changes after spheroidizing annealing.

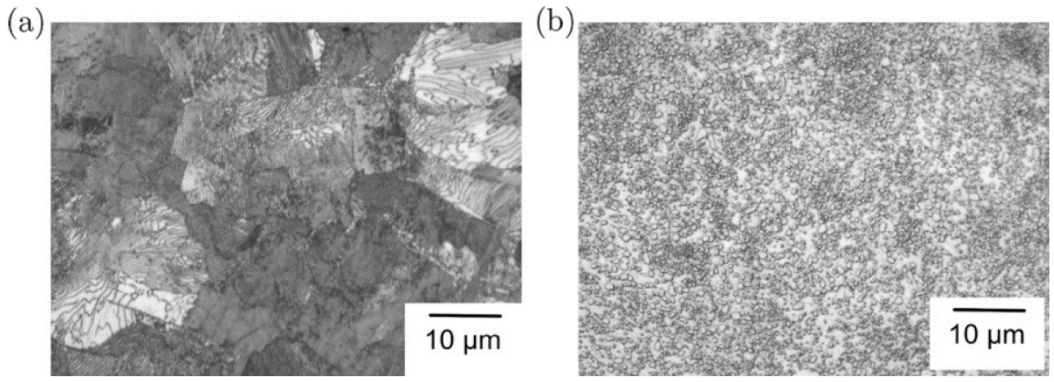

Figure 4. Microstructure of the steel 100Cr6 after hot rolling (a) and after spheroidizing annealing (b). [3]

The traditional spheroidizing annealing process is slightly higher than A_{C1} (lowest temperature at which austenite begins to form in steel under equilibrium conditions) temperature (for example, 780~810°C for 100Cr6) and then slowly cooled in the furnace after holding (25°C/h). Then it is air-cooled from the furnace below 650℃. If the cooling rate is too fast, the carbides will be smaller and dispersed and the hardness will be higher. If the cooling rate is too slow, the carbides will accumulate and grow and the hardness will be lower. The heat treatment time of this process is long (over 20 h), and the carbide particles after annealing are not uniform, which affects the structure and performance of subsequent cold working and final quenching and tempering. After that, according to the transformation characteristics of undercooled austenite, an isothermal spheroidizing annealing process was developed: after heating, it was quickly cooled to a temperature range below A_{r1} (690~720℃) for isothermal, and the austenite transformation to ferrite and carbide was completed in the isothermal process. Then it can be directly discharged from the furnace and air-cooled after the transformation is completed. The advantage of this process is to save heat treatment time (the whole process is about 10~18 h), and the carbides in the treated structure are fine and uniform. Another time-saving process is to periodically repeat the spheroidizing annealing: heating to 810°C for the first time and then cooling to 650°C, then heating to 790°C and then cooling

to 650°C and then air cooling. Although the process can save a certain amount of time, the process operation is relatively complicated and is subject to certain restrictions in actual production applications. [6~7]

2.3. Heat treatments and microstructures of 100Cr6 bearing steel:

Among the many alloys studied in the history of bearing steels, only two types of steels are used in most bearings. [8] Here we will study those hardened to a martensitic or bainitic condition. We would see that within these types, only a few alloys dominate the market for the simple reason that they are the best at meeting all the manufacturing and engineering requirements. This section will mainly study the heat treatment processes for steels tempered or isothermal transformed at temperatures below 300℃.

2.3.1. Martensitic quenching and tempering process：

Spheroidization is pretreatment of the heat treatment processes. The conventional final heat treatment is quenching and low temperature tempering.

Austenitising:

For 100Cr6 steels, the general heating temperature is 830 ~ 880 ℃ which is the austenitic zone (the specific temperature is determined according to the steel type and the size of the workpieces), and the holding time is determined according to the wall thickness of the workpieces, usually 0.6 ~ 0.8 h per 100 mm, and the minimum heat preservation is 10 min.

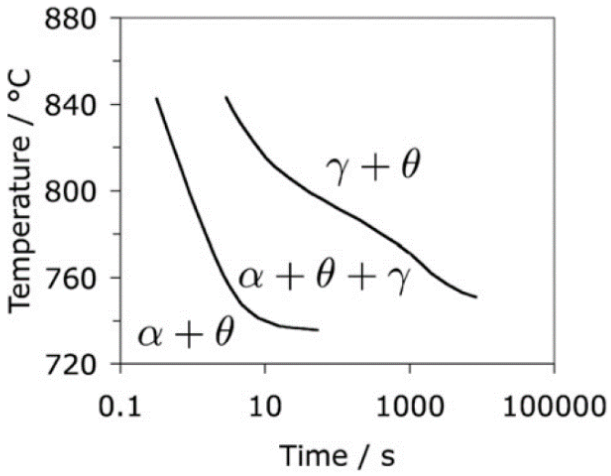

Figure 5. Isothermal transformation diagram for the austenite generation. [3]

Figure 5 shows an isothermal transformation diagram for austenitisation. Although the steel becomes completely austenitic at temperatures above about 900°C, this is under equilibrium conditions. It has been found in practice that austenitisation at 1040°C for 20 min completely

dissolves the cementite in 100Cr6 steels with a content of up to 1.1 wt.% carbon, resulting in austenite grain sizes of 40 to 60 μm.

Figure 6 shows how austenite grain size changes with austenitizing temperature. There will be a significant increase when carbides are dissolved at the higher temperatures.

Rapid heat treatment can generate even finer grain sizes, and while these studies were done with molten metal baths, short-duration austenitisation is realistic in commercial induction hardening.

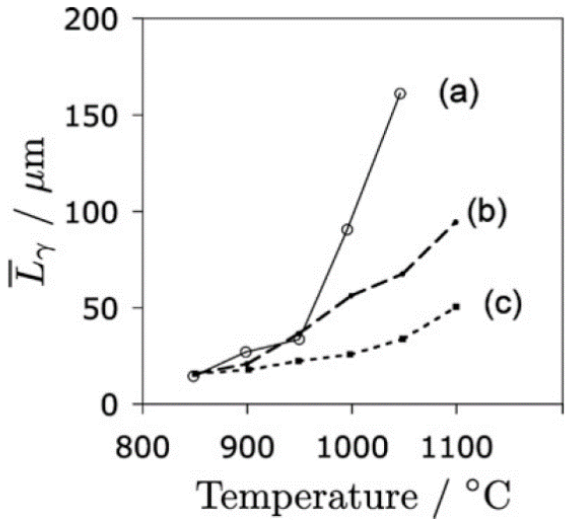

Figure 6. The austenite grain size defined as the average lineal intercept of a 100Cr6 steel, austenitizing for 1 h at the indicated temperature. [3]

A semi-empirical time–temperature parameter based on Avrami theory could be used to model the kinetics of cementite dissolution. Prior to austenitisation, the carbide dissolving process can be fastened by cold working the steel. Because equilibrium is not maintained in commercial heat treatments, a degree of superheating is required above the A_{cm} temperature to promote the formation of austenite. Austenite begins to form at A_{c1} = 756°C with heating at 2°C s^{-1}, and ferrite is disappeared when 790°C is reached.

At 840°C, about 3~4% of cementite remains undissolved, with the exact amount depending on the austenitisation time and initial microstructure. The cementite in the final microstructure aids in the steel's wear resistance. Austenitisation reaches equilibrium in approximately 20 min.

Quenching and tempering:

After austenitic holding, a quenching medium (oil bath or salt bath) with sufficient cooling capacity is used and appropriate stirring is performed to ensure that the workpiece is cooled to a certain temperature below the M_s point at a cooling rate higher than the critical cooling rate.

The M_s point is the temperature at which austenite starts to transform into martensite (high carbon chromium bearing steel M_s is about 220°C), and the M_f point is the temperature at which austenite stops transforming into martensite (high carbon chromium bearing steel M_f is about -70°C). The temperature of M_s point and M_f point is mainly determined by steel grade and heating conditions.

The structure of conventional martensite quenched is composed of martensite, retained

austenite and undissolved carbides for example microstructure shown in Figure 7. Under TEM we could find obvious twinning due to the fact that the martensite formed on quenching is heavily twinned. Twinned martensite is known to contribute to the strength of the alloy, but it generally results in poor toughness. In addition, high carbon steels are generally susceptible to microcracking. Microcracks appear at the tips of impinging martensitic plates and are a consequence of the accommodation of transformation strains. Austenitisation at high temperatures results in dissolution of carbides. However, with greater carbon in solution, larger transformation stresses are associated with the subsequent quenching, and the microcracking tendency increases.

After quenching, it should be tempered immediately to eliminate internal stress, improve toughness, and stabilize structure and size. The tempering temperature of 100Cr6 steel is 150~160℃, and the tempering time is 2~3 h. The tempered structure is tempered martensite, uniform fine carbides and a small amount of retained austenite. In order to eliminate the grinding stress generated during the grinding process, and further stabilize the structure and size, an additional tempering could be performed after the grinding process. The tempering temperature is 120~150℃, and the tempering time is 2~3 h.

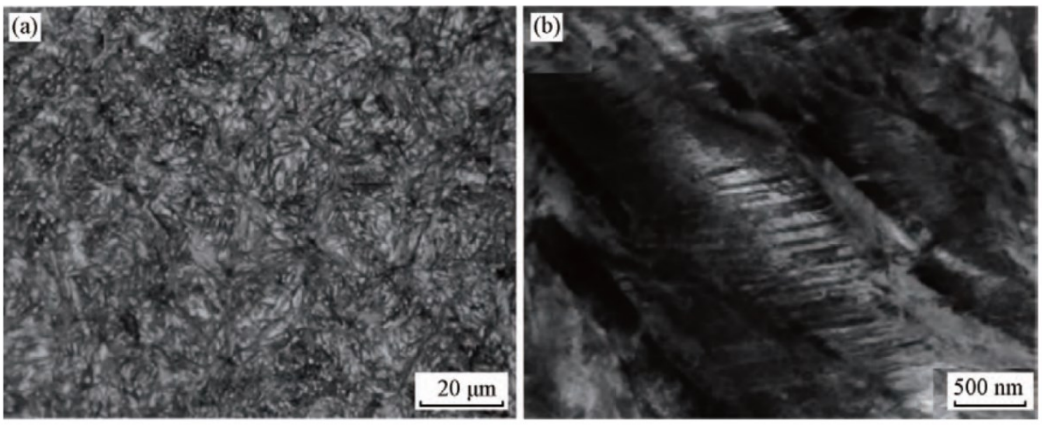

（a）OM；（b）TEM。

Figure 7. Microstructure of 100Cr6 martensite bearing steel after quenching and tempering in OM and TEM, respectively. [3]

Quenching from the austenitizing temperature results in a microstructure containing martensite, around 3~4% cementite particle and 6% retained austenite s that did not dissolve during the austenitisation process. These particles are usually uniformly dispersed and are about 0.4~0.6μm in diameter, as shown in Figure 8. The steel is then tempered at 160°C, which might result in the retained austenite decomposition and the precipitation of various Fe transition carbides from the supersaturated martensite. These carbides include both η- Fe_2C and χ- Fe_5C_2. For strength, the martensite relies on solid solution carbon and fine transition carbides of Fe, primarily ε-carbide, after the low temperature tempering.

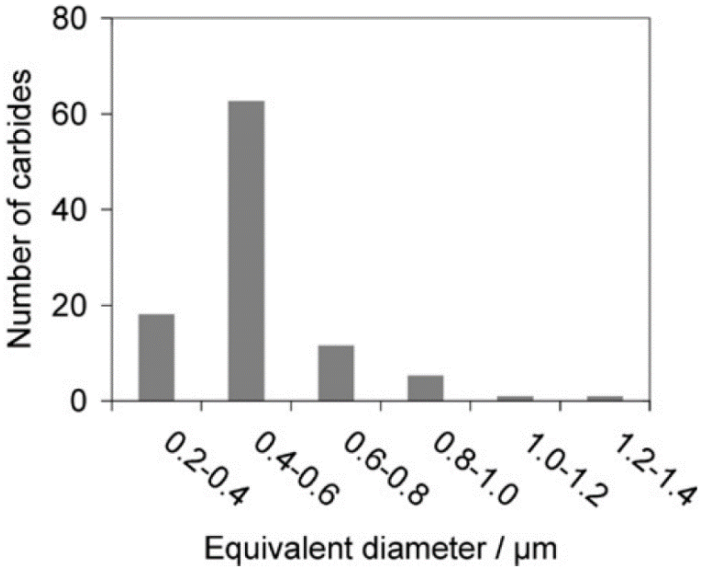

Figure 8. Typical distribution of undissolved carbides after austenitisation, 100Cr6 steel in its quenched and tempered state. [9]

The final structure in room temperature is about 85% martensite + 8% spherical carbide + 7% retained austenite. The quenching of bearing steel is to heat to the two-phase zone, holding for a period of time to form a certain proportion of austenite/carbide, and then rapidly cooling to room temperature. Carbides remain, most of the austenite is transformed into martensite, and there is a small amount of retained austenite. Many researchers have conducted qualitative studies on the dissolution mechanism of carbides and the influence of alloying elements on the dissolution process during the heating and holding of the two-phase zone. The quenching temperature determines the ratio of austenite and insolubilized spherical carbides, which determines the carbon content in the austenite and the final retained austenite content after quenching.

In recent years, the development of the martensitic quenching and tempering process of conventional high carbon chromium bearing steel is mainly divided into two aspects: on the one hand is on the effect of quenching and tempering process parameters on the structure and performance, such as the structure transformation in the quenching and tempering, decomposition of retained austenite, toughness and fatigue properties after quenching and tempering. On the other hand, the process performance of quenching and tempering, such as the influence of quenching conditions on size and deformation, dimensional stability, etc.

2.3.2. Bainite isothermal quenching process:

Although the traditional martensitic quenching and tempering process could greatly increase the strength of 100Cr6 bearing steel, mostly the ultimate tensile strength of steel is under 2000MPa. In addition, the high hardness of martensite in traditional high carbon chromium bearing steel makes this steel has good wear resistance and excellent contact fatigue resistance. However, due to poor toughness, residual tensile stress is likely to exist on the surface of the workpiece during quenching,

and the high sensitivity of hydrogen embrittlement greatly reduces the service life of high carbon chromium bearing steel in a working environment with high performance requirements.

Therefore, on the basis of the traditional martensitic quenching and tempering process, bainitic isothermal quenching process was developed. Isothermal transformations appear to be particularly appealing since they have the ability to provide optimal strength-toughness combinations by carefully controlling microstructure. Bainitic structures are essential because they allow a product of deformed ferrite and carbide to be produced that closely matches the structure of tempered martensite when the right isothermal temperatures are used. Martensite and bainite duplex structures could also be beneficial.

The bainitic transformation occurs at a temperature between that of ferrite and pearlite which are high temperature transformations, and martensite which is low temperature transformation. Bainite consists of aggregates of ferrite flakes or laths separated by phases such as martensite or austenite.

Isothermal transformation in the temperature range 200~450°C can make the 100Cr6 steels bainitic, with lower bainite dominating the microstructure when the transformation temperature is below 350°C. In contrast to tempered martensite, where the carbide is ε-carbide, the carbide in lower bainite is cementite. The difference is due to the fact that the initial excess carbon dissolved in the bainitic ferrite is subjected to two demands: partitioning into retained austenite and precipitation. When the former dominates, the precipitation mainly comes from carbon-enriched austenite. The lower bainitic microstructure observed in TEM after isothermal transformation at 200℃ and different holding time (6 h and 12 h, respectively) are shown in Figure 9.

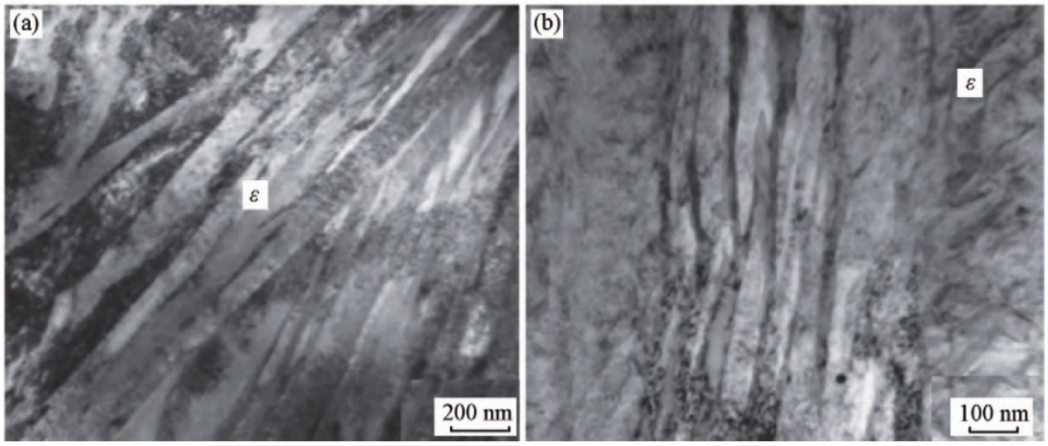

(a) 6 h; (b) 12 h。

Figure 9. Microstructure of 100Cr6 steel after bainitic isothermal transformation under different holding time. [10]

It can be observed that they are composed of lath bainite ferrite, thin film retained austenite and ε-carbide. The final structure is measured and corrected by the average line intercept method, and it is concluded that the structure is a nanobainite lath with an average thickness of about 50nm±15nm.

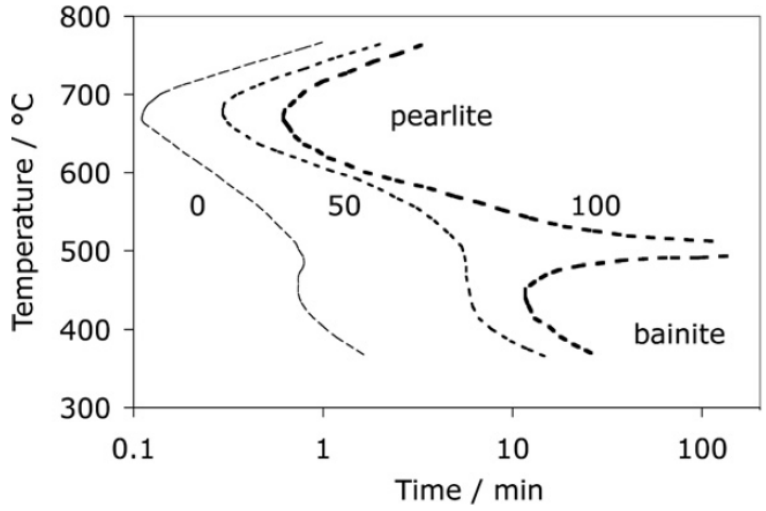

Figure 10. Isothermal transformation diagram for the 100Cr6 steels, completely austenitised at 1040°C for 30 min obtaining the austenite grain size of 40~60 μm. [3]

Figure 10 shows a time–temperature transformation measured for 100Cr6 steel. Figure 11 shows another diagram, drawn on the same horizontal scale, with nearly the same steel that has been austenitised at a lower temperature to reduce the carbon concentration in the austenite. The increased driving force for transformation causes the bainitic reaction to accelerate. Due to the higher concentration of carbon dissolved in the austenite, the formation of pearlite is faster when the austenitizing temperature is higher as shown in Figures 10 and 11.

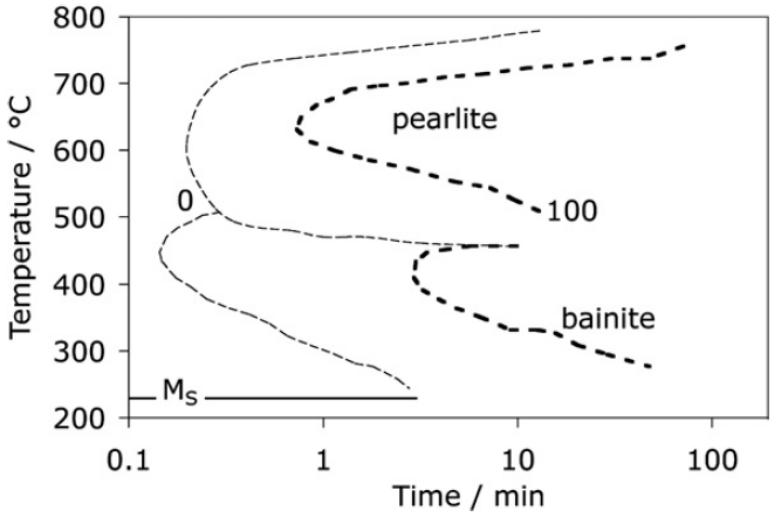

Figure 11. Isothermal transformation diagram of the 100Cr6 steel, austenitised at 845°C for 20 min. The numbers represent the transformation percentage. [3]

The austenitisation process of the bainite isothermal transformation process and the martensite quenching and tempering process is the same, and then the same quenching medium is used and appropriate stirring is performed to ensure that the workpiece is cooled to lower bainite transformation temperature zone at a cooling rate greater than the critical cooling rate, and

isothermal for sufficient time (about 4 h isothermal transformation at 240℃) to obtain the final structure composed of lower bainite, a small amount of retained austenite and carbides.

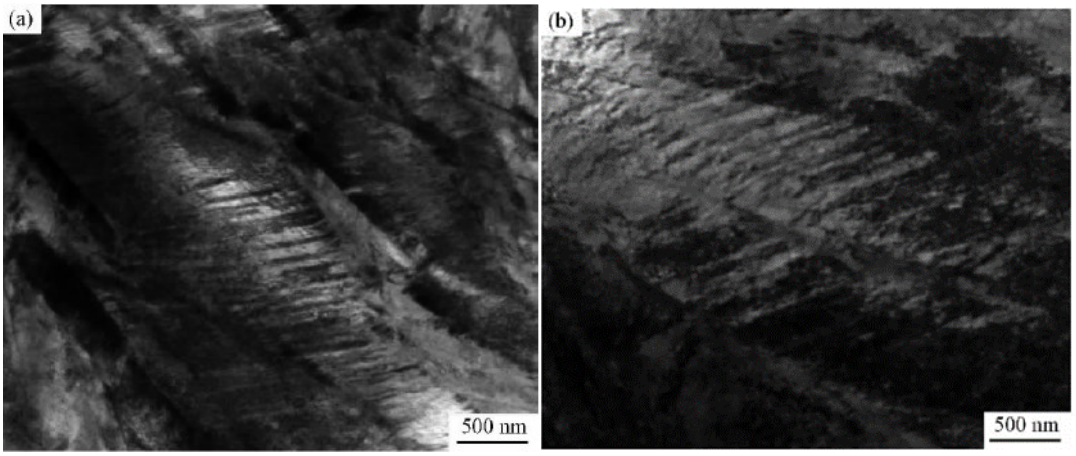

Figure 12. TEM images showing microstructure of the steel after different heat treatments (a) quenching and low temperature tempering; (b) bainite isothermal quenching. [8]

As shown in Figure 12, the martensite, bainite flakes and rod-like carbides distributed on the sample after the martensite quenching and tempering and bainite isothermal treatment are observed under high resolution TEM.

As shown in Figure 12(a), after quenching and tempering, the dispersed and precipitated rod-shaped carbides are distributed in parallel in the flaky martensite.

As shown in Figure 12(b), the dispersed and precipitated carbides after bainite isothermal treatment are fine flakes or fine grains which are distributed at an angle of 55°~60° with the axial direction on the ferrite matrix. The substructure of lower bainite ferrite is entangled dislocations, and no twin substructure is found. Therefore, compared with lamellar tempered martensite, it is one of the reasons for the higher toughness.

Since lower bainite has more carbides dispersed and precipitated, the degree of carbon supersaturation of bainite ferrite is lower than that of martensite, so the solid solution strengthening effect is smaller. Among the factors that affect strengthening, solid solution strengthening makes the toughness drop the most prominent, so the toughness of bainite is better than martensite. The low carbon content dispersed and precipitated in the lower bainite is the main factor for the strengthening of the bainite, but the presence of these carbides has little damage to the toughness and in the tempered martensite, the decomposition of the flaky coherent ε-carbide is the main reason for the formation of shell-like cementite at the martensite interface and the increase in brittleness. In addition, the flaky carbides precipitated along the twin planes during tempering of high carbon martensite form a high energy barrier to the movement of dislocations, resulting in a high concentration of stress at the ends of the cracks and reducing toughness. There are no twins in lower bainite, which is an important aspect of lower bainite's toughness better than tempered martensite.

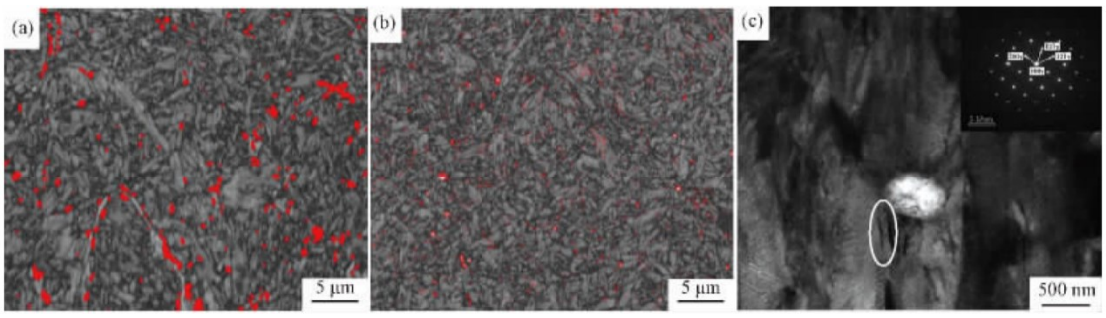

Figure 13. Morphology and distribution of the residual austenite of 100Cr6 steel (a) quenching and tempering EBSD; (b) bainite EBSD; (c) bainite TEM. [8]

The Figure 13 shows the retained austenite EBSD and TEM results of the sample processed by isothermal transformation for 4 h at 240°C. It can be seen that, compared with quenching and tempering, the distribution of retained austenite after bainite isothermal treatment is more dispersed and finer. There are two main distribution forms of retained austenite in high carbon chromium bearing steel: massive forms are distributed at grain boundaries, as shown in (a) and (b) in red areas; thin films are distributed between laths (as shown in (c) Inside the white box). It can be seen that after the bainite isothermal treatment, the fine and dispersed retained austenite is distributed in the matrix. The austenite is almost completely consumed. As a result, the retained austenite percentage is low, below 1%, and isothermally transformed structures of this type are dimensionally stable. The heat treatments used in bainitic process also help to reduce the risk of quenching cracking, which is not only harmless but can also increase overall performance.

World-renowned bearing companies such as Germany's FAG and Sweden's SKF have successfully applied the bainite isothermal process to railways, automobiles, rolling mills, cranes, drilling tools and other bearings that are resistant to impact and poor lubrication.

2.3.3. Martensite and bainite duplex structure quenching process:

When compared to the quenched and tempered condition, the entire transformation to bainite at a temperature just above M_s (i.e., 230°C) can take up to 4 h, increasing the heat treatment cost. It is possible to speed up the reaction by quenching it for less than a minute at a temperature around 20°C below M_s and then bringing it to the bainitic range. Step quenching of this type, although within the bainite transformation range, has been known to speed up transformation kinetics at higher temperatures for some time. The two-steps process of bearing steel has been shown experimentally to reduce heat treatment time without reducing hardness, but it remains to be established whether the process could be applied to industrial use. The researchers found that transforming 100Cr6 steel completely at 210°C for 33 h yields a hardness of 60.1 HRC. Transformation of the most of the austenite for 9 h at the same temperature followed by heating to 250°C for 1 h, yields a fully bainitic microstructure with a slight reduction in hardness to 59.9 HRC. [11]

The austenitisation process could be also same as before, and then the same quenching medium is used and appropriate stirring is performed to ensure that the workpiece is cooled to a temperature M_d between the M_s point and M_f point at a cooling rate greater than the critical cooling rate, to

transform austenite in the workpiece partially into martensite. The lower the M_d temperature, the more austenite transforms into martensite. After the temperature of the core of the workpiece is cooled to M_d, the workpiece is immediately transferred to the appropriate medium (Such as air, hot oil or salt bath) heated to the lower bainite transformation temperature, and isothermal for a certain period of time, to transform the retained austenite in the workpiece into lower bainite, and the formed martensite is tempered, and finally obtained by tempered martensite, lower bainite, carbide and a small amount of retained austenite.

By comparing the temperature-expansion curve of conventional isothermal transformation and isothermal transformation with a pre-quenched process simulated by the dilatometer, the kinetic curve of bainite isothermal transformation can be obtained, as shown in the Figure 14. It can be seen that the partial transformation at a lower temperature in advance to form a small amount of martensite can accelerate the subsequent bainite transformation at a higher temperature. This may be related to the strain induced nucleation caused by the pre-transformed structure. The strain-promoting effect of the bainite accelerates the nucleation of the α phase in the bainite, which accelerates the bainite transformation, and greatly shortens the incubation period. The bainite temperature change treatment obviously shortens the bainite transformation time without affecting the performance.

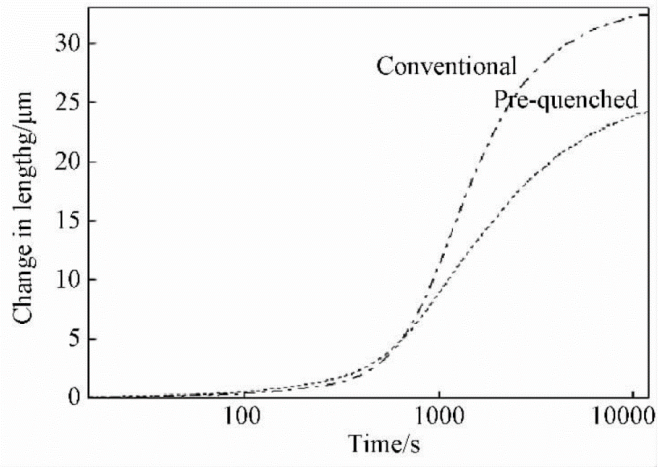

Figure 14. The kinetics of bainite isothermal transformation. [8]

2.3.4. Bainite temperature varying quenching process:

In recent years, many new bearing bainite quenching methods have been invented, which are suitable for the quenching of precision bearings and high-temperature bearings (The 100Cr6 steel is not intended for elevated temperature service). The technical solution studied here is a high-carbon chromium bearing steel bainite temperature varying quenching method which could also significantly shorten the bainite transformation time and have good overall performance.

The austenitisation process could be also same as before. There are two types of quenching/cooling methods: It is possible to shorten the holding time of the bainite isothermal transformation to a period of time. Then Increase the temperature by 15~20℃ and wait for a period of time. Or, wait for a period of time in the bainite isothermal transformation, then air cooling to below the M_s point temperature, after that increase the temperature by 15~20℃, and wait for a

period of time. [12] The two quenching process routes are different, and the treatment effect is the same. In addition, this technology can be combined with Martensite and Bainite duplex structure quenching technology which the pre-quenched process is added giving full play to the advantages of the two and giving full play to the potential of the material as shown in Figure 15, Process 4.

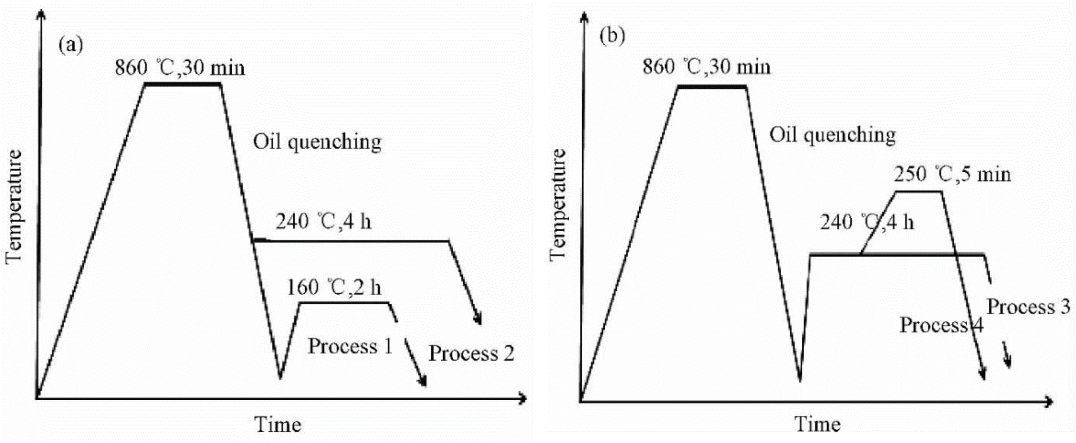

Figure 15. Scheme of different heat treatments which Process 1: quenching and tempering, Process 2: isothermal transformation, Process 3: pre-quenched isothermal transformation, Process 4: bainite temperature varying quenching. [8]

The beneficial effect of the invention is that compared with the traditional lower bainite quenching process, after the parts are subjected to the bainite isothermal transformation at 230~250℃, the second isothermal stage has a small increase in temperature. The second isothermal stage makes the residual stress generated by the bainite isothermal transformation released. The martensite and lower bainite duplex structure is quenched and tempered, and the retained austenite continues to transform into lower bainite, which makes the hardness decrease little.

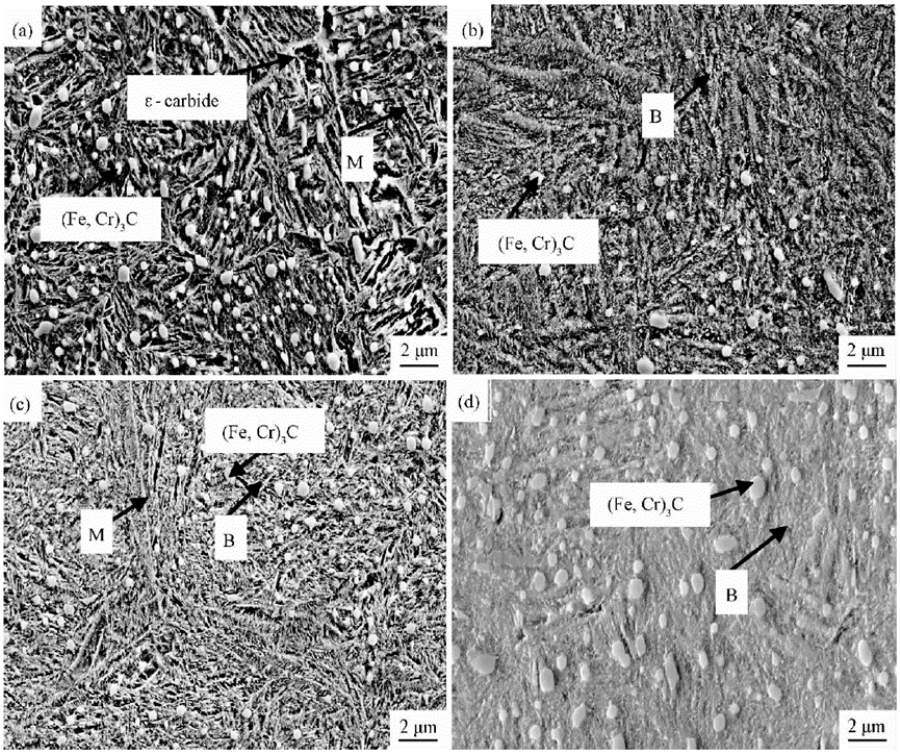

Figure 16. Microstructures of the steel 100Cr6 after different heat treatments. [8]

The overall microstructure and their inclusions of the different processes studied are shown in the Figure 16. The pretreatments are all spheroidizing annealing, while the final heat treatments are different which results in distinct microstructures, thereby affecting the mechanical properties of the steels.

2.3.5. Analysis of retained austenite and dimensional stability:

In order to quantitatively analyze the retained austenite under different heat treatment process conditions, the researchers carried out phase analysis on the X-ray diffractometer. The test results are shown in the Figure 17(a) which is the state of spheroidizing annealing, Figure 17(b), (c), (d), (e) are the results of 4 heat treatment processes. Here P, B, M in XRD patterns represent in fact the peaks of α-ferrite in pearlite, bainite and martensite, respectively. Since pearlite is a structure composed of α-ferrite and cementite lamellae, bainite is a metastable structure formed by α-ferrite and its dispersed carbides, while martensite is a supersaturated solid solution of carbon in α-ferrite. We could evaluate the structures of 100Cr6 steel by detecting the α-ferrite in XRD.

It can be seen from Figure 17(a) that in the spheroidizing annealing state the structure is mainly spherical carbides distributed on the pearlite matrix, and there are mainly two peaks of pearlite (P) and carbide (M_3C) on the XRD pattern. Figures 17(b), (c), (d), (e) show that the amount of retained austenite (RA) is the largest after the process 1, reaching 12.5%, and the main structure is tempered martensite and retained austenite. After the process 2, the retained austenite content is less than 3.88%, and the structure is mainly bainite and carbide. After the process 3, the retained austenite content is only 3.50 %. After process 4, the retained austenite content is 7.80% and the room temperature structure is mainly bainite, carbide and retained austenite.

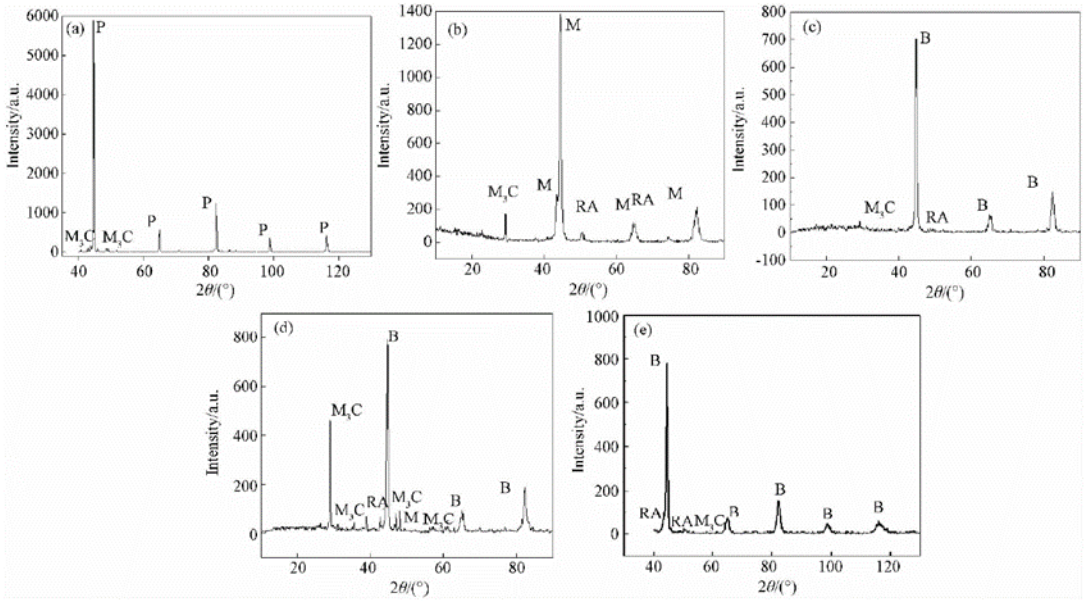

Figure 17. XRD patterns of 100Cr6 steel after different heat treatments. [8]

The dimensional stability of high carbon chromium bearing steel can be divided into stability during heat treatment and stability during service. Generally, the stability during heat treatment can

be measured by the dimensional change before and after heat treatment, while the stability during service is often characterized by the amount of retained austenite and the carbon content of retained austenite. The Table 2 shows the dimensional change, the amount of retained austenite, and the carbon content of retained austenite after the samples are processed by different treatments. The results show that the dimensional change after bainite transformation and the amount of retained austenite are lower than the martensite quenching and tempering transformation. It can be seen that different degrees of bainite transformation can improve the dimensional stability of the high carbon chromium bearing steel.

	Process 1	Process 2	Process 3	Process 4
Residual austenite/%	10. 80	3. 88	3. 50	7. 80
Elongation/μm	36. 2	4. 3	3. 6	7. 0

Table.2. Residual austenite (%) and elongation (μm) of different samples. [8]

2.4. Mechanical properties of 100Cr6 bearing steel:

2.4.1. Hardness:

Heat treatment induced hardness is a significant variable. The Rockwell C hardness at operating temperature must be 58 or above for most rolling bearings.

The hardness of 100Cr6 steels can occasionally be approximated using a mixing rule assuming that the hardness of martensite, bainite, pearlite, and austenite are 64, 35, 29, and 17 HRC, respectively. As long as there is not much bainite in the steel, the method seems to be fairly accurate, as it would not be reasonable to assign a single value of 35 HRC to this phase, due to the fact that isothermal transformation to full bainite at 250°C after austenitisation at 840°C will result in a hardness approaching 60 HRC.

Figure 18(a) shows the hardness values under different heat treatment conditions. From the data, it can be seen that the hardness of lower bainite is lower than that of martensite (close to 800 HV or 72 HRC) in the process 1 which is completely martensitised. The hardness of the structure is the highest, and the hardness of the fully bainitic structure in process 2 is the lowest. The hardness of 100Cr6 steel decreases with the decrease of martensite and the increase of bainite. After the bainite temperature varying quenching process, the hardness is equivalent to that obtained by the bainite isothermal treatment process, and the hardness of the martensite and bainite duplex structure is in the middle position.

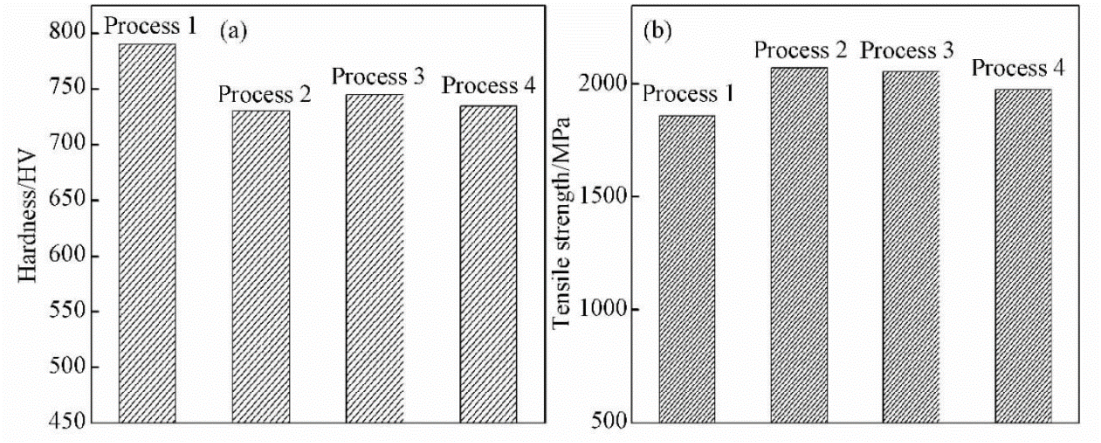

Figure 18. Mechanical properties of 100Cr6 steels after different heat treatment processes. [8]

In general, the higher the bearing steel's hardness at operating temperature, the longer the bearing steel's life. A relationship has been developed that approximates the effect of bearing material hardness on fatigue life:

$$LF = \exp\{m[(\mathrm{RC})_\mathrm{T} - 60]\}$$ [13]

where m is an exponent related to material hardness and life (usually m=0.1) and $(\mathrm{RC})_\mathrm{T}$ is the Rockwell C hardness at operating temperature. All components in the rolling bearing (i.e., the rolling elements and the races) were assumed to be of the same hardness for the purposes of this relationship, which was obtained for 100Cr6 steel. This equation was also assumed to be applicable to various bearing steels. An increase of hardness of 3% can lead to a 35% bearing life increase. Most bearing steels, except for 100Cr6 steel and other low temperature tempering bearing steels, could maintain their hardness in room temperature after soaking at increased temperatures.

Hardness in the 59~66 HRC range has been found to correlate positively with rolling contact fatigue life, and higher hardness is linked to less bearing track wear.

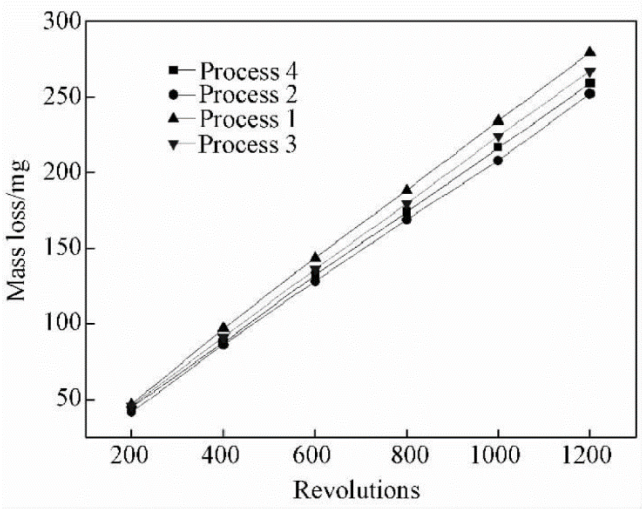

Figure 19. Curves of mass loss vs number of revolutions of 100Cr6 steel specimens after different heat treatments. [8]

Figure 19 shows the pin and disc wear curves of the four structures as shown in Figure 16 after different revolutions. It can be seen from the curve that the wear of different samples increases linearly with the increase of the number of revolutions, and the mass loss of different samples is close. The wear performance of the lower bainite structure obtained by the bainite isothermal treatment is better than that of the martensite structure obtained by quenching and tempering, but the difference is not big. It can be seen that when the hardness is similar, the wear resistance of the lower bainite structure is better than that of the tempered martensite structure.

2.4.2. Strength vs. ductility:

Steels like 100Cr6 steel are not particularly ductile when quenched and tempered. The elongation under tension is just 1~2%, therefore, meaningful tensile test data is difficult to come by, and hardness or bending strength is often provided instead.

According to some general statements, 100Cr6 steel has a 0.2% proof strength in the range 1400~2200MPa and an ultimate tensile strength in the range 2150~2450 MPa in its typical martensitic condition (with 12% γ_r) or when transformed to lower bainite range at temperatures below 300°C (without γ_r). The higher values correspond to martensite, and as the bainite transformation temperature rises, the strength drops. Figure 20 shows some specific data for the influence of the bainite transformation temperature. As the transformation temperature increases, the hardness of the material decreases continuously. The ultimate tensile strength peaks at around 220°C. With a transformation temperature of 220~240°C, the yield strength looks to be at its peak. For low transformation temperatures, total plastic elongation to fracture is low, but between 240 and 300°C, it increases significantly.

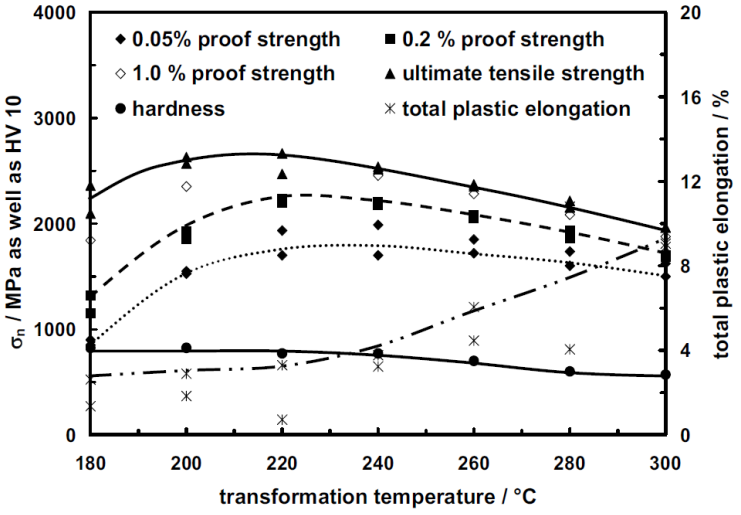

Figure 20. Results of the hardness and tensile tests for the effect of the isothermal transformation temperature. [14]

The individual tensile test curves reveal that the highest strength is found between 200°C and 240°C, while the total elongation to fracture is greater at higher transformation temperatures as shown in Figure 21. The tensile behavior after transformation at 180°C is remarkable: the slope of

the tensile test curve changes around 850 MPa, indicating that the isothermal transformation resulted in a material state with retained austenite that is unstable in the tensile tests and transforms stress or strain induced during tensile tests into martensite.

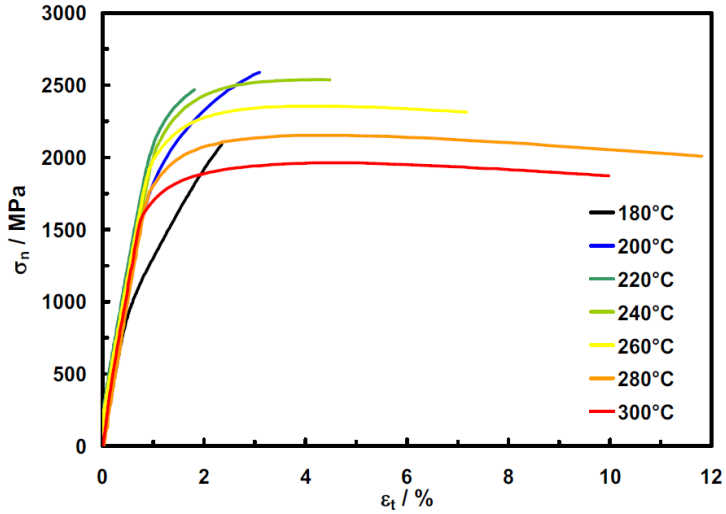

Figure 21. Individual tensile test curves. [14]

The ductility in the bainitic condition is always greater than the minimal plasticity exhibited by the tempered martensitic structure of 100Cr6 steel. This might give the reason why the lower bainitic bearings operating in water-containing environments have a longer life than quenched and tempered bearings

Figure 18(b) shows the ultimate tensile strength under different heat treatments measured by the normal temperature tensile test. The strength of the lower bainite and martensite and bainite duplex structure is higher than that of the typical tempered martensite which definitely exceeds 2000Mpa as we expected. (We could also have tempered martensite whose tensile strength is above 2000Mpa by varying the austenitisation and tempering parameters.) The analysis reasons are: On the one hand, the carbides in the lower bainite structure are uniformly dispersed and precipitated so that the bainite structure is strengthened. On the other hand, considering the stress state after heat treatment, the surface of martensite structure after the quenching and tempering treatment is tensile stress and the core is compressive stress. This stress distribution is unreasonable. The surface of the workpiece after bainite treatment is compressive stress, and the core is tensile stress. Obviously, the latter is beneficial to increase the strength. Finally, for the martensite and bainite duplex structure, the lower bainite precipitated first divides the untransformed undercooled austenite which could refine the austenite grains, so that the later transformed martensite is refined. At the same time, because the specific volume of martensite is larger than austenite, in the process of transforming into martensite from the undercooled austenite, the lower bainite will be squeezed by the expansion of martensite so that certain deformation strengthening is produced.

2.4.3. Fracture toughness:

One of the failure modes of bearing parts is the occurrence of cracks and fractures. For example, the inner ring of a rolling mill bearing mainly fails in the form of axial fracture. Therefore, the

research on improving the fracture toughness (K_{IC}) of 100Cr6 bearing steel has attracted more and more attention. Fracture toughness characterizes the ability of a material to prevent crack propagation. It is independent of the shape, size and applied stress of the crack itself. It is an inherent characteristic of the material and is barely related to the material itself, processing technology and heat treatment.

The fracture toughness tends for hardened 100Cr6 steel which the hardness exceeds about 50 HRC have values in the range 15~20 $MP.m^{1/2}$, the lower values corresponding to larger carbon concentration within the steel, as shown in Figure 22.

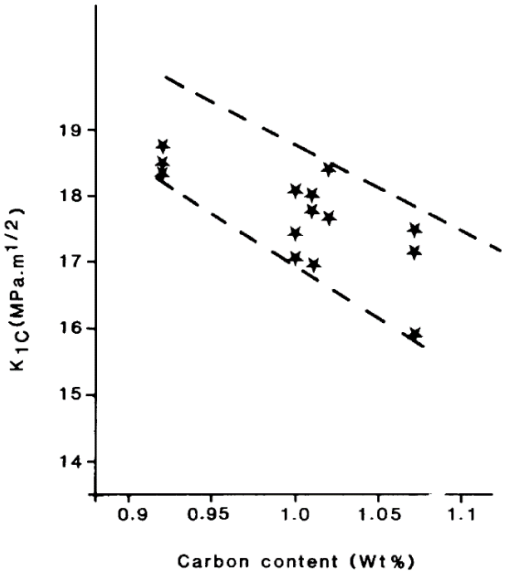

Figure 22. Carbon content related to K_{IC} for martensitic hardening at 860°C for 20 min and tempering at 160 °C for 1.5 h. [15]

Bearing parts always have some defects or microcracks. Before the stress intensity factor K_I at the crack tip reaches K_{IC}, that is, before the instability fracture, the crack is in stable growth. Therefore, the fatigue crack growth rate da/dN of the material is also a very important fracture mechanics parameter. As the austenitizing temperature decreases and the tempering temperature increases, the fatigue crack growth rate da/dN decreases as shown in Figure 23.

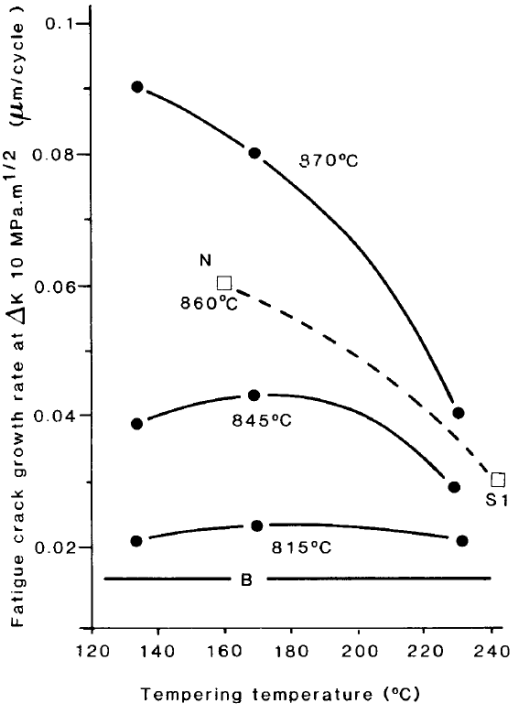

Figure 23. Crack growth rates at $\Delta K = 10\ MP.m^{1/2}$ in related to tempering temperature for martensitic-hardened 100Cr6 steel. [15]

It could be seen in the Table 2 that different processes can obtain different amounts of retained austenite. The higher the retained austenite content, the higher the K_{IC} and the lower the fatigue crack growth rate da/dN. In 100Cr6 steel, martensitic microstructures with high levels of retained austenite have higher fracture mechanics properties but lower blunt notch toughness than martensitic microstructures with lower levels of retained austenite. High fracture and blunt notch toughness are produced by bainitic microstructures in 100Cr6 steel with little retained austenite. This is because when the crack meets the retained austenite, the crack tip undergoes considerable passivation. At the same time, the austenite induces martensite transformation due to the stress field at the crack tip, causing stress relaxation and crack propagation to occur difficultly. However, at different quenching temperatures, the amount of retained austenite has an opposite effect on K_{IC} and da/dN. This is obviously the beneficial factor of retained austenite on K_{IC} are concealed by unfavorable factors such as the increase in the amount of solid solution carbon amount in martensite, the coarsening of bulk grains and the increase in the amount of twin martensite.

As the austenitizing temperature decreases, the fracture toughness K_{IC} value of 100Cr6 steel increases. The average K_{IC} values related to austenitizing temperature are shown in Figure 24. The lower austenitizing temperatures result in low carbon austenite and, subsequently, lower carbon tougher martensite upon quenching.

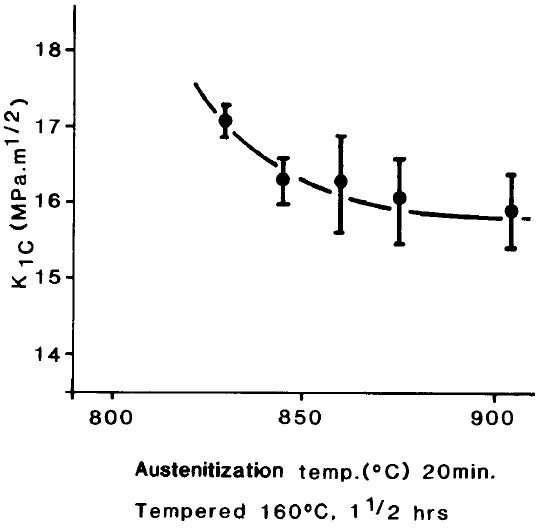

Figure 24. Fracture toughness related to austenitizing temperature for martensitic-hardened 100Cr6 steel. [15]

Figure 25 shows the K_{IC} and notch impact toughness against tempering temperature at a 1 m/ s^{-1} impact velocity. Increased tempering temperatures increased dynamic toughness significantly, but the K_{IC} was only slightly affected. K_{IC} increases slightly after tempering at temperatures up to about 210 °C. At 240 °C, austenite is completely decomposed, and K_{IC} shows a slight decrease. Tempering in the range of 180°C to 240°C improves notch toughness significantly, and such toughness test shows no signs of embrittlement.

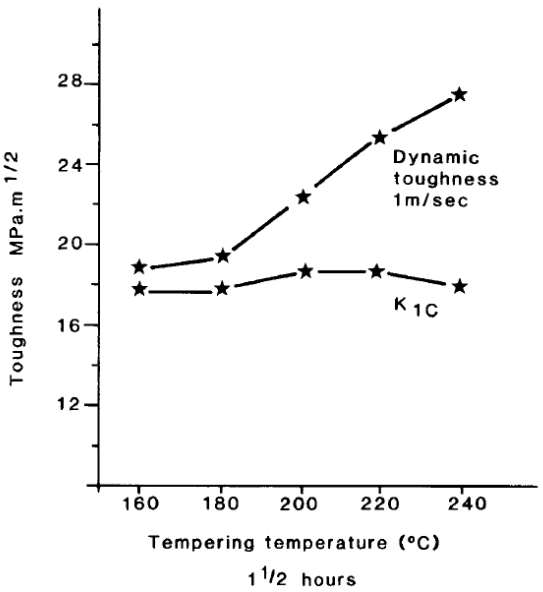

Figure 25. Toughness related to tempering temperature. [15]

The dynamic stress intensity K_{ID} is a parameter that determines the speed at which a crack propagates. Although it is not a single-valued material parameter like K_{IC}, it represents the resistance of the material to dynamic crack growth which is often referred to as dynamic fracture toughness. The dynamic toughness increases significantly as tempering temperatures increasing, but has very little effect on the K_{IC}.

Comprehensive research results show that the impact toughness of the bainite structure is about 3 times higher than that of the conventionally quenched and low temperature tempered martensite structure. The impact toughness of the martensite structure is increased by 30% to 50%, and the fracture toughness is increased by 20% than that of the martensite structure tempered at the same temperature. The wear resistance is lower than the martensite structure of quenching and low temperature tempering, close to or slightly higher than the martensite structure of tempering at the same temperature as shown in Figure 19.[16]

Compared with martensite structure, bainite structure has a lower carbon supersaturation and a small solid solution strengthening effect. Among the factors that affect strengthening, solid solution strengthening makes the toughness drop the most prominent, so bainite has more excellent toughness than martensite. Bainite structure has good toughness, which can hinder the growth of cracks. The flaky ε-carbides which precipitated along the twin plane during tempering of high elastic martensite form a high degree of energy barrier to dislocation movement, causing stress concentration at the end of the crack and reducing toughness.

2.4.4. Fatigue:

Since rolling contact fatigue (RCF) has dominated the failure mode of rolling bearings, the service life of the bearing has been restricted by the RCF life. Researchers have done a lot of work to improve the fatigue performance of bearing steel. The specific methods mainly include improving metallurgical quality and innovating heat treatment processes.

In recent decades, the chemical composition of 100Cr6 bearing steel has not changed much, but its contact fatigue life has been increased by more than 100 times. This is inseparable from the rapid progress and development of bearing steel smelting technology. Reduction of oxygen content and the number and size of metal inclusions has greatly increased the fatigue life of bearing steel. Specifically, the control of metallurgical quality includes three aspects: chemical composition, inclusion and carbide control.

Impurity elements in bearing steel, such as O, S, N, Ti, directly affect the fatigue life and microstructure of the steel. To improve the fatigue life of bearing steel, the content of these impurity elements must be strictly controlled. Researchers have found that the contact fatigue life of bearing steel is inversely proportional to the oxygen content or sulfur content in the steel. Among them, when the oxygen mass fraction in the steel decreases from 0.004% to 0.001%, the contact fatigue life L_{10} of the steel can be increased by 10 times.

Non-metallic inclusions in steel are mainly composed of deoxidation products during refining and precipitates during solidification. In general, non-metallic inclusions are non-metallic elements in steel such as compounds of C, N, S, P, and O, which O and S compounds are the main ones. In the smelting process before the molten steel solidifies, the inclusions in the steel continuously interact with the components in the molten steel, thereby changing its size, composition, shape and position.

Regarding the influence of various non-metallic inclusions in 100Cr6 steel on fatigue performance, researchers believe that fatigue life is inversely proportional to the square root of the size of the inclusions, so clean steel with smaller and fewer non-metallic inclusions has longer fatigue life as shown in the Figure 26, at the same time, as the depth of inclusions increases, fatigue

life also shows an increasing trend.

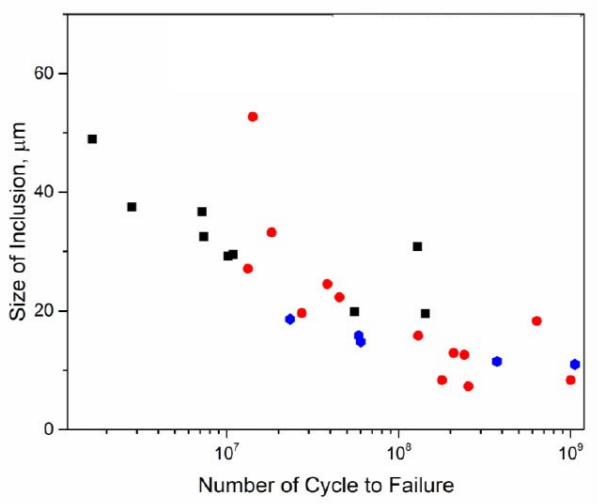

Figure 26. The relationship between inclusion size and fatigue life (N_f). [17]

Common non-metallic inclusions in bearing steel mainly include sulfides, Al_2O_3 inclusions, silicate inclusions and nitrides. Figure 27(a) shows a typical oxide inclusion observed by the metallographic method. The Ti and N elements in bearing steel usually exist in the steel in the form of TiN inclusions as shown in Figure 27(b). Such inclusions have sharp edges and corners, and stress concentration is easily formed at the edges and corners, which have a greater impact on the fatigue life of the steel.

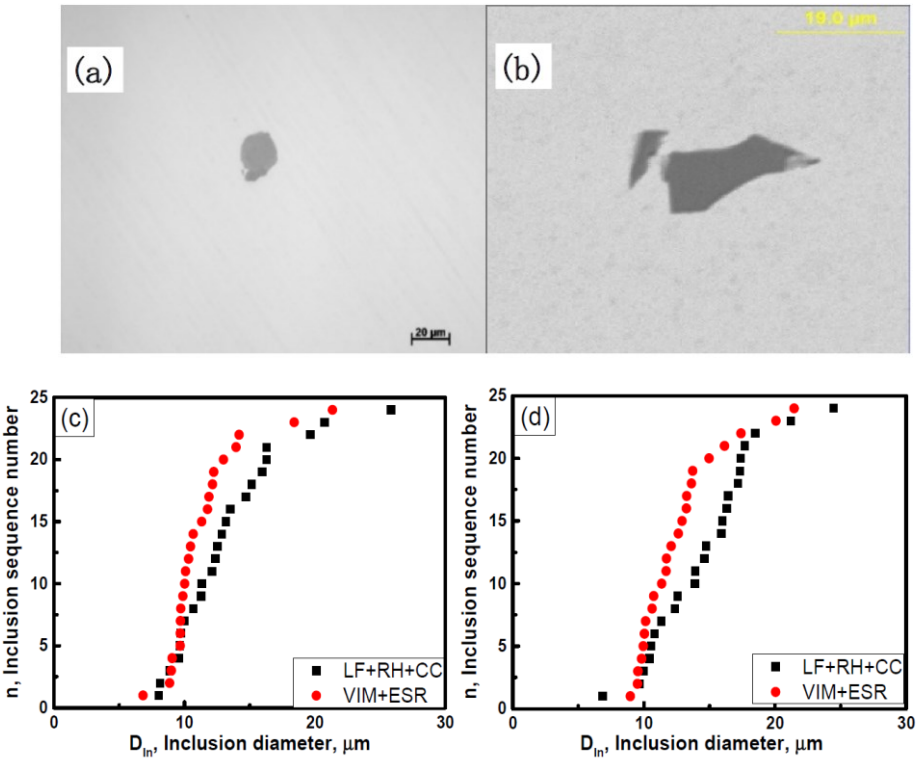

Figure 27. (a) Typical oxide inclusions (CaO-MgO-Al_2O_3) examined by the metallographic method, (b) typical TiN inclusions exhibited by the SEM, (c), (d) the largest inclusions of LF + RH and VIM + ESR in descending order of the inclusion size. [18]

The non-metallic inclusions of LF + RH steel are mainly oxide inclusions, while that of ESR steel is mainly oxide inclusions and titanium nitride inclusions, both of which belong to brittle inclusions and are extremely unfavorable to fatigue life. The size of the bearing steel fabricated by LF + RH is clearly larger than that of the bearing steel fabricated by VIM + VAR.

In the process of refining bearing steel using new technologies such as ESR, it is necessary to grasp the composition of the slag system and the setting of the solidification parameters, so that the content and size of TiN inclusions in the bearing steel can be controlled, and the cleanliness of the bearing steel can be achieved.

Comparing with the metallographic method, the SEM is very useful for revealing the difference in the inclusions in terms of their size and distribution. However, both the metallographic method and SEM underestimate the size of the maximum inclusions, the rotated bending fatigue method successfully examined the maximum inclusion size. Through rotated bending fatigue experiment, we could get the maximum inclusion size and the S–N curve as shown in Figure 28. At room temperature, the S-N curve of 100Cr6 bearing steel has the characteristics of a stress plateau, which is stepped. It is easy to find that the electroslag steel has longer life under the same stress condition. The size range of inclusions observed at the fracture of electroslag steel during the rotary bending experiment is much smaller than that of the degassed steel.

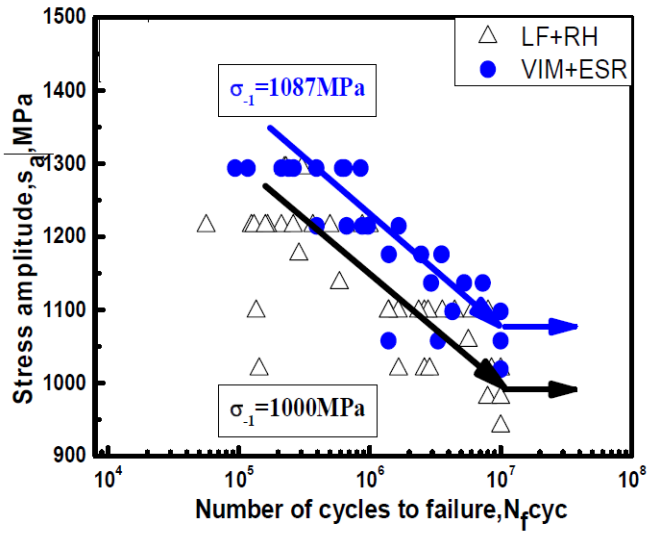

Figure 28. S-N curves of LF+RH steel and VIM+ESR steel. [18]

The distribution of the maximum inclusions could not be described based on the inclusion size by the classical Weibull distribution which could give the accuracy of the measurement of the inclusion size, whereas the inverse Weibull distribution of the maximum inclusion size could be well applied based on the inverse value of the maximum inclusions.

In addition, the rotated bending fatigue life is not only determined by the loading stress amplitude but also by the maximum inclusion size. The relationship between the rotated bending fatigue cycle number, the loading stress amplitude, and the maximum inclusion size was established and shown to accurately predict the dependence among these three parameters.

Researchers generally believe that the failures caused by contact fatigue can be divided into two categories: failures caused by the surface and failures caused by the subsurface. It is found that

high contact stress increases the probability of surface failure, which makes the steel fail at a relatively low number of cycles, and fatigue at a higher number of cycles (greater than 10^7) is more affected by the subsurface microstructure. Large, non-metallic inclusions can become stress concentration and crack initiation. In fact, for high cycle cycles (greater than 10^5), almost all cracks originate from non-metallic inclusions.

Some scholars believe that the interface conditions between the matrix and the inclusions have a great influence on the control of crack nucleation and propagation during the RCF process. The strength and adhesion of the interface are the same as the size of inclusions, which are important factors that determine the nucleation of cracks. Therefore, they put forward the concept of "inclusion engineering", hoping to achieve a good combination of matrix and inclusions through processing.

In the sample with crack initiation caused by internal inclusions, the fracture surface will show a "fish-eye" morphological feature as shown in Figure 29, and the "fish-eye" contains a bright white coarse and fine-grained area (FGA) attached to the surrounding inclusions. Although the fisheye is only a few hundred microns and the FGA is only a few tens of microns, as a characteristic area of crack initiation, it controls 95% of the fatigue life.

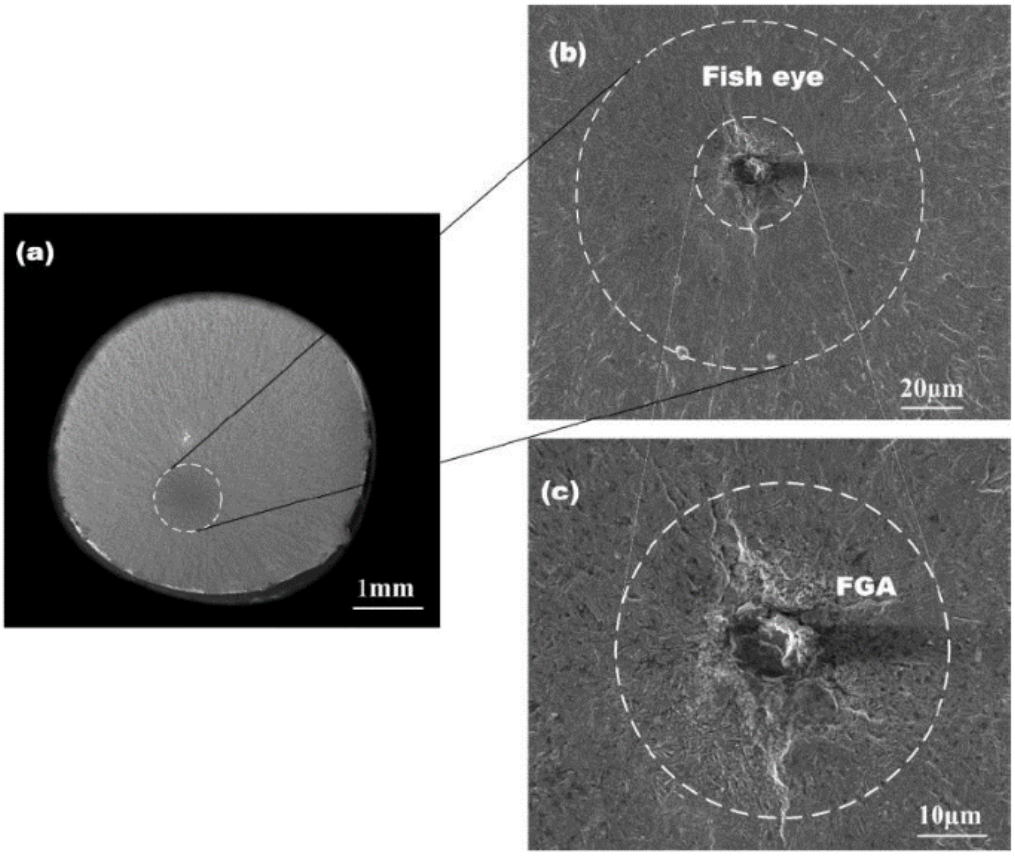

Figure 29. Very high cycle fatigue fracture fisheye morphology. [19]

Some researchers believe that the FGA zone is produced because of the accumulation of "hydrogen" and proposed a "hydrogen embrittlement model" as shown in Figure 30. The hydrogen captured by non-metallic inclusions in the smelting process overflows during heat treatment and causes brittle failure under the action of alternating loads. When the first stage of crack propagation is completed, the effect of hydrogen basically disappears, and smooth fatigue cracks usually appear on the fracture surface.

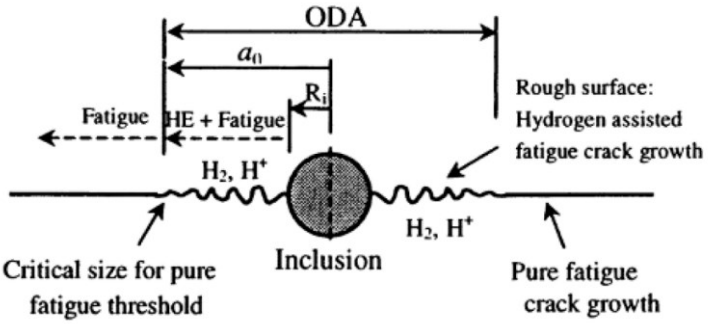

Figure 30. The mechanism of hydrogen assisted crack growth. [20]

During the formation of FGA, the local plastic deformation is extremely uneven. In addition to the inhomogeneous structure at the inclusions, there will be serious incompatibility of plastic strain, which may lead to corresponding crack initiation. Therefore, it can be considered that the initiation of cracks is the result of the incompatibility of plastic strain during the formation of FGA, while the formation of FGA is mainly caused by the process of grain refinement in the accumulation process of plastic strain, which is also called the quasi-dynamic recrystallization process (as shown in Figure 31.). As a characteristic area of crack initiation, FGA's formation mechanism has always been the focus of researchers' attention. Although a variety of mechanism models have been proposed, they all have counterexamples that cannot be explained, and more models need to be developed.

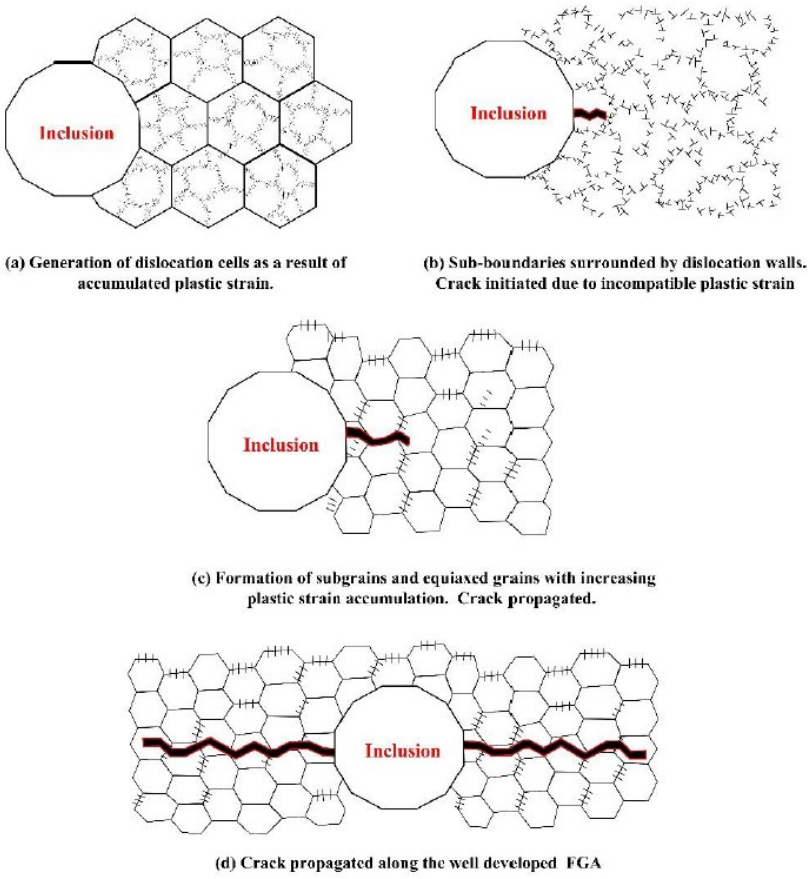

Figure 31. Schematic illustration of the FGA formation. [19]

In short, the non-metallic inclusions in the bearing steel reduce the fatigue performance of the steel. By improving the smelting process to reduce the number of non-metallic inclusions in the steel, reduce the size of the inclusions, and even the distribution of the inclusions can greatly improve the contact fatigue life of the bearing steel.

Although more research has been conducted on the influence of non-metallic inclusions in bearing steel on contact fatigue life, the influence of carbides and retained austenite on contact fatigue life cannot be ignored.

Through high-temperature diffusion, controlled rolling and controlled cooling, spheroidizing annealing and other processes of 100Cr6 bearing steel, the band-like distribution, network-like distribution of carbides in the steel, and the phenomenon of carbide liquefaction have been significantly controlled and improved, so as to achieve higher contact fatigue life. In addition, the uniformity of carbide distribution also affects the contact fatigue life of bearing steel. The uniformity of carbide distribution ultimately depends on the solidification structure, so the control of the solidification process of molten steel is particularly critical.

Retained austenite is a soft metastable phase. Under certain conditions (such as tempering, natural aging or the use of parts), its instability will lead to decompose into martensite or bainite. The consequence of decomposition is that the hardness of the parts increases, the toughness decreases and the size changes during storage or use, which affect the normal operation of the parts. Therefore, for bearings with high dimensional accuracy requirements, in order to ensure dimensional stability, it is generally desirable to have retained austenite as little as possible, such as supplementary water cooling or deep cryogenic treatment after quenching, and higher temperature tempering. However, retained austenite can improve toughness and crack growth resistance. Under certain conditions, the retained austenite on the surface of the workpiece can also reduce contact stress concentration and increase the contact fatigue life of the bearing. In this case, certain measures are taken in the process and material composition to have a certain amount of retained austenite and improve its stability, such as adding austenite stabilizing elements Mn for stabilization or adding Si. Si is actually not an austenite stabilizing element, but it might have an indirect effect by avoiding carbides and keeping C in the austenite. [21]

Generally, the contact fatigue life of bainite structure is lower than that of quenched low temperature tempered martensite structure, and close to the same temperature tempered martensite structure. However, under poor lubrication conditions (such as coal slurry or water), The contact fatigue life of the bainite structure shows obvious advantages, and it has a much higher contact fatigue life than the low temperature tempered martensite structure. The bainite quenching heating equipment basically uses a protective atmosphere or a controllable atmosphere, which can ensure no decarburization, or carry out carburization or carburization as needed, so that the machining allowance after heat treatment can be greatly reduced.

The use of some innovative heat treatment processes can also greatly increase the contact fatigue life of 100Cr6 bearing steel. The effect of double-stage quenching on the contact fatigue life of ultra-clean 100Cr6 bearing steel was studied. Figure 32 shows the microstructure of 100Cr6 bearing steel after single-stage quenching and double-stage quenching. It can be seen from Figure 31 that the two-stage quenching greatly refines the size of grains and carbides and improves the distribution of carbides. This optimization of the microstructure not only improves the strength and hardness, but also improves the contact fatigue life. Figure 33 shows the change of contact fatigue

life under different heat treatment conditions. It can be seen from Figure 32 that the double-stage quenching heat treatment increases the contact fatigue life of the bearing steel by 5 times. In addition, 100Cr6 bearing steel was carburized, which increased the surface hardness and retained austenite content, and increased the contact fatigue life to 10 times. In addition, 100Cr6 bearing steel was carburized by researchers, which increased the surface hardness and retained austenite content, and increased the contact fatigue life to 10 times the original, as shown in Figure 34.

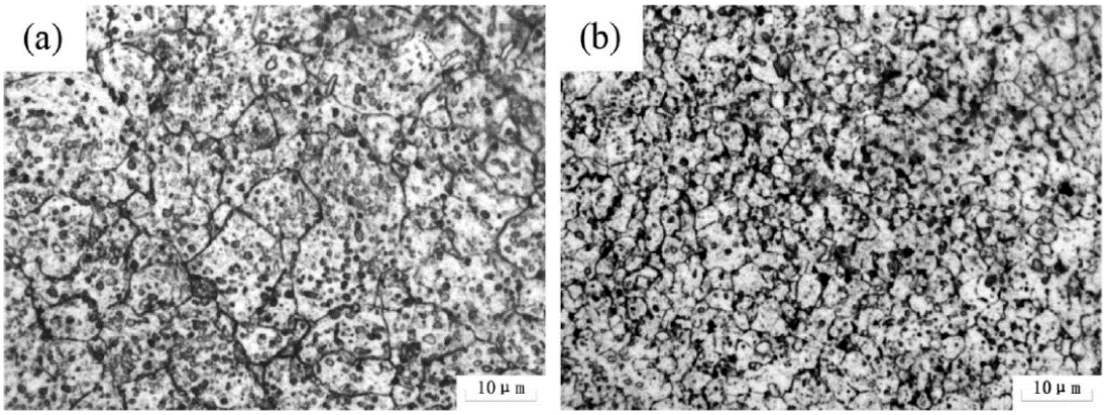

Figure 32. Microstructures of 100Cr6 treated by different heat treatment. (a) Single quenching and tempering and (b) Double quenching and tempering. [22]

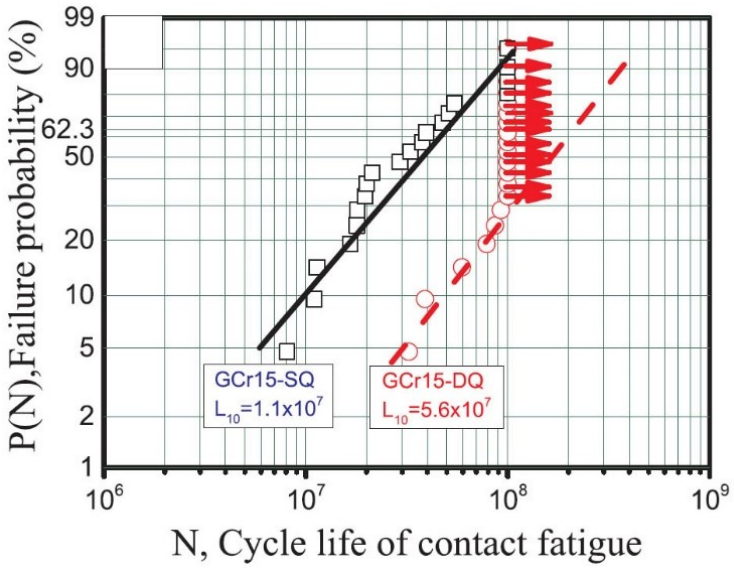

Figure 33. Weibull distribution of the RCF-life in 100Cr6 subjected to different heat treatments. [23]

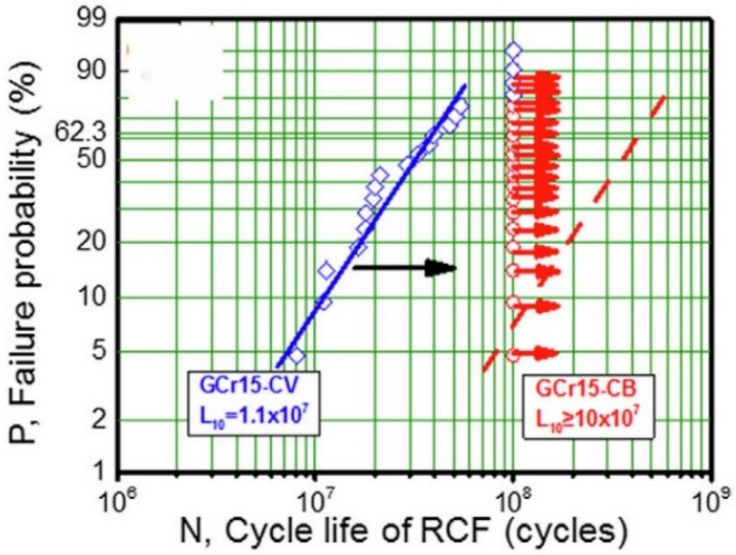

Figure 34. Effect of carburizing treatment on RCF life of 100Cr6. [23]

2.5. Discussion:

Bearing steel is an important mechanical equipment manufacturing material which plays a vital role in the performance of bearings. In order to meet the long-life and high-reliability requirements of high-end bearings, bearing steel in the future should continuously improve the metallurgical quality through advanced smelting processes such as VD and inclusion homogenization.

Improvement of heat treatment is another key factor to achieve long life of bearing steel. Surface modification heat treatment technologies such as carburizing, nitriding, carbonitriding and special heat treatments such as double stage quenching are important directions for future research.

The research and development of new bearing steels should focus on excellent comprehensive performance, and the innovation of alloy system and the alloy design are also the key points in R&D.

3. Medium-carbon engineering steels

The earliest mechanical engineering steel is AISI 4130 (United States grade). In order to obtain better strength and toughness, it adopts high temperature quenching and tempering process, however, its strength is not so high. In 1950, on the basis of AISI 4130, the carbon content was increased to 0.43%, and a certain amount of nickel was added to improve the hardenability and toughness of the steel, hence a new steel of nickel, molybdenum, and chromium with medium carbon content, AISI 4340 steel, was developed which is included in the standard ASTM-A29/A29M–04 as shown in Table 3.

Grade Designation	Heat Chemical Ranges and Limits, %							
	Carbon	Manganese	Phosphorus, max	Sulfur, max	Silicon[A]	Nickel	Chromium	Molybdenum
4028	0.25–0.30	0.70–0.90	0.035	0.035–0.050	0.15 to 0.35	...	...	0.20–0.30
4032	0.30–0.35	0.70–0.90	0.035	0.040	0.15 to 0.35	...	...	0.20–0.30
4037	0.35–0.40	0.70–0.90	0.035	0.040	0.15 to 0.35	...	...	0.20–0.30
4042	0.40–0.45	0.70–0.90	0.035	0.040	0.15 to 0.35	...	...	0.20–0.30
4047	0.45–0.50	0.70–0.90	0.035	0.040	0.15 to 0.35	...	...	0.20–0.30
4130	0.28–0.33	0.40–0.60	0.035	0.040	0.15 to 0.35	...	0.80–1.10	0.15–0.25
4135	0.33–0.38	0.70–0.90	0.035	0.040	0.15 to 0.35	...	0.80–1.10	0.15–0.25
4137	0.35–0.40	0.70–0.90	0.035	0.040	0.15 to 0.35	...	0.80–1.10	0.15–0.25
4140	0.38–0.43	0.75–1.00	0.035	0.040	0.15 to 0.35	...	0.80–1.10	0.15–0.25
4142	0.40–0.45	0.75–1.00	0.035	0.040	0.15 to 0.35	...	0.80–1.10	0.15–0.25
4145	0.43–0.48	0.75–1.00	0.035	0.040	0.15 to 0.35	...	0.80–1.10	0.15–0.25
4147	0.45–0.50	0.75–1.00	0.035	0.040	0.15 to 0.35	...	0.80–1.10	0.15–0.25
4150	0.48–0.53	0.75–1.00	0.035	0.040	0.15 to 0.35	...	0.80–1.10	0.15–0.25
4340	0.38–0.43	0.60–0.80	0.035	0.040	0.15 to 0.35	1.65–2.00	0.70–0.90	0.20–0.30
E4340	0.38–0.43	0.65–0.85	0.025	0.025	0.15 to 0.35	1.65–2.00	0.70–0.90	0.20–0.30

Table 3. Steel grades and chemical composition of 40 series medium carbon steel. [24]

AISI 4340 steel is a typical representative of low alloy ultra-high strength steel. The tempering temperature of this steel is generally 200℃ or slightly lower than 200℃. Because of its excellent comprehensive mechanical properties, it has been widely used in manufacturing of key components in engineering. It is mainly applied in the manufacture of power transmission gears, aircraft landing gear, shafts and automobile industries to manufacture gears, shafts, pins, bearings, spindles, couplings, chucks and cams which requires tight geometric tolerances, long service life and high surface quality. As a structural material, AISI 4340 steel must meet the static strength design requirements of components. In addition, it is often subjected to cyclic loads during service. Therefore, its basic mechanical properties and fatigue properties are the key indicators affecting its engineering application.

In 1952, the United States International Nickel Company developed 300M steel. 300M steel is developed on the basis of AISI 4340 steel by increasing the silicon content and adding 0.05% to 0.10% vanadium, which improves the strength while avoiding low temperature tempering brittleness. 300M steel has been used in key aircraft components such as aircraft landing gear since 1966. So far, almost all civil aircraft use 300M steel in large quantities.

The United States developed D6AC in the early 1960s. It is a low alloy ultra-high strength steel improved by increasing molybdenum, carbon and chromium content and reducing nickel content on the basis of AISI 4340 steel and adding about 0.08% vanadium. The hardenability is better than that of AISI 4340 steel, and it does not show temper brittleness at high temperatures, and it can maintain high strength at high temperatures. It is widely used in the manufacture of tactical and strategic missile engine casings and aircraft structural parts. [25] The medium carbon engineering steels studied in this section is as shown in Table 4.

	C	Si	Mn	Cr	Ni	Mo	V
AISI4340	0.38 ~ 0.43	0.20 ~ 0.35	0.60 ~ 0.80	0.70 ~ 0.90	1.65 ~ 2.00	0.20 ~ 0.30	—
300M	0.41 ~ 0.46	1.45 ~ 1.80	0.65 ~ 0.90	0.65 ~ 0.95	1.60 ~ 2.00	0.30 ~ 0.40	≥0.05
D6AC	0.45	0.22	0.60 ~ 0.90	0.80 ~ 1.05	0.40 ~ 0.70	0.90 ~ 1.10	0.05 ~ 0.10

Table 4. Steel grades and chemical composition of the medium carbon engineering steels studied in this section. [26]

3.1. Machining processing of engineering steels:

The AISI 4340 is a highly commercialized medium carbon low alloy steel in the hard-to-cut material category. Because of its high hardness (45~60 HRC), hard turning has become a popular alternative to conventional grinding for machining AISI 4340 in recent decades.

Most researchers have used CNC lathe machines during their experiments as shown in Figure 35. This is because the use of CNC machines provides more precision products compared to the conventional machine tools.

Figure 35. The CNC lathe machine used in the experiments. [27]

Hardened steel is typically machined under dry conditions in hard turning operations, which could improve surface quality and extend tool life. However, machining in dry conditions generates a large amount of heat at the tool-work specimen interface due to friction between the tool and the work material surface, which has a significant impact on the metallurgical properties of the work surface, as well as the formation of a white layer and the distribution of tensile residual stress on the workpiece.

As a result, the use of coolant is critical for reducing frictional force and competent heat removal from the machining zone. The coolant is directly applied over the machining zone during the MQL (Minimum Quantity Lubrication) technique, allowing for easy heat removal from the tool-workpiece interface. MQL technique not only removes the heat generated during machining, but also provides better machining performance than dry machining.

The surface topography of the workpiece is altered as a result of heat generation in the

machining zone. Cryogenic cooling is being used to prevent these phenomena. Because cryogenic cooling produces very little heat at the machining zone, the change in microstructure is minimal compared to other cooling environments. Among other cooling environments, using cryogenic cooling with the MQL environment provides longer tool life and the best surface finish.

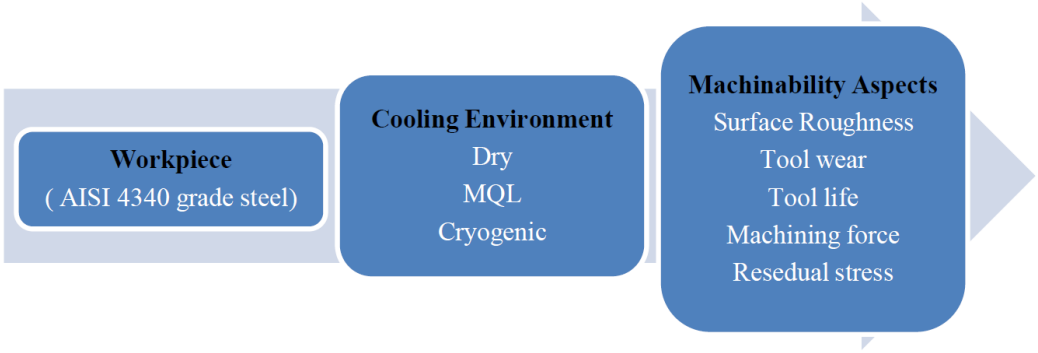

Figure 36. Schematic view of machining aspects. [28]

In addition, coated tool provides lower machining temperature, better surface finish and longer tool life compared to uncoated tool.

We can evaluate machining performances through the study of tool life, tool wear, surface roughness, machining force and residual stress as shown in Figure 36.

Future research should be linked to environmentally friendly methods for improving machining performance under industry-implemented cutting conditions. Machining AISI 4340 steels in a MQL Environment results in cleaner manufacturing, reduces environmental impact, and further increases sustainability.

3.2. Heat treatment and microstructures of engineering steels:

3.2.1. Annealing(spheroidization) of engineering steels:

The AISI 4340 steel is easy to machine and preferably has a coarse lamellar pearlite structure or a spheroidized structure.

AISI 4340 steel should be annealed at a nominal temperature of 830ºC, cooled to 730ºC, and furnace cooled at a rate of 11ºC per hour to 610ºC, and then air cooled to obtain a pearlitic structure on certain parts for machining. Full annealing is a time-consuming process involving slow cooling over the entire temperature range from the austenitizing temperature to well below the transformation completion temperature.

To obtain a spheroidized structure in AISI 4340 steel involves austenitizing at 750°C, furnace cooling to 705°C and then cooling to 565°C at a rate of 3°C per hour. This structure would most likely be easier to machine than the coarse lamellar pearlite structure obtained through the full annealing process. [29]

3.2.2. Normalizing of engineering steels:

This process is defined as heating the steel to a temperature above the ferrite to austenite transformation temperature, and then cooling it in air to a temperature well below the transformation temperature. This treatment might be used on forged products as a conditioning treatment before final heat treatment. Normalizing also helps to refine the structure of forgings that might have cooled evenly during the forging operation. The nominal normalizing temperature for AISI 4340 steel is 815ºC, but production experience might need a temperature 10ºC above or below this temperature. The upper limit on the normalizing temperatures is used when forgings are normalized prior to carburizing or quenching and tempering. The lower temperature range is used when normalizing is the final heat treatment.

3.2.3. Quenching and tempering of engineering steels:

The purpose of heat treatment is to obtain an excellent microstructure to exert the excellent potential of the material. In general, quenching and tempering are the accepted methods for producing strengthening in medium carbon engineering steels mainly due to the fine dispersed precipitation of alloy carbides during tempering.

3.2.3.1. Structure of the as-quenched martensite of AISI 4340 steel:

The morphology of martensite is shown in Figure 37 OM (optical microscope) and TEM (electron transmission microscope), consisting mainly of dislocated martensite laths. Isolated examples of internal twins could be also seen in some plates. The thickness of the twinned wafer layer is between 30 and 50 nm. Typically, laths about 100~200 nm wide are separated by low angle boundaries and each martensite lath consists of many dislocation cells. Its density is reported to be as high as 10^{12}cm^2. [30]

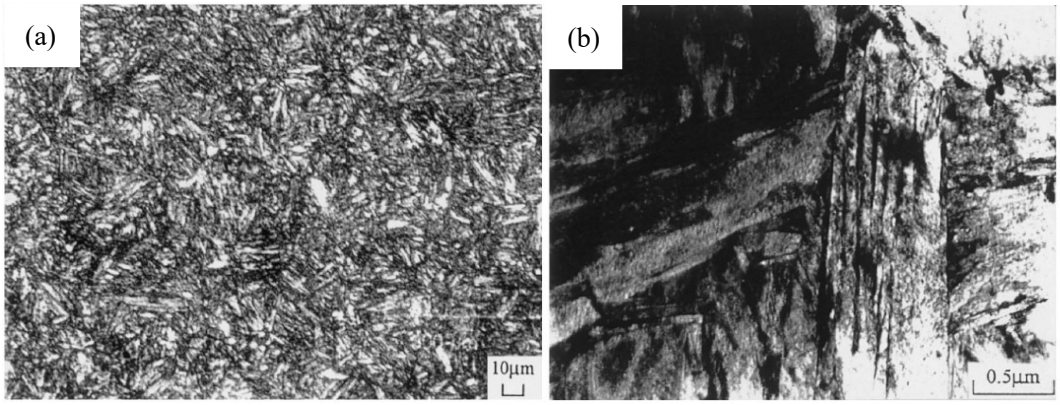

Figure 37. (a) OM and (b) TEM images of the as-quenched martensite of the AISI 4340 steel. [31]

Since M_s of AISI 4340 steel is above room temperature, it exhibits autotempering behavior in the as-quenched structure, allowing carbon atoms to redistribute themselves for some brief periods in quenched martensite. Because the stress fields in lath martensite are located around individual dislocations and cell walls, some defect interstitial lattice sites close to these locations

provide lower carbon energy than normal sites. When comparing the carbon in an interstitial site near a dislocation with that in a 'normal' one, such migration could be detected either by metallography or by carbon's smaller contribution to electrical resistivity or internal friction. Autotempered precipitation are not present in any twinned plates but only resolved in dislocated laths and untwinned plates. This strongly suggests that dislocated laths and untwinned plates form first near M_s, while twinned plates form at lower temperatures, i.e., near M_f.

In addition, no matter whether the AISI 4340 steel is fast quenched or slow quenched, there is only a very little carbides near the prior austenite grain boundaries in the steel, so it is not sensitive to the quenching cooling rate. [32]

3.2.3.2. The effect of austenitizing temperature on the structure of AISI 4340 steel:

In the study of AISI 4340 steel, it was found that the amount of retained austenite in the structure after high-temperature austenitisation is higher than that of conventional temperature austenitisation and quenching. The austenitic grain size gradually increased with austenitizing temperature as shown in Table 5. OM also revealed that the martensitic plate size increases as austenitic grain size increases.

Effect of Austenitizing Treatment on Austenitic Grain Size

Austenitizing Temperature, K (°F)	1144 (1600)	1255 (1800)	1366 (2000)	1477 (2200)
ASTM Grain Size	8	5	3½	1

Table 5. Effect austenitizing treatment on austenitic grain size. [33]

OM in Figure 38(a) and (b) revealed that the step quenched (1200 to 870°C/oil) heat treatment's prior austenite grain size was an order of magnitude larger than the grain size attained with a commercial heat treatment (870°C/oi1). The coarse-grained material had an average grain size of ASTM 0~1, while the specimens austenitized at 870°C had an average grain size of ASTM 7~8. For both heat treatments, OM revealed no ferrite or upper bainite.

Both heat treatments (1200 to 870°C/oil and 870°C/oil) resulted in mixed microstructures containing autotempered martensite, untempered martensite, and small amounts of lower bainite, according to TEM shown in Figure 38(c) and (d). Large lenticular plates and bundles or packets of fine parallel laths were found among the martensite. The large martensite plates would often extend across an entire grain in the fine-grained structure, but this was never seen in the coarse-grained structure. The large plates in the coarse-grained structure originated from prior austenite grain boundaries and only protruded partially across the grain.

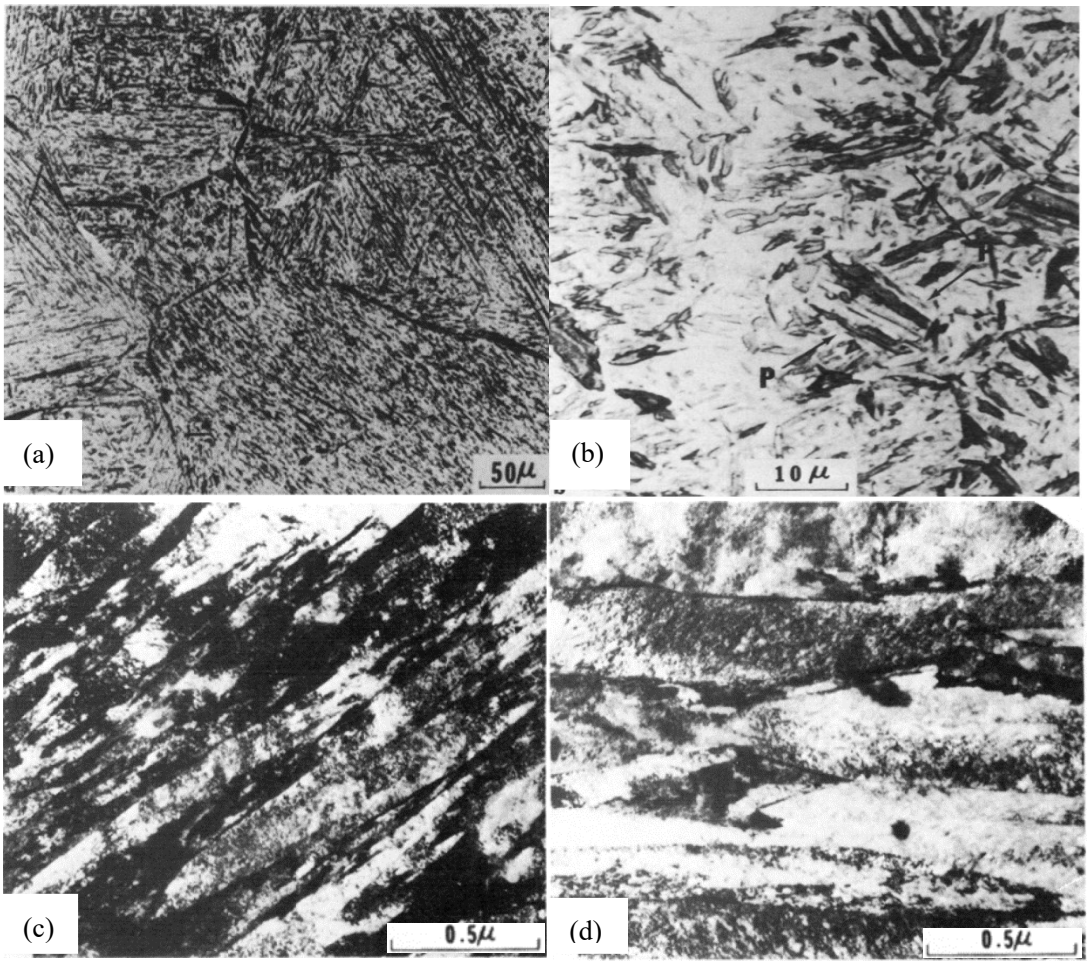

Figure 38. (a) and (b), OM micrograph, illustrate these aspects of grain size and martensite morphology at 1200°C and 870°C. (c) and (d), TEM at 1200°C and 870°C. [34]

The martensite exhibited a substructure which varied with the two heat treatments. Use of the high temperature step austenitizing treatment resulted in the elimination of twinned martensite plates. Meanwhile, with the increase of austenitizing temperature, the amount of twinned martensite in the microstructure decreases. All the plate martensite heat treated at the higher austenitizing temperature was dislocated and exhibited extensive autotempering.

3.2.3.3. The effect of tempering temperature on the structure of AISI 4340 steel:

Tempering, a process of heating martensite to high temperatures to make it more ductile, involves a number of basic processes, including carbide precipitation, decomposition of retained austenite and the recovery and recrystallization of martensite structure.

When the studied AISI 4340 steel [31] was tempered at 200°C for 2 h, ε-carbide ($Fe_{2,3}C$, HCP) precipitated at this temperature. This is different from the found martensitic high carbon steel, the carbide precipitated in the first stage of tempering is η-carbide or η-Fe_2C. Figure 39(b) shows the microstructure at this temperature, where the high-density dislocation tangles and smaller dislocation units are the two primary features in the dislocation structures. In addition, ε-carbide

precipitates could be found in lath martensite.

Dendritic carbide (Fe_3C, orthorhombic) forms after 2 h of tempering at 300°C, and its initial morphology in martensite is platelike, as shown in Figure 39(c). At low temperatures, the nucleated site of the carbide is frequently martensite lath boundaries, while at higher temperatures is ferrite grain boundaries.

When the quenched structure is tempered at high temperature for example, 650°C for 2 h, the microstructure consists of equiaxed ferrite grains and various small rod-like carbides which are distributed in specific directions in the ferrite matrix, as shown in Figure 39(d). In addition, the dislocation cell boundaries and the random dislocations that exist between these cell boundaries vanish as a fine cellular structure emerges.

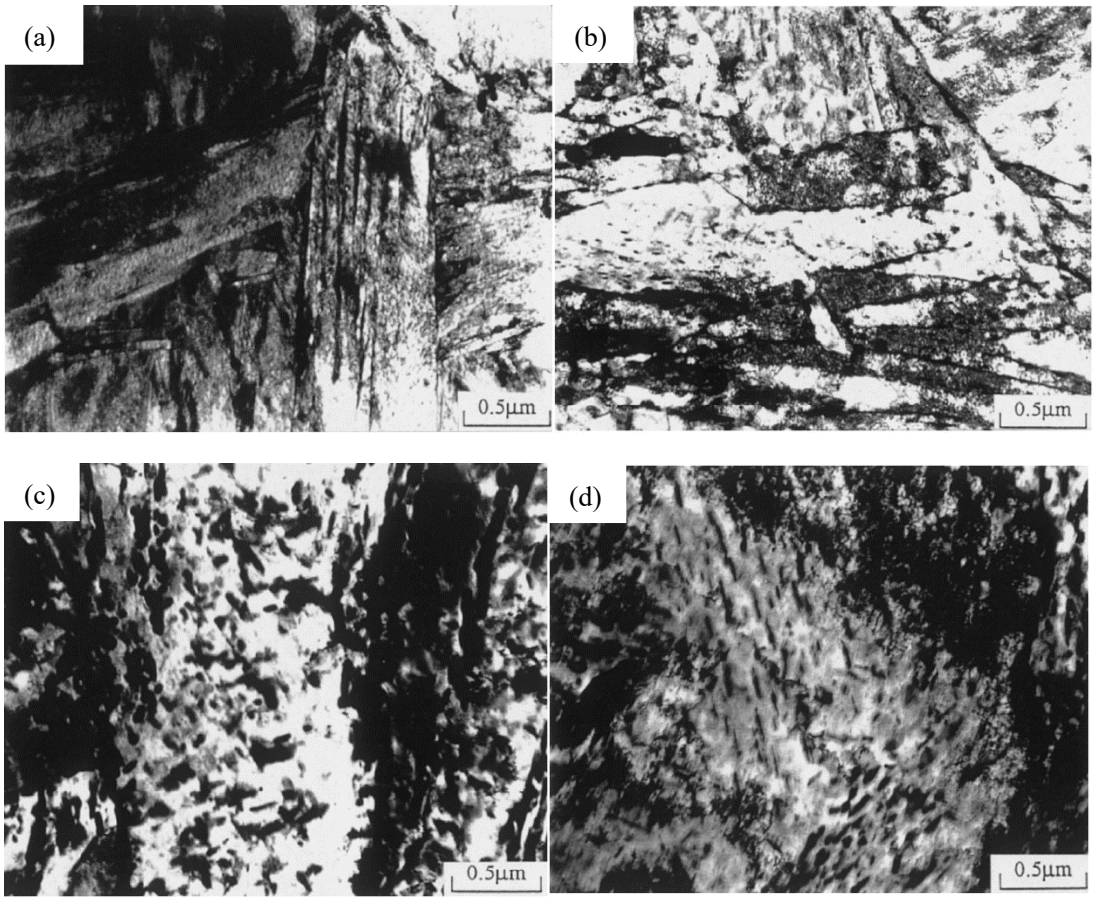

Figure 39. TEM images of a specimen (a) quenched at 850°C for 30 min in oil, (b) tempered at 200°C for 2 h, (c) tempered at 300°C for 2 h, (d) tempered at 650°C for 2 h. [31]

The TEM in Figure 40 shows that some laths grow to larger ones after tempered at 200°C for 48 h. The growth of the lath should be controlled by two operating mechanisms which are the movement of lath boundaries and the elimination of lath boundaries as a result of the movement and annihilation of dislocations at the boundaries. High density dislocations with precipitated carbides are present in most of the laths under this tempering condition, but only few could be seen. These carbides immobilize the dislocations, preventing them from forming low energy dislocation arrays like those found at small-angle grain boundaries.

Similar dendritic carbide structures could also be seen in the case tempered at 300°C for 48 h. The precipitated carbide growth with tempering holding time is also visible.

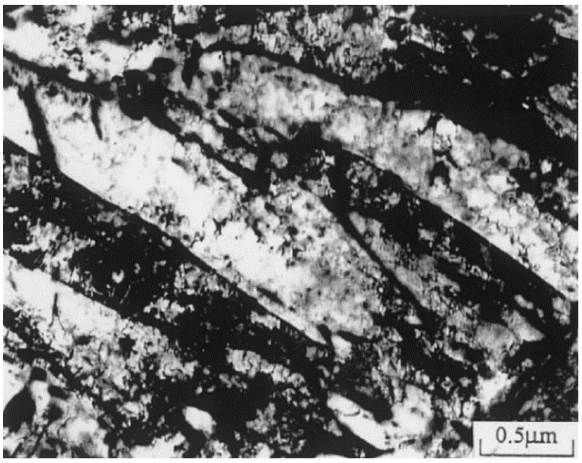

Figure 40. TEM image of a specimen quenched at 850°C for 30 min in oil and tempered at 200°C for 48 h. [31]

The AISI 4340 steel has a ferrite matrix with carbides scattered throughout it as shown in Figure 41 after being tempered at 650°C for 48 h, at such a high temperature and for such a long time. The only kinetic processes after recrystallization are carbide particle and ferrite grain growth. Recrystallisation occurs at this tempering temperature, resulting in a rapid decrease in dislocation density and internal strains.

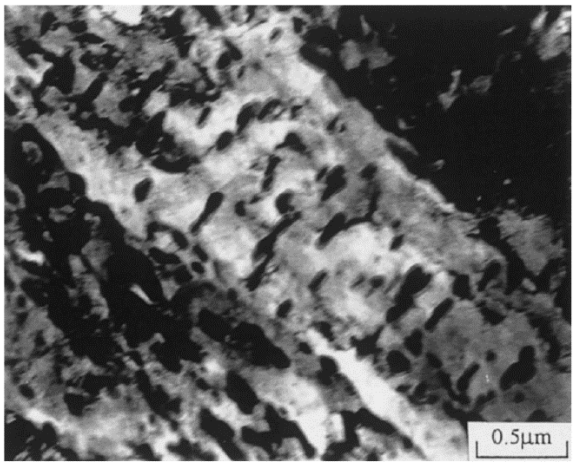

Figure 41. TEM image of a specimen quenched at 850°C for 30 min in oil and tempered at 650°C for 48 h. [31]

It is worth noticing that when the quenched structure is tempered at a high temperature, e.g., 650°C, the reaction of Fe_3C to Cr_7C_3 occurs, resulting in different types of carbide as shown in Figure 41. The Fe_3C does not directly transform into Cr_7C_3, but actually dissolves in the ferrite matrix, while Cr_7C_3 precipitates grow elsewhere. At low temperatures, Fe_3C has a needle-like structure as shown in Figure 39(b), while Cr_7C_3 has a spheroidal structure at 650°C as shown in Figure 41. To reduce surface energy, Fe_3C appears to have taken on both a plate-like and a spheroidal shape. As a result, Cr_7C_3 is most likely formed when Fe_3C reacts with the matrix.

3.2.3.4. The effect of austenitizing temperature on the structure of 300M steel:

TEM of the as-quenched structure of 300M steel revealed several significant features: The 300M steel which is quenched at austenitizing temperature of 870°C contains evenly distributed undissolved particles, however, undissolved particles are not observed in the specimens which is quenched at austenitizing temperature over 870°C.

The undissolved particles vary in size with diameters between 100 and 200nm. The structure was identified as FCC by electron diffraction with a lattice parameter of 1.05nm. Figure 42 shows a specimen austenitized at 870°C in the untempered condition which these undissolved particles is visible. They exist inside the plates, laths and also at their boundaries. Such particles are not found in specimens austenitized at 982°C and above do.

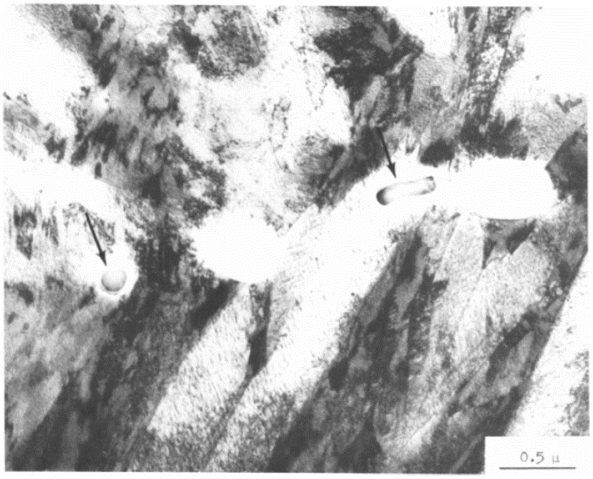

Figure 42. 300M steel specimen austenitized at 870°C and quenched. The presence of undissolved particles is shown (indicated by arrows). [33]

In all the as-quenched structures the martensitic substructure consists mainly of plates and laths with few partially twinned plates. The extent of twinning is low (less than 5% of the martensitic plates were twinned). The dissolution of the above-mentioned particles in the specimens austenitized over 870°C is not accompanied by any observable change in martensitic substructure.

Autotempering is also extensive for 300M steel with almost every plate and lath exhibiting autotempered ε-carbides. They are very fine and could be observed in Figure 43.

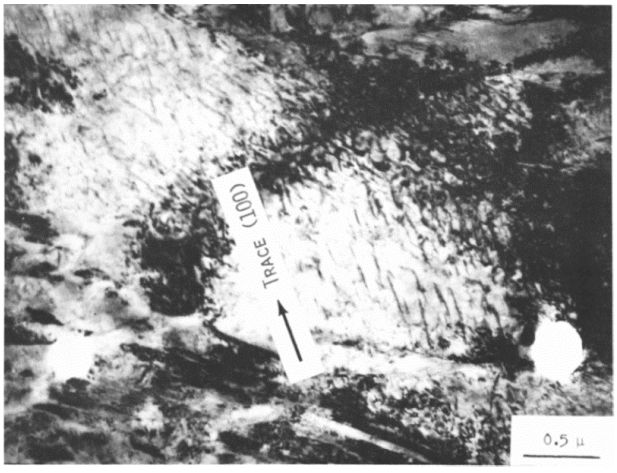

Figure 43. 300M steel specimen austenitized at 870°C and quenched. Autotempered ε-carbide in a martensitic plate is shown. [33]

In addition, the retained austenite in the as-quenched martensite occurs in such low amount that conventional X-ray diffraction techniques barely revealed its presence. The austenite, in most cases, outlines the lath and plate boundaries and in some instances occurs in thin platelets. Figure 44 shows a specimen austenitized and quenched from 870°C.

It was found by extensive observation that the extent of the inter-lath and plate austenite is quite comparable in the specimens austenitized at 870°C and the specimens austenitized over 870°C, and no significant differences in the quantity of retained austenite could be detected.

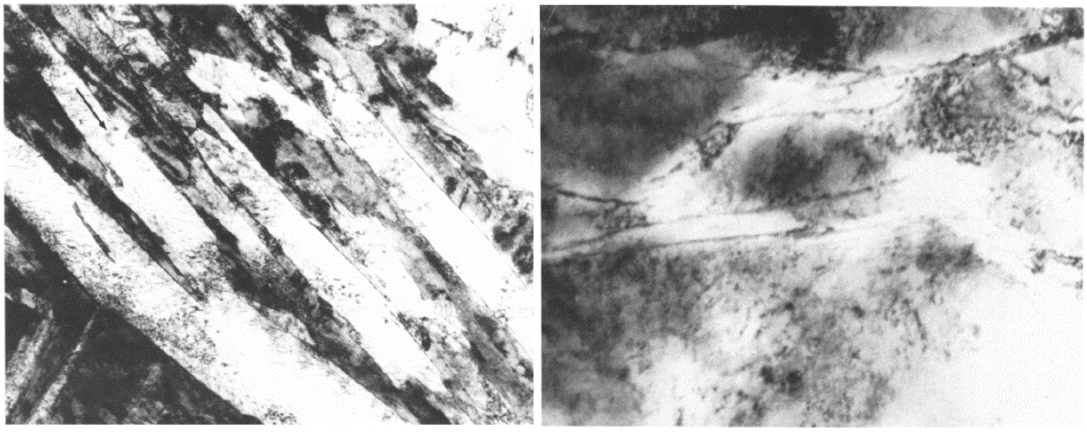

Figure 44. 300M steel specimen austenitized and quenched from 870°C and double tempered at 427°C. Autotempering is evident in the laths. [33]

According to some recent studies, using a higher austenitizing temperature followed by oil quenching but no subsequent tempering in some commercial steels results in high toughness. The as-quenched structure is uniformly martensitic with small amounts of austenite at the lath and plate boundaries, according to OM and TEM results. Since all of the as-quenched fracture specimens failed transgranularly, the austenite at the lath and plate boundaries could not mitigate brittle failure in the as-quenched condition.

3.2.3.5. The effect of tempering temperature on the structure of 300M steel:

The tempered structure is tempered martensite. A small amount of film-like retained austenite is dispersed in the martensite ε-carbide martensite lath, and there are no undissolved particles observed.

All of the specimens that were tempered at 200°C and 316°C have ε-carbide precipitates that are coarser than those seen in the as-quenched structure. Retained austenite is still present at the boundaries and is clearly observed in the structure. The cementite particles are partially spheroidized after tempering at 427°C. Retained austenite at the lath boundaries decomposes to cementite and, presumably, ferrite leaving a network of lath boundary carbides. The specimen austenitized at 870°C and tempered at 427°C is shown in Figure 45, where distinct cementite precipitates can be seen at the lath boundaries. In addition, isolated occurrences of retained austenite could be discovered. The cementite was spheroidized during the 538°C tempering process, and these spheroids could be seen matrix and the boundaries as shown in Figure 45. The retained austenite is totally absent.

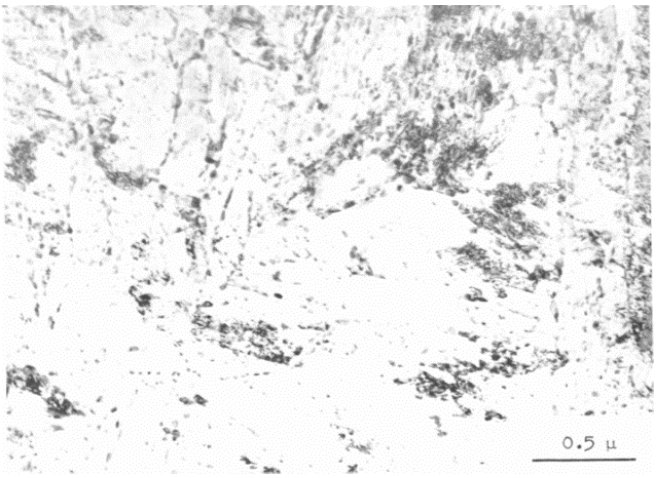

Figure 45. 300M steel specimen austenitized at 1204℃ and double tempered at 538℃ which spheroidized cementite precipitates at the lath and plate boundaries are shown. [33]

3.3. Mechanical properties of engineering steels:

3.3.1. Hardness:

In recent years, due to the strict requirements to obtain high quality products in the industry, mainly in the automotive and machine tool sector, steel with a hardness higher than 448 HV (45 HRC) is required.

The hardness values of the lower bainite and the upper bainite are much lower than that of martensite. Therefore, from the view of hardness, the bainite is less preferred. [35]

The as-quenched AISI 4340 steel which only the martensite left provided higher hardness values than as-received material. Low tempering does not significantly change hardness, for example, the tempering at 300°C results in less than 8% reduction in the hardness in quenched state. However, higher tempering temperature affects the size of precipitated carbides, making it easier for dislocations to move, resulting in a sharp decrease in hardness.

In addition, as researchers confirmed, hardness gradually decreased as tempering temperature increased, indicating that tempering temperature plays a significant role in hardness reduction due to carbon rejection softening of the martensitic matrix. In the case of AISI 4340, similar hardness values have been reported when tempering temperature is varied. In this way, the higher tempering temperatures provide sufficient mobility for the substitutional alloying elements to cause cementite growth, resulting in a continuous decrease in hardness and strength during tempering.

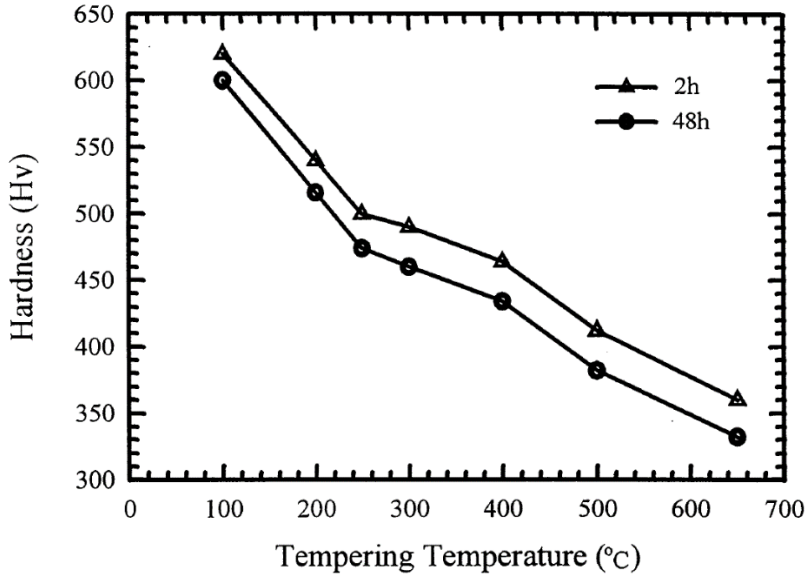

Figure 46. Hardness as a function of tempering temperature for 2 h and 48 h. [31]

3.3.2. Strength vs. ductility:

3.3.2.1. The effect of alloying elements and smelting processes on strength and ductility:

The strength of AISI 4340 steel is guaranteed only if martensite is obtained. The strength of martensite mainly depends on the content of carbon atoms in its interstitial solid solution, alloying elements do not contribute much to the strength, and the effect of adding other alloying elements is to improve other properties of the steel, including directly improving properties (such as ductility and toughness) and indirectly affects performance by participating in phase transitions.

Carbon atoms play the role of solid solution strengthening when the alloy steel undergoes martensitic transformation to obtain ultra-high strength. In the low temperature tempered 0.2% ~ 0.5% C medium carbon low alloy steel, the tensile strength (R_m) has a linear relationship with the carbon content (w_c, mass fraction):

$$R_{\mathrm{m}} = (294 \times w_{\mathrm{c}} + 82) \times 9$$

During low temperature tempering, ε-carbides are coherently precipitated from the martensite, but do not cause a re-increase in strength. Increasing the carbon content will damage almost all properties other than strength, so it should be reduced as much as possible under the premise of ensuring strength.

Generally speaking, the addition of chromium, nickel, molybdenum, vanadium, manganese, niobium, silicon and other alloying elements to steel can improve the hardenability of steel and ensure that the steel can easily obtain martensitic structure.

The number of lamellar twinned martensite in the quenched state of the double vacuum smelting (VIM+VAR) steel (Figure 47(a)) is significantly more than that in the ordinary smelting (EAF) (Figure 47(b)). The researchers revealed that the nano-twin boundary can not only effectively hinder the dislocation slip, improve the strength, but also can absorb and store dislocations as the

slip surface of dislocation, and improve the ductility of the material. [36]

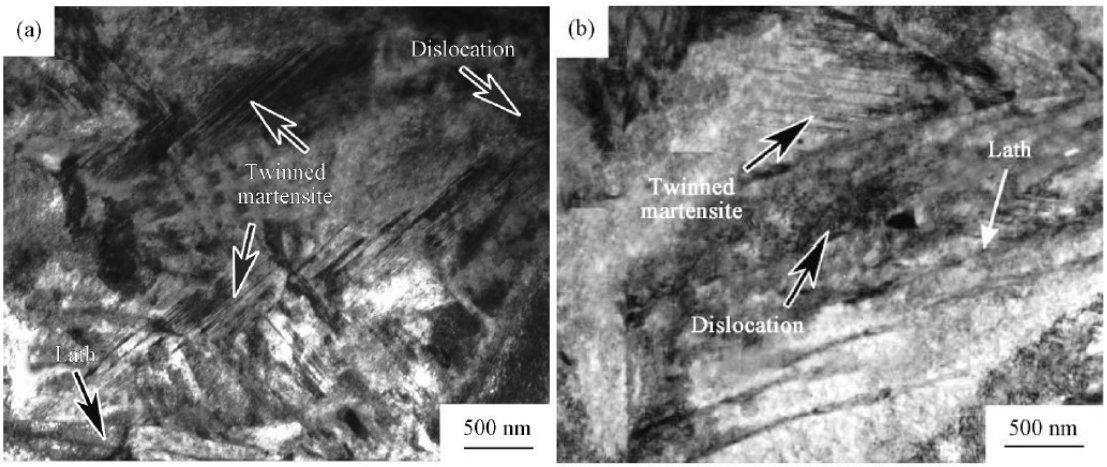

Figure 47. TEM images of as-quenched microstructure of (a) the ordinary smelting and (b) the double vacuum smelting AISI 4340 steel after heat treatments. [37]

The thickness of twinned martensitic sheets in AISI 4340 steel is between 20 and 50 nm. The existence of twinned martensite sheets in AISI 4340 steel will improve the strength and ductility of the material. This should be one of the reasons for the simultaneous improvement of the strength and ductility of AISI 4340 steel in the quenched state and 350℃ tempered state by double vacuum smelting.

3.3.2.2. The effect of heat treatment on strength and ductility:

It has been well known that high strength martensitic steel heat-treated to obtain the optimal combination of strength, ductility and toughness might mainly result from different heat treatment processes.

When studying the heat treatment process of AISI 4340 steel, it was found that in the quenched condition, the material has the highest strength and hardness with the lowest ductility. This could be explained in terms of the phase transformation of the steel during quenching, where the lattice structure of the steel is immediately transformed from FCC (γ phase) to BCT (martensite). At the same time, a large amount of deformation occurs during the formation of martensitic platelets, resulting in a rapid increase in strength and hardness. The figure shows the tensile properties of AISI4340 steel in different states. The quenched steel has excellent tensile properties, the tensile strength exceeds 2000 MPa, and the elongation is close to 10% as shown in Figure 48.

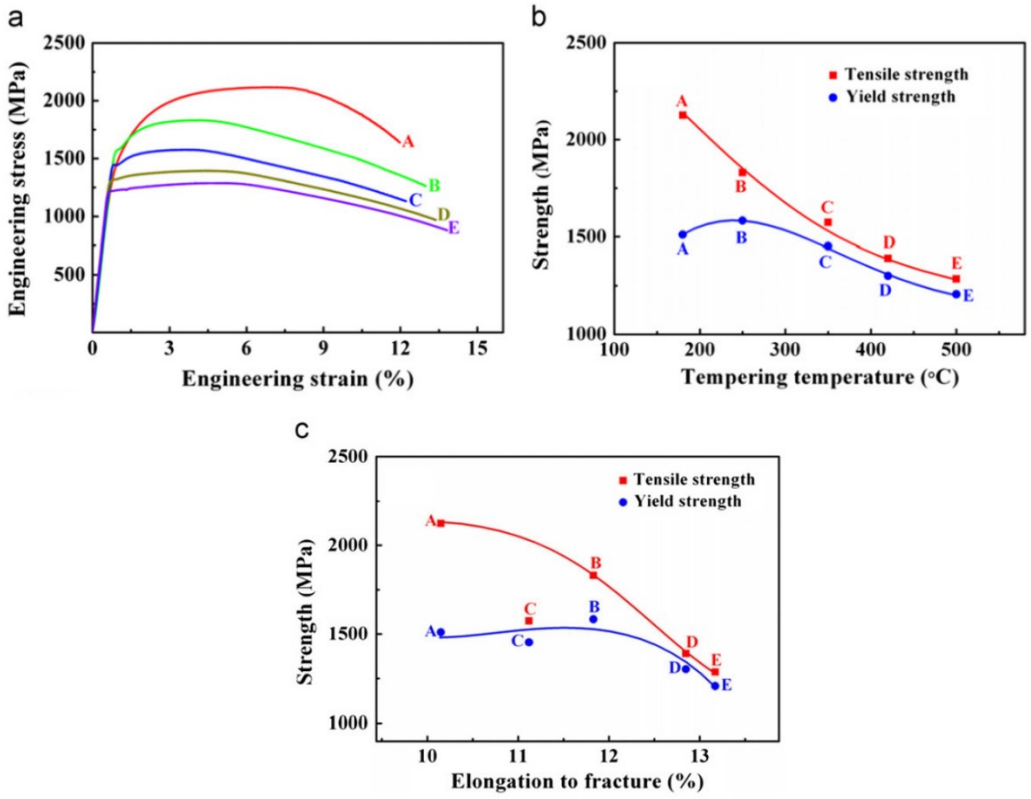

Figure 48. Tensile properties of AISI 4340 steel: (a) engineering stress-strain curves; (b) the relation between strength and tempering temperature; (c) relation between strength and elongation to fracture. [38]

For the tempered case, the hardness and strength of the AISI 4340 steel as a function of tempering temperature and holding time are shown in Figure 46 and 49, indicating that:

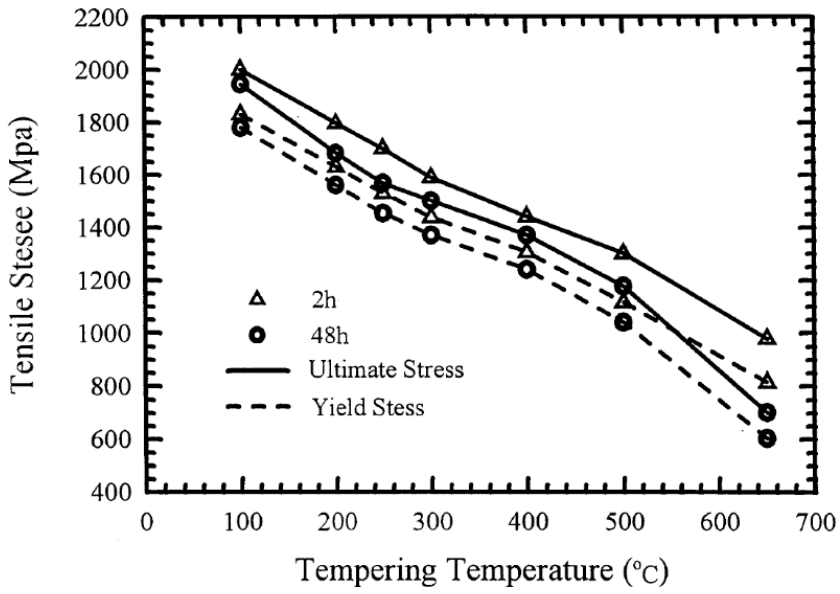

Figure 49. Ultimate stress and yield stress as a function of tempering temperature for 2 h and 48h. [31]

Within a certain tempering temperature range, the mechanical properties of the material are obviously affected by the tempering temperature and holding time. The tensile strength of tempered martensite gradually decreases as tempering temperature and holding time increasing. The effect of temperature is more significant than that of holding time, while the elongation increases with tempering temperature and holding time but does not change much, but the ductility suddenly decreases when tempering at 300°C, Figure 50 shows that the area reduction and elongation of the tested samples as a function of tempering temperature and holding time. It may be due to the thermal instability of the tempered interlaminar austenite in the quenched state, which often leads to the formation of carbide films that this phenomenon is analogous to temper brittleness which will be discussed in next.

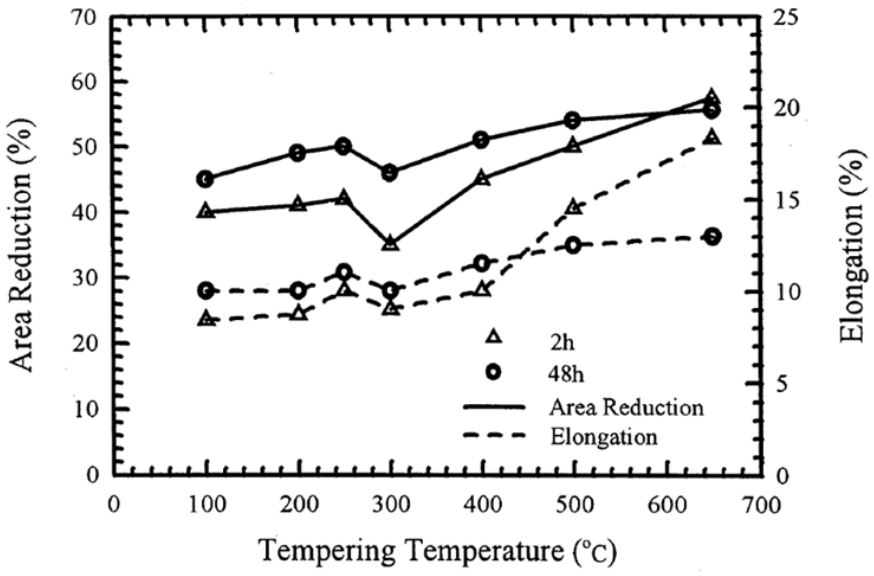

Figure 50. Reduction in area and elongation as a function of tempering temperature for 2 h and 48 h. [31]

Further research found that regardless of the holding time, the strain hardening exponent n of the material decreased as the tempering temperature increasing. Figure 51 shows that the yield stress and the strain-hardening exponent n have a linear relationship, demonstrating that for steel properties, high strength cannot coexist with high work hardening. As a result, obtaining both a high strength and a high rate of work hardening in AISI 4340 steel is difficult. The microscopic analysis is the same as the literature, [33] with the increase of the tempering temperature, the quenched martensite gradually decomposes, the lamellar twinned martensite gradually disappears, the dislocation density decreases, and the carbides tend to spheroidize, which is advantageous to plastic deformation.

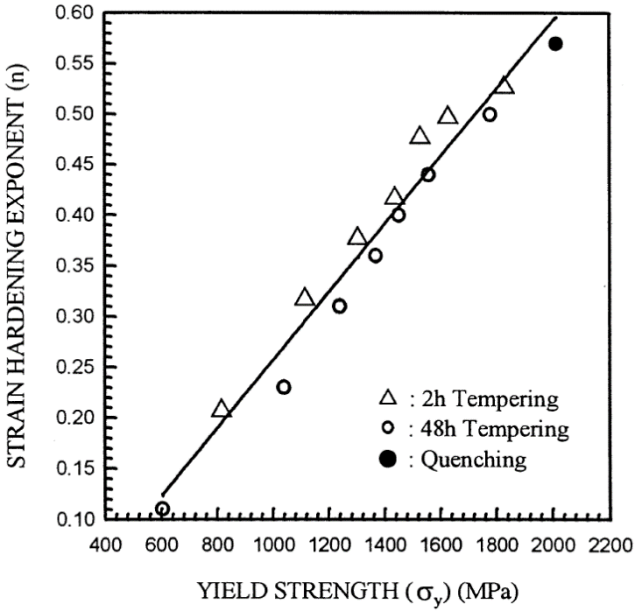

Figure 51. Effect of the yield stress on the strain-hardening exponent of AISI 4340 steel. [31]

In addition, tensile strength successively decreases as tempering temperature increases, however, elongation to fracture and reduction in area gradually increase as tempering temperature increases, which is consistent with other steels. On the other hand, the yield strength first slightly increases and then decreases, which is consistent with 300M steel [39] and some other ultra-high strength steels which are tempered below 200°C.

Figure 48(c) shows the yield strength and ultimate tensile strength versus elongation to failure of the AISI 4340 steel. Elongation to failure decreases continuously with increasing yield strength and ultimate tensile strength, which is consistent with the trade-offs between strength and elongation in steels.

3.3.3. Fracture toughness and impact toughness:

When the chemical composition of low alloy medium carbon steel is determined, its toughness mainly depends on the microstructure of the steel, and different smelting processes, rolling and heat treatment processes which could significantly affect the structure of the steel and thus its properties. At present, the properties of steel are mainly optimized from two aspects: First, a reasonable microstructure is obtained by heat treatment. Second, control the content and shape of non-metallic inclusions.

3.3.3.1. The effect of heat treatment on toughness:

Within a certain tempering temperature range, with the increase of the austenitizing temperature, the strength of the alloy steel does not change much, but the fracture toughness

increases and the impact toughness decreases. The researchers studied the heat treatment process of 300M steel, and the results show that the best strength and toughness treatment of the material is austenitizing vacuum oil quenching at 982°C(1255K) and salt bath tempering in the temperature range of 204~316°C(477~811K) as shown in Figure 52. [33] The tempered structure is tempered martensite (dispersed ε-carbides in the martensite and a small amount of film-like retained austenite between the martensite laths), no undissolved phase, and the fracture morphology is quasi-cleavage and dimples mixed morphology.

When austenitizing at a lower temperature of 870℃, there is an undissolved phase in the quenched structure, and the impact property after tempering is higher than that of austenitizing at a lower temperature, indicating that the elimination of the undissolved phase is beneficial to the impact property of the steel.

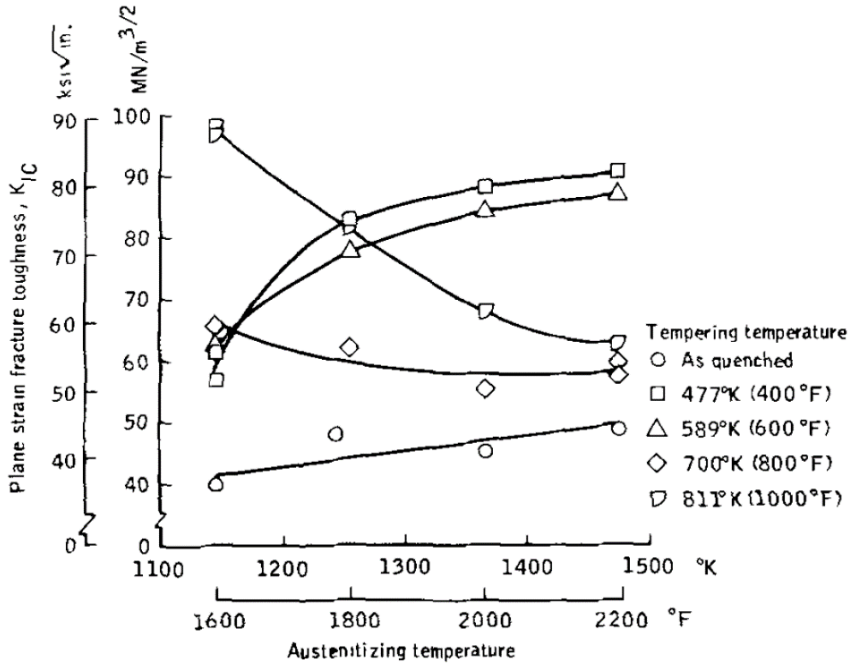

Figure 52. Effect of austenitizing temperature on the fracture toughness of 300M steel. [33]

The fracture toughness of 300M steel is affected by both the austenitizing temperature and the tempering temperature. The fracture toughness increases with the increase of the austenitizing temperature when tempered at a lower temperature, while the fracture toughness increases when tempered at a higher temperature. The toughness K_{Ic} decreases with the increase of the austenitizing temperature. This is because during low temperature tempering, the austenitizing temperature dominates, resulting in the increase of retained austenite and the elimination of twins, while during high temperature tempering, the tempering temperature dominates, and the retained austenite decomposes and disappears. The coarsening of carbide precipitation particles can lead to a decrease in K_{Ic}.

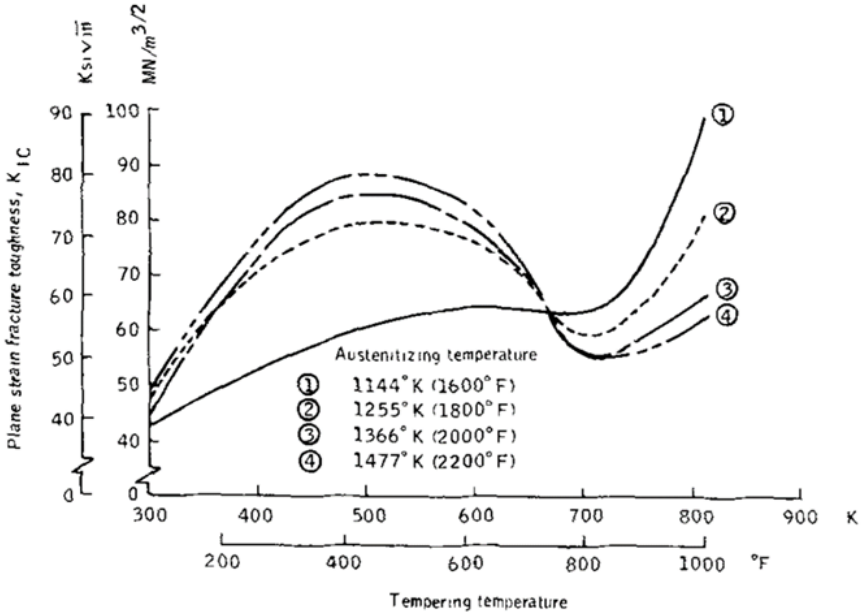

Figure 53. Effect of tempering temperature on the fracture toughness of 300M steel. [33]

In the study of AISI 4340 steel, it was found that the high temperature austenitisation at 1200℃ was higher than the conventional austenitisation at 870℃, and the amount of retained austenite in the structure after quenching is more. The amount of twinned martensite decreases as the austenitizing temperature increases. The mechanical properties test results as shown in Table 6 show that the fracture toughness of austenitizing at 1200℃ is much higher than that at 870 ℃. In addition, although there are also twinned martensitic structures in the austenitizing staged quenching structure at 1200℃ ~ 870℃, the film-like retained austenite in the microstructure is much more than that of directly quenched at 870℃. The mechanical property index shows that the fracture toughness of the staged quenched is higher than that of the directly quenched at 870℃, and it is comparable to the fracture toughness of the directly quenched at 1200℃, which indicates that the increase of retained austenite and the elimination of twinned martensite are beneficial to the fracture toughness.

Room Temperature Fracture Toughness Properties for Alloy 4340 in the As-Quenched Condition

Austenitizing Temperature, °C	Quench	Test Speciman Number	$\frac{P_{max}}{P_Q}$	Plane† Strain Fracture Toughness K_I		Critical Stress Intensity K_{crit}	
				ksi-in.$^{1/2}$	NM/m$^{3/2}$	ksi-in.$^{1/2}$	MN/m$^{3/2}$
1200	Oil	1	1.12	65.3	71.8	81.8	89.9
		2	1.15	60.9	66.9	88.9	97.7
		39	1.08	49.6	54.5	62.8	69.0
1200	Water	5	quench cracked				
		6	quench cracked				
1200	IBQLN	3	quench cracked				
		4	1.19	49.8	54.7	51.7	56.8
1100	Oil	41	1.07	40.0	44.0	45.3	49.8
1200-870	Oil	9	1.02	63.8	70.1	69.4	76.3
		10	1.01	66.6	73.2	68.7	75.5
		35	1.11	52.0	57.1	65.3	71.8
		46	1.00	61.2	67.2	61.2	67.2
1200-870	Oil + LN	43	1.07	55.6	61.1	63.7	70.0
1200-870	Water	11	1.14	59.3	65.2	74.6	82.0
		12	1.31	59.8	65.7	97.5	107.1
1200-870	IBQLN	7	1.14	60.5	66.5	84.5	92.9
		8	1.24	52.2	57.4	85.4	93.8
870	Oil	15	1.08	31.1	34.2	38.8	42.6
		16	1.00	39.0	42.9	39.4	43.3
		34	1.00	32.3	35.5	32.3	35.5
870	Oil + LN	45	1.00	33.1	36.4	33.1	36.4
870	Water	17	quench cracked				
		18	quench cracked				
870	IBQLN	13	quench cracked				
		14	quench cracked				
1200-870-870*	Oil	37	1.08	38.9	42.7	46.5	51.1

*Step quenched into oil (1200-870) and then re-austenitized at 870°C for one hour and oil quenched.
†K_I values are valid K_{Ic} when $P_{max}/P_Q < 1.1$.

Table 6. Fracture toughness properties at room temperature for AISI 4340 steel in the as-quenched condition. [34]

Here we analyze the reasons why the fracture toughness of AISI 4340 steel with higher temperature austenitization increases and the impact properties decrease. The impact toughness of the Charpy V-notch specimens of the 1200°C high temperature austenitizing specimens are lower than those of the 870°C austenitizing specimens, because the grain boundary embrittlement occurs and critical fracture stress is reduced during the higher temperature austenitization, which reduces the impact toughness. The reasons why high temperature austenitization can improve fracture toughness are: the dissolution of the undissolved phase increases the solid solubility of alloying elements, improves the impact toughness of the steel and improves the hardenability of the steel. The amount of retained austenite of the martensitic lath boundary increases and the amount of twinned martensite decreases, the grain size of austenite increases and the minimum distance (characteristic distance) when the front of the sharp notch crack reaches the critical fracture stress increases. [40]

	σ_y (MPa)	σ_b (MPa)	ε (%)	K_{IC} (MPa m$^{1/2}$)	F_{max} (kN)	$2.5(K_{IC}/\sigma_y)^2$ (mm)
	1355	2061	10.29	41.07±0.61	0.8 (B=4 mm)	2.30
180 °C	1550	1933	10.75	55.00±3.07	1.0 (B=4 mm)	3.15
240 °C	1473	1810	9.31	58.58±1.87	1.4 (B=4 mm)	3.95
350 °C	1430	1606	9.40	75.64±0.71	6.5 (B=8 mm)	6.99
420 °C	1320	1452	9.63	91.73±3.34	49.1 (B=25 mm)	12.07
500 °C	1185	1264	13.29	127.72±3.46	92.8 (B=30 mm)	29.04

Table 7. Yield strength, ultimate tensile strength, elongation, fracture toughness, the maximum load for valid specimen and the critical valid sample thickness for K_{Ic} test of AISI 4340 steel tempered at different temperatures. [41]

The mechanical properties data tempered at different temperatures are shown in the Table 7, and it can be seen that the fracture toughness K_{Ic} increases with the increase of tempering temperature. The strength and toughness of AISI 4340 steel exhibits a traditional inversion relationship, as shown in Figure 54, its tensile strength ranges from 1200 to 2100 MPa, and its fracture toughness ranges from 40 to 130 MPa·$m^{1/2}$.

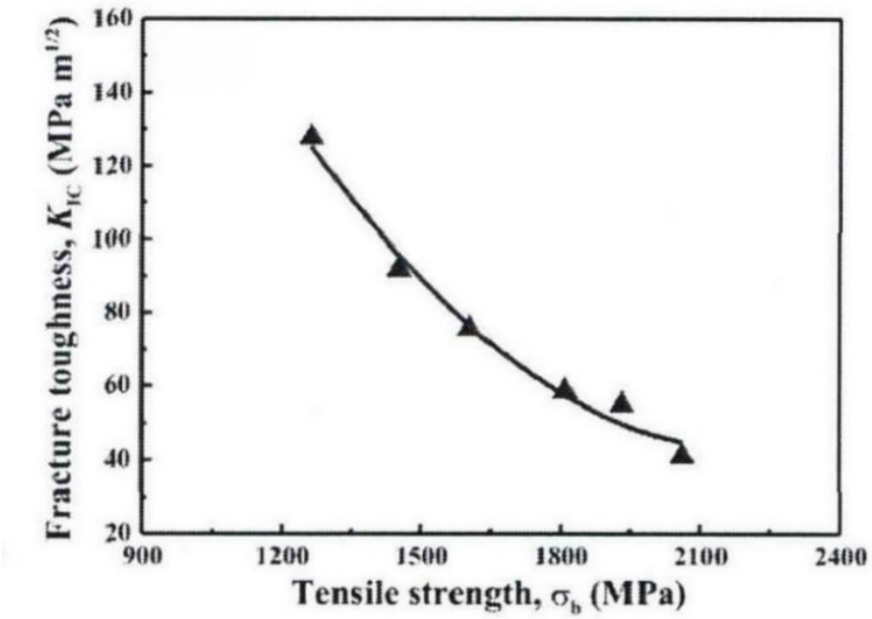

Figure 54. The trade-off relationship between the fracture toughness K_{Ic} and ultimate tensile strength. [41]

Many studies have found that when a material is tempered at a certain temperature, a sudden decrease in ductility and toughness occurs. Figure 55 shows tempered martensite embrittlement (TME) as a microstructural constraint associated with the decomposition of interlath retained austenite into M_3C films during tempering at temperatures ranging from 250°C to 400°C. Interlath Widmanstatten F_3C forms from ε-carbide. In comparison to prior austenite, the fracture is transgranular. In upper bainite the situation is similar. This TME failure is distinct from temper embrittlement (TE), which occurs at higher tempering temperatures (approximately 500°C) and is caused by impurity segregation ((principally sulfur in the present work) at prior austenite grain boundaries, resulting in intergranular fracture along those boundaries. Depending on the tempering conditions, both failures can occur in the same steel.

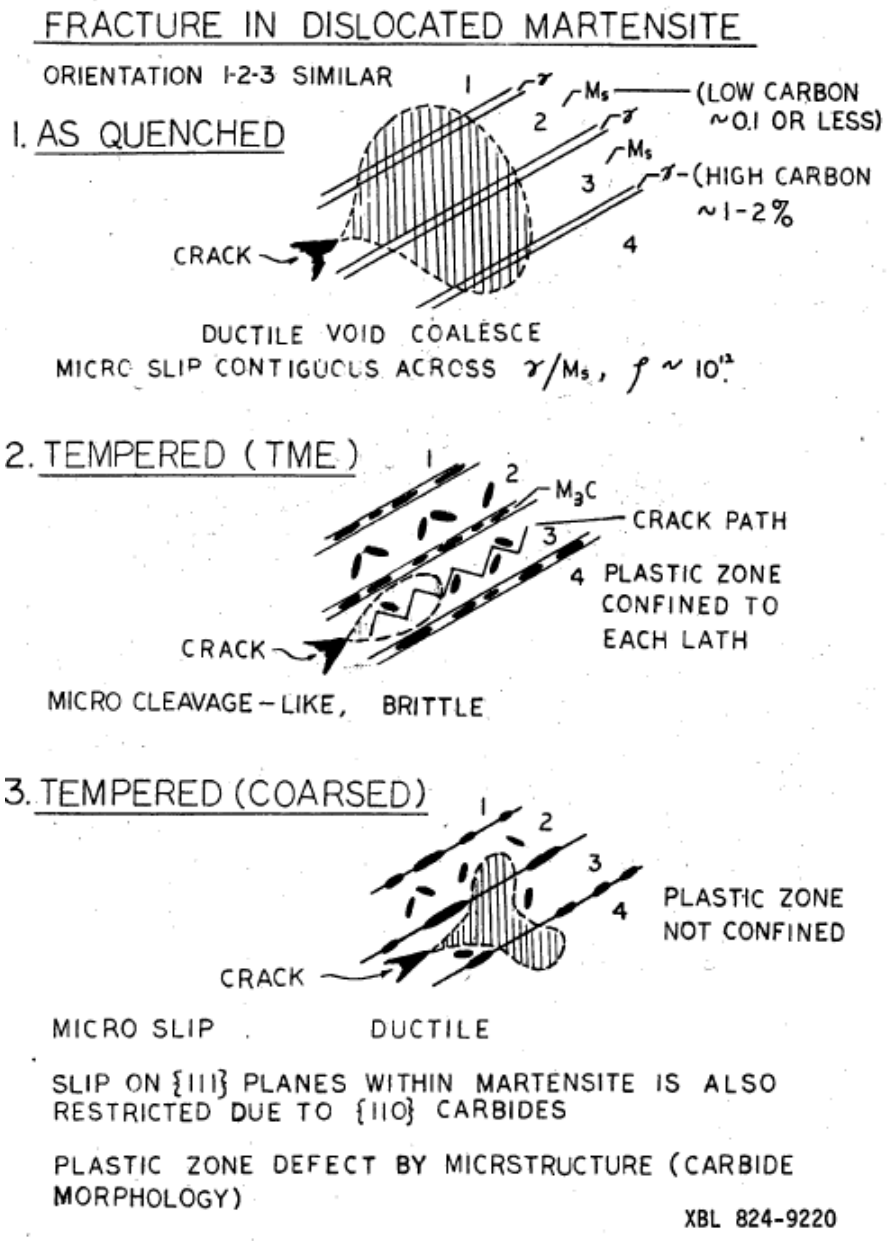

Figure 55. Scheme showing the observations of foil in-situ fracture, demonstrating the effect of microstructure on plastic zone and fracture path. [42]

3.3.3.2. The effect of smelting methods and rolling on toughness:

In the process of smelting and rolling, with the change of temperature, non-metallic inclusions inevitably exist in steel materials.

The relationship between non-metallic inclusions and steel properties is studied, [43] and it is found that the strength is mainly affected by the microstructure, and the size distribution and morphology of the non-metallic inclusions have a great influence on the ductility and toughness. When the researchers studied non-metallic inclusions in AISI 4340 steel, they found that the inclusions were mainly M_nS.

In the study of non-metallic inclusions in AISI 4340 steel processed by electroslag remelting

(ER) process and vacuum arc remelting (VAR) process, it was found that VAR can significantly reduce the content of M_nS in AISI 4340 steel. [44] Comparing the composition of AISI 4340 steel smelted by double vacuum smelting and ordinary smelting, it is found that the content of sulfur (S) element in AISI 4340 steel processed by ordinary smelting process is 0. 014 mass%, while that of AISI 4340 steel processed by double vacuum smelting process is 0.014 mass%. The content of S element is only 0.0027 mass%. It can be seen that double vacuum smelting significantly reduces the content of impurity element S in AISI 4340 steel, thereby reducing the content of M_nS inclusions, which has a positive effect on improving the plasticity and toughness of the steel.

In addition to the optimization of the smelting method, the rolling treatment can also change the morphology of the inclusions, thereby affecting the properties of the steel. When the effect of hot rolling deformation on AISI 4340 steel was studied and it is found that when the hot rolling deformation was reduced from 98% to 80%, M_nS changed from a rectangle to an ellipse, and the fracture toughness K_{Ic} of the steel increased by 20 MPa·$m^{1/2}$. [45]

In addition, adding calcium to AISI 4340 steel to modify sulfide inclusions, the process of feeding calcium-silicon wire can change the sulfide from band-like M_nS to granular C_aS, which increases the K_{Ic} by about 37 MPa· $m^{1/2}$ [30], and can improve the cold-brittle transition temperature.

The influence of inclusions on the properties of D6AC steel was studied, and it was found that the impact toughness of steel decreased with the increase of inclusion content and the decrease of inclusion spacing. If the inclusions in front of fatigue pre-crack were aggregated and distributed, the pre-crack would be affected. Crack propagation accelerates and reduces impact toughness. In addition, studies have shown that elliptical inclusions have little effect on the ductility and toughness of steel, while elongated inclusions have greater damage to ductility and toughness. It can be seen that the content, shape, distribution and size of inclusions in steel can significantly affect the properties of steel. [46]

3.3.4. Fatigue:

As a structural material, AISI 4340 steel must meet the static strength design requirements of components. In addition, it is often subjected to cyclic loads during service. Therefore, its basic mechanical properties and fatigue properties are the key indicators that affect its engineering application.

3.3.4.1. The effect of heat treatment on fatigue:

The very-high-cycle (10^9 cycles here) fatigue properties of AISI 4340 steel with different heat treatments are studied, and it is found that with the increase of tensile strength corresponding to different heat treatments or the decrease of stress amplitude, the fatigue damage mechanism will gradually change from the control of intrinsic defects (grain boundaries, dislocations and precipitation, etc.) to the control of process defects (voids, non-metallic inclusions, scratches, etc.).

There are four types of fatigue crack origin modes, which correspond to the crack initiation modes of high strength steels: (a) surface scratch, (b) surface inclusion, (c) subsurface inclusion and (d) inner inclusion. The average diameter of the inclusion in AISI 4340 steel is typically greater than

20 μm. In addition, a special granular bright and rough area, called Granular-bright-facet (GBF), appears around the inclusion, as indicated by the blue cycle in Figure 56(d), but is not visible in Figure 56(c).

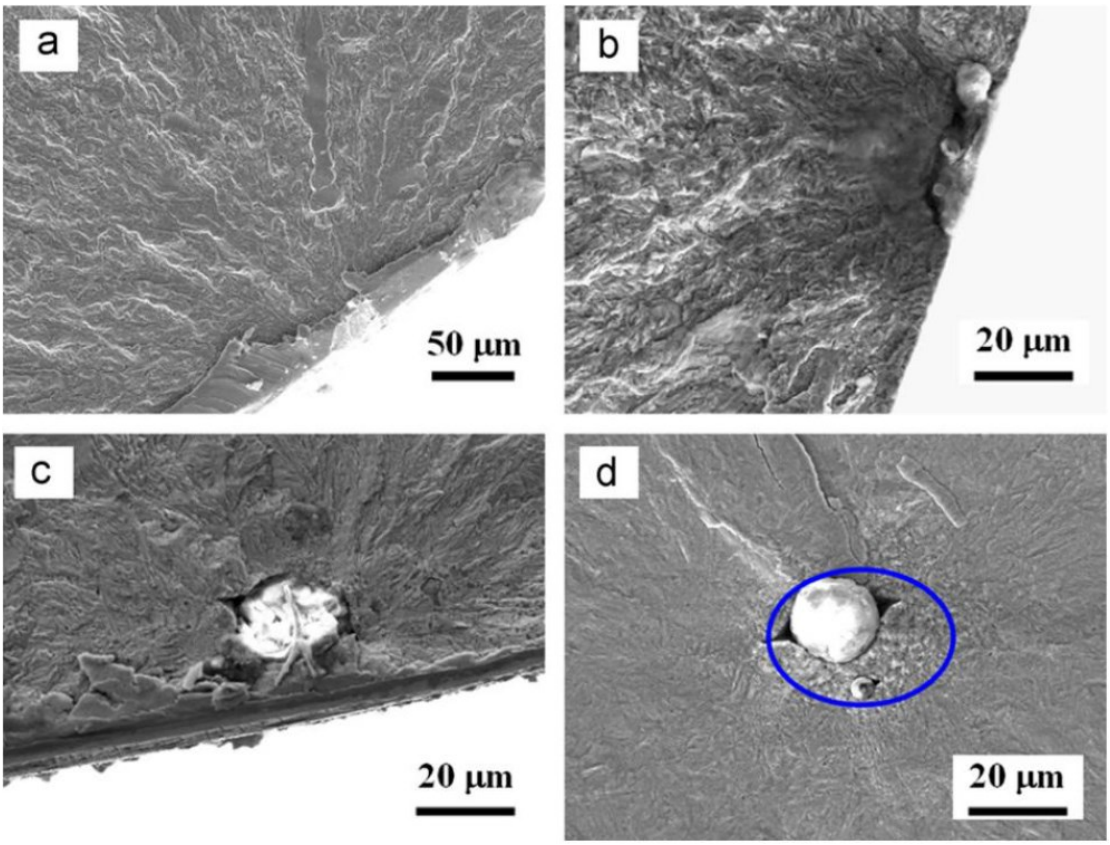

Figure 56. Crack origin of fatigue in AISI 4340 steel: (a) surface scratch; (b) surface inclusion; (c) subsurface inclusion and(d) inner inclusion. [38]

Broadly speaking, the four crack initiation modes could be divided into two types based on the fatigue cracking site: i.e., surface (surface scratch, surface/subsurface inclusion) and inner (inner inclusion). The statistic ratio of surface and inner cracking sites for the VHC fatigue test is shown in Figure 57. With increasing tensile strength, the ratio of inner cracking sites gradually increases. As tensile strength increases, the ratio of surface cracking sites gradually decreases. Nearly all fatigue cracks originate from surface defects when tensile strength is less than about 1200 MPa. Almost all fatigue cracks originate from inner inclusion when the tensile strength is over about 2000 MPa. The fatigue crack initiation gradually transitions from surface defects to inner inclusions when the tensile strength is within 1200~2000 MPa.

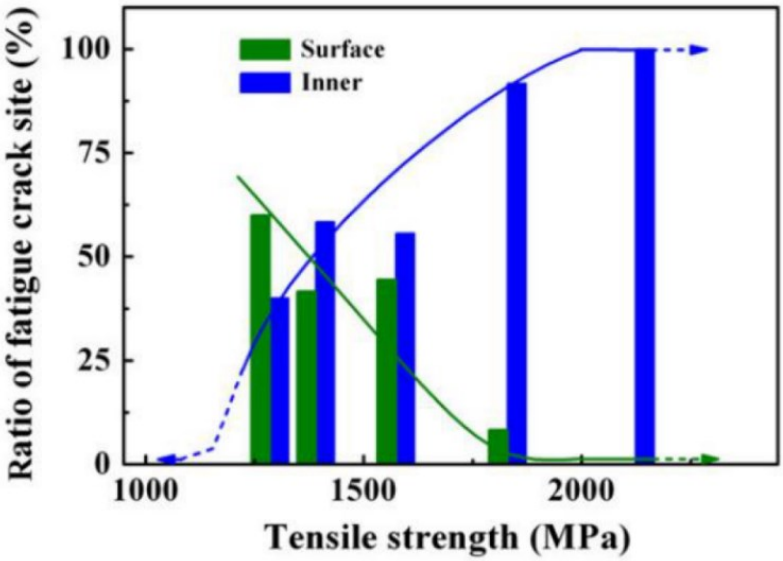

Figure 57. Relation between the fatigue crack sites ratio and tensile strength in AISI 4340 steel. [38]

The VHC fatigue strengths of AISI 4340 steel are found to increase first, then decrease as tensile strength increasing, which increases monotonically with decreasing tempering temperature. The specimen with the highest fatigue strength has a tensile strength of 1830 MPa, which is not the highest tensile strength implying that higher tensile strength does not always lead to higher fatigue strength. This is also found in other high-strength materials. In contrast, as tensile strength increases to a certain extent, fatigue strength begins to decrease.

However, the fatigue strength with the highest tensile strength is typically very close to the highest fatigue strength, implying that the fatigue testing result for the highest tensile strength but lower fatigue strength is also reliable.

The relationship between the fatigue strength and tensile strength of AISI 4340 steels under various heat treatments is shown in Figure 58(a).

We find a general fatigue strength formula to describe the intrinsic relationship between fatigue strength and tensile strength for the AISI 4340 steel at different tensile strength levels to gain a better understanding of the varying trend of fatigue strength at different tensile strength levels:

$$R = \sigma_w / \sigma_b = 0.70 - 1.85 \times 10^{-4} \sigma_b$$

which is drawn in Figure 58(b), it could be found that the fatigue strengths are basically within the 5% error band which is pretty satisfying.

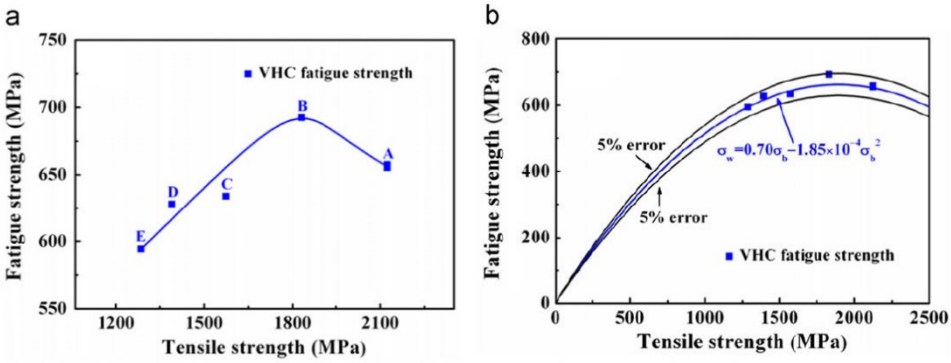

Figure 58. (a) Relation between tensile and fatigue strengths of the AISI 4340 steel; (b) Fitting curves of tensile and fatigue strengths. [38]

For high/very-high-cycle fatigue, S-N curve is a principal reference to determine fatigue strength and design criterion. As expected, the curves show that by reducing the stress, the number of failure cycles increases and the durability limit or fatigue limit is commonly observed in many steels.

However, the S-N curves are not always linear, hence we can utilize Basquin relation to express well the VHC fatigue S-N curves of AISI 4340 steel tempered at different temperatures and those S-N curves show decreasing type, of which step-wise or duplex type would not be found.

Basquin expressed them in logarithm ordinate and abscissa and found a simple linear formula such that:

$$\log\sigma_a = \log\sigma_f^{'} + b\log(2N_f) \quad [47]$$

Where σ_a is the stress amplitude, $\sigma_f'$is the fatigue strength coefficient, N_f is the number of failure cycles, $2N_f$ is the number of reservals to failure and b is the fatigue strength exponent on a log-log plot and also known as Basquin exponent which is the absolute value of the fitting curve slope. As shown in Figure 59, the fatigue data without tempering (curve A) are within the 15% error band, but others are within the 5% error band.

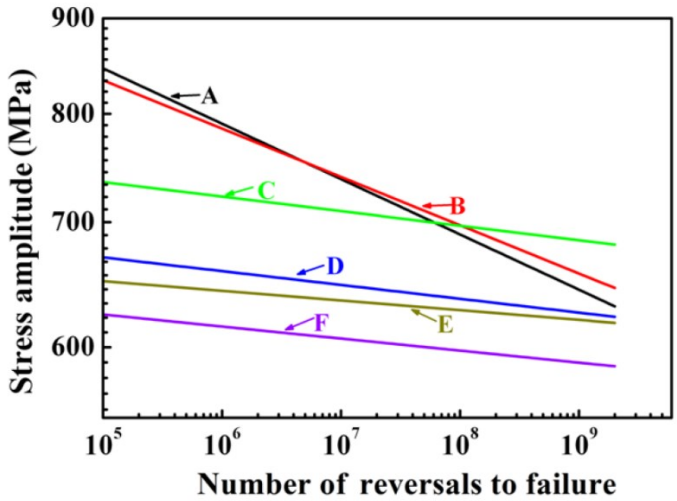

Figure 59. Six VHC Fatigue S-N curves expressed by Basquin relation for AISI 4340 steel which curve A is untampered and from B to F, the tempering temperatures are decreasing. [47]

The ideal material loaded under the stress amplitude of fatigue strength coefficient (σ_f') will pause for 10^9 cycles, which means that the S-N curve should be a level line and σ_f' can be called an ideal fatigue strength. However, local damages will occur in a real material after alternating loads due to various defects (point defects, dislocations, boundaries, inclusions, and so on), making the S-N curve not a level but various types. As a result, the fatigue strength exponent b could also be referred to as the fatigue damage exponent.

There are three ways to improve fatigue strength listed here:

(1) The fatigue strength coefficient σ_f' remains constant, while the fatigue strength exponent b increases. The higher the fatigue strength exponent, the greater the fatigue strength.

(2) The fatigue strength exponent b remains constant, while the fatigue strength coefficient σ_f' increases. The higher the fatigue strength coefficients, the greater the fatigue strength.

(3) Both the fatigue strength coefficient σ_f' and the fatigue strength exponent b increase in this case.

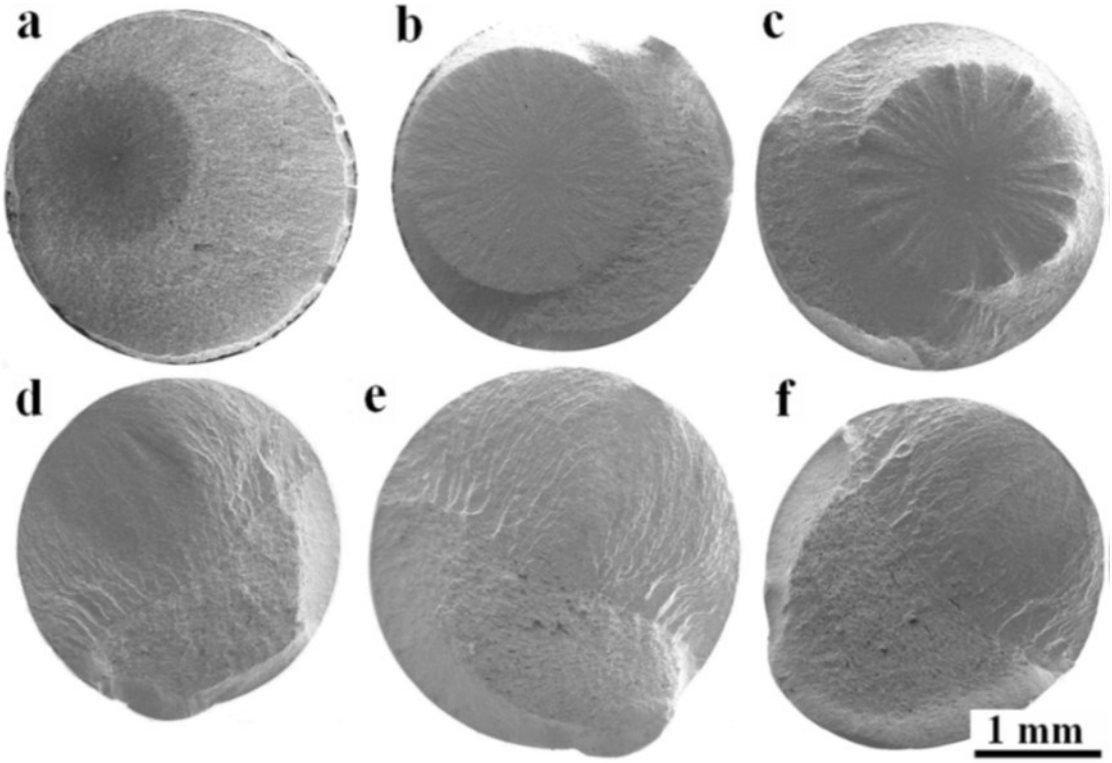

Figure 60. The macroscopic morphologies of fatigue samples for AISI 4340 steel tempered at different temperatures which a is untempered, from b to f, the tempering temperatures are decreasing. [47]

In addition, there are also some differences in the microstructure and fractographs of AISI 4340 steel tempered at different temperatures. Here is a rough explanation of the corresponding mechanism: Untempered sample (a) has an indistinct dividing line between the crack growth area and the final fracture area, as well as a flat fracture surface as shown in Figure 60(a). Samples (b)~(f) tempered at 180, 250, 350, 420, and 500°C have distinct dividing lines and growth ridges as shown in Figure 60(b)~60(f), especially sample (c) showing some regular fan shaped zones as shown in Figure 60(c). This implies that they have different plastic deformation abilities. The reason for this could be that sample (a) with full martensitic microstructure has so many defects such as

supersaturated interstitial carbon atoms, high density dislocations, subgrain boundaries and so on, that plastic deformation ability is limited and tensile strength is high. Since the fatigue sensitivity to defects is much higher in this case and fatigue damage degree is a major cause of fatigue crack initiation, sample (a) has the lowest fatigue strength exponent b.

3.3.4.2. The effect of cryogenic treatment on fatigue:

Besides tempering, after cryogenic treatment, the fatigue limit of the steel is also improved as shown in Figure 61. This is due to the higher hardness and strength of the material with this treatment. Results reported in the literature indicate that cryogenic treatment has some beneficial effects in the case of AISI 4340 steel members subjected to fatigue loads.

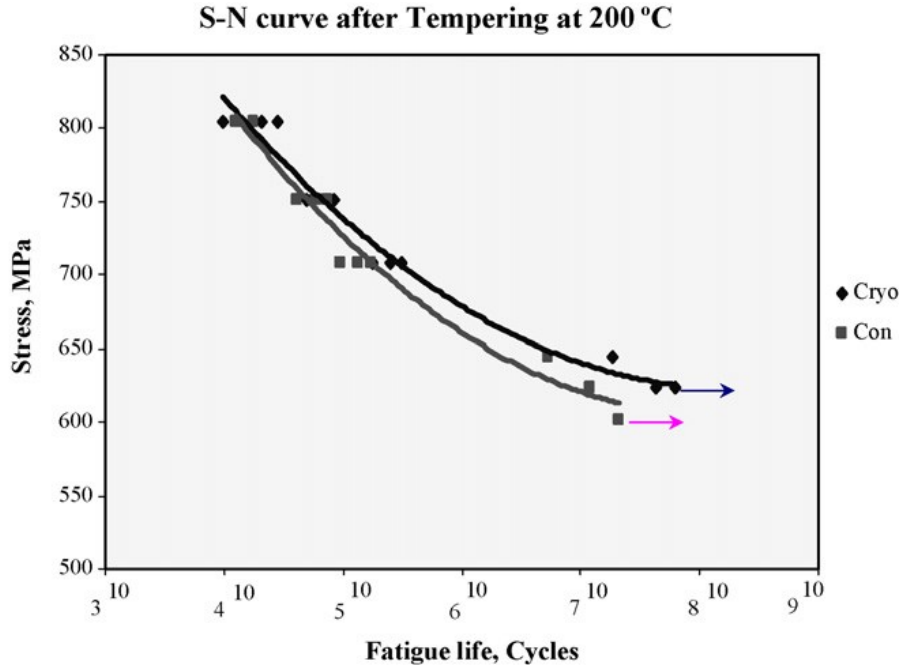

Figure 61. S-N curves tempering at 200°C with and without cryogenic treatment. [48]

In addition, neutron diffraction techniques have shown in Figure 62 that the main microstructural effect of cryogenic treatment is a slight reduction in the amount of "retained austenite", which could be the transformation to martensite by cryogenic treatment. This leads to an increase in hardness due to the higher amount of martensite. This effect persists even after tempering. The use of cryogenic treatment showed a slight detrimental effect (14.3% reduction) on the impact energy toughness before tempering. The fracture characteristics of the cryogenic treated steel showed fewer shear lips, indicating less energy absorption, than the conventionally treated ones.

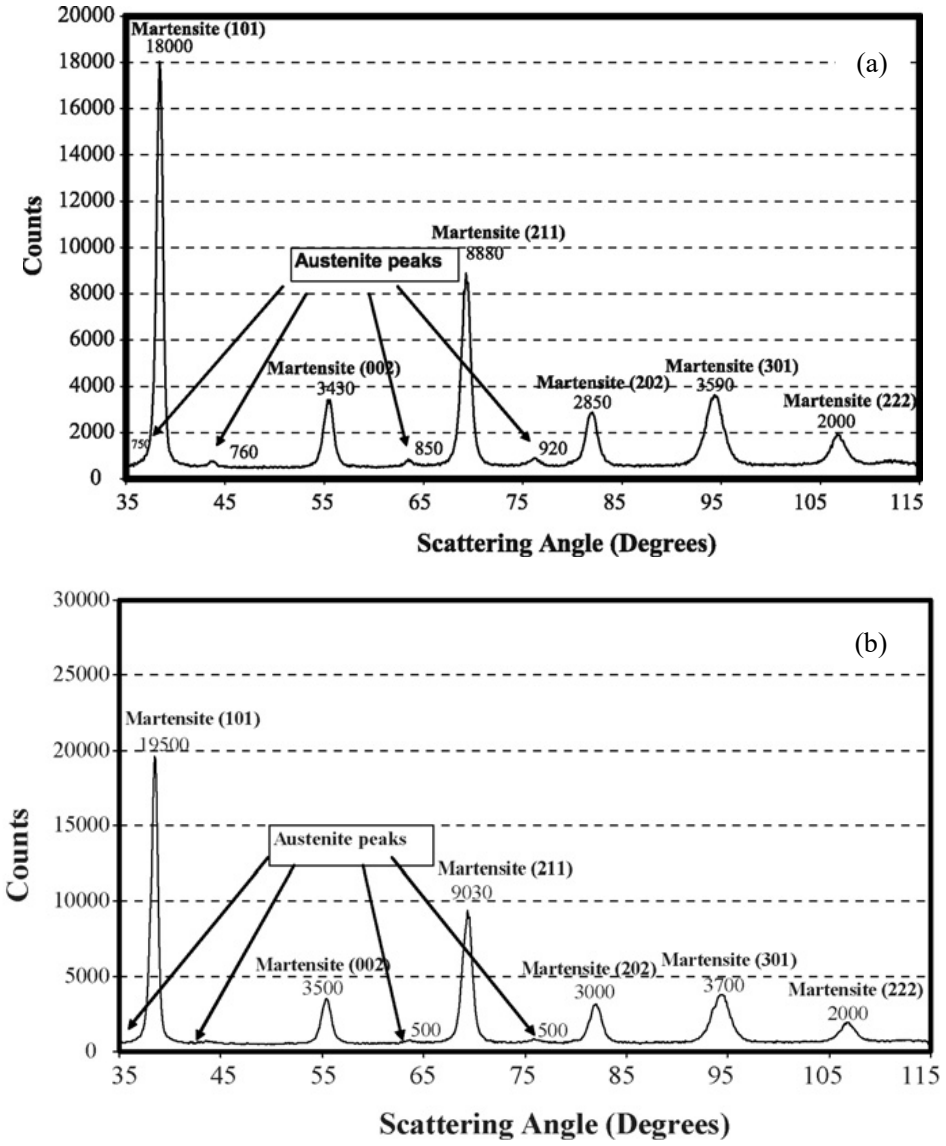

Figure 62. The neutron diffraction profile for AISI 4340 steel austenitized at 845°C (a) without cryogenic treatment. And (b) with cryogenic treatment. [48]

3.3.4.3. The effect of smelting methods on fatigue:

It has been reported in the section before that the content and size of inclusions have an obvious effect on the fatigue properties of high strength steels. The double vacuum smelting process of vacuum induction melting (VIM) and vacuum arc remelting (VAR) can greatly reduce the inclusions in the steel content, vacuum smelting can significantly reduce the size of inclusions and control the distribution of inclusions. Therefore, compared with ordinary smelting, double vacuum smelting can improve the high/very-high-cycle fatigue properties of steel.

3.4. Improvement of heat treatment process of engineering steels:

The heat treatment method of conventional low alloy medium carbon engineering steel is quenching and low temperature tempering, resulting in a mixed structure, generally lath martensite with high density dislocation, thin film retained austenite on the lath bundle boundary, and a small amount of twinned martensite. There is sometimes a small amount of lower bainite structure, which has high strength and good ductility and toughness. However, in the face of the demand for higher strength and higher toughness of this type of steel in practical applications, it is very important to explore the heat treatment process with better strength and toughness.

Low alloy ultra-high strength steel is added with alloying elements vanadium, niobium, titanium and other strong carbide forming elements. When the content is large, stable carbides can be formed in the steel. These carbides are insoluble in austenite at the usual austenitizing temperature. This reduces the stability of supercooled austenite, inhibits the transformation of pearlite, and enables the bainite transformation to occur. According to the isothermal temperature, it can be divided into two types of austempering above the M_s point and below the M_s point.

When the isothermal treatment of AISI 4340 steel above the M_s point, it is found that the structure of the steel varies with the isothermal temperature. The acicular lower bainite and martensite structures (as shown in Figure 63.) are obtained by isothermal transformation at 320°C, and the lower bainite divides prior austenite grains, which give a better combination of strength and toughness, and the best strength and toughness are obtained at the lower bainite volume fraction of about 25%, which may be due to the fine grain size of the lower bainite split prior austenite. Isothermal transformation in 400℃ obtain massive upper bainite and martensite structure, the upper bainite and martensite are closely connected to fill the prior austenite grains. Such a structure is very detrimental to the strength and toughness of the material.

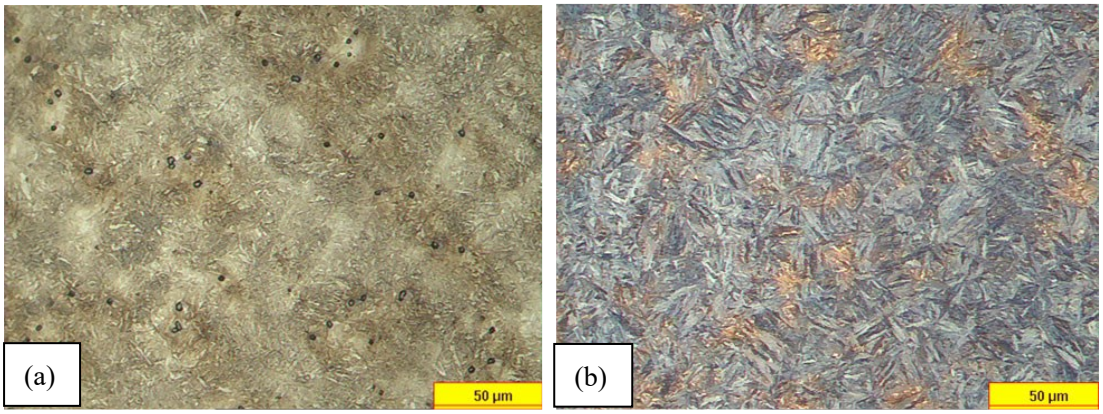

Figure 63. OM of transverse section of (a) Q&T specimen and (b) austempered specimen. [49]

At comparable elastic strain amplitudes in strain-life fatigue testing and at comparable stress amplitudes in stress-life fatigue testing, the austempered steel had longer high/very-high-cycle fatigue lives than the conventional quenching and tempering samples. In strain-life testing, however, the Q&T samples had longer low-cycle fatigue lives than the austempered samples at comparable plastic strain amplitudes. Despite the fact that both materials had similar fatigue fracture characteristics, the Q&T samples' overload regions were entirely composed of dimple rupture, while the austempered samples had both dimple rupture and quasi-cleavage as shown in Figure 64.

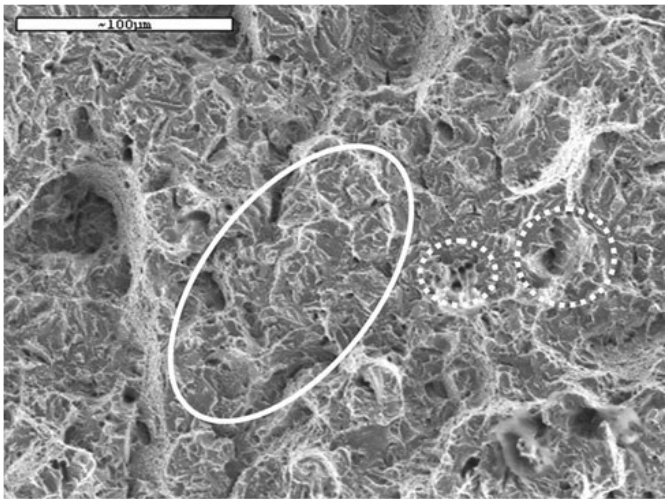

Figure 64. SEM image of quasi-cleavage within solid ellipse and dimple rupture within dashed circles. [50]

When studying the isothermal bainitic transformation of 300M steel above the M_S point, it is found that the isothermal transformation of 300M steel above the M_S point also obtains a mixed structure of bainite and retained austenite, and the isothermal transformation around 350℃ is that retained austenite film of 12%~18% volume fraction divides the carbide-free upper bainite structure, which obviously improves the fracture toughness and impact toughness of the steel, but the strength is slightly reduced. While the isothermal transformation is above 374℃, we obtain a large number of blocks in which the retained austenite is closely combined with the upper bainite. It damages various performance of the steel as shown in Figure 65. This is because the film retained austenite is relatively stable and is not prone to phase transformation during subsequent plastic deformation, which can hinder the expansion of cracks. However, the bulk retained austenite is prone to strain-induced martensitic transformation during plastic deformation, resulting in brittle untempered martensite, which is prone to brittle fracture.

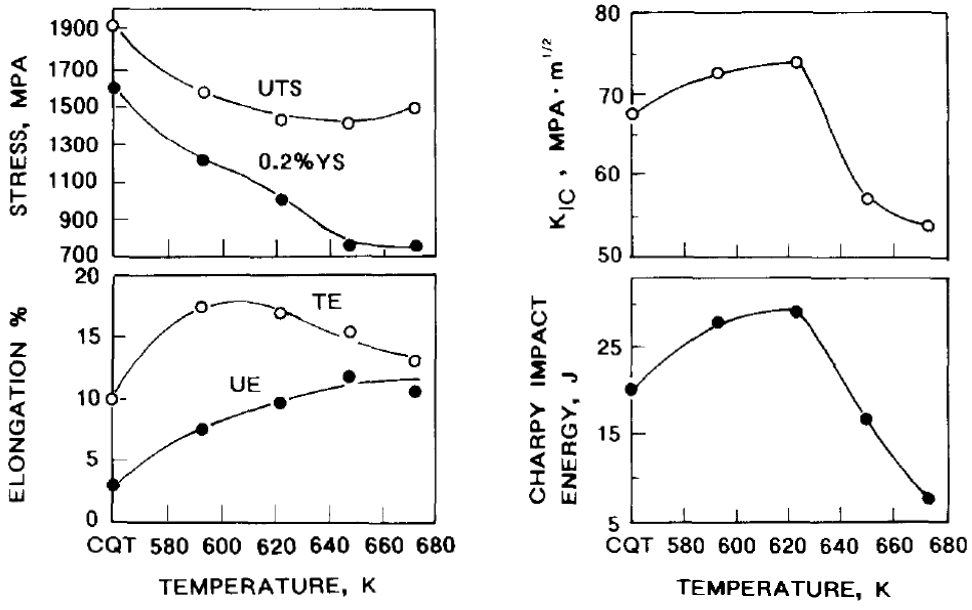

Figure 65. Effect of transformation temperature on mechanical properties of 300M steels. [51]

In addition, the steel obtained isothermally below the M_S point is generally a mixed structure of lower bainite, martensite and retained austenite. When the isothermal time is short, the lower bainite divides the prior austenite However, with the extension of isothermal time, the content of lower bainite in the mixed structure gradually increases, which is slightly detrimental to the strength of the material, but the plasticity and toughness are significantly improved. It can be seen from the above that the properties of low alloy medium carbon engineering steel during isothermal transformation are very sensitive to isothermal temperature and holding time.

The main purpose of other improved heat treatment processes (staged heat treatment, cyclic heat treatment) is also to change the substructure of the steel, obtain more retained austenite and refine the structure, and finally obtain performance that meets the requirements of use.

3.5. Discussion:

At present, scholars have mainly conducted a lot of research on quasi-static mechanical properties in smelting, heat treatment, etc., and have achieved many results. But there are still few researches on large/high strain rate dynamic loads. The static and quasi-static mechanical properties of low alloy medium carbon engineering steel should be improved by newer process. While ensuring high strength, the fracture strength and ductility are significantly improved. For the mechanical properties under dynamic loads, the current research mainly focuses on the evolution of microstructure and failure mechanism.

4. Low-carbon high strength hot-stamped steels

It has been more than a hundred years since the birth and development of the automobile industry at the end of the 19th century. Its products have gradually developed from simple customized models to mass-produced models that are sold simultaneously all over the world. With the continuous increase of automobile production, the fuel economy and related environmental issues of automobiles have received special attention. Consequently, the trend in the automotive industry in recent years has been to reduce fuel consumption, reduce emissions, and at the same time minimize the negative impact on the environment.

On the premise of ensuring the safety of automobile collision, automobile lightweight technology is one of the effective ways to achieve the above goals. According to relevant statistics, every 10% reduction in the weight of a car can reduce fuel consumption by 6~8% and carbon dioxide emissions by 13%. [52]

There are three main ways to reduce the weight of automobiles: one is to optimize the car frame and structure, and the redundant structure is removed by optimizing the structure of the car body, engine and other parts. The other is to use high specific strength materials, such as high-strength steel and aluminum alloys, magnesium alloy, carbon fiber materials, etc. The third is to use advanced manufacturing processes, such as hot stamping, laser welding, internal high pressure forming and other technologies, to manufacture lightweight automotive parts. The above three methods are complementary.

With the rapid development of materials and metallurgical science, more and more Advanced High Strength Steel (AHSS) and Ultra High Strength Steel (UHSS) have been developed and gradually applied to the manufacture of automotive body safety components. Compared with traditional automotive steel, AHSS/UHSS has higher specific strength, which can reduce the thickness of the body plate without losing the strength of the body components, thereby reducing the weight of the vehicle.

However, the improvement of the strength of the steel plate and the reduction of the thickness would reduce the formability. The traditional cold stamping process for forming AHSS/UHSS is prone to forming defects such as cracking, wrinkling and spring-back and other unfavorable factors such as severe wear and low dimensional accuracy. Therefore, hot stamping was introduced to high-precision stamping of AHSS/UHSS. The Swedish company Plannja (now acquired by Swedish Steel AB Group) proposed and applied for a patent for hot stamping of boron steel in 1977, mainly for the production of some tools. [53] By 1984, the Swedish Saab (SAAB) automobile company took the lead in using hardened boron steel plate to make the body parts of the SAAB9000 model. Between 1987 and 1997, the production of hot stamped parts increased from 3 million pieces/year to 8 million pieces/year. Since 2000, hot stamped parts have been increasingly used in automobile bodies, and the annual production volume has reached 100 million in 2007. [54] In the newly developed XC90 car of Volvo, which is famous for its safety, the amount of hot-stamped steel has reached 30%, and the amount of hot-stamped steel in the new models of other companies has also increased significantly, such as Benz C class. Hot stamping technology for automotive steel uses both high specific strength materials and advanced manufacturing processes.

Figure 66 shows the application of hot-stamped steel in the body safety structure. Hot stamping technology is currently mainly used to produce automotive body structures and crash safety parts,

such as: automotive A-pillars, B-pillars, front and rear bumper reinforcement beams, door anti-collision beams, roof rails, door sill reinforcement beams, middle tunnel parts.

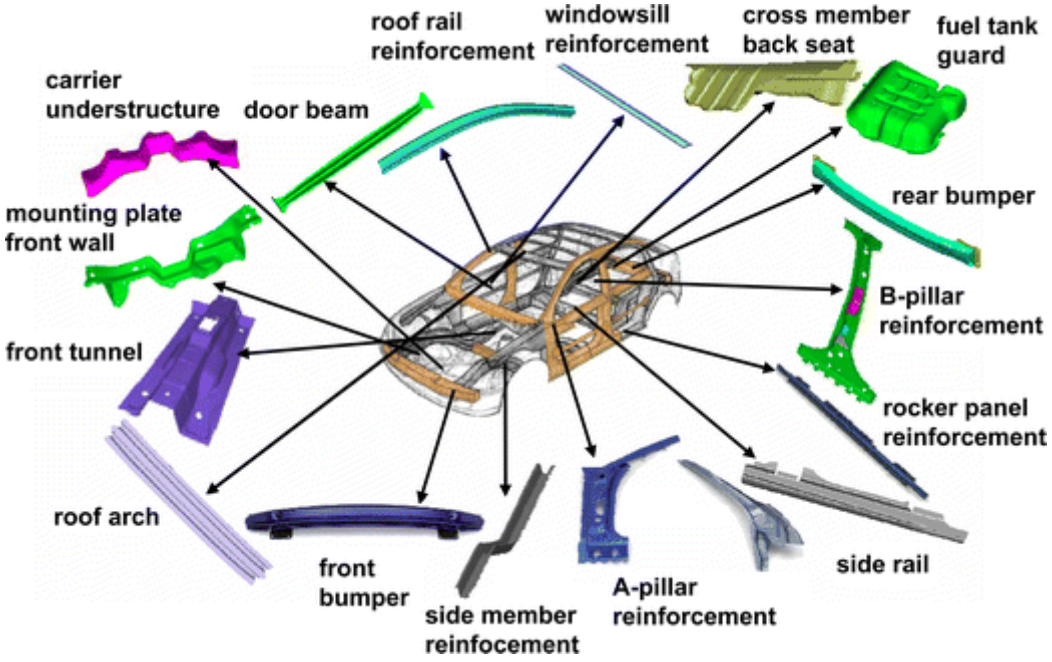

Figure 66. Application of hot stamped parts in car bodies. [55]

A widely used steel grade for hot stamping is Mn-B alloy steel. The steel for hot stamping contains boron without exception, and the content of boron is controlled between 0.001~0.005%. Among them, 22MnB5 steel is the first available commercial steel grade, and it is still the most widely used hot stamping steel in the automotive industry. For boron steel series hot stamping steel, the grades of 22MnB5 steel produced by different iron and steel enterprises in different countries are different, but the composition is very similar, and the content of main elements is not very different. Its chemical composition is listed in Table 8.

Commercial name	Steelmaker	C	Si	Mn	P	S	Cr	Ti	B	Fe
USIBOR 1500	ArcelorMittal	0.22	0.25	1.23	0.025	0.008	0.2	0.037	0.004	Bal.
MBW 1500	ThyssenKrupp	0.25	0.4	1.4	0.025	0.01	0.5	0.05	0.005	Bal.
Docol Boron02	SSAB	0.2~0.25	0.20~0.35	1.0~1.3	0.019	0.01	0.14~0.26	/	0.005	Bal.

Table 8. Chemical compositions of 22MnB5 hot-stamped steels produced by different steelmakers. [56~58]

ArcelorMittal, the world's largest steel group, has launched the USIBOR series of boron steel for hot stamping, which includes USIBOR 1500 for bare plate, USIBOR 1500P (or USIBOR 1500-AS) for Al-Si coated plate, USIBOR 1500-GI for galvanized plate, and USIBOR 1500-GA for zinc-iron coated plate. USIBOR series sheets are in an annealed state. The microstructure is uniform ferrite and finely dispersed pearlite. The initial yield strength is 350~550 MPa, and the tensile strength is 500~700 MPa. After hot stamping, the microstructure of the sheet is transformed into a

uniform lath martensite structure, the yield strength can reach 1100MPa and the ultimate tensile strength can exceed 1500MPa. [59] ThyssenKrupp Steel of Germany can provide MBW series manganese boron steel for hot stamping, including MBW-K1500 for cold-rolled sheet, MBW-W1500 for hot-rolled sheet, and MBW1500+AS for aluminum-silicon coated sheet. [60]

Although the strength of these 22MnB5-based steels after hot stamping can reach the 1500 MPa level, with the further improvement of the lightweight requirements of automobile companies, more ultra-high strength hot stamping steels have been successively developed by major steel companies in the world. There are mainly two grades of 1800 and 2000 MPa. German ThyssenKrupp company developed 1900 MPa hot stamping steel MBW-1900 based on 34MnB5 composition. Sweden SSAB Group launched 2000 MPa hot stamping steel Docol2000Bor based on 37MnB4 composition, Korean POSCO company Developed 2000 MPa class hot stamping steel HPF 2000. ArcelorMittal also developed 2000 MPa class hot stamping steel USIBOR 2000. [61] The grades, compositions and mechanical properties of the other corresponding steel grades after stamping are shown in the Table 9. The mechanical properties of the final stamped parts mainly depend on their C content. As an important alloying element, B has the greatest influence on hardness and hardenability. Mn and Cr elements have a certain influence on the hardness. Si element improves the strength of the material by means of solid solution strengthening and can inhibit the growth of austenite grains to a certain extent.

Steel	Composition (mass fraction / %)										YS	UTS
	C	Si	Mn	Cr	Ti	B	N	Ni	Al	Fe	MPa	MPa
27MnCrB5	0.25	0.21	1.24	0.34	0.042	0.002	0.004	0.01	0.03	Bal.	1097	1611
28MnB5	0.28	0.40	1.30	–	–	0.005	–	–	–	Bal.	1135	1740
34MnB5	0.34	0.40	1.30	–	–	0.005	–	–	–	Bal.	1225	1919
37MnB4	0.37	0.31	0.81	0.19	0.046	0.001	0.006	0.02	0.03	Bal.	1378	2040

Table 9. Chemical composition and corresponding strength of M-B steel after quenching. [62]

4.1. Hot stamping process:

A new manufacturing technology for ultra-high-strength stampings. The so-called hot stamping is to heat the steel plate to above the A_{c3} point for austenitization. And then the sheet material is stamped and quenched from the point above A_{c3} transformation in the stamping die. The stamping process of stamping and transformation quenching is realized at the same time. It is also known as hot forming or press hardening process.

There are two types of hot stamping processes: direct hot stamping and indirect hot stamping, as shown in Figure 67. In direct hot forming, the boron steel hot stamping technology process is as follows: in roller heath furnaces (sometimes also with conduction heating or induction heating) high-strength boron steel sheet is heated to austenitizing temperature and hold for a period of time to make it fully austenitized. Then quickly transfer it to the mold which is installed on the fast press. The mold is equipped with the water-cooled system. The pressure is held for a period of time after stamping, and then quench in the mold to obtain a complete martensitic structure and make the shape and size of the part tend to be stable. The yield strength of the part material after quenching can reach 1100 MPa, and the ultimate tensile strength can reach 1500 MPa. Post-processing includes

shot blasting to remove the oxide scale, both for paint adhesion and for ease of spot welding. Geometry could be refined through machining such as trimming, cutting, and/or piercing. Usually, laser machining is conducted.

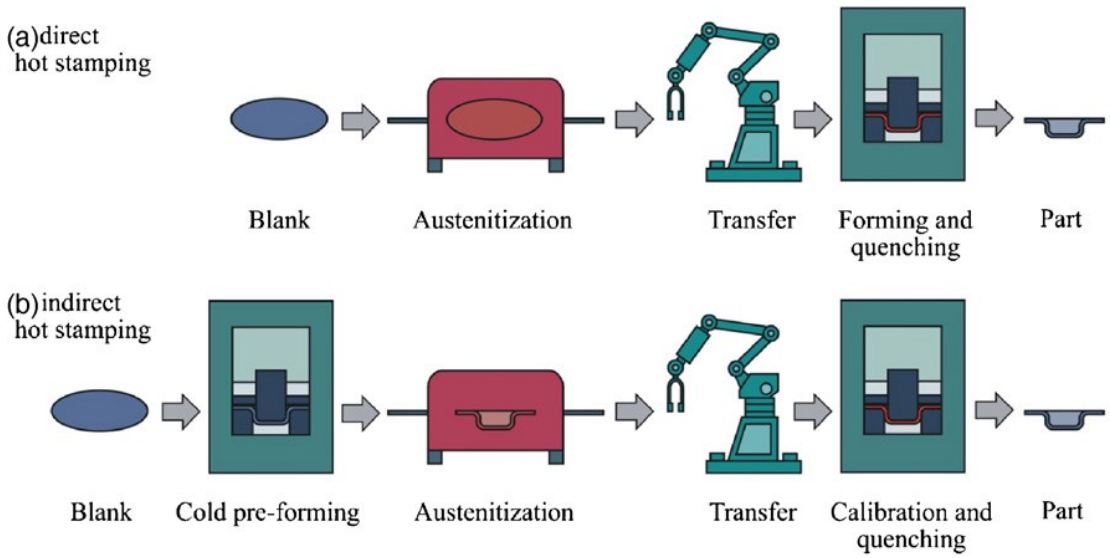

Figure 67. Basic hot stamping process flows: (a) direct hot stamping, (b) indirect hot stamping. [63]

In indirect hot stamping, the high-strength boron steel sheet is first transferred to a stamping die, and then cold stamped into a pre-formed part which is then heated in a heating furnace and transferred to a water-cooled forming mold. It is calibrated and quenched until it is finally stamped into a fully formed part. The main advantage of indirect hot stamping is that it avoids liquid metal embrittlement (LME) and is therefore compatible with galvanized sheet steel providing cathodic corrosion in the final part. However, due to the lower cost and higher production efficiency of the direct hot stamping process than the indirect process, direct hot stamping has more widespread use in the automotive industry.

It is worth noticing that the blank must be transferred from the furnace to the press as quickly as possible in order to avoid cooling the part before forming. Furthermore, forming must be finished before the start of the martensite transformation. Therefore, the prerequisite for successful process control is a fast tool closing and forming process. In addition, most of hot stamping tool systems use a distance blank holder as shown in Figure 68, to avoid the quenching of the blank between the die and the blank holder during the hot stamping process.

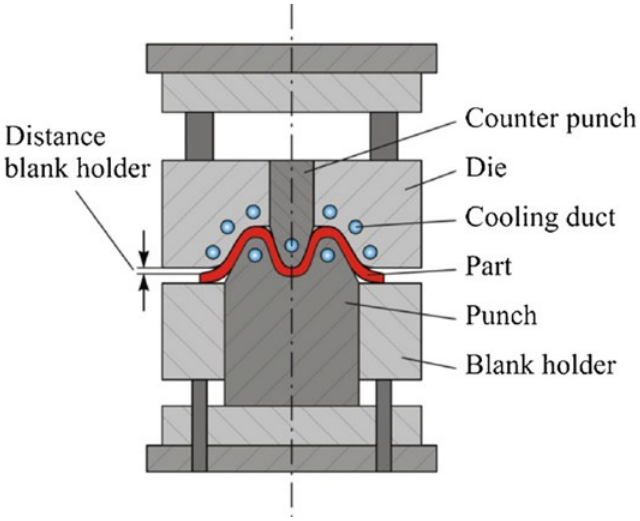

Figure 68. Tool design for the hot stamping process. [63]

Hot stamping with working media is another process variant. Hot gas formation and simultaneous quenching of the formed parts both use temperature as a process parameter. The forming step is carried out using the working media after the tool is closed as shown in Figure 69. The air could be the working medium with a pressure as high as 600 bar. The advantage of hot gas forming compared to traditional hot forming is the free forming of the part at the start of the forming process.

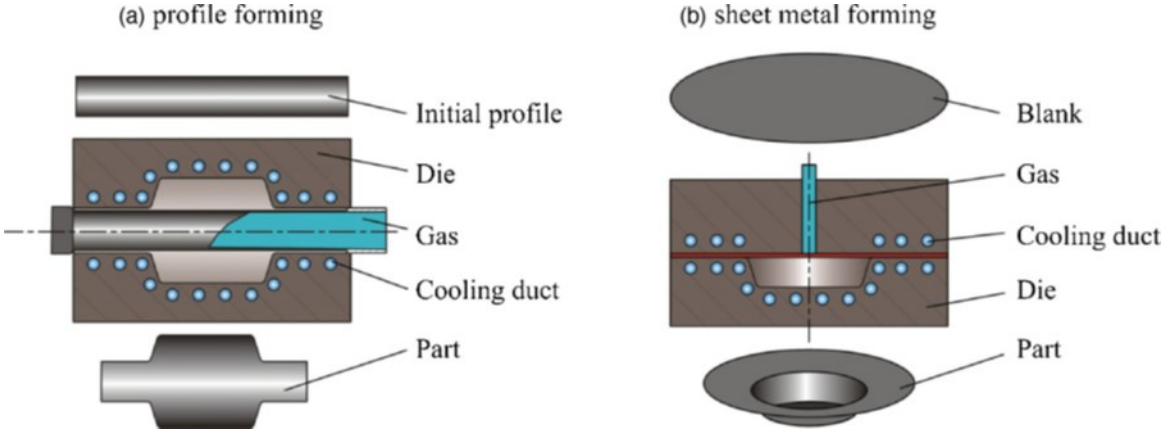

Figure 69. (a) Gas forming of profile and (b) sheet. [63]

The birth of the hot stamping process of high-strength boron steel meets the production development needs of the automobile industry. It combines hot forming and heat treatment in one process, greatly improving production efficiency and creating a precedent for the integrated forming process. Compared with the traditional cold stamping process, the hot stamping process has the following advantages: the material has good plasticity at high temperature, good ductility, high forming limit, low deformation resistance, high forming accuracy, small spring-back, and complex formable geometry. The parts after mold quenching have high strength, about 50% less weight than parts of the same strength level and excellent welding performance.

At the same time, there are also the following disadvantages: a special mold with a cooling system is required. The design is complex, and the processing cost is high. The surface of the heated

sheet is easily oxidized so that requires coating or gas protection. The manufacturing process requires heating and heat preservation energy consumption. The high strength of the stamped parts makes the subsequent processing difficult, and the cost of laser cutting is high and the efficiency is low.

4.2. Heat treatment and microstructure of hot-stamped steels:

4.2.1. Annealing(spheroidization) of hot-stamped steels:

The annealing process heats the strip above the recrystallization temperature, and cools it at a certain speed, together with a certain flat rate, so that the strip can obtain the required mechanical properties and surface structure. For hot-stamped steel, in order to meet the shearing and pre-forming (via the indirect hot stamping method) process before stamping, the hot-formed steel in the annealed state is required to have lower strength and good formability. This presents a challenge for steelmakers, because the product must have inherent strength to satisfy mechanical property specifications in hot-stamped parts.

The industrial production results show that when the annealing temperature is 700~800℃, the steel strip with excellent mechanical properties and surface can be obtained. The annealing process curve is shown in the Figure 70. Due to the high content of C, B and other elements in the hot-stamped steel, not only the annealing time is required to be prolonged, but also the B and Mn elements can improve the hardenability, which limits the cooling rate after annealing.

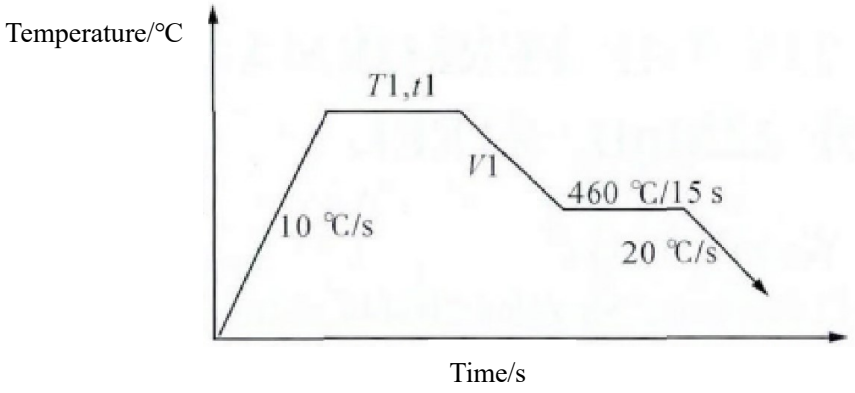

Figure 70. Continuous annealing curve of hot galvanizing. [64]

The structure perpendicular to the rolling direction is shown in the Figure 71. The A_{c1} temperature of 22MnB5 steel is about 740°C. When the annealing temperature is lower than A_{c1}, the ferrite recrystallized grains begin to form, however, the ferrite retains the thin rods or filaments that have been rolled along the rolling direction. With the increase of the annealing temperature, the matrix grains begin to grow and the ferrite recrystallization is carried out in a large amount until the recrystallization is basically completed. The pearlite has not obvious changes.

The structure after annealing at 740°C shows that there are fine grains at the recrystallized grain boundaries (see the arrow position in Figure 71(d)). As the annealing temperature continues to increase, the number of small grains in the structure is obviously increasing, and the grains are obviously refined. When heated above A_{c1}, the pearlite in the matrix dissolves and transforms into

austenite. During the subsequent cooling process, the austenite transforms into ferrite and bainite (or a small amount of martensite).

In addition, since the annealing at a temperature lower than A_{c1} requires a longer time to achieve better mechanical properties. If the annealing temperature is higher, the annealing time can be shortened, the production efficiency can be improved, and it is also convenient to switch between different steel grades during production, avoiding the use of transition coils and saving costs.

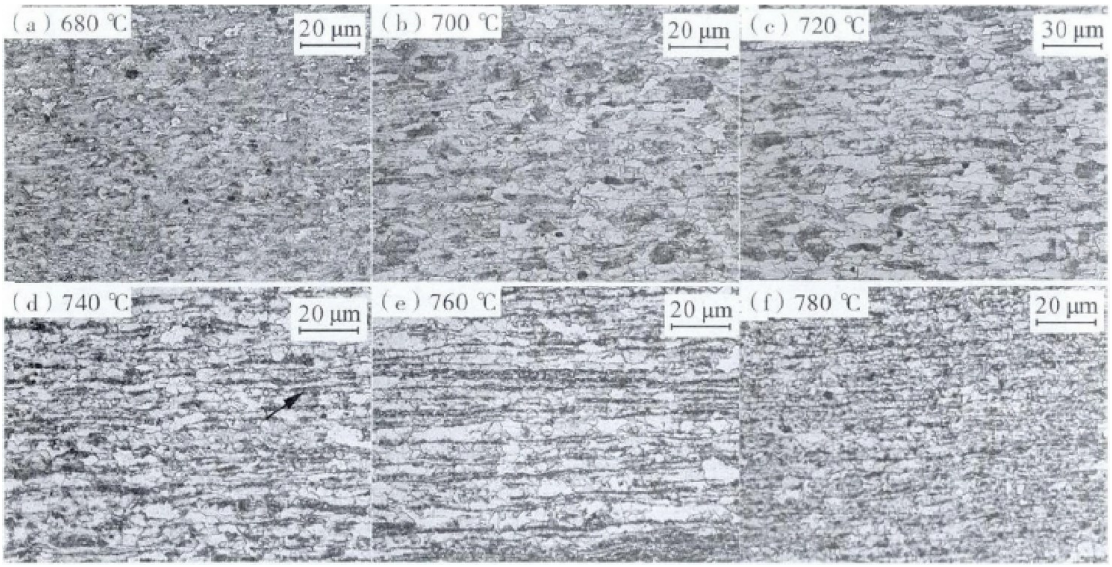

Figure 71. Metallograph structure after different annealing temperatures. [64]

The current demand for batch annealing has decreased while the demand for continuous annealing has increased. For many steelmakers, it is unimaginable to use batch annealing to produce a large amount of cold-rolled 22MnB5 steels to supply the now enormous hot-stamped sheet steel market. Therefore, cold-rolled 22MnB5 steels are mostly produced by continuous annealing routes and combined with pressure filling the continuous annealing lines to a maximum capacity (these cold rolled products might be insufficient in quantity and could only be produced by continuous annealing routes, such as DP and HSLA steels).

The continuous annealing route actually makes it more challenging to meet cold-rolled specifications because it promotes harder and more brittle fine ferritic–pearlitic or even bainitic products due to unfavorable process constraints, especially higher cooling rates. [65]

4.2.2. Quenching and tempering of hot-stamped steels:

The as-received blank sheet is first heated to above A_{c3} at about 900℃ in the furnace and kept for about 5 min to form a uniform full austenite structure. The manipulator transfers it to the press, and the temperature is 700~800℃ during clamping and stamping. At this time, it is the fully austenitic state. The cooling water system in the mold maintains the surface temperature of the mold at 50~100℃, and the heat-conducting quenching of the mold forms a full martensitic structure during stamping. The scheme of process described here is shown as Figure 72.

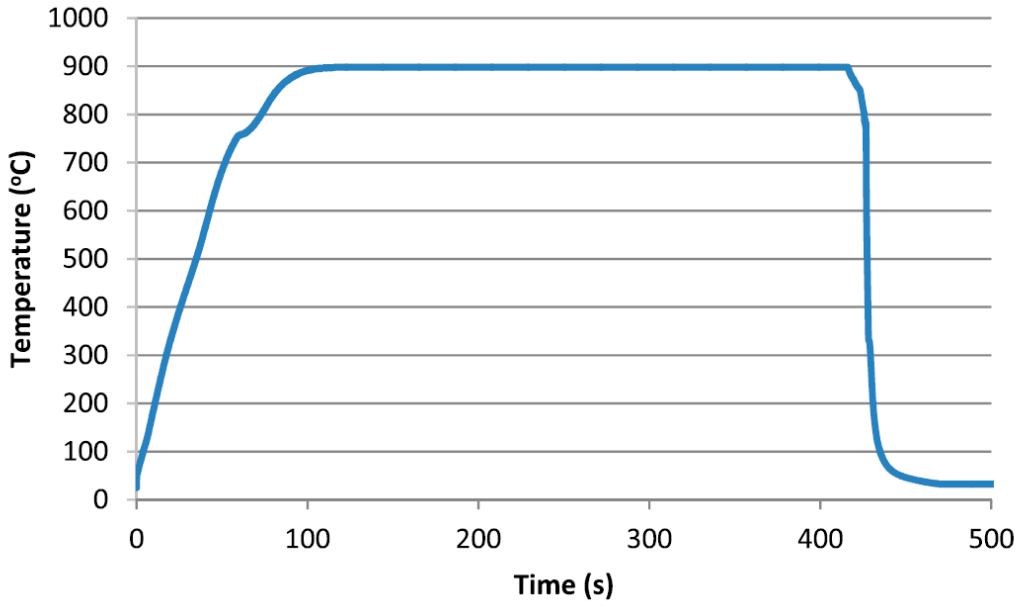

Figure 72. Thermal cycling of the direct hot stamping process for 22MnB5 steel. [65]

After the sheet steel is hot stamped and the final parts are welded and assembled, the body-in-white is painted and baked in the paint shop (between weld shop and assembly shop as shown in Figure 73.), and the temperature is kept at 150~180°C for 10~20 min. The baking process is actually a low temperature tempering of the parts to make the martensitic structure high strength steel have good elongation and fracture toughness at the same time, ensuring good deformation resistance and fracture resistance.

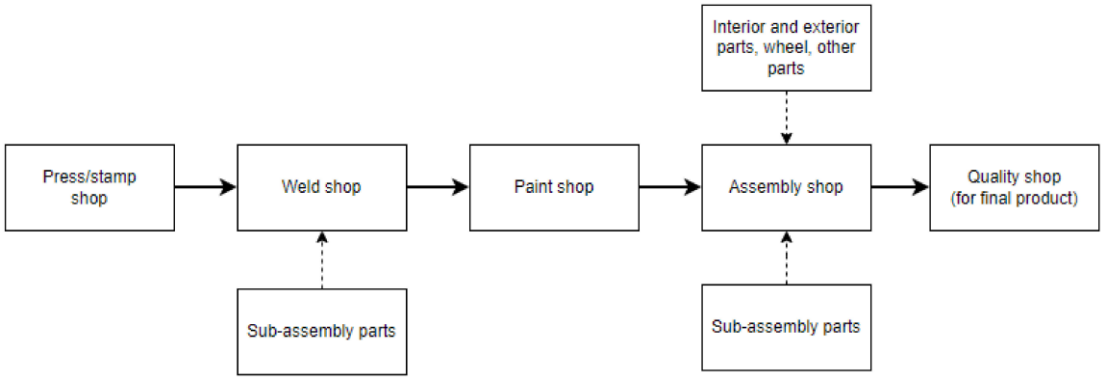

Figure 73. A general automotive manufacturing process. [66]

4.2.2.1. Structure of the as-quenched martensite of 22MnB5 steel:

It is revealed that the final quenching microstructure of the hot-stamped steels includes martensite, ferrite bainite and retained austenite under low cooling rate conditions while bainite and ferrite disappear gradually as the cooling rate increases.

The most innovative aspect of hot stamping technology is the ingenious combination of sheet hot forming and die quenching. However, the cooling rate of die quenching is much smaller than

that of water quenching. In order to obtain a complete martensitic structure, in hot stamped steel the critical cooling rate of martensitic transformation must be reduced, which makes martensitic transformation easier to occur.

Figure 74 shows the experimentally determined continuous cooling transformation diagram for 22MnB5 steel from which it could be seen that the critical cooling rate is -27℃/s. (A_{c3} is about 860℃ at this time) The martensitic transformation occurs at 425℃ (martensitic transformation start temperature M_s) and ends at 280℃ (martensitic transformation end temperature M_f). Due to the specific chemical composition of the material and the test method, the critical cooling rate of different boron steels is slightly different.

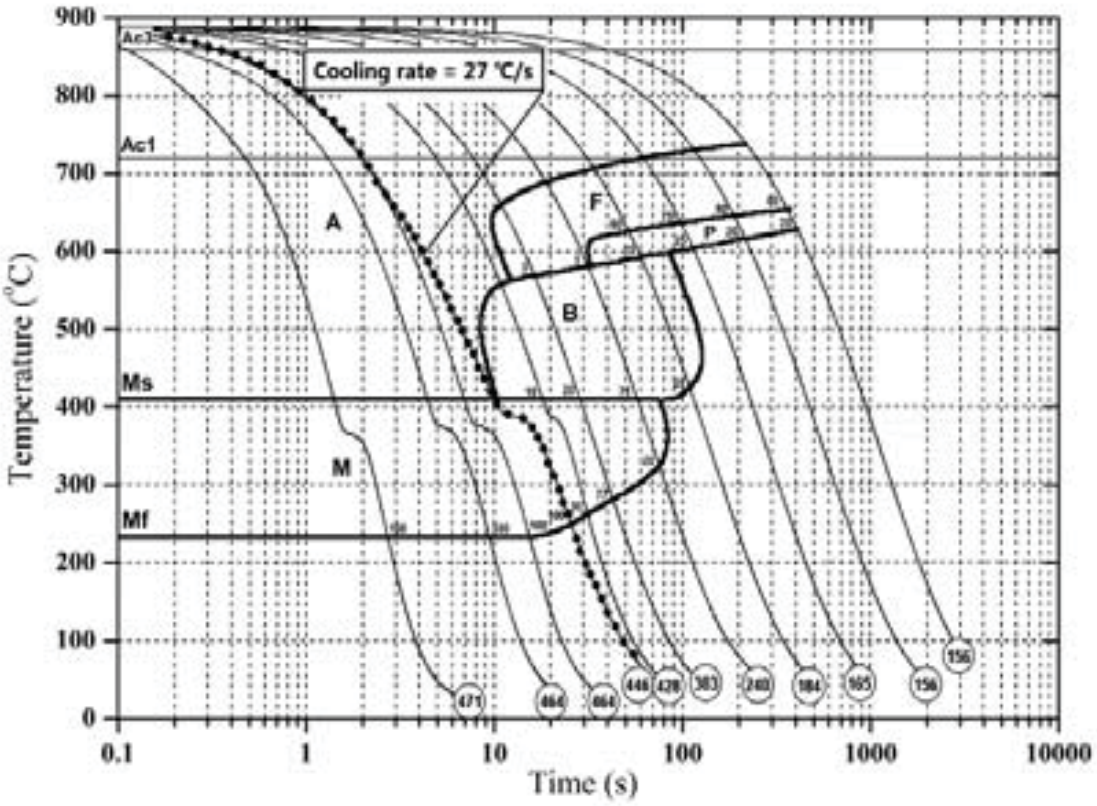

Figure 74. CCT Diagram of 22MnB5 Steel Austenitized at 900°C. [67]

Figure 75 shows the microscopic metallographic diagram of 22MnB5 before and after quenching. It can be seen that the microstructure of 22MnB5 before quenching is mainly ferrite and pearlite, and the microstructure after quenching is martensite. Due to the low carbon content (0.22%) of 22MnB5, low carbon lath-like martensite is mainly formed after quenching, and its microscopic substructure is dislocation structure. It can be seen that the key of 22MnB5 hot forming technology is to quench the sheet material at the same time of forming to obtain lath-like martensite, so that the substructure of its microstructure remains dislocation type, then the formed parts have both high strength and high toughness.

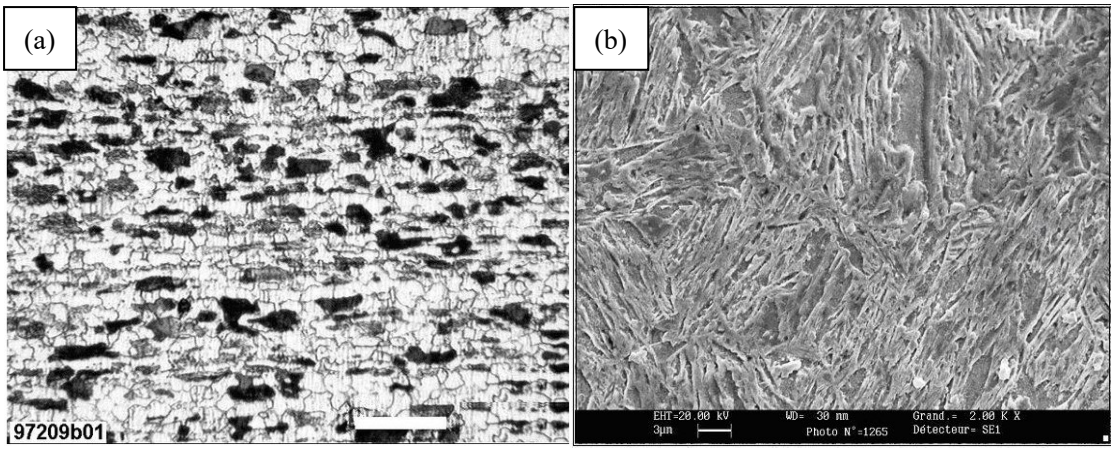

Figure 75. Microstructure of 22MnB5 steel (USIBOR 1500) (a) before hot-stamping heat treatment (as-delivered condition) and (b) after quenching. [68]

4.2.2.2. The effect of austenitisation on the structure of 22MnB5 steel:

The austenitizing process is the first step in most heat treatment processes, as well as the first step in the hot stamping process. The published data of high-strength hardenable boron steels that have been commercially produced are studied: the influence of heating temperature and holding time on microstructure and properties.

The target soak temperature is typically 850~950°C.The heating temperature is typically maintained for a holding time of 3~8 min (depending on coating and gauge) to ensure homogenous and complete austenisation, sufficient austenitic grain growth to improve hardenability and substrate-coating interlamellar alloying (depending on coating). But these data are definitely affected by the specific steel composition, sheet thickness and heating method.

Researchers from the University of Padova in Italy [69] studied the grain change law of 1.5mm thick 22MnB5 steel under different heating temperatures and holding times, and obtained a full austenitisation at 900 °C for 5 minutes (non-transformed ferrite is not present any more) without significant grain coursing as shown in Figure 76(b).

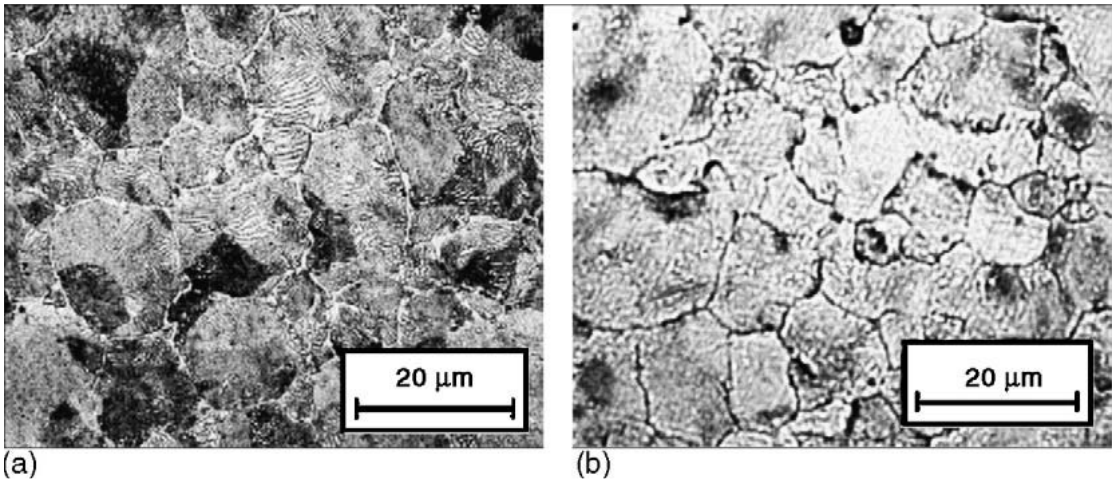

Figure 76. Micrographs of austenitized 22MnB5 steel: (a) after 5 min at 850 °C and (b) after 5 min at 900 °C. [69]

The specific grain size data are shown in Figure 77. When the austenitizing temperature is 850°C, the austenitic grains will first coarsen and then refine, while at 900 and 950°C, the austenitic grain size will increase before full austenitisation after holding for less than 5 minutes. After that, increasing the holding time will cause the grains to gradually become coarser, and the lower the austenitizing temperature, the more obvious the effect. In addition to holding at 900°C, the grain size increases to varying degrees at other austenitizing temperatures.

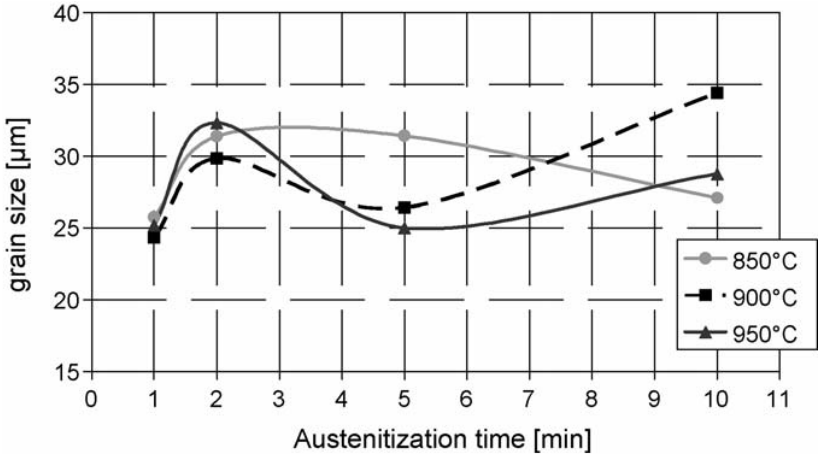

Figure 77. Austenitic grain size of quenched 22MnB5 steel after different austenitisation times and temperatures. [69]

It is also clear that the blank heated to a certain temperature and then immediately taken out of the furnace has not yet developed a homogenous microstructure as shown in Figure 78. The ferrite matrix's incomplete transformation is shown by the light spots in the micrograph. In the still visible prior austenitic grains, the resulting microstructure represented by the dark regions consists of needle-like structures indicating that martensite has been formed.

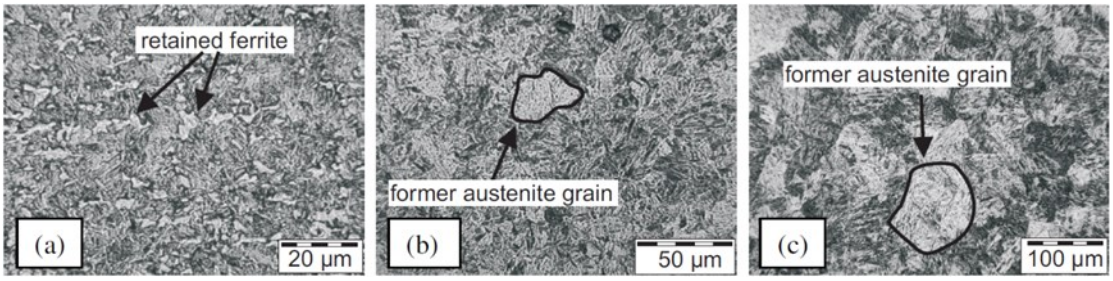

Figure 78. Micrographs of 22MnB5 steel austenitized in 950°C after (a) 0 min, (b) 4 min and (c) 50 min austenitisation time. [70]

The specimens which were exposed to the 4 min austenitisation consisted of martensite. Needle-like structures could be seen with some prior austenite grains still visible. The coarse structure does not appear to affect the phase transformation. The dispersed martensite structure is still formed.

After quenching, the microstructure of the specimen is almost all needle-shaped martensite, but after inspection, it can be found that there is a small amount of ferrite at the prior austenite grain boundaries.

In addition, it is found that prior austenite grain size refinement can effectively refine the

martensite packet and martensite block. [71] When the heating temperature is 1000℃, the microstructure of the specimen is close to 100% martensite structure, but the martensite grain size has grown significantly relative to 900℃. The reason is that under the condition of overheating, the grain boundaries of austenite grains undergo a certain migration under the action of a certain driving force, which leads to the growth of austenite grains and thus the growth of martensite grains.

Table 10 are the quantitative analysis data of the microstructure after quenching. It can be seen that the characteristic length of martensite austenitized at 1000°C is close to 20μm, while that at 900°C is about 10μm.

Austenitizing temperature / °C	Martensite fraction / vol%	Ferrite fraction / vol%	$\bar{L}_M$ / μm
900	90	10	11.4 ± 0.8
950	95	5	12.3 ± 1.3
1000	100	—	18.5 ± 2.7

Table 10. Quantitative metallographic data of 22MnB5 steel heated to different austenitizing temperatures. [72]

The austenitizing heating and holding time of high-strength boron steel sheet is a key factor affecting hot stamping. The heating temperature and holding time of the sheet all affect the microstructure of the hot stamping. From the metalogical point of view, the sheet metal has the best formability when it is in the state of uniform and fine austenite structure. At this time, the flow stress is low, the plasticity of the metal is good and the forming limit is high. When the heating temperature is too low or the holding time is too short, it is easy to cause incomplete austenitization of the sheet metal and there is a small amount of residual ferrite in the microstructure of the part after forming and quenching, so that the part cannot achieve the expected mechanical properties. On the contrary, if the heating temperature is too high or too long holding time, it may cause austenitic grains to grow resulting in coarse microstructure of the final part. If the sheet is not treated with anti-oxidation, surface decarburization will occur, affecting the surface mechanical properties of the part. Underheating and overheating have a great influence on the mechanical properties and microstructure of the final stamping parts, so it is of great significance to study the heating process and austenitizing transformation behavior of boron steel.

4.2.2.3. The effect of tempering temperature on the structure of 22MnB5 steel:

The Figure 79 shows the SEM microstructure of 22MnB5 steel at different tempering temperatures, the microstructure is tempered martensite and the martensite is lath-like. It can be seen that the lath bundle of tempered martensite does not change significantly in the range of 150~200℃ and the lath martensite structure is still clear. This is because when the low-carbon martensite is tempered below 200℃, the energy state of C atom segregation is lower than that of precipitation carbide, and C atoms are still segregated near the dislocation line. At the tempering temperature of 250℃, the martensitic lath bundles become blurred, and carbide precipitation was observed at the same time. The carbon content in the ferrite matrix decreased. When tempering at 300℃, the supersaturation of the matrix decreases. The lath bundles of the lath are no longer obvious

and if it is almost unobservable under OM, the supersaturated carbon precipitation of lath martensite during tempering causes the matrix lattice structure to transform into ferrite between body-centered cubic (BCC) and body-centered tetragonal (BCT). Between the ferrite, the morphology of martensite is still maintained, and fine carbide particles are precipitated.

When the tempering temperature increases, the interface between the lath bundles is also difficult to identify, and the carbon content in the martensite decreases continuously. The carbides precipitate, aggregate and grow. The solid solution strengthening effect is also reduced.

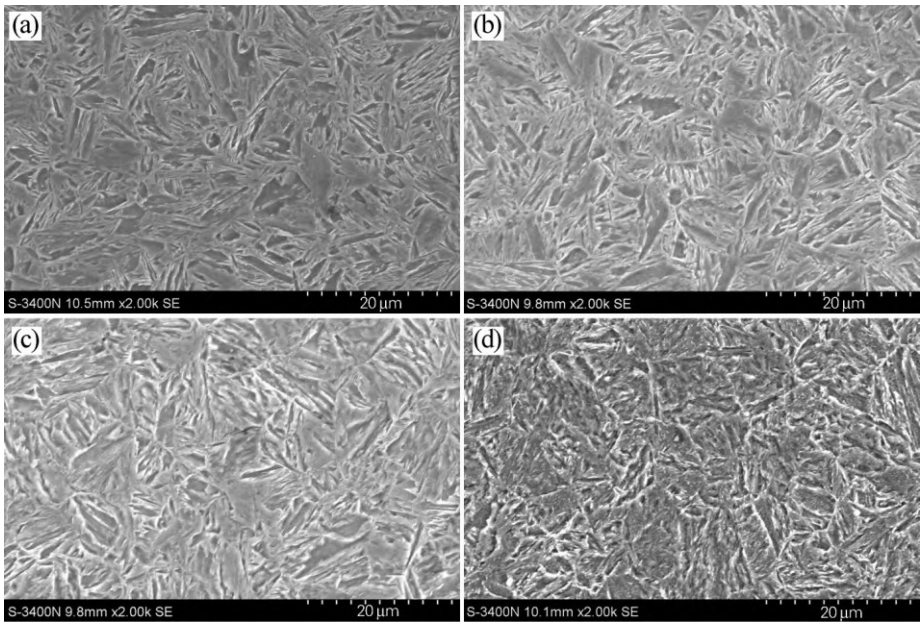

Figure 79. SEM morphologies of the 22MnB5 steel tempered at different temperatures (a) 150℃; (b) 200℃; (c) 250℃; (d) 300℃. [73]

Figure 80 shows the TEM image of 22MnB5 steel at a tempering temperature of 150℃. When the tempering temperature is between 150 and 300℃, the microstructure of 22MnB5 steel is lath martensite, and the mechanical performances are best at 150℃. There are a large number of high-density dislocations in the material and the higher the dislocation density, the stronger the plastic deformation resistance of the material. Through the observation and analysis of TEM structure, it is found that when tempering at 150℃, the second phase structure is obviously precipitated in the martensite lath. Figure 80 (b) and (c) show the bright and dark field TEM images of the second phase. TEM observation showed that the size of the second phase is small and dispersed, with a length of about 30 nm.

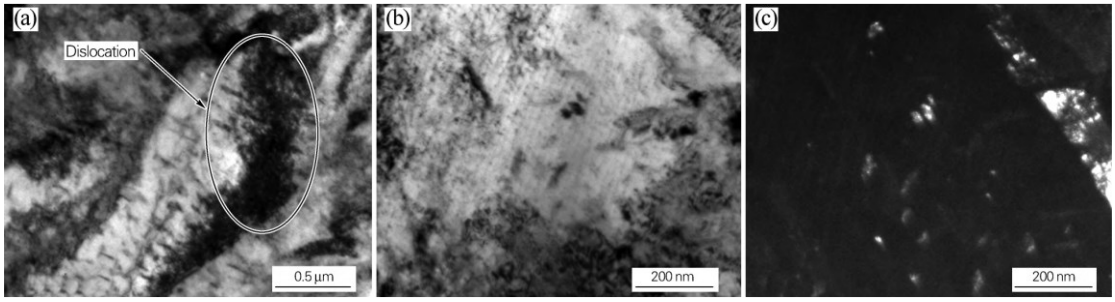

Figure 80. TEM images of the 22MnB5 steel tempered at 150℃ (a) dislocation; (b) bright field image of the second phase; (c) dark field image of the second phase. [73]

After tempering at high temperature, the precipitated cementite begins to aggregate and coarsen. At this time, the small carbide particles are dissolved, and the large carbide continues to deposit and grow. After tempering, the length of some acicular carbides increases to above 500 nm. When the tempering temperature is above 400°C, some martensitic laths have recrystallized as shown in Figure 81 to form quasi-polygonal ferrite. Although part of the lath-like martensite fine structure can be seen, the lath interface is obviously diluted and there are no high-density dislocations inside. The martensite after high temperature tempering is fully recovered and partially recrystallized and the martensite is desolubilized and decomposed without supersaturated carbon (a large amount of carbides are precipitated). The non-equilibrium structure of the quenched state turns to subequilibrium or partial equilibrium state.

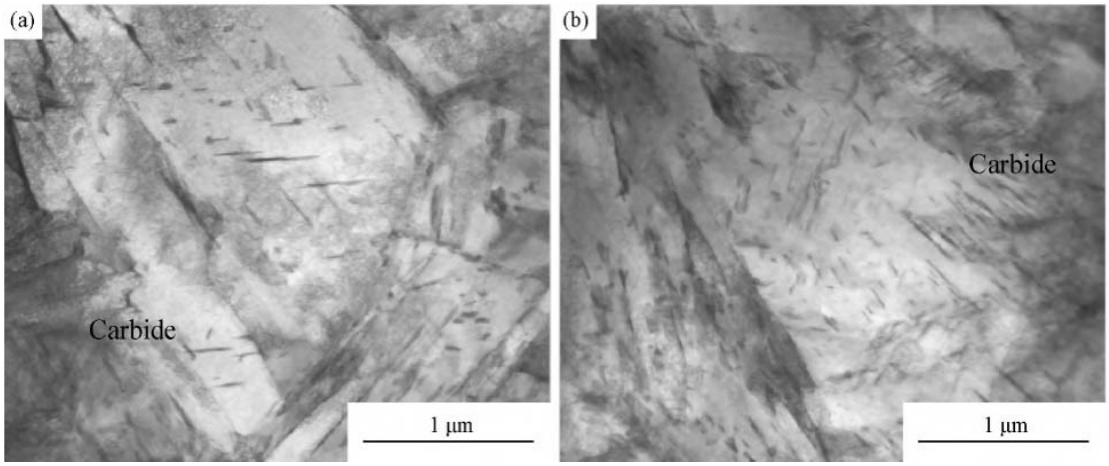

Figure 81. TEM images showing microstructure of the 22MnB5 steel tempered at high temperatures (a) 400℃; (b) 600℃. [74]

In short, with the increase of tempering temperature, the recovery degree of martensite lath increases, dislocation slip and offset become more severe. Lath martensite gradually evolves from supersaturated metastable state to equilibrium state. The martensite boundaries are widen by merging and engulfing each other and the dislocation defects gradually disappear which the softening of tensile strength is pronounced.

4.3. Mechanical properties of hot-stamped steels：

4.3.1. Hardness:

The hot stamping process transforms the structure of the high-strength boron steel from austenite to martensite, so that the stamping parts are hardened. The surface hardness of the parts can exceed 500 HV. Its hardness is second only to ceramics, but it still has the toughness of steel.

The hardness of the 22MnB5 steel in the as-delivered condition investigated is about 150 HV. When the hardness is over 450 HV, a fully martensitic structure is assumed, while from 200 HV to 450 HV, a heterogeneous structure consisting of ferrite, martensite, bainite, and other phases is assumed. Figure 82 shows the soaking hardness of 22MnB5 steel at different austenitizing

temperatures. At 900°C the peak hardness occurs.

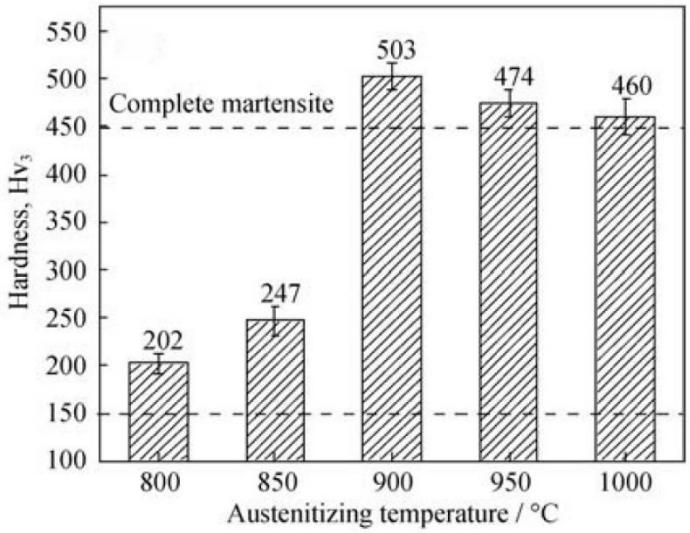

Figure 82. Vickers hardness of 22MnB5 steel heated to different austenitizing temperatures. [72]

Because when the heating temperature reaches 900°C, the structure can be fully austenitized and avoid overheating which could result in coarse austenite grains and coarse martensite grains thus reduction in hardness and other mechanical properties. Hence the actual heating temperature during production is also around 900°C.

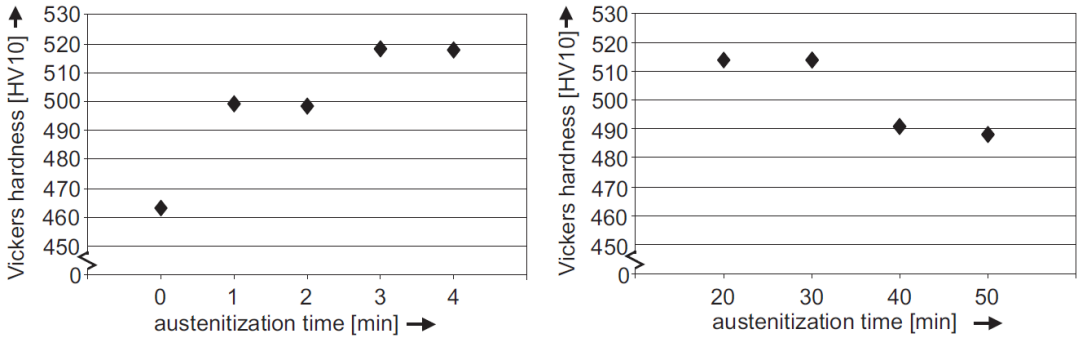

Figure 83. Vickers hardness results at different austenitisation time. [70]

Figure 83 shows the dependency of the Vickers hardness on the austenitisation time. It could be seen that the hardness increases with increasing austenitisation time. In terms of hardenability, austenitisation time of three to four min should be kept to a minimum. Austenitisation times of 20 min or more result in a hardness reduction. The full austenitisation time is bounded to be at least 3 or 4 min but not more than 20 min. The reason is that the ferritic matrix is not transformed into a homogeneous austenitic matrix at the shorter austenitization time. Longer time causes grain growth, which results in lower hardness.

A semi-empirical formula is shown in Figure 84 which indicates the relationship between soaking time and hardness and other mechanical properties. The increase of martensite volume fraction makes the curve go up first, and then the increase of grain size makes the curve drop.

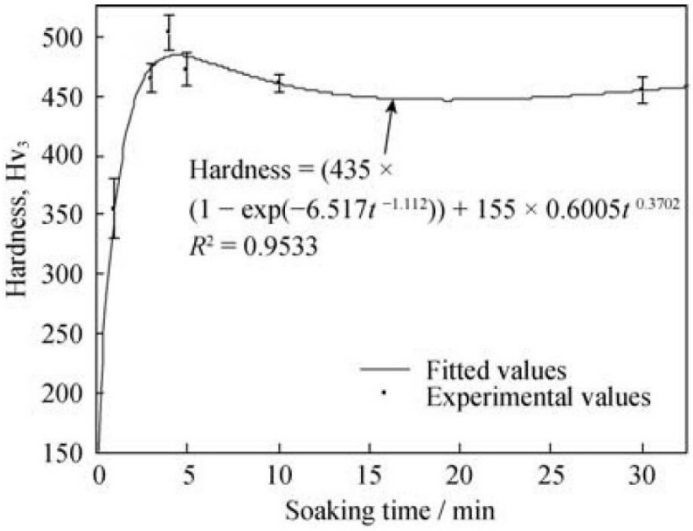

Figure 84. Semi-empirical formula between soaking time and hardness. [72]

With the increase of tempering temperature, the hardness of 22MnB5 steel decreases significantly. The tempering process is actually the process of martensite decomposition, and it is also the desolubilization of supersaturated solid solution carbon from ferrite and the formation of carbides. The higher the tempering temperature, the more fully the martensite decomposes and the more fully the growth of the decomposition products. Combined with the microstructure before, it can be seen that the tempered products are all tempered martensite. With the increase of tempering temperature, carbide precipitation increases, and the solid solution carbon in ferrite decreases which makes carbon solid solution strengthening effect weaken thus the hardness decreases.

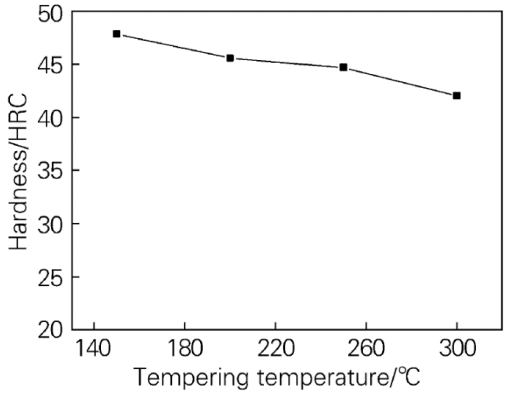

Figure 85. Effect of tempering temperature on hardness of the 22MnB5 steel. [73]

4.3.2. Strength vs. ductility:

In order to ensure crash safety, automotive components made of hot stamped steels need to have sufficient resistance to collision intrusion to ensure that the components are deformed within the allowable range to prevent occupants from being injured. At the same time, with good deformability the energy brought by the collision is absorbed. The scholars revealed that the impact

resistance force (F_{av}) of the steel sheet is positively correlated with the tensile strength (σ_U) and the thickness of the steel plate (t): [75]

$$F_{\mathrm{av}} = K \cdot E^{0.4} \cdot \sigma_{\mathrm{U}}^{0.6} \cdot t^{1.8}$$

where K is a constant and E is the elastic modulus. It can be seen from formula that under the premise of ensuring the original energy absorption, the thinning of the part can be achieved by increasing the strength of the material.

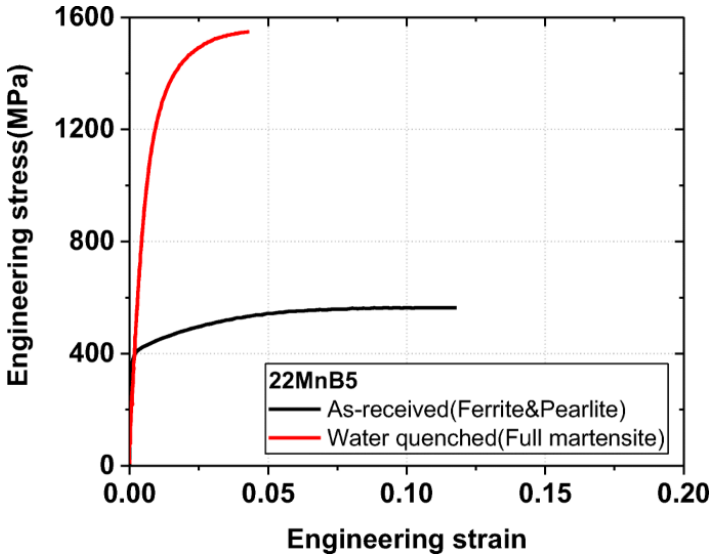

Figure 86. Stress-strain curves of as-received and water-quenched 22MnB5 sheet. [76]

Typical stress-strain curves of 22MnB5 sheets before and after hot stamping are shown in Figure 86. It can be seen that the tensile strength of 22MnB5 before quenching is only about 500MPa, and the tensile strength after quenching is increased to about 1500MPa. The strength after quenching is about 3 times that before quenching. The strength is significantly improved. At the same time, the elongation of 22MnB5 steel is greatly reduced from the original close to 12% to 4%, and the hardening index is also reduced indicating that after quenching the ductility of 22MnB5 steel decreases. The hardness increases, and it is extremely difficult to stamping. The hot stamping technology can realize the precise forming of 22MnB5 steel and quench it at the same time and obtain complex high-strength parts, thus solving the contradiction between high strength and poor formability.

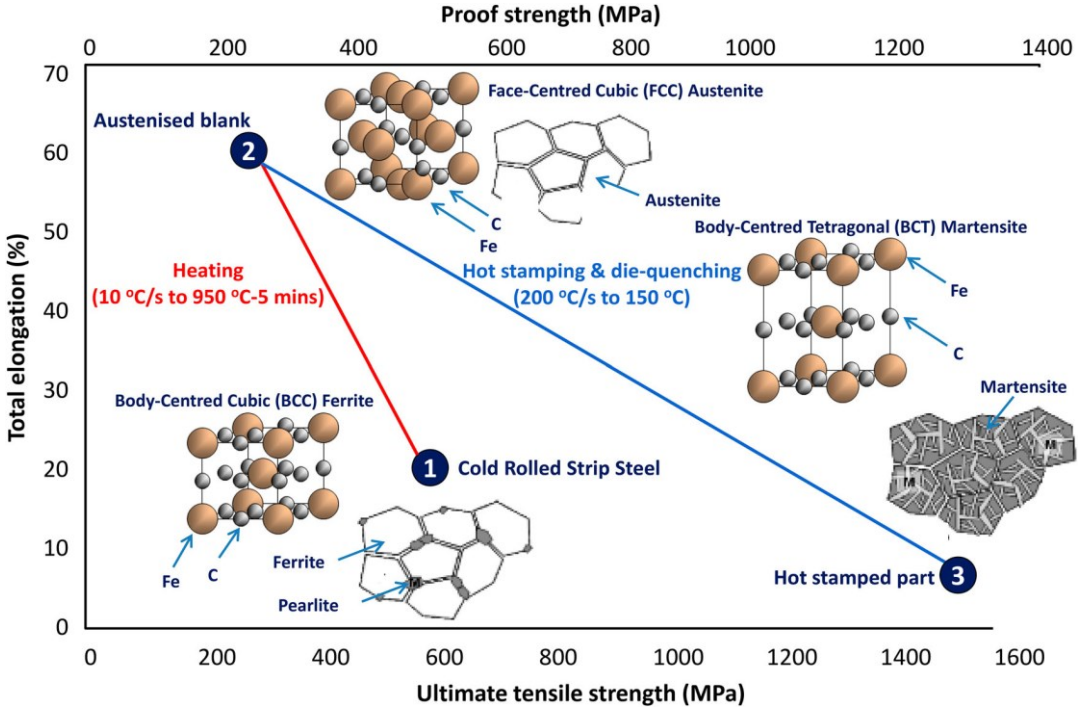

Figure 87. Scheme of tensile strength versus total elongation showing the transient mechanical properties and the microstructural evolution during hot stamping. [65]

Work hardening which exists in cold forming can be eliminated by (dynamic) recrystallization during hot forming. The FCC crystal structure of austenite dominates the microstructure above the A_{C3} temperature. As shown in Figure 87, the FCC crystal structure of austenite exhibits preferential slip when compared to the BCC crystal structure of ferrite due to the presence of close-packed planes. All of these factors combine to reduce yield strength, increase ductility, increase plastic isotropy and consequently increase formability significantly during hot forming. At each stage of the process: from softn and ductile during the forming to extremely hard in the final part, hot stamping enables the steel to keep in the optimal microstructural state and to show the optimal mechanical properties.

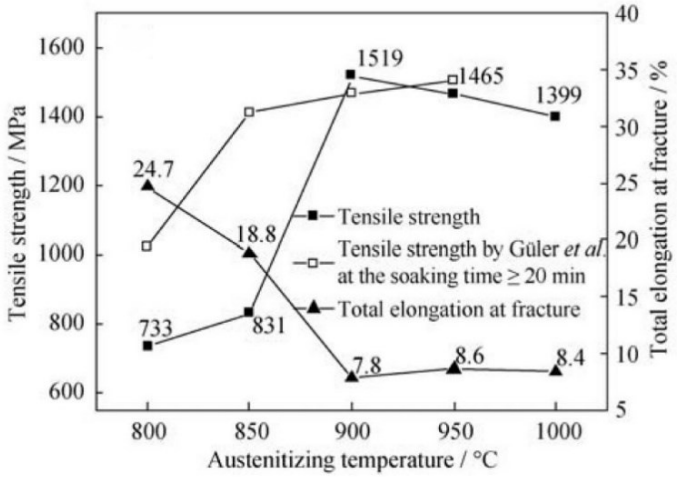

Figure 88. Tensile strength and elongation of 22MnB5 steel heated to different austenitizing temperatures. [72]

Figure 88 shows the tensile strength and total elongation at fracture of specimens heated to different austenitizing temperatures. The total elongation at fracture decreases with increasing austenitizing temperature while the tensile strength initially increases and then decreases with increasing austenitizing temperature. At 900°C, which is a watershed of austenitizing temperature, the maximum tensile strength also occurs. Tensile strength and hardness have the similar tendency with respect to austenitizing temperature, suggesting that these two properties are controlled by the same determinants.

If the temperature is less than 900°C, as the austenitizing temperature increases, the tensile strength dramatically increases and the total elongation at fracture remarkably decreases. On the contrary, the tensile strength slightly decreases as the austenitizing temperature further increases, and the change in total elongation at fracture is small.

If the soaking time is longer than 20 min, an austenitizing temperature of 850°C could also achieve high strength. Due to the different thickness and chemical composition of blanks, the optimal temperature and time for austenitisation must be carefully chosen.

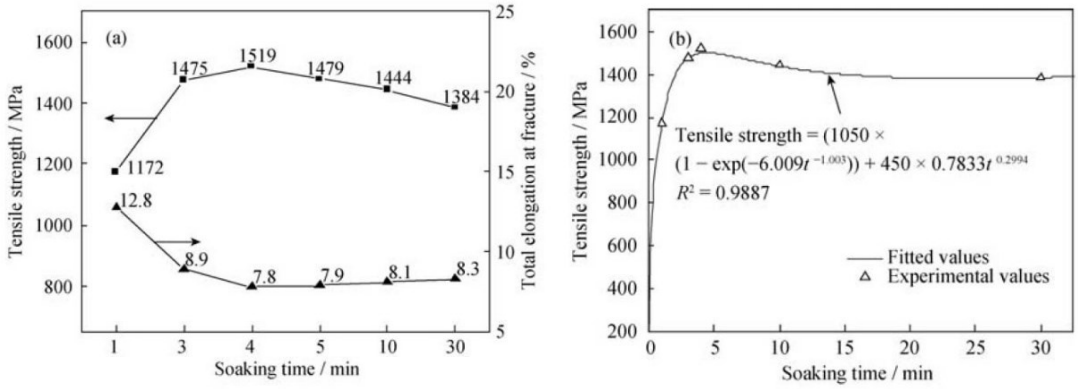

Figure 89. (a) Tensile strength and elongation of 22MnB5 steel after different soaking time. (b) Semi-empirical formula between soaking time and tensile strength. [72]

Figure 89 shows the tensile strength and elongation of specimens that were soaked for different time along with its fitting curve. When the specimen is soaked for less than 4 min, the tensile strength increases dramatically with increasing soaking time and decreases gradually with increasing soaking time when the specimen is soaked for more than 4 min.

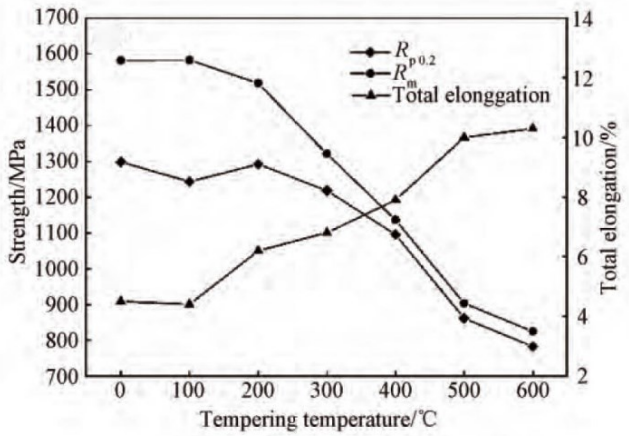

Figure 90. Tensile strength and elongation of 22MnB5 steel at different tempering temperatures. [74]

It can be seen from Figure 90 that with the increase of tempering temperature, the tensile strength gradually decreases, and the total elongation gradually increases. The yield strength does not decrease monotonically with the increase of tempering temperature, but first decreases. After tempering at 200℃, it increased slightly. When the tempering temperature exceeds 200℃, both the tensile strength and the yield strength decrease significantly. When tempered at 100℃, the tensile strength and elongation did not change greatly, and the tensile strength was basically the same as that of the quenched sample, which is near 1600 MPa, and the elongation was extremely low. After tempering at high temperature, the tensile strength decreased significantly to even lower than 1000 MPa, but the total elongation could increase to over 10%.

Therefore, by comprehensively comparing the mechanical properties at each tempering temperature, it can be found that when the tempering temperature is 200°C, the strength has no significant change compared with the quenched case. The ductility is significantly improved and the comprehensive mechanical properties meet the requirements for the use of automotive structural parts after hot forming or anti-collision bars after high-frequency induction heating and quenching.

4.3.3. Fracture toughness:

The microstructure uniformity and phase composition of hot-stamped steel will change greatly at different temperatures, and the performance indicators such as strength and toughness will be greatly different. In addition, safety components, as the core components of automotive passive safety systems, have complex load-bearing characteristics. The materials selected not only require good strength and ductility matching, but also have relatively excellent fracture toughness.

At present, the K_{IC} method has high requirements on the thickness of the sample, and the ultra-high strength steel sheet with a thickness of 2~3mm cannot meet the test requirements. Among the methods used at this stage, the K_{IC}-type fracture toughness has a strong linear correlation with the tear test results, which can well reflect its fracture failure mode.

The fracture toughness of 22MnB5 steel is characterized by Kahn tear test, mainly based on three parameters: tear strength (TS), initiation energy (IE), and propagation energy (PE). Due to the different thickness of different materials, the unit crack initiation energy UIE and the unit crack propagation energy UPE are generally used as indicators to measure the fracture toughness, and the relevant calculation formula and the curve is shown in the Figure 91.

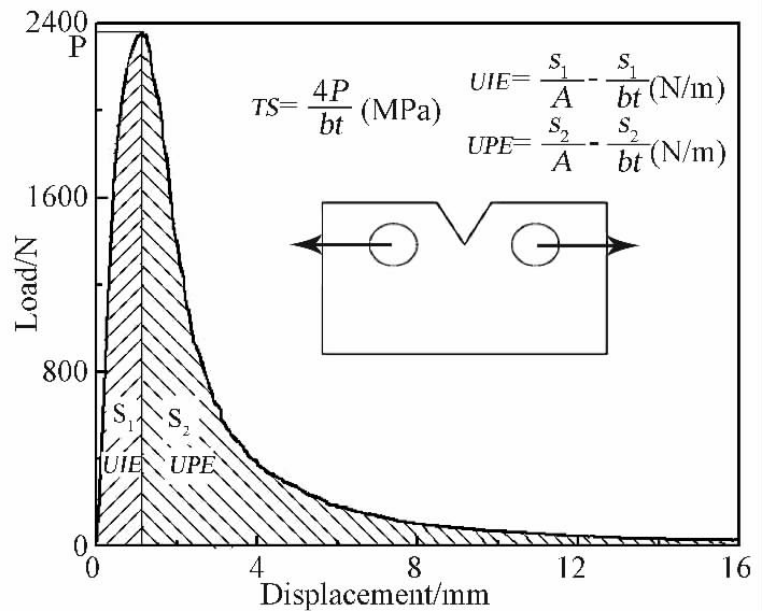

Figure 91. Diagram of Kahn tearing test method in Force-Displacement curve. [77]

Among them, P is the maximum applied load, A is the effective cross-sectional area of the sample, b is the minimum width at the notch of the sample, t is the thickness of the sample. UPE is directly and linearly related to fracture toughness K_{IC}^2, so by comparing the change trend of UPE at different temperatures, the change of corresponding fracture toughness can be obtained.

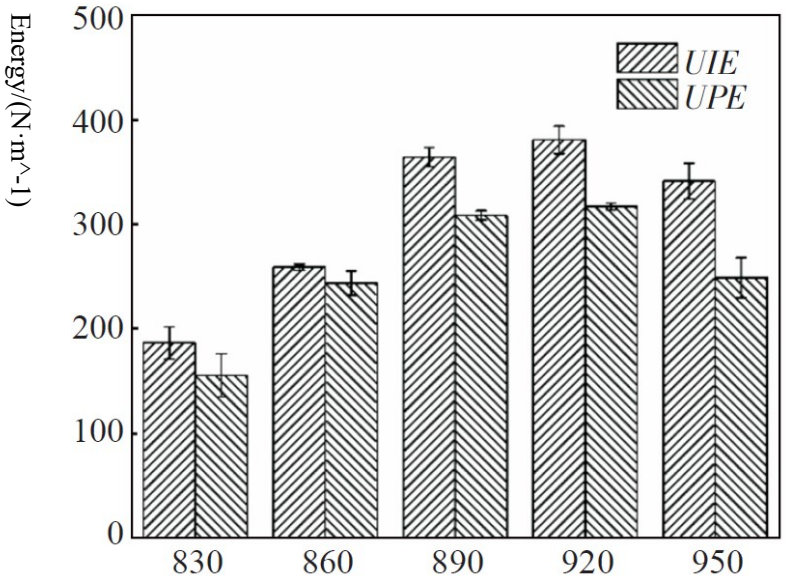

Figure 92. Changes of tear property parameters of 22MnB5 steel at different austenitizing temperatures. [78]

Figure 92 shows the change of tear properties of 22MnB5 steel at different austenitizing temperatures. It can be seen that after heat treatment, 22MnB5 steel is affected by the coupling effect of the increase of martensite content (ductility reduction) and grain refinement (ductility increase). The UIE and UPE reach peaks when quenched at 920°C, and both showed a trend of first increasing

and then decreasing, which matched the change trend of strength-ductility product. When the austenitizing temperature continues to increase, the martensitic laths become coarse and the amount of retained austenite increases resulting in a decrease in UPE. Since the fracture toughness has a direct linear relationship with the UPE, the change trend of the UPE is exactly the same as that of the fracture toughness. Therefore, in terms of fracture toughness, when the austenitizing temperature is 920°C, the fracture toughness of the corresponding 22MnB5 steel is the highest, which is consistent with the change of ductility with austenitizing temperature.

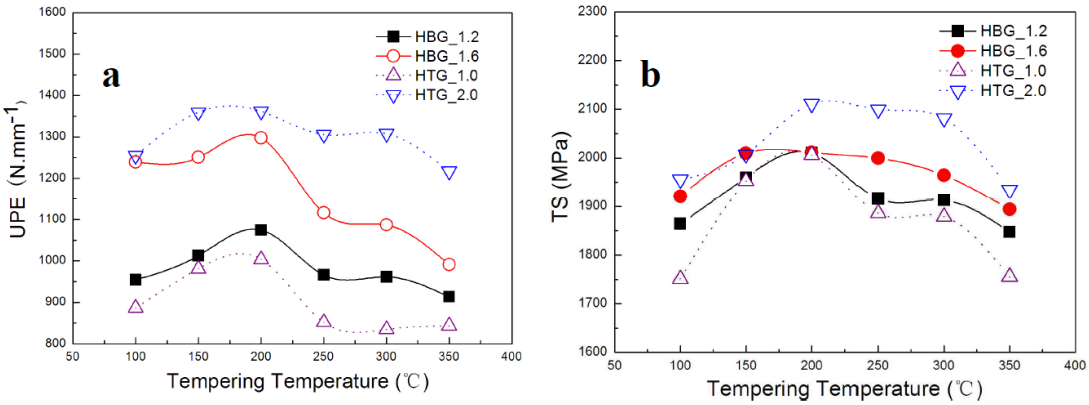

Figure 93. Effect of tempering temperature of high strength steels on (a) UPE and (b) TS. [77]

After different tempering processes, the fracture toughness of hot-stamped 22MnB5 steel has been improved, and the UPE and TS of samples with different thicknesses have different degrees of change but have the same trend. As the thickness of the samples increases, the Kahn specimen will store higher elastic energy, and the UPE and TS of the hot-stamped samples will also increase resulting in an increase in fracture toughness.

In the range of 100 ~ 200℃, with the continuous increase of the tempering temperature, the UPE and TS of the samples also increased as shown in Figure 93. This is because the tempering temperature is in the range of 100~200℃, by continuously increasing the tempering temperature, the lath martensite will be increased and the twinned martensite will be reduced or eliminated so as to improve the UPE and TS of the sample. According to the Cottrell air mass theory, a large number of dislocations in the quenched 22MnB5 steel structure do not disappear during low temperature tempering. Under the external force, the dislocations still have a certain migration ability, making it difficult to produce cracks. Therefore, the fracture toughness and strength of steel increase with increasing tempering temperature.

In the range of 200~350℃, with the continuous increase of tempering temperature, the UPE and TS of 22MnB5 steel decreased. When the sample was tempered at 200℃, its UPE and TS both reached the peak value. The main reason is that carbides are precipitated from martensite. With the increase of precipitates, the retained austenite also begins to decompose and a brittle cementite film is formed on the grain boundary, which makes the grain boundary brittle. Under the external force, the tendency of brittleness to fracture along the grain boundary increases which increases the difficulty of dislocation movement. Hence the fracture toughness and strength of 22MnB5 steel decrease with the increase of tempering temperature, which also significantly reduces the UPE and TS of the sample. When the tempering temperature is too high, the strength loss is not conducive to the improvement of the fracture toughness of hot-stamped 22MnB5 steel. Therefore, a properly

designed tempering treatment can significantly improve sheet strength and fracture toughness.

4.3.4. Cold bending properties:

The vast majority of automobile body structural parts undergo bending deformation during the collision process and the deformation state of the components is close to plane strain bending. The crash properties of hot-stamped steel components are related to their flexural properties under plane strain.

In the VDA 238-100 three-point bending test standard developed by the German Automobile Industry Association, the width of the steel plate with bending deformation is much larger than its thickness and the radius of the bending punch is extremely small resulting in the steel plate still under the stress state of plane strain. Because of this, this method is widely used in the automotive industry to quickly measure the fracture strain of hot-stamped steel.

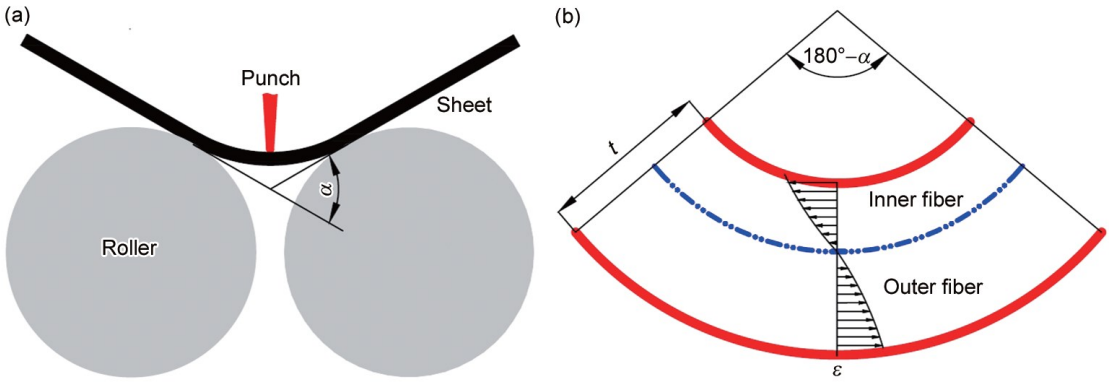

Figure 94. (a) Scheme of VDA 238-100 bending process and (b) strain state during bending (α, ε and t represent bending angle, principal strain in the circumferential direction and sheet thickness, respectively). [79]

Figure 94 (a) is a schematic diagram of the bending of VDA 238-100, where α is the bending angle. During the bending process, the inner layer of the material is subjected to compressive stress and the outer layer of the material is subjected to tensile stress as shown in Figure 94(b). When the bending load reaches the peak value, the outer surface of the material is affected by the tensile stress and begins to crack and the bending angle at this time also reaches the maximum value (that is, the maximum bending angle α_{max}). Since α_{max} can evaluate the bending properties of materials, many automobile companies in the world use α_{max} and tensile properties as indicators to measure the mechanical properties of materials. In addition, when the bending angle is α_{max}, the strain on the outer surface of the material reaches the maximum strain value that it can withstand without breaking under the condition of plane strain, that is, the bending fracture strain. Compared with α_{max}, the bending fracture strain (the equivalent strain on the outer surface of the material corresponding to α_{max}) can more directly evaluate the fracture limit of the material under the condition of plane strain. The result can be directly used as the fracture limit strain of the material for CAE of the whole vehicle collision analysis. It has become an important parameter to judge whether the component has crashed and failed. A higher α_{max} signifies that the material has a higher flexural rupture strain. Therefore, improving the α_{max} of hot-stamped steel has also become

one of the key directions of the current hot stamping steel development.

4.4. Recent advances in hot-stamped steels:

In the past 20 years, the development of hot-stamped steel is mainly reflected in three aspects: First, on the basis of the original hot-stamped steel, by adjusting the C content, either high strength is pursued, but it will lead to reduced toughness, or high toughness is pursued but C needs to be reduced. strength to achieve. Second, by adding micro-alloying elements such as Nb and V, dispersed nano-precipitated phases are introduced into the martensite matrix and the toughness is improved by refining the grains. In addition, these nano carbides act as hydrogen traps and can improve the hydrogen embrittlement resistance of hot-stamped parts. The third is to design new grades for example steel suitable for quenching and partitioning (Q&P) treatment by appropriately adjusting the composition of existing hot-formed steels to achieve the goal of high strength and high toughness.

4.4.1. New steels by adjusting the C content:

The C element is the most commonly used element for improving the strength of steel materials. The C content of the existing hot-stamping steel is generally less than 0.4%. As the C content increases, the strength of the steel also increases. But too high C content will also bring a series of problems. For example, the ductility and weldability of the steel will deteriorate. In addition, with the increase of C content, the martensite transformation temperature M_S decreases continuously.

Based on 22MnB5, the researchers increased its C content to 0.33%, and the tensile strength after quenching could reach 2000 MPa, but its elongation after fracture was only 2.5%. [80] In fact, 1800 and 2000 MPa grade hot-stamped steels for example 34MnB5 and 37MnB4 generally have low toughness problem. Therefore, simply increasing the C content in the steel to improve the strength of the hot-stamped steel will inevitably lead to a substantial decrease in its toughness and ductility, which cannot achieve the purpose of reducing the weight of automobiles.

For the parts of the car body that require high toughness, major steel mills and hot stamping enterprises have developed corresponding high-toughness and low-strength hot-stamped steels by decreasing the C content. The tensile strength of these hot-stamped steels is about 500 MPa, but the total elongation can reach 20%, and the composition is shown in Table 11. The existing Ductibor1000 steel has a tensile strength of not less than 1000 MPa, a total elongation of more than 6%, and a cold bending angle of not less than 80°.

Commercial name	Steelmaker	C	Si	Mn	P	S	Al	Nb	Fe
Ductibor 500	ArcelorMittal	0.05~0.08	< 0.5	< 1.4	< 0.03	< 0.01	0.02~0.04	0.03~0.07	Bal.
MBW 500	ThyssenKrupp	< 0.10	< 0.35	< 1.0	< 0.03	< 0.025	> 0.015	< 0.1	Bal.
PHS-Ultraform 490	Voestalpine	< 0.11	< 0.5	< 1.4	< 0.03	< 0.025	< 0.015	< 0.1	Bal.

Table 11. Grades and chemical compositions of high ductility and toughness steels with strength of 500 MPa. [62]

4.4.2. New steels adding micro-alloying elements:

In order to solve the problem of inversion of strength and toughness, some researchers try to improve the strength of hot-stamped steel through composite strengthening mechanism, so as to avoid the damage of toughness caused by single strengthening mechanism. Based on the alloy composition of 22MnB5, a new-generation hot stamping steel 34MnB5V with V micro alloying was designed. While increasing the C content from 0.22% to 0.34%, 0.11%~0.30% V was added.

The VC precipitation particles can pin the austenitic grain boundaries, inhibit the growth of the grains, and refine the austenitic grains and the substructure size of the martensite lath group and lath bundle after quenching. Figure 95(a) and (b) are the prior austenite grain boundaries of 22MnB5 and 34MnB5V heated at 900°C for 4 min, respectively. The average grain size of prior austenite in 22MnB5 is 8.7μm, while that in 34MnB5V under the same heating conditions is 3.9 μm. As shown in Figure 95(c) and (d), observed by TEM, the microstructure of 34MnB5V after quenching is lath martensite, and a large number of VC precipitation particles of 5~20 nm are dispersed in the martensitic lath.

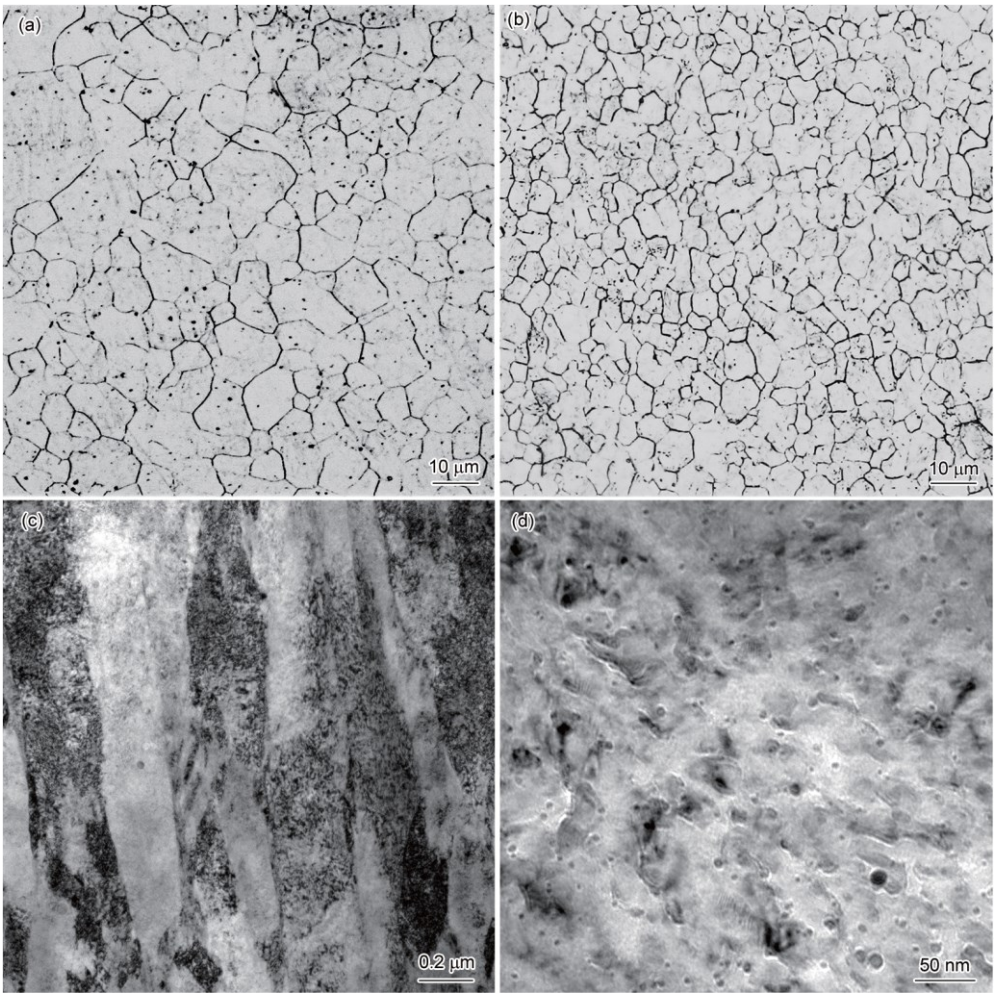

Figure 95. (a) Prior austenite grain boundaries of 22MnB5 steel and (b) 34MnB5V steel austenitized at 900℃ for 4 min, and (c) TEM images of quenched lath martensite and (d) VC precipitation particles in 34MnB5V steel. [81]

According to the alloy design of 34MnB5V, only a part of the V element is in solid solution at 900℃ through the calculation of the solid solubility product. Therefore, most of the nano-VC in the initial structure will not dissolve during the short-term heating process of austenitisation. The addition of Ti to the hot-stamped steel ensures that the solid solution B improves the hardenability. The thermodynamic stability of the composite carbide formed by V and Ti will be further improved and a large number of nano-VC particles are dispersed in the austenite and finally retained in the martensite.

Studies show that when the C content in martensite exceeds 0.3%, a large amount of twinned martensite will be formed, which will seriously deteriorate the fracture resistance of steel. [82] Although 0.34% C was added to 34MnB5V, the precipitation of VC reduced the C content in the martensite, so the formation of twinned martensite was effectively suppressed.

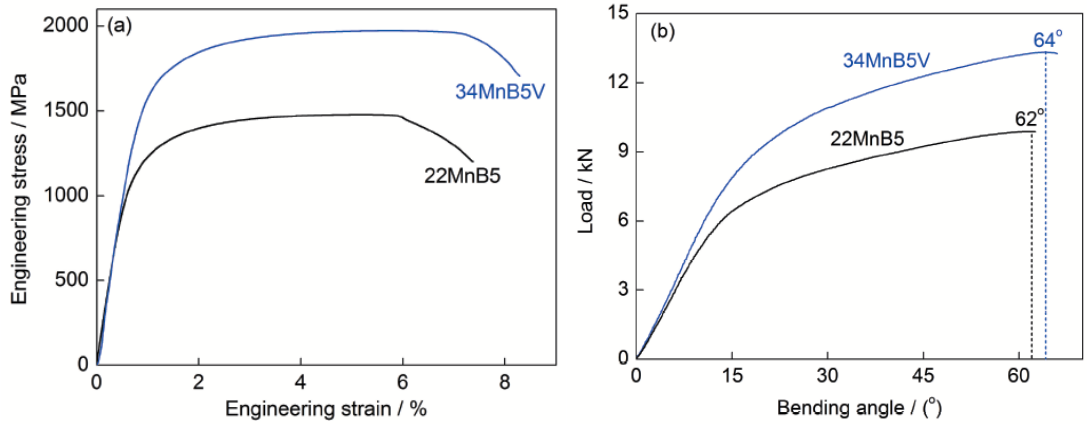

Figure 96. (a) Tensile curves and (b) three points bending load angle curves of 34MnB5V and 22MnB5 steels. [81]

Figures 96(a) and (b) are engineering stress-strain curves (JIS5 standard specimens) and three-point tip bending angle-load curves of 22MnB5 and 34MnB5V steels after hot stamping and simulated coating (170℃, 20 min) tempering.

The strength improvement of 34MnB5V after hot stamping is mainly due to the precipitation strengthening effect of nano-scale VC precipitation particles and the grain refinement caused by VC precipitation. In general, the fracture resistance of steel decreases with the increase of strength, while the strength of 34MnB5V is greatly improved compared with 22MnB5, and its elongation are also improved. The three-point tip bending angle is equivalent. Nano-scale VC particles are the main factor to improve the elongation of 34MnB5V. Dislocations need to bypass the VC particles to continue to move. A large number of geometrically necessary dislocations are generated and accumulated around the second phase particles. The obstruction of dislocation motion can realize precipitation strengthening and improve its work hardening ability. Precipitation strengthening itself cannot improve toughness and ductility. For martensite with poor inherent ductility, improving the work hardening ability of the material can delay the occurrence of necking. and improve its uniform elongation.

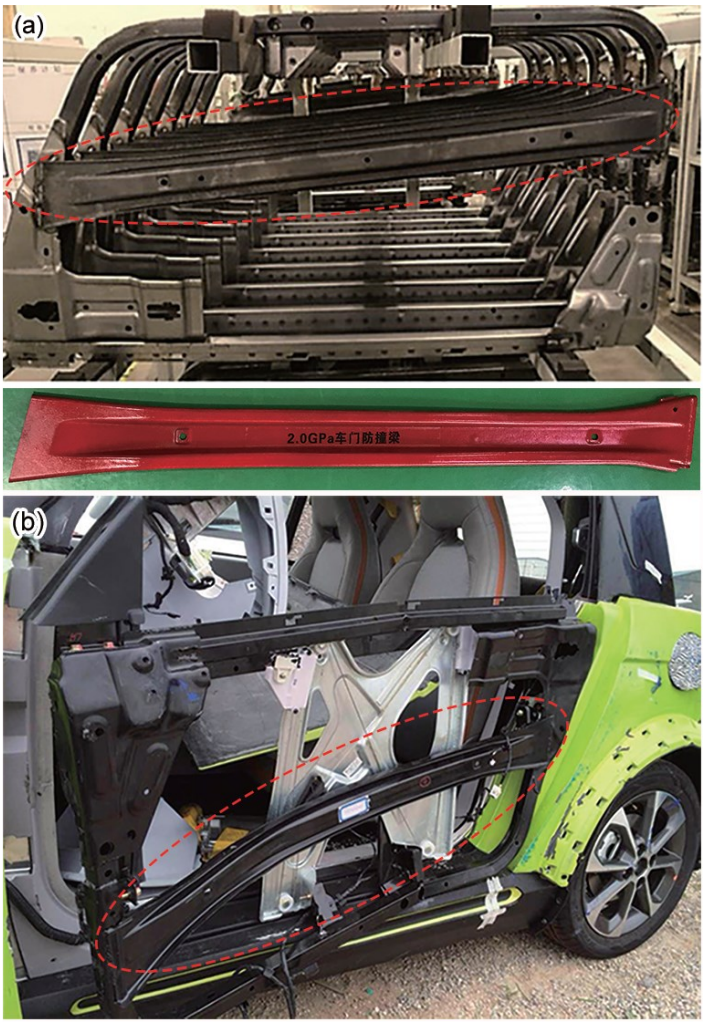

Figure 97. (a) Door beam made of 34MnB5V hot-stamped steels and (b) vehicle crash test. [79]

As shown in Figure 97, in 2017, the world's first batch industrial application of 2000 MPa hot-stamped steel. During the real vehicle crash test of 34MnB5V steel parts, the door anti-collision beam undergoes a large amount of deformation to absorb the collision energy without breaking. This fully shows that the material has good ductility and high fracture toughness.

In addition to V micro-alloyed hot-stamped steel, NbV composite micro-alloyed hot-stamped steel has also been successfully applied in car loading. The hot-stamped steel is based on the conventional 22MnB5 steel composition with the addition of 0.04% Nb and 0.04% V. The hardened layer depth of the NbV micro-alloyed samples is 13~14 mm which is higher than that of the traditional 22MnB5 steel by 3~5 mm, that is, adding Nb and V elements to the traditional 22MnB5 steel can significantly improve the hardenability of the material as shown in Figure 98. And the cold bending angle of the NbV micro-alloyed samples after hot stamping, 65°~70°, is about 8° larger than that of the traditional 22MnB5 steel, 58°~65°. This shows that the addition of Nb and V elements at the same time can make the cold bending performance more excellent.

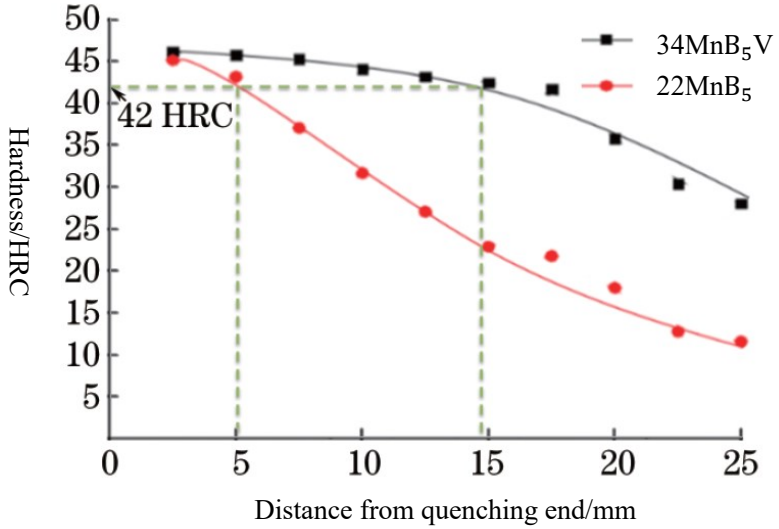

Figure 98. Rockwell hardness vs distance from quenching end curves of two tested steels. [83]

Nano-sized Nb and V carbides can be observed by TEM as shown in Figure 99.

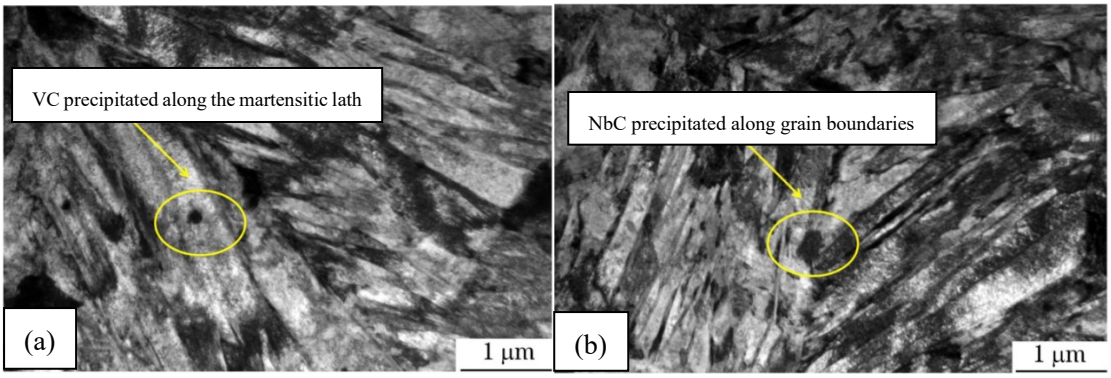

Figure 99. TEM micrograghs of nano-sized Nb and V carbides. [83]

Using the isotope deuterium D of H as a tracer element, it was found that D element is mainly distributed in the carbides of Nb and V elements. Therefore, these dispersed nano-sized carbons can act as H traps by electrochemical hydrogen charging method, thereby reducing the concentration of diffusible H in the matrix. The researchers found that VC can be used as H trap by using thermal hydrogen desorption method (TDS). [84] They believed that the interface between the VC precipitation and the ferrite matrix, that is, the C vacancy on the (001) plane played the role of the H trap.

Therefore, NbV composite micro-alloying can also introduce dispersed nano-sized carbides into the martensite matrix. These carbides can effectively pin the original austenite grain boundaries and refine the original austenite grains, thereby improving the toughness of hot-stamped steel. On the other hand, these dispersed nano-sized carbides can act as hydrogen traps to pin the diffusible hydrogen in hot-stamped steels, thereby improving the hydrogen embrittlement resistance.

4.5. Material Surface Protection – AlSi coating and Zinc-based coating of hot-stamped steel:

The hot stamping process requires heating the steel plate to above the austenitizing temperature (900~950°C) for about 5 min. If there is no inert atmosphere or the protection of the steel sheet coating, the steel sheet is prone to oxidation and surface decarburization at such a high temperature. The roller hearth furnace used in the hot stamped production line is generally protected by an inert gas, such as N_2. In addition to inert atmosphere protection, major steel mills and hot stamping companies have developed or are developing protective coatings. At present, there are two main types of coatings for hot-stamped steel sheets in commercial applications: one is AlSi coating, and the other is zinc-based coating.

4.5.1. AlSi coating:

A typical AlSi coating consists of 10% Si + 90% Al, and the thickness of the original coating before austenitisation is about 25μm. When the AlSi coated steel sheet is heated, the Fe atoms in the matrix will diffuse into the AlSi coating, and the final Al-Si-Fe layer thickness is about 40μm. [61] Since the diffusion of Fe atoms into the AlSi coating is a kinetic process, the final microstructure and properties of the coating are closely related to the holding time above the austenitizing temperature. The coating properties have a great influence on the spotwelding properties and surface phosphating and coating effects of the final hot-stamped parts. The austenitisation time determined in hot stamping production is generally 5min. The determination of this parameter should not only ensure complete austenitisation, but also ensure the quality of the A1Si coating.

The advantage of the AlSi coating is that it can prevent de-C and oxidation on the surface of the steel sheet during austenitisation. Moreover, the coating can isolate the steel sheet substrate from the external environment, so it has a certain anti-corrosion effect.

4.5.2. Zinc-based coating:

Zn has good cathodic protection, so the corrosion resistance of Zn-based coatings is high. In 2008, hot-stamped steel sheets with pure Zn coating (GI) were introduced. Zinc-iron alloying (GA) is a form of zinc-based coating.

At present, zinc-based coatings cannot be widely used due to the limitations of two main problems. One is the volatilization of Zn during austenitisation. Second, the brittle fracture of the substrate caused by liquid Zn will occur in the zinc-based coating sheet, that is, the liquid metal brittleness. When the coating is heated to 850°C, liquid Zn will enter the austenite grain boundaries of the base steel and diffuse along the grain boundaries resulting in embrittlement of the austenite grain boundaries. Embrittled grain boundaries produce surface microcracks reducing the fatigue life of hot-stamped parts and deteriorating cold-formability.

From the formation mechanism of the liquid metal embrittlement phenomenon of zinc-based coated sheets [85], it can be seen that two conditions need to be met for the occurrence of this phenomenon: one is that the coating is in a liquid phase (the melting point of Zn is about 420°C), and the other is that the galvanized steel sheet is subjected to stress. Therefore, liquid metal embrittlement can be avoided by indirect hot stamping. First, most of the deformation (90% to 95%) is completed in the cold stamping process, and then only further shape correction is required in the

hot stamping process. In this way, the amount of deformation in the hot stamping process is very small, thereby avoiding the problem of liquid metal brittleness.

The advantage of zinc-based coated sheet is that it has good corrosion resistance. The disadvantage is that there is an oxide layer on the surface of the coating after the hot stamping is completed. In order to meet the requirements of spot welding and coating of the hot-stamped parts, additional surface treatment is required for the hot-stamped parts, such as sandblasting or shot peening to remove the surface oxide layer.

4.6. Discussion:

Hot-stamped steel and its application require steel mills, automobile manufacturers, equipment manufacturers and industry associations to collaborate. So that research on the whole chain in the development of new steel grades, the innovation of the process, the use of service evaluation methods and the formulation of their labels. Finally shorten the development cycle of advanced hot-stamped steel and application technology.

In the design strategy of lightweight and multi-materials for automotive manufacturing, the types of hot-stamped steel used for key safety structural parts of automobiles and their processes should also be adapted to the requirements of different car models, different safety (regulatory) standards, different environments, and even the customization requirements of different structures and properties on the same part. Therefore, the hot-stamped steel for lightweight automobiles is also coexistence of various components and new processes.

In short, with the continuous improvement of the strength, toughness and economical requirements of hot-stamped steels for automotive safety structural parts, through the collaborative innovation, the performance of hot-stamped steel is better, and the technology is becoming more mature. The advantages over cold-formed steel will continue to increase.

5. Armor and wear resistant steels

5.1. Armor steels:

After more than 100 years of development, armor steel has become the main protective structural material which is widely used in the manufacture of tank, armored vehicle body and turret as well as armor plate. Armor steels have high strength, high toughness and hardness and reasonable hardenability. The low or medium carbon armor steels such as Mn-Mo, Cr-Mo or Ni-Cr-Mo-(V) low alloy steels are typically used. With the continuous development of armor steels, the standardization of armor steel has also developed rapidly. From the initial RHA (rolled homogeneous armor steel) (MIL-DTL-12560) to HHS (high hardness armor steel) (MIL-DTL46100), then to UHHS (ultra-high hardness armor steel) (MIL-DTL-32332).

5.1.1. Series and chemical composition of Armor steels:

The R&D and production of Swedish armor steel is currently in a leading position. It has formed a relatively complete material series from low and medium hardness RHA to HHS and UHHS, mainly including Armox series, Ramor series and Swebor series. Armox and Ramor armor steels are produced by the Swedish SSAB. Swebor armor steel is produced by Swebor STAL SVENSKAAB. Armox steel is mainly used for protection of medium and large caliber ammunition. Ramor and Swebor are dual-use armor steel which can be also used for walls, doors, window frames, reception counters, shutters and other parts of a building against dangerous assault. In this section, we focus on Armox armor steels.

Armox steels include Armox 370T (Class 1, 2), Armox 440T, Armox 500T, Armox 600T and Armox Advance. Armox steels are all fine-grained steels. Since grain size affects hardenability and critical plastic flow properties. The grain refinement is the only way to increase strength and toughness at the same time, therefore, armor steels are expected to have very small grain size. The main alloying elements are Mn, Ni, Cr, Mo, Si, etc., and the C content is between 0.21 and 0.47 as listed in Table 12.

Grade	C	Si	Mn	P	S	Cr	Ni	Mo	B
Armox 370T Class1	0.32	0.4	1.2	0.01	0.003	1	1.8	0.7	0.005
Armox 370T Class2	0.32	0.4	1.2	0.01	0.003	1	1.8	0.7	0.005
Armox 440T	0.21	0.5	1.2	0.01	0.003	1	2.5	0.7	0.005
Armox 500T	0.32	0.4	1.2	0.01	0.003	1	1.8	0.7	0.005
Armox 520T	0.32	0.4	1.2	0.01	0.003	1	1.8	0.7	0.005
Armox 560T	0.37	0.7	1	0.01	0.003	1	1.8	0.5	0.005
Armox 600T	0.47	0.7	1	0.01	0.003	1.5	3	0.7	0.005
Armox 620T	0.46	0.7	1	0.01	0.003	1	2.5	0.6	0.005
Armox Advance	0.47	0.7	1	0.01	0.003	1.5	3	0.7	0.005

Table 12. Chemical composition (ladle analysis) of the armor steels (the element content is the maximum). [86]

5.1.2. Processing of Armor steels*:*

Armor steel production processes consist of a few important steps in order to reach their required mechanical properties. The first of these steps is the continuous casting of slabs ore with a high chemical purity. The next step is the rolling of the slabs at a temperature of around 1250°C so as to refine its microstructure and reach the desired thickness and width. The next step is the cutting of the steel into sheets of manageable lengths. Then the sheets are quenched from a temperature of about 1000°C by rapidly and evenly distributing cooling with water to obtain its high strength properties. Next step is the tempering of sheets at temperatures between 200~500°C to make the hardened more ductile. The final step is cutting to delivering length and application of corrosive paint.

Armox 370T~600T are delivered in Q&T (quenched and tempered) condition, Armox 620T and Advance are delivered in quenched condition and the manufacturer does not recommend further heat treatment.

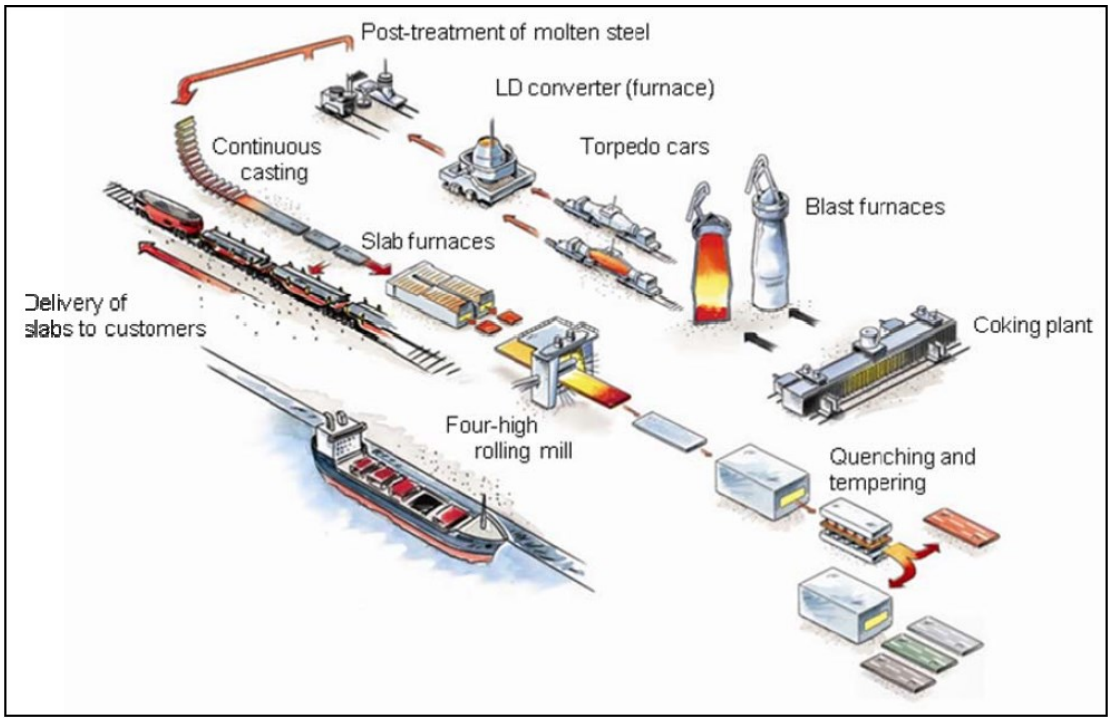

Figure 100. Production flow of SSAB for armor steel plate manufacture. [87]

Sweden SSAB has the world's most advanced four-high rolling mill with a rolling mill grade of $1x10^5$kN. At the same time, it has the world's most advanced high-automation quenching line which can perform heat treatment, leveling, coating, handling and other processes as shown in Figure 100. The uniformity of the properties along the thickness direction of the steel plates produced is due to the substantial reduction in the thickness of the billet during rolling. The grain size control benefits from the precise control of the thickness and temperature of the billet during rolling.

5.1.3. Microstructure of Armor steels:

The microstructure resulting from described heat treatment is fine tempered martensite as shown in Figure 101. A characteristic feature of the martensite in low and medium-carbon steels is its three-level hierarchy in morphology—it is composed of laths, blocks and packets. Martensite laths making a block are characterized by the same crystallographic orientation, and hence they represent the same variant of the created martensite structure.

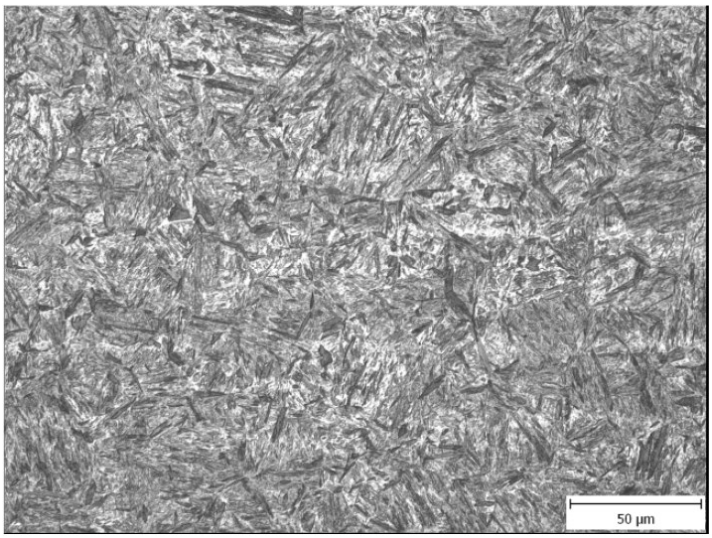

Figure 101. Microstructure of Armox 500 delivered state. [88]

The over tempering of Armor steel or any other steel with similar production processes occurs at using the secondary production processes based on heat transfer (cutting, welding, shaping, banding and others) which the affected microstructure is shown in Figure 102. Therefore, the producer recommends the secondary processing at temperatures lower than the tempering temperature (200°C) due to accidental over tempering and the degradation of mechanical properties in heat affected zones (HAZ).

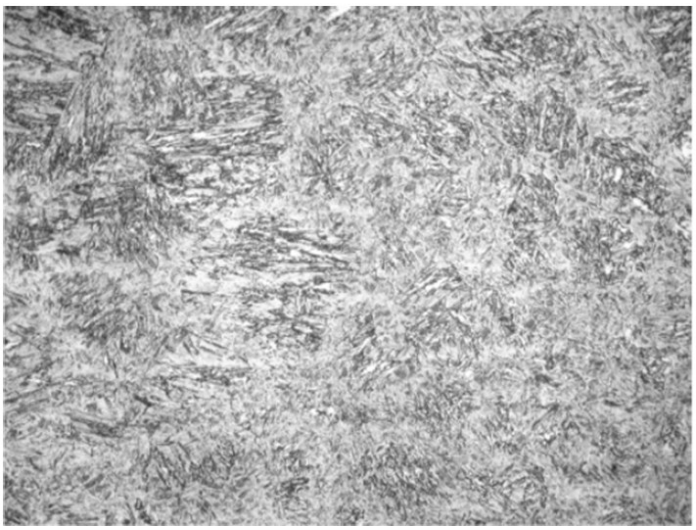

Figure 102. Microstructure of Armox 500 affected by over tempering with temperature below A_1. [88]

5.1.4. Mechanical properties of Armor steels:

As the most important performance parameter of armor steels, the general relationship between hardness and ballistic resistance is very dependent on the armor-piercing fracture form. The hardness change of armor steel plate and the form of armor-piercing fracture is shown in Figure 103. At low hardness values, plastic flow controls the ballistic resistance and the steel plate will fail through plastic hole reaming. At this time, most armor steel plates are RHA. As the strength of the target plate increases, the probability of localized failure through full thickness adiabatic shearing increases which will eventually fail due to soft ram plugs, while the armor-piercing projectile steel core remains intact. As the hardness increases further, the steel core begins to gradually erode or break and the bullet shape becomes blunt. The shape of the blunt tip strongly promotes a plunger failure which is called a hard plunger. There is little deformation of the target plate. As the projectile is eroded, most of the impact energy will be dissipated. Generally speaking, under this hardness condition, the harder the target plate material, the greater the erosion and the better the anti-ballistic performance. At this time, the armor steel plate belongs to HHS. As the hardness level increases further, the toughness decreases to a very low level. The target itself is only broken in a very brittle manner and provides no structural support. Theoretically, ballistic resistance may continue to improve, but its value as structural armor has been lost.

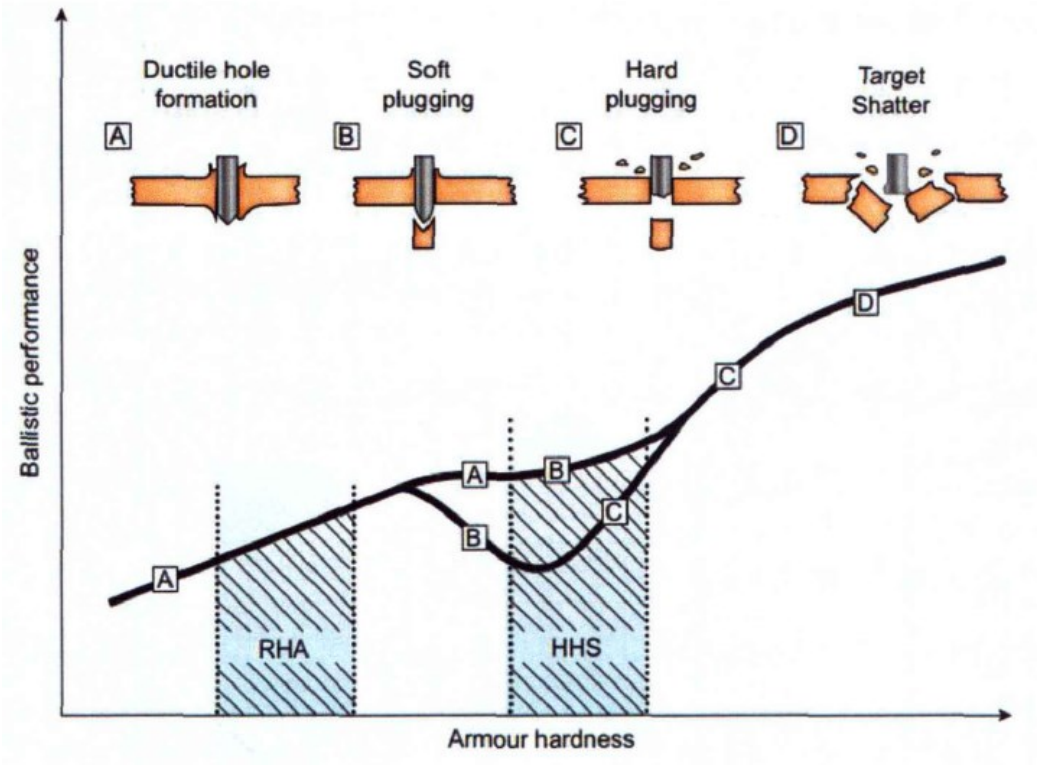

Figure 103. Schematic diagram of the general relationship between hardness and ballistic resistance of armor steel plates. [89]

Armox 370T class 1 has excellent high toughness and penetration resistance with a hardness range of 325 to 405 HBW as the thickness decreases. Armox 370T class 2 has excellent impact

resistance and toughness with a hardness range of 280 to 330HBW. Armox 440T has excellent penetration resistance and impact resistance, the hardness range is 420~480HBW. Armox 500T has high toughness and high hardness, and the hardness range is 480~540HBW. Armox 600T has very good penetration resistance and ultra-high hardness with a range of 570 ~640HBW which is suitable for occasions with more stringent quality requirements. The tensile strength is up to 2100Mpa as shown in Table 13. Armox Advance is Sweden's highest-performance armor steel with a hardness range of 58 to 63HRC. At present, some performance data are still confidential, such as strength and ballistic resistance.

Armox® product range	Thickness (mm)	Typical Hardness (HBW/HRC)	Typical Yield Strength (MPa)	Typical Tensile strength (MPa)	Typical Impact toughness at -40 C (J)*
Armox® 370T Class 1	3.0–19.9 20.0–39.9 40.0–100.0	405 360 325	1200 1040 935	1300 1125 1040	35 55 80
Armox® 370T Class 2	3.0–100.0	310	880	950	100
Armox® 440T	4.0–80.0	450	1200	1425	75
Armox® 500T	3.0–80.0	515	1400	1690	45
Armox® 600T	4.0–20.0	605	1540	2100	25
Armox® Advance	5.0–7.0	58–63			10

Table 13. Main mechanical properties of some armor steel plates. [90]

For these structural armor steels, weldability is also an important indicator of armor materials. In order to ensure the weldability of armor steels, the carbon equivalent of the alloy should not be too high. High carbon equivalent means that the need for preheating during welding is relatively high. Generally, the carbon equivalent is required to be less than 1, usually about 0.8.[91] Typical values for Armox steels are given in Table 14.

Steel grade	Thickness range	CET[1] [%]	CEV[1] [%]
Armox 370T CL1 & CL2	3–100 mm	0.46–0.50	0.67–0.73
Armox 440T	4–80 mm	0.39–0.42	0.67–0.73
Armox 500T	3–80 mm	0.46–0.50[2]	0.67–0.73[2]
Armox 600T	4–20 mm	0.58–0.61	0.83–0.86
Armox Advance Class 1	4–12 mm	0.64–0.68	0.89–0.96

Table 14. Carbon equivalents which is valid for plate thicknesses up to 70 mm. Typical CET values for plate thicknesses of 70.1~80 mm are in the range of 0.50~0.53%, and typical CEV values are in the range of 0.73~0.93% [92]

The definitions of the carbon equivalents CET and CEV are given below:

$$CET = C + \frac{(Mn + Mo)}{10} + \frac{(Cr+Cu)}{20} + \frac{Ni}{40}$$

$$CEV = C + \frac{Mn}{6} + \frac{(Mo+Cr+V)}{5} + \frac{(Ni+Cu)}{15}$$

In addition to welding properties, armor steel is also required to have good cold bending

properties and cutting properties. The most important performance of armor steel is anti-ballistic performance, anti-detonation performance and anti-multiple shot performance.

Armor steel has excellent ballistic resistance, multi-shot and detonation resistance. Armox 370T is the best ductile steel produced by SSAB in Sweden. The composition design of Armox Advance gives this steel excellent resistance to multiple shot. As the best toughness steel on the market, Armox Advance armor steel ultra-high hardness is even comparable to the hardness of ceramics.

From 1990 to 2010, Swedish company successively developed Armox 500T, Armox 600T and Armox Advance armor steel. For a 5.56 M193/SS92 projectile threat with a velocity of 937 m/s at 0° inclination, the thicknesses required for Armox 500T, Armox 600T and Armox Advance are 9 mm, 6 mm and 4.5 mm, respectively as shown in Figure 104. The areal density is reduced 50%, and the anti-ballistic performance is continuously improved.

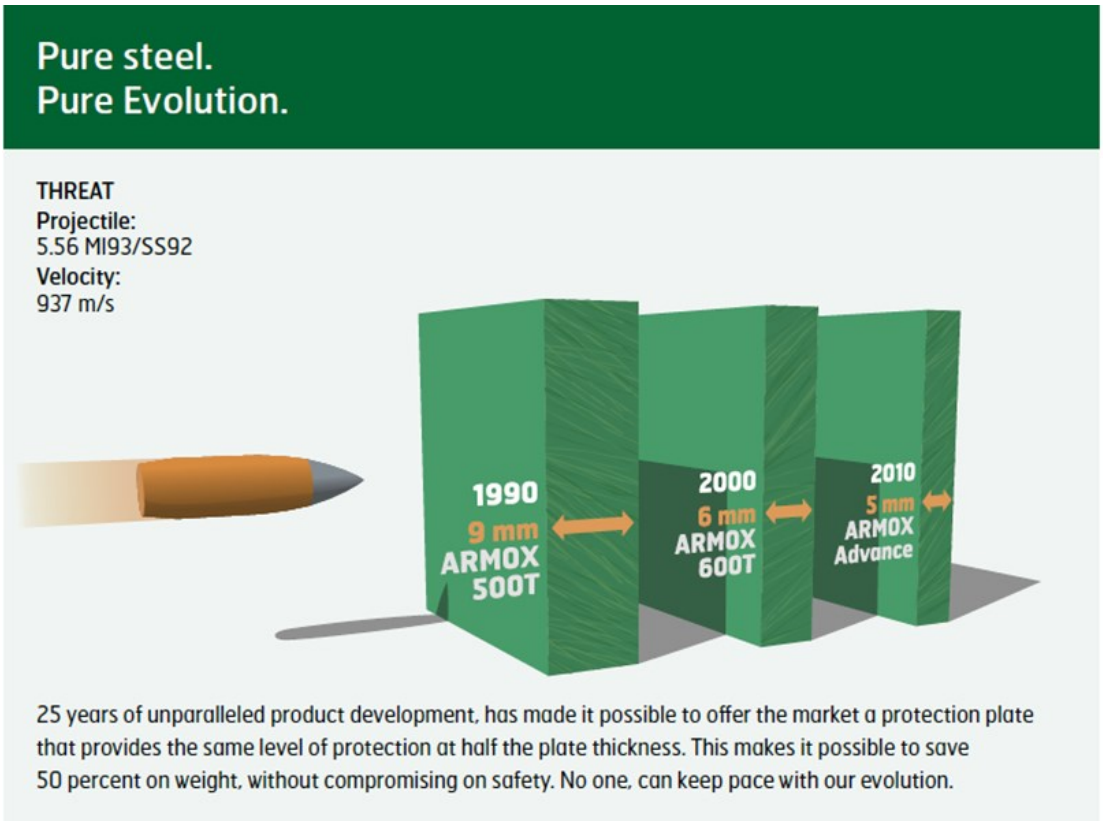

Figure 104. Armor plate thickness evolution in past 30 years. [90]

The U.S. Army Research Laboratory and the Swedish SSAB company [93] jointly studied the V50 ballistic test of Armox 370T/370X, 500S, 560S, 600S/600T against 7.62 mm APM2 bullets, 12.7 mm APM2 bullets, 14.5 mm B32 bullets and 30 mm APDS bullets. The test results were compared with the corresponding U.S. military standards MIL-A-12560 (RHA) and MIL-A-46100 (HHS). It was found that the candidate armor grade 4b steel plates met or exceeded the ballistic requirements of the U.S. military standard RHA. For the same projectile, Armox 500S/T plate provides higher performance. As a grade 4a steel plate, it can be used in non-structural parts. The maximum thickness of the Swedish HHS plate is 80 mm, which exceeds the maximum thickness (50mm) of the U.S. military standard HHS plate. UHHS Armox 560 and 600 steel plates were also tested, and performance data significantly exceeded U.S. military specifications.

5.1.5. Strengthen of the armor:

In recent years, researchers have developed some new UHHS to strengthen armor, such as nanocomposite bainite-austenite, named NANOS-BA. [94] The total amount of alloying elements is about 6% by mass as shown in Table 15 which is comparable to the total content of alloying elements in current quenching and tempering steels used for armor.

C	Mn	Si	P	S	Cr	Co	Mo	V	Ti	Al
1.00	2.39	2.00	0.015	0.017	1.37	1.7	0.80	0.120	0.023	0.800
0.49	1.82	1.57	0.008	0.010	0.01	0.0	0.27	0.086	0.000	0.014

Table 15. Range of the elements content in the investigated experimental melts of the high carbon, medium–alloy bainitic steels, mass %. [94]

The developed parameters of thermo-mechanical and heat treatment of NANOS-BA steel leads to formation of nano-composite structure in final products as shown in Figure 105. The structure is composed of carbide-free nanobainitic laths with high dislocations density and nano-laths and nano-grains of retained austenite, and its volume is determined to be 15~25%.

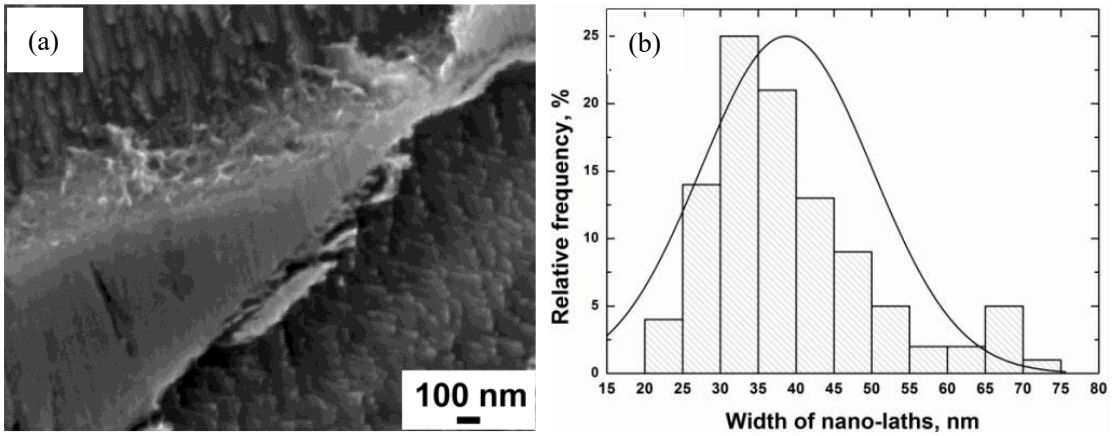

Figure 105. a) Structure of nano-bainite (SEM), b) distribution of bainite nano-laths width. [94]

NANOS-BA steel sheet is produced under semi-industrial conditions and has high strength and good ductility: As shown in Figure 106, the strength is close to 2000MPa, the yield stress is higher than 1400MPa, and the total elongation in the tensile test is 12~20%.

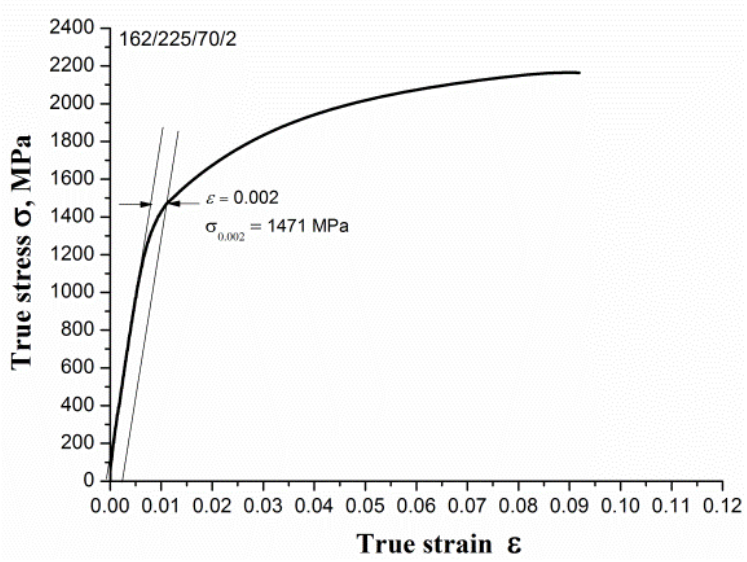

Figure 106. Typical true stress-strain curve for uniaxial tensile test of NANOS-BA steel. [94]

Such level of mechanical properties generates possibility to use NANOS-BA steel for production of shields of improved protective properties, protecting against projectile firing, in comparison with the available steel plates for armors of the highest protection grade as shown in Figure 107.

Ballistic tests have shown that NANOS-BA steel provides better protection when firing a 12.7 mm B-32 projectile than Armox 500T plates or Armox 600T plates in application conditions.

Tests of NANOS-BA steel plates mounted on RHA, Armox 500T, and Armox 600T base plates using 12.7 mm B-32 projectiles have shown that, in the conditions, NANOS-BA steel exhibits better protective properties than commercial plates of 500BHN and 600BHN grades. Armox 500T and Armox 600T plates have been protected from piercing by NANOS-BA steel plates with a minimum 5 mm thickness.

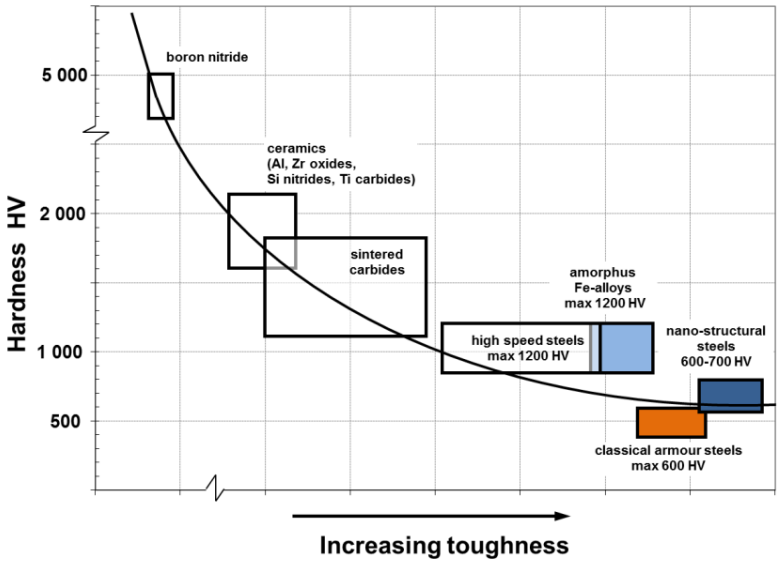

Figure 107. The level of hardness and toughness of selected hard materials applied in the technology, compared to the properties of new generation of hard steels and iron alloys. [94]

NANOS-BA steel is a promising material for armor which may reduce armor weight and/or improve armor protection compared to currently used structures. Due to the very high protective capacity, the monolithic sheet of NANOS-BA steel can be used as one of the layers of composite armor as well as for the protection of selected areas of the surface of lightly armored vehicles. The premise is to ensure the parameters of the vehicle's steel sheet like thickness, strength and stiffness are compatible with Armox 500T or Armox 600T steel plate. In addition, the NANOS-BA steel plate is fixed to the vehicle plate (for example by screws).

5.1.6. Discussion:

Although many ground vehicles are now actively adopting lightweight armor materials which include low-density metals such as aluminum, magnesium, titanium alloys, etc., armor steels with high hardness are still very competitive in certain ballistic and structural applications.

With the continuous development of armor steel optimized composition design, smelting process and heat treatment process, high-performance armor steel continues to emerge. Armor steel develops from low or medium strength to high hardness, ultra-high hardness, high strength and high toughness. In addition, new types of armor steels and their structures are also being developed, such as chiseled armor steels, low-density armor steels, and foam steel armored panels. These armor steels will reduce areal density enabling further weight reduction for tank and armored vehicles.

5.2. Wear resistant steels*:*

For steel materials, in addition to fracture and corrosion, wear is also one of the main forms of workpiece failure. Wear resistant steel is a general term for steel materials with good wear resistance and it is the most used material in wear resistant materials today. There are many kinds of wear resistant steel which can be roughly divided into high manganese steels, low and medium alloy wear resistant steels, chrome-molybdenum-silicon-manganese steels, cavitation resistant steels and special wear resistant steels. As an important category of wear resistant steel, low alloy high-strength wear resistant steel is a promising wear resistant material due to its low alloy content, good comprehensive performance, convenient and flexible production, and low price.

5.2.1. Series and chemical composition of wear resistant steels:

As the world's leading manufacturer of high-strength steel, the Swedish SSAB has the world's leading high-end quenching and tempering heat treatment technology, and is the world's largest developer and producer of wear resistant steel. Its wear resistant steel plates are divided into Hardox 400, 450, 500, 550, 600 and Extreme according to the hardness level. The hardness of Hardox Extreme wear resistant steel launched in recent decades is as high as 700 HB, which can play an important role in wear resistant structural parts facing extremely severe wear such as in mines,

cement and brick mold production industry, etc. It explored a road to the field of special ultra-high-strength wear resistant steel for the world's low alloy wear resistant steel industry. These steels are all fine-grained steels. The chemical composition is largely dependent on the plate thickness, since the goal is to obtain high hardness levels with similar values throughout the cross-section which are at the same time a derivative of a homogeneous material structure. The element content of some wear resistant steel plates is listed in Table 16.

Grade	C	Si	Mn	P	S	Cr	Ni	Mo	B
Hardox 400 (sheet&plate)	0.32	0.7	1.6	0.025	0.01	2.5	1.5	0.6	0.004
Hardox 450 (sheet&plate)	0.26	0.7	1.6	0.025	0.01	1.4	1.5	0.6	0.005
Hardox 500 Tuf	0.3	0.7	1.6	0.02	0.01	1.5	1.5	0.6	0.005
Hardox 500 (sheet)	0.27	0.5	1.6	0.025	0.01	1.2	0.25	0.25	0.005
Hardox 500 (plate)	0.3	0.4	1.3	0.02	0.01	2.2	2	0.4	0.005
Hardox 550	0.44	0.5	1.3	0.02	0.01	1.4	1.4	0.6	0.004
Hardox 600 (sheet)	0.4	0.5	1	0.015	0.01	1.2	1.5	0.6	-
Hardox 600 (plate)	0.47	0.7	1.5	0.015	0.01	1.2	2.5	0.7	0.005
Hardox Extreme	0.47	0.5	1.4	0.015	0.01	1.2	2.5	0.8	0.005

Table 16. Chemical composition (heat analysis) of the wear resistant steels (the element content is the maximum). [95]

5.2.2. Microstructure of wear resistant steels:

Hardox 400~550 are delivered in Q or Q&T (quenching or quenching and tempering), and Hardox 600 is delivered in quenching condition. The information on the structure of Hardox Extreme steel in the delivery state provided by the manufacturer is not very precise. In the catalogue card, in the State of Delivery section there is information that the steel is delivered in the hardened state. However, in the Production and Other Recommendations section, more details are added—namely, that Hardox Extreme steel reaches its mechanical properties by quenching, and if necessary, by yet another tempering process.

The microstructures of Hardox Extreme steel in the delivery state are shown in Figure 108. The structure of steel in the delivery state is tempered martensite with visible boundaries of prior austenite grains.

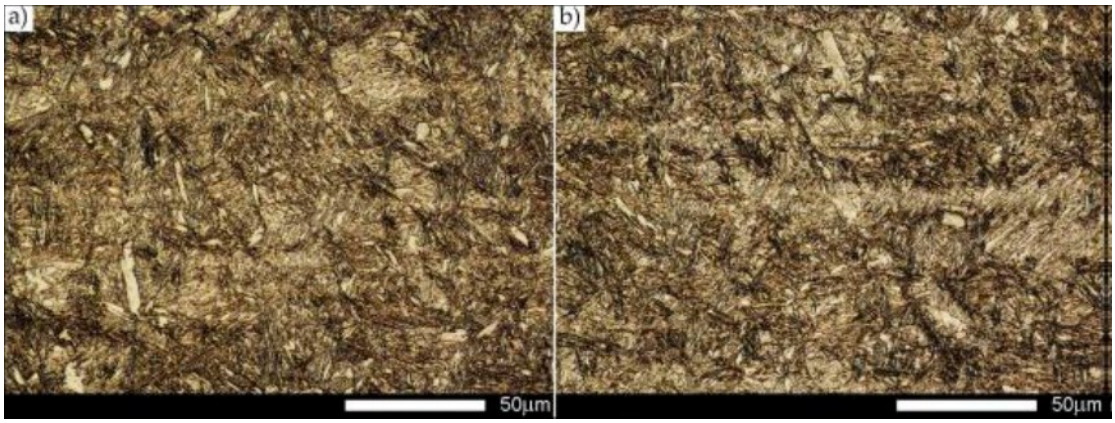

Figure 108. OM of delivered wear resistant steel. (a) Longitudinal orientation. (b) Transverse orientation. Quenched and tempered martensite with fine-lath morphology structure in two dimensions. [96]

Moreover, in both directions of rolling direction, it could be observed bright bands which indicates slightly increased carbon content in these areas. The bands are longer and wider in the case of longitudinal direction comparing Figure 109(a) and (b) which leads to slight hardness difference.

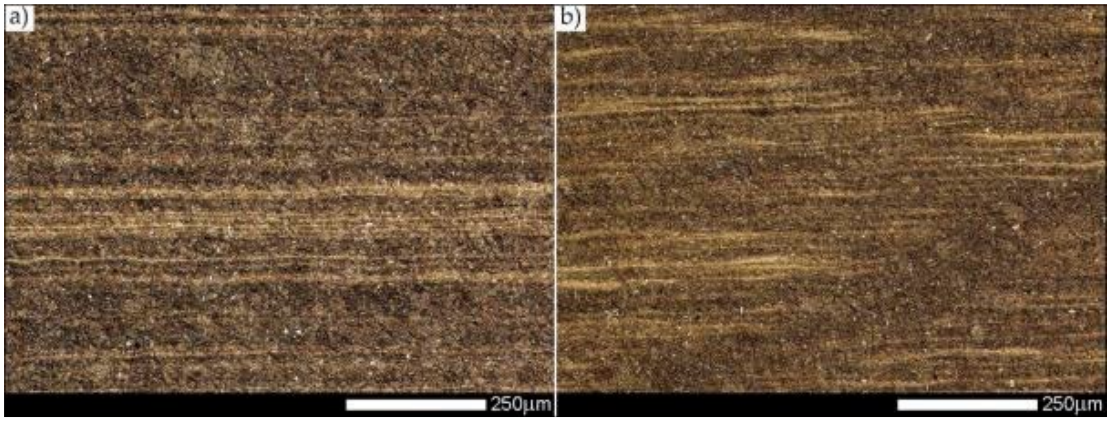

Figure 109. Delivered wear resistant steel microstructure with clearly distinct banding pattern resulting from thermomechanical rolling. (a) Longitudinal orientation. (b) Transverse orientation. [96]

5.2.3. Mechanical properties of wear resistant steels:

Same as armor steels, the hardness is the main parameter cited by manufacturers. In some cases, hardness can even be considered as the main wear resistance criterion of wear resistant steel. Regarding the relationship between hardness and wear resistance, JFE Company used SiO_2 as abrasion to conduct wear analysis on their own low alloy wear resistant steel and obtained the relationship between its hardness and relative wear resistance, as shown in Figure 110. It can be seen that when the Brinell hardness is 300HB and below, with the increase of hardness, the relative wear resistance increases less. When the Brinell hardness exceeds 300HB, the relative wear resistance increases with the increase of hardness in an almost linear way. Among the commonly used low alloy wear resistant steels, the Brinell hardness exceeds 300HB. Therefore, the most effective way to improve the wear resistance of low alloy wear resistant steels is to increase the

hardness.

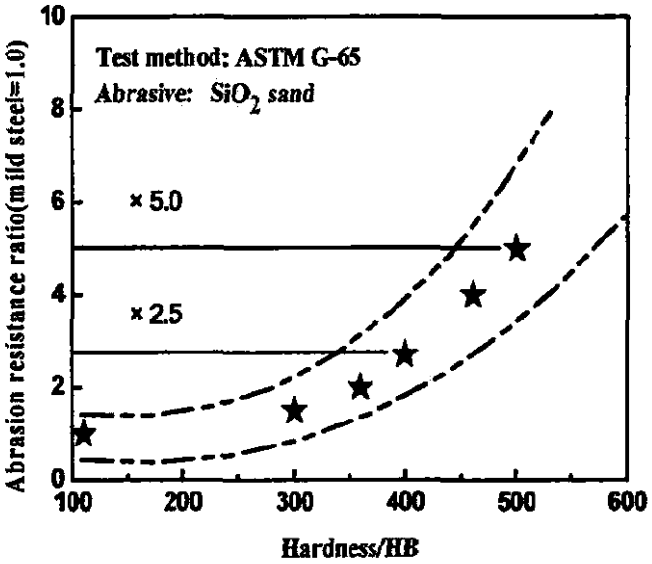

Figure 110. Relation between hardness and abrasion resistance ratio. [97]

The wear resistant steels' distinctive wear resistance and structural strength are a result of its hardness. Hardness minimizes wear since it makes it difficult for abrasive material's "edges" to cut into the material. Throughout the entire service life of the plates, they provide high wear resistance. The structure with high hardness also has excellent yield and tensile strengths, as shown in Table 17, which prevent deformation.

Brinell HBW 10 mm 29.4 kN	Vickers 98 N	Rockwell HRC	Approximate tensile strength MPa	Approximate corresponding grade
400	401	40	1245	Hardox® 400
450	458	44.5	1412	Hardox® 450
500	514	49	1580	Hardox® 500
600	627	55	1940	Hardox® 600

* Tested by SSAB on standard production samples. The data is for guidance only, not as a basis for design and acceptance testing.

Table 17. Approximate hardness and strength of some wear resistant steels. [98]

For some wear resistant steel with a hardness of 700HB, the strength is more than 2400Mpa although its ductility is very poor as shown in Figure 111.

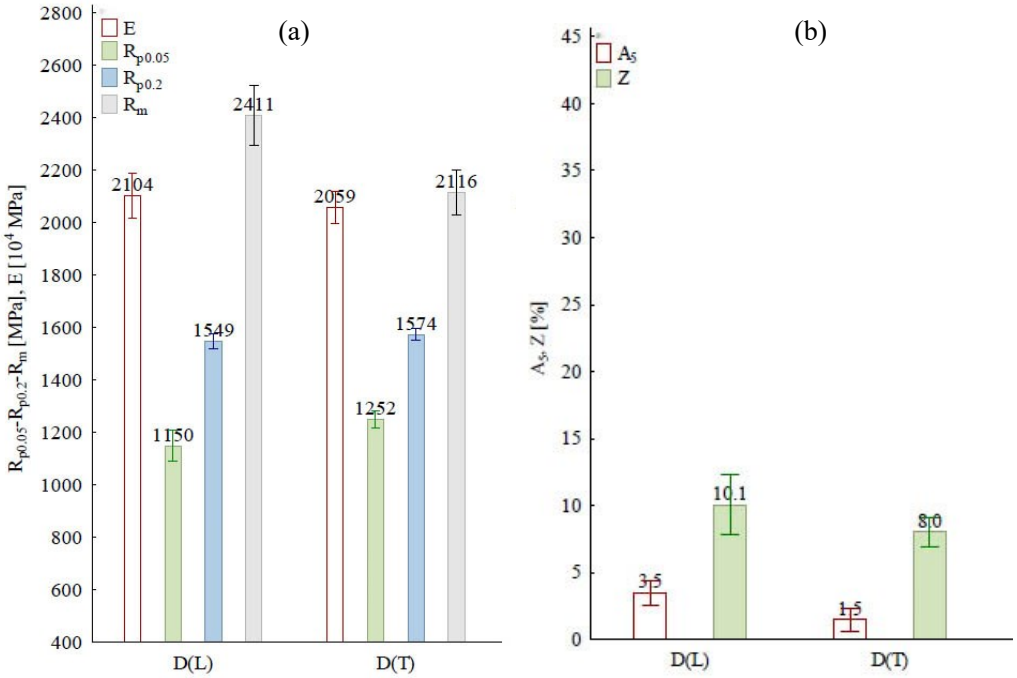

Figure 111. (a) Tensile strength (R_m), yield strength ($R_{p0.2}$), elastic limit ($R_{p0.05}$) and Young' s modulus (E), (b) Elongation (A_5) and reduction in area (Z) at break, of Hardox Extreme steel in delivery states. [96]

With the same hardness, improving the toughness and ductility of the material can also improve its wear resistance. From the main application conditions of wear resistant steel and cutting, fatigue, and corrosion wear rates, it can be seen that wear resistant steel requires a certain degree of toughness and ductility to ensure anti-fracture or other requirements in order to ensure the safety of the service process. Therefore, certain toughness and ductility are very necessary for wear resistant steel, both in terms of wear resistance and safety of the manufactured equipment.

Making hardness and toughness work together is the other strong point of wear resistant steel plates as shown in Table 18. Toughness allows the material to be bent, formed, and welded without cracking when hardness makes it strong and wear resistant. If a wear resistant plate is stressed beyond its yield point and plastically deformed (either intentionally in the shop or hit by heavy stones in the field) it will resist cracking and if a localized crack occurs it will resist propagation.

Despite mostly designed as wear resistant plates, the unique combination of hardness and toughness allows for better performance as a load bearing component in applications such as buckets, dumper bodies and containers, and for longer service times.

HARDOX® PLATE AND SHEET					
Hardox® grade	Hardness nominal HBW	Impact toughness CVL typical for 20 mm (¾") J at -40°C (ft-lb at -40°F)	Relative service life interval[1]	CEV/CET typical for 20 mm (¾")[2]	Thickness range mm (inches)
Hardox® HiTuf	350	95 (70)		0.55/0.36[3]	40-160 (1.57-6.3)
Hardox® 400	400	45 (33)	1	0.44/0.28	2-130 (0.079 -5.12)[4]
Hardox® 450	450	50 (37)	1.1-1.7	0.56/0.38	2.5-130 (0.098-5.12)[4]
				0.39/ 0.31	0.7-2.1 (0.028-0.083)[5]
Hardox® 500	500	37 (27)	1.3-2.1	0.63/0.41	3-103 (0.118-4.06)
Hardox® 500 Tuf	475-505	45 (33)	1.3-2.1	0.52/0.36	4-25 (0.079-0.985)
Hardox® 550	550	30 (22)	1.5-4.0	0.72/0.48	8-65 (0.315-2.56)
Hardox® 600	600	20 (15)	1.8-8.0	0.76/0.58	6-65, metric only
Hardox® Extreme	650-700	15 (< 11)	2.0-18.0	0.65/0.54	8-19, metric only
Hardox® HiTemp	350-400	60 (44)		0.59/0.40	5-51 (0.197-2)

All plates are produced according to Hardox® wear plate guarantees or better.
1. Max/min sliding wear by SSAB WearCalc (mild steel 0.2-0.8)
2. CEV=C+Mn/6+(Cr+Mo+V)/5+(Cu+Ni)/15;CET=C+(Mn+Mo)10+(Cr+Cu)/20+Ni/40
3. 70 mm (2.76")
4. Up to 160 mm (6.30") available upon request
5. Hardox® 450 CR

Table 18. Key performance data such as Hardness, toughness, service life, welding properties and thickness of some wear resistant steel plates and sheets. [98]

Hardox 400 and 450 are multi-purpose wear steels that can also be used for load bearing purposes in some applications due to their high toughness, good bending and welding properties. Hardox 500 is a bendable and weldable wear steel that can be used in applications where higher wear resistance is required. Hardox 550 mainly aimed at users and manufacturers who use high manganese steel castings or wear resistant steel plates with a Brinell hardness of over 500. When upgrading from Hardox 500 steel plate to this product, the Brinell hardness increased by 50 units, extending the wear life without losing the toughness of the steel plate. The hardness value of Hardox 600 and Hardox Extreme reached an average hardness of 600 or 700HB, but their toughness is greatly reduced.

In addition, these wear resistant steels have consistent properties from one plate to the next. Low carbon equivalent and excellent cleanliness also make these wear resistant steels easy to weld.

5.2.4. Optimizing the choice of wear materials:

Wear comes in different forms and has various effects on practical applications. The most common types of wear are sliding wear and impact wear. Typical wear resistant steel plates have excellent resistance to impact and sliding wear for hard and soft rock at all impact angles. However, when facing severe sliding wear conditions when large volumes of material are processed, some specific steel plates are preferred as shown in Figure 112.

(a)

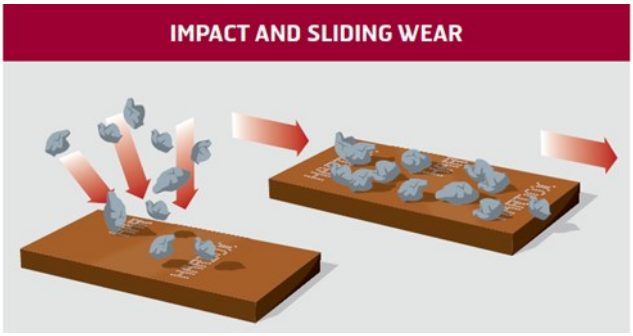

(b)

Figure 112. Different application conditions of (a) Hardox and (b) Duroxite steel plate. [99]

An extremely wear resistant composites could be created by welding chromium carbides or complex carbides onto a Duroxite base plate. The optimized carbide concentration provides consistently high wear resistance from the top surface to 75% of the overlay thickness. As shown in Figure 113, this results in a longer life for wear parts than other similar overlay products and better performance in specific wear environments.

(a)

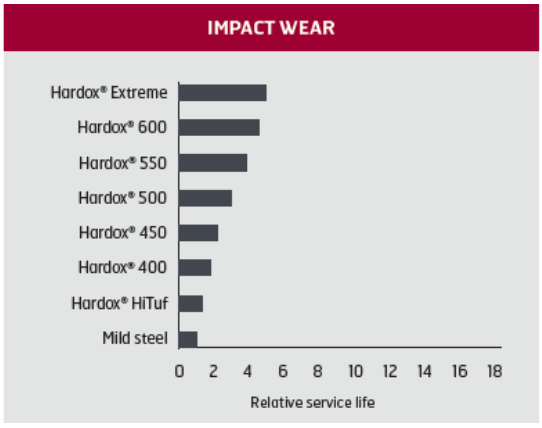

(b)

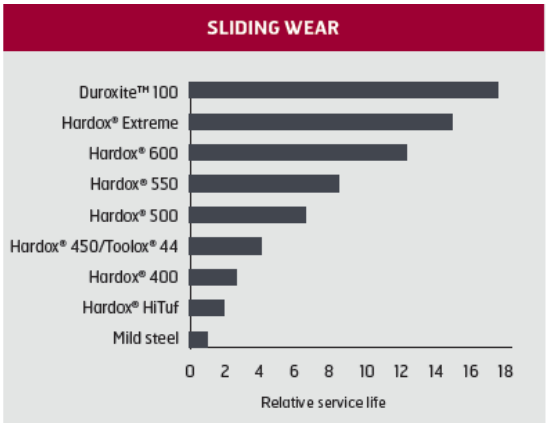

Figure 113. Calculated relative service life and (a) impact wear, (b) sliding wear of hard rock at 20 degrees angle of incidence. [99]

The service life in real applications depends on the volume, size, and hardness of the processed material as well as the size of the machines used. Extremely hard materials are more susceptible to impact, vibration, and stress levels and more higher processing and material costs.

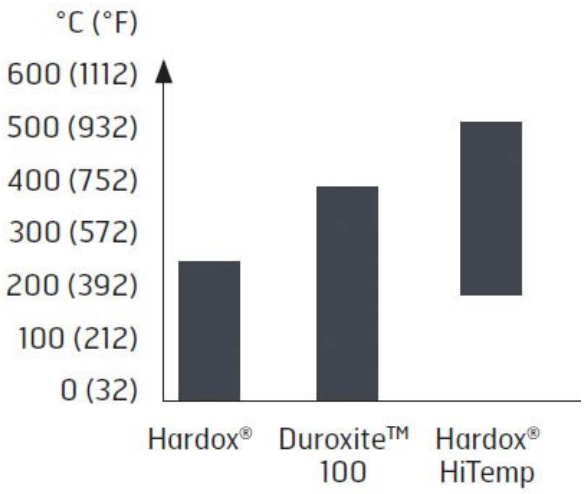

Figure 114. Recommended working temperature intervals of wear resistant steels. [99]

In addition, most wear resistant steels recommend a maximum working temperature of around 250°C. Duroxite 100 overlay plates which withstand sliding and moderate impact wear could work up to 350°C. Special high temperature grades, for example, HiTemp are also emerged as shown in Figure 114.

5.2.5. Discussion:

In comparison with regular steel, wear resistant steels reduce weight and increase the service life of steel structures. Light truck container made of the wear resistant steel has a 10~20% increase in load capacity or even more in some applications. It not only reduces the number of trucks on the road, but also saves fuel and reduces emissions. In addition, 2/3 of the steel used in auto parts is used for maintenance, and most of them fail due to the reduction of the service life of the parts caused by wear and tear. Therefore, improving the quality of wear resistant steel and developing new high performance wear resistant steel to reduce the wear loss is of great significance for developing the automotive industry in the future.

6. Nanobainitic steels

Nanobainitic steels can be obtained by a simple heat treatment process and is known as the first large-scale nanostructured metal. This material has received extensive attention since it was developed by Caballero and Bhadeshia et al. in 2001. Nanostructured bainite is formed by supercooled austenite in the low temperature bainite transformation zone for a long time isothermally. It consists of bainitic ferrite and retained austenite with a lath width of only tens of nanometers. [100] Generally, the lath width (20~40 nm) of nanobainite is much smaller than the lath width (about 200 nm) that can be achieved by martensitic transformation. Therefore, through the refinement effect, nanobainitic steel not only has the comparable hardness to martensitic steels while exhibiting higher toughness than conventional lower bainitic steels. [101] On the other hand, the refinement of the bainite lath also helps to obtain ultrafine film-like carbon rich retained austenite, which can realize the Transformation-Induced-Plasticity (TRIP) effect during the material deformation process and suppress micro defects and cracks. The strength and ductility of the steel material are further improved [102]. Nanobainite is a high strength and tough structure with excellent comprehensive properties and relatively simple production process. Due to its good strength, ductility, toughness and impact and fatigue resistance, it has broad application prospects in the field of not only bearings, but also railway tracks, gears, etc.

At present, the development limitations of nanobainitic steel are mainly the dependence on composition and the requirement on heat treatment time, while the two affect each other. The thickness of nanobainite lath is mainly affected by the driving force of phase transformation and the stress state of austenite. The choice of bainite isothermal temperature is an important condition affecting these two factors. In general, the lower the isothermal temperature, the smaller the thickness of the nanobainite lath and the higher the structural strength, but at the same time, the martensitic transformation point of the material is required to be reduced. This thermodynamic condition can generally be achieved by adding effective alloying components (Mn, Cr, Ni, etc.) as shown in Table 19. But the bainite interfacial migration rate tends to be low due to solute drag effect and the extremely low diffusion coefficients of substituting elements.

Steel	C	Si	Mn	Cr	Mo	V	Nb	Co	Al
First generation									
NANOBAIN 1	0.79	1.59	1.94	1.33	0.30	0.11	–	–	–
NANOBAIN 2	0.83	1.57	1.98	1.02	0.24	–	–	1.54	–
NANOBAIN 3	0.78	1.49	1.95	0.97	0.24	–	–	1.60	0.99
Second generation									
NANOBAIN 4	0.99	1.58	0.76	0.45	–	–	–	–	–
NANOBAIN 5	1.00	1.53	0.75	0.51	–	–	0.02	–	–
NANOBAIN 6	1.01	1.51	0.82	0.46	0.10	–	–	–	–
NANOBAIN 7	0.98	2.90	0.77	0.45	–	–	–	–	–
NANOBAIN 8	0.88	1.54	0.69	0.50	–	–	–	–	–
NANOBAIN 9	0.67	1.60	1.25	1.50	–	–	–	–	–
NANOBAIN 10	0.61	1.45	0.76	2.42	–	–	–	–	–
NANOBAIN 11	0.64	1.60	1.27	1.50	–	–	0.03	–	–
NANOBAIN 12	0.58	1.63	1.29	1.43	0.1	–	–	–	–

Table 19. Chemical composition of nanostructured bainitic steels. [103]

The thermodynamic temperature of nanobainite transformation can be reduced by increasing the alloy composition. Compared with that, increasing the C content can achieve the dual requirements of reducing the thermodynamic temperature of bainite transformation and forming nanobainite. The high carbon nanobainitic steel successfully developed can already be comparable

to some maraging steels in performance and the alloy cost is greatly reduced. But even so, the isothermal time corresponding to the bainite transformation is very long, and the bainite reaction in NANOBAIN 1 steel takes 2 to about 90 days to complete the transformation in the temperature range of 125~325 °C, as shown in Figure 115. For some alloys with slightly higher alloying elements, the calculated nanobainite nucleation takes one year [104]. Room temperature transformation is up to hundreds of years. Such a long-term low temperature isothermal heat treatment seriously hinders the practical application of nano-bainite steel, and the development only for high carbon steel will also limit the processing, forming and welding properties of nanobainite steels.

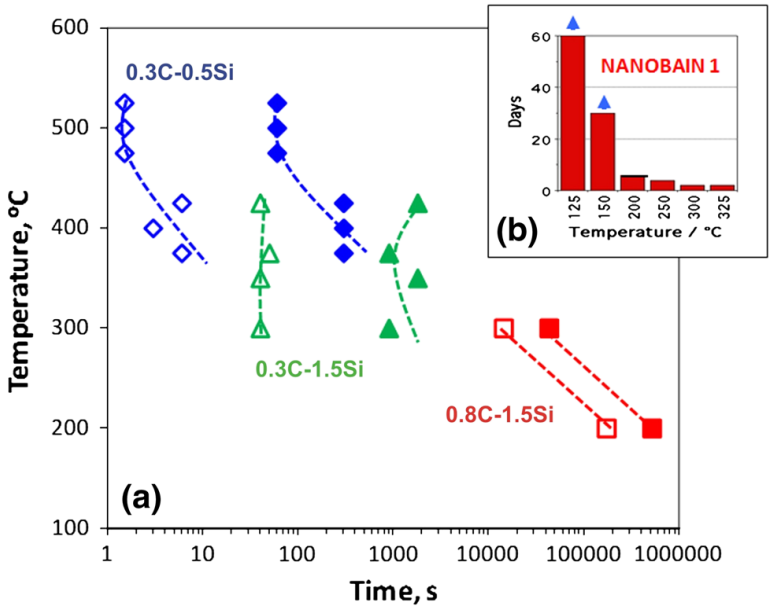

Figure 115. (a) Kinetics results in terms of start and end bainite reaction times as a function of transformation temperature in steels with different C and Si. (b) The time required to complete bainite reaction of the first generation nanostructured bainitic steels at different temperatures. [103]

How to speed up the transformation rate of nanobainite while ensuring the formation of nanobainite will help nanobainite to be applied in a wider range of alloy systems and more complex service environments. Therefore, the acceleration technology of bainitic transformation has become a research hotspot in the development of nanobainitic steels in recent years.

At present, the development of nanobainite transformation mainly focuses on reducing the transformation time by improving the alloy composition, changing the austenitisation process, changing the heat treatment process of the cooling process, applying pre-stress and pre-strain, and external magnetic field.

6.1. Alloy design of nanobainitic steels:

The first step in accelerating transformation is to increase the magnitude of the free energy change accompanying the decomposition of austenite ($\Delta G^{\gamma\alpha}=G^{\alpha}- G^{\gamma}$), i.e., the transformation is driven by controlling additions of substitutional solutes to the steel. Both nucleation and growth rates could be expected to increase as a function of $|\Delta G^{\gamma\alpha}|$.

Si and Al are important alloying elements of nanobainitic steel, which can effectively inhibit the formation of cementite during bainitic transformation. At the same time, Al and Co elements can change the stacking-fault energy of austenite and increase the driving force of bainite transformation. The addition of Co and Al (detailed composition in Table 19) to the first generation NANOBAIN increased $|\Delta G^{\gamma\alpha}|$, resulting in an increase in the transition rate. By controlling the addition of Al and Co at concentrations below 2 wt.%, the transformation is significantly accelerated and processing can be completed in hours (in contrast to days). The related research is mainly aimed at the traditional bainitic transformation process, but also has important reference value for the alloy design of nanobainitic steel.

Some researchers found by adding 0.5~1.5 wt.% Al element to 0.25C~2Mn low carbon low alloy steel: with the increase of Al content, the nucleation driving force of bainite increases at the same temperature; The addition of Si has no effect on the driving force of bainite nucleation, but delays the growth of bainite, as shown in Figure 116.

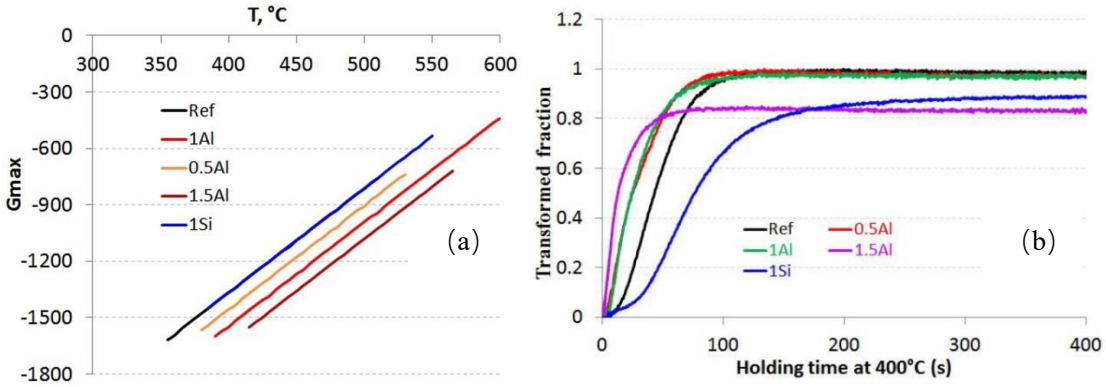

Figure 116. (a) Driving force which is calculated for nucleation in the different steels. (b) Transformation kinetics at 400 °C after soaking at 1100°C for 5 min. [105]

In order to suppress the formation of cementite, other researchers added a small amount of Si element to 100Cr6 steel and performed nanobainite heat treatment, and found that it needs to be kept at 200°C for 72 h before the bainite transformation is basically completed.

It is believed that Al and Si have similar effects in inhibiting the formation of cementite, and the addition of Al can reduce the C content required to form nanobainite. Compared with the increase of Co content, the reduction of Mn will greatly accelerate the transformation process of bainite. In summary, it can be seen that although Si plays an important role in inhibiting the precipitation of cementite during the bainite transformation process and also delays the growth of bainite to a small extent, Si has a significant effect on the refinement of bainite. The effect will have a greater impact on the morphology of the nanobainite lath. Al element and Co element have similar promoting effect on bainite transformation, but Al element can also inhibit cementite precipitation.

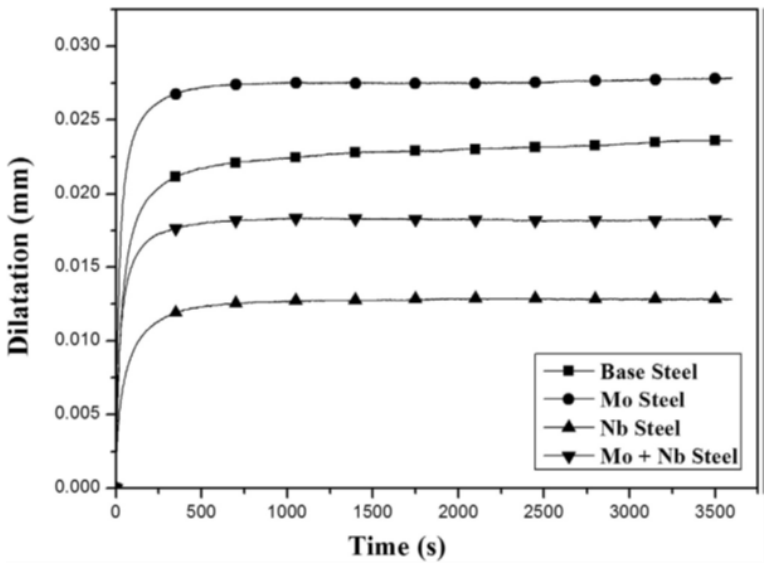

Figure 117. Dilation curves recorded by dilatometer on thermal simulator during bainitic transformation at 350°C. [106]

In addition to Al, Si, Co and Mn that have a great influence on the bainite transformation, some studies have shown that a small amount of Mo element can accelerate the bainite transformation process, while the addition of Nb will slow down the bainite transformation kinetics as shown in Figure 117. Some scholars believe that for low carbon bainitic steel, the addition of Mo can inhibit the transformation of Widmanstatten stucture/ferrite, expand the C curve of bainite transformation and make austenite mainly transform into refined bainite structure. Nb has an important drag effect on the migration of austenite grain boundaries which can effectively refine austenite grains leading to the increase of bainite nucleation, reduce the driving force of bainite transformation and delay the occurrence of bainite bulk phase transitions.

In NANOBAIN 4~12 alloys (Table 19), the rate increment is possible as kinetics data in Figure 118 illustrate by reducing C, Mn, Cr, and Mo contents and by refining the prior austenite grain size with the help of Nb additions.

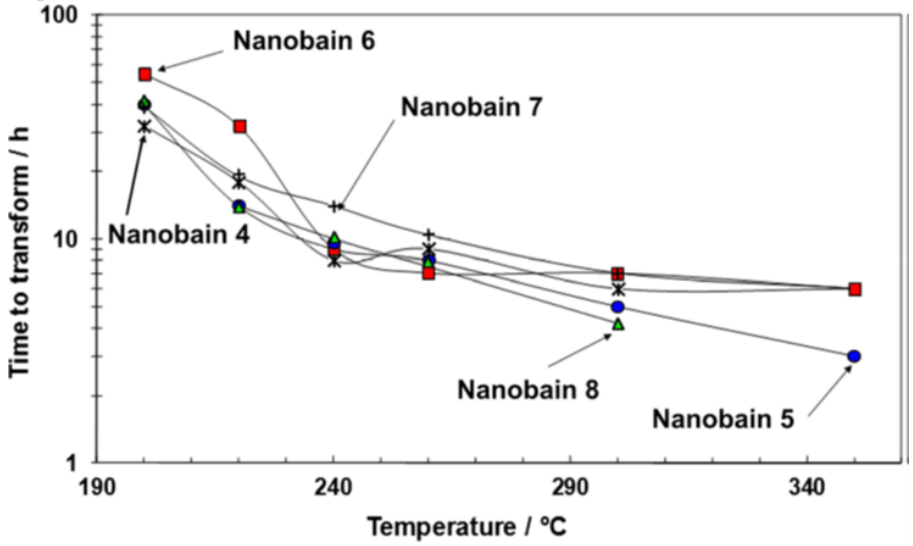

Figure 118. The required time to complete bainite reaction at different temperatures in the second generation of nanostructured bainitic steels. [103]

In addition, fine VC particles could be generated in austenite grains through medium temperature holding and then carried out low temperature bainite transformation. The results showed that fine precipitation particles can greatly reduce the incubation period of bainite and the increase the overall bainite transformation rate, as shown in Figure 119. The bainite nucleation activation energy for nucleation on VC particles was reduced by 15.24 kJ/mol.

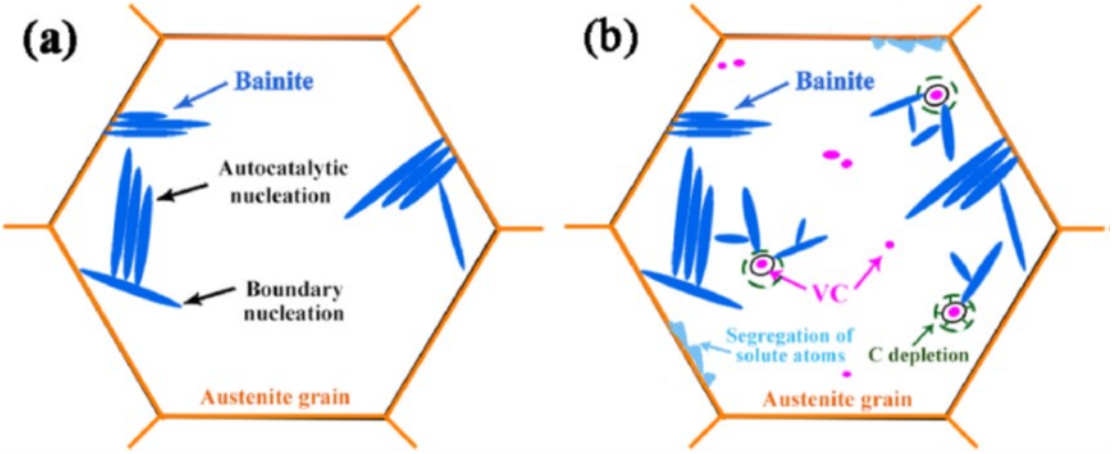

Figure 119. Schematics of bainite nucleation and growth for (a)without VC, (b)with VC. [107]

6.2. Microstructure of nanobainitic steels:

Figure 120(b) shows a bright-field TEM image of a first generation nanostructured bainitic steel transformed at 125℃ for 60 days. Some of the bainite plates are incredibly long and thin (20~40 nm), resulting in an ultrafine scale structure consisting of an intimate mixture of ferrite and austenite. In both the austenite surrounding and the bainitic ferrite, the dislocation debris is visible. In the samples after extensive aging at 200°C for 14 days, only a small amount of ultrafine (20 nm wide and 175 nm long) cementite particles were found in bainitic ferrite, while any significant carbide precipitation was not detected by extensive TEM in this low-temperature bainite.

Ferrite laths in a bainite sheave have almost the same crystallographic orientation. In OM, the sheaves are sometimes called packets because they resemble lath martensite. The prior austenite grains are divided into packets in lath martensite, that is, lath groups with the same habit plane (or the same parallel close-packed plane relationship) as austenite, and each packet is further divided into blocks. Each martensite block contains the same orientation laths, which is called covariant packets.

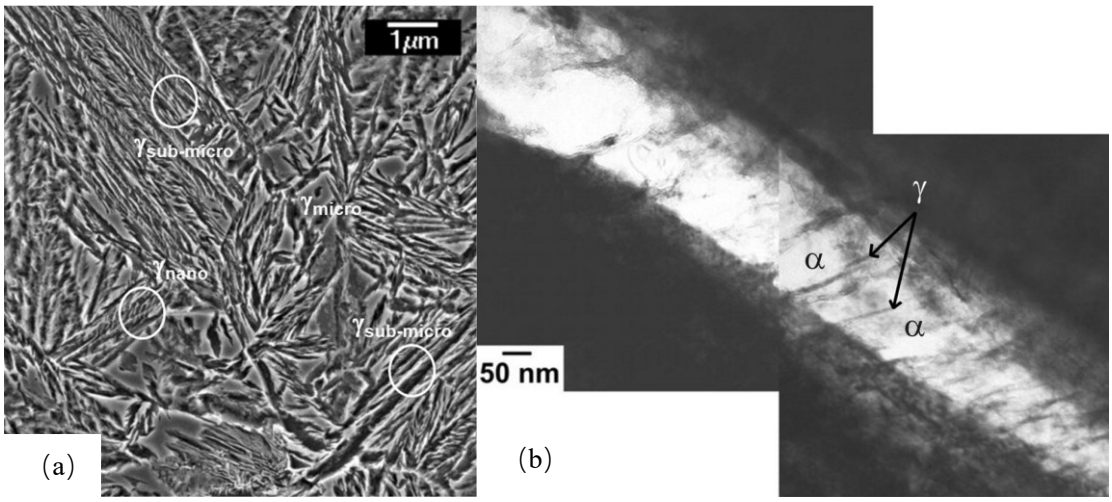

Figure 120. (a) SEM of microstructures by isothermal transformation at 220℃. (b) TEM of microstructure at 125℃ for 60 days. [103]

Microstructural refinement to the nanoscale does not exclude bainitic ferrite because retained austenite is trapped between the ferritic slender plates, as shown in Figure 120 (a) and (b), the size of the nanofilms also smaller than 100 nm. In the past, the term austenite block has been used to describe unetched surface pools of austenite whose sizes are tens of μm, sandwiched between bainite sheaves. In low temperature bainitic alloys, the term microblock is used to denote blocks of retained austenite whose sizes are greater 1000 nm, and submicron blocks are those between 100 nm and 1000 nm.

6.2.1. Effect of prior austenite grains:

Any method of increasing the nucleation rate would accelerate the transformation, and the most common method is to refine the austenite grain size. The number density of nucleation sites increases with the austenite grain size decreases. The austenite grain boundary area per unit volume could be further increased by deforming austenite, which is often referred to as "pancaking" the austenite grains. The grain surface area increase could be quantitatively predicted. If the austenite is in a deformed state, other defects such as dislocations and shear bands might also have an effect on the nucleation rate. In the case of displacive transformations, however, such defects could hinder the kinetics through a phenomenon which is known as mechanical stabilization.

It is found that the austenite grain can be refined by selecting a lower isothermal temperature during the austenitisation process. Figure 121 shows OM of steels quenched from various austenitizing temperatures to temperatures just above the A_{CM} and allowing the formation of pro-eutectoid cementite along the prior austenite boundary. It is clear from the OM that the prior austenite grain size decreases as the austenitizing temperature decreases. The refinement of the prior austenite grains is beneficial to increase the nucleation rate of bainite at the prior austenite grain boundaries, thereby accelerating the nano-bainite transformation.

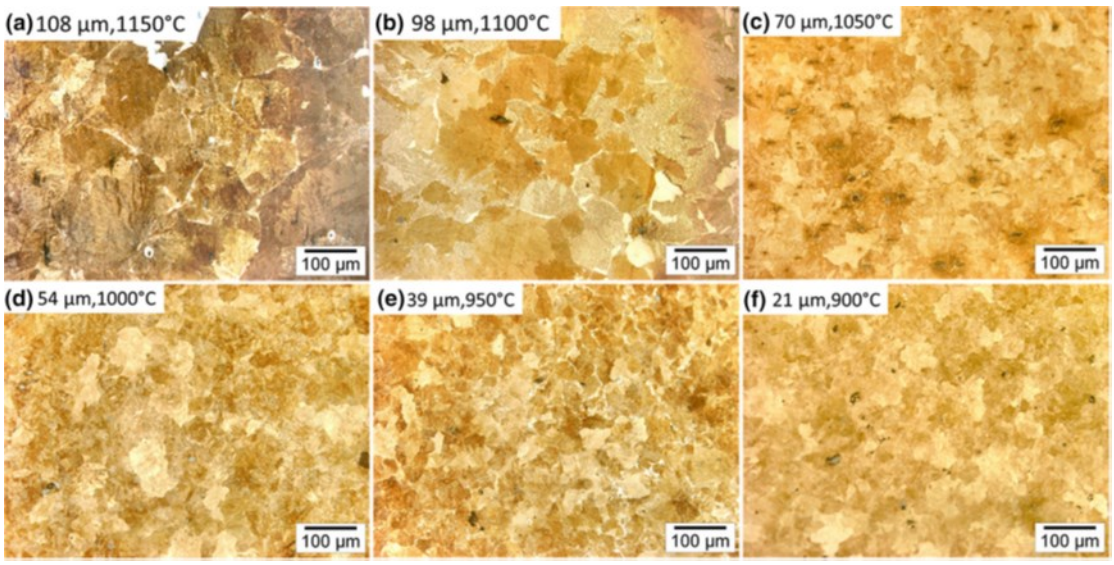

Figure 121. OM used for determining the prior AGS (a) 1150°C, (b) 1100°C, (c) 1050°C, (d) 1000°C, (e) 950°C, and (f) 900°C. Pro-eutectoid (white network) cementite is observed at the grain boundaries. [108]

Other researchers also adjusted the austenitizing temperature of high carbon steel and obtained different austenite grains with grain size distribution ranging from 3 μm to 53 μm. The study found that when the austenite grains are reduced to the micron level, although the phase transformation is significantly accelerated, the bainite formed a large number of irregularly shaped carbide-free bainite with a high fraction of massive retained austenite. The optimal match of nanobainite formation efficiency and good mechanical properties is 18 μm, as shown in Figure 122.

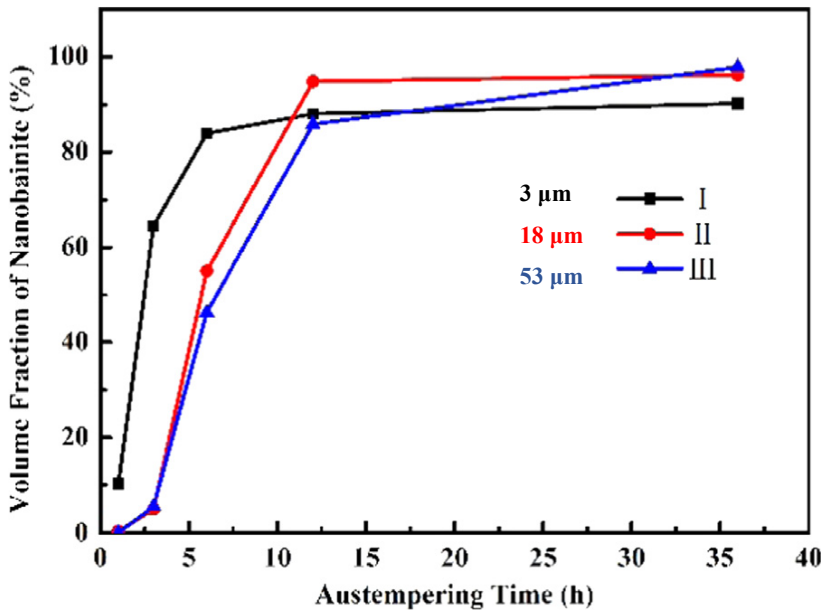

Figure 122. Volume fraction of bainite for different austenitization temperature and austempering time. I, II, III for austenitization at 820°C for 10 min, 900°C for 10min, 980°C for 1 h, respectively. [109]

However, some scholars believe that the increase of the nucleation rate at the prior austenite

grain boundary may not be conducive to the acceleration of bainite transformation. A large amount of nucleation will lead to premature and frequent soft impingement of the bainitic substructure to hinder the phase transformation. [110]

6.2.2. Effect of heat treatment process to nanobainitic steels:

In addition to adjusting the austenite transformation process to change the prior austenite grain size, the related process of changing the low temperature bainite transformation also has a significant effect on the bainite transformation. The research results show that the phase transformation rate of nanobainite in two-steps austempering treatment process is significantly higher than that in one-step austempering treatment process, as shown in Figure 123 which is analogous to Figure 15, process 4.

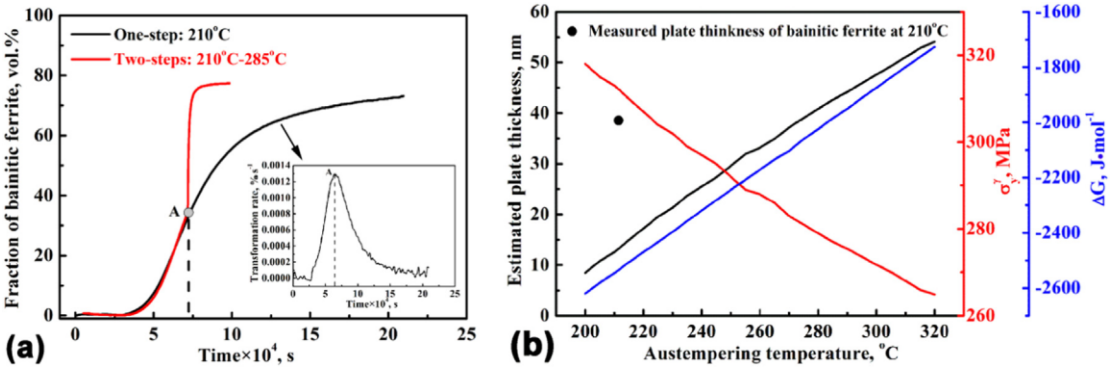

Figure 123. (a) Transformation kinetic of one-step and two-steps treatment processes. (b) The variation of bainitic ferrite plate thickness, $\Delta G^{\gamma\alpha}$ and σ_y^{γ} as a function of austempering temperature. [111]

Compared with one-step austempering treatment process, the nanobainite lath formed by the final two-steps austempering treatment process does not have obvious coarsening due to the increase of the bainite/austenite interface to accelerate the autocatalytic nucleation of bainite as shown in Figure 124. Compared with the one-step austempering, the tensile strength of the nanobainitic steel by two-steps austempering is increased by about 200 MPa, the toughness is increased by 47%, and the ductility is also slightly improved. This is mainly due to the fact that in the process of bainitization, two-steps austempering can obtain more nanobainite and the second-step high temperature isothermal is conducive to the distribution of carbon elements which improves the stability of retained austenite.

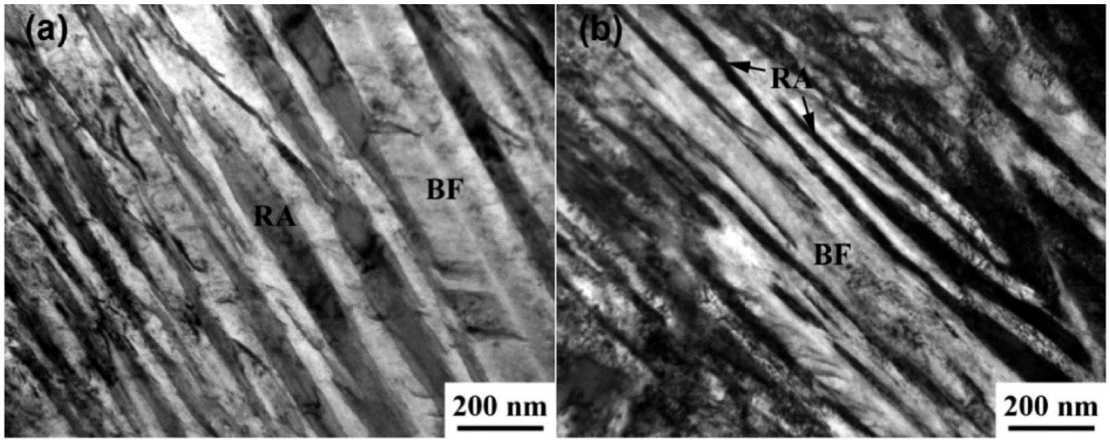

Figure 124. TEM images for the (a) one-step and (b) two-steps specimens. [111]

In addition, the pre-quenching process which is analogous to Figure 15, process 3 can also accelerate the bainite transformation rate. After complete austenitisation, first reduce the temperature below the M_S point to form a small amount of martensite, and then increase the temperature to the bainite transformation temperature range, as shown in Figure 125. This is because the pre-existing martensite can be used as a potential nucleation site for bainitic ferrite which increases the nucleation rate of bainitic ferrite.

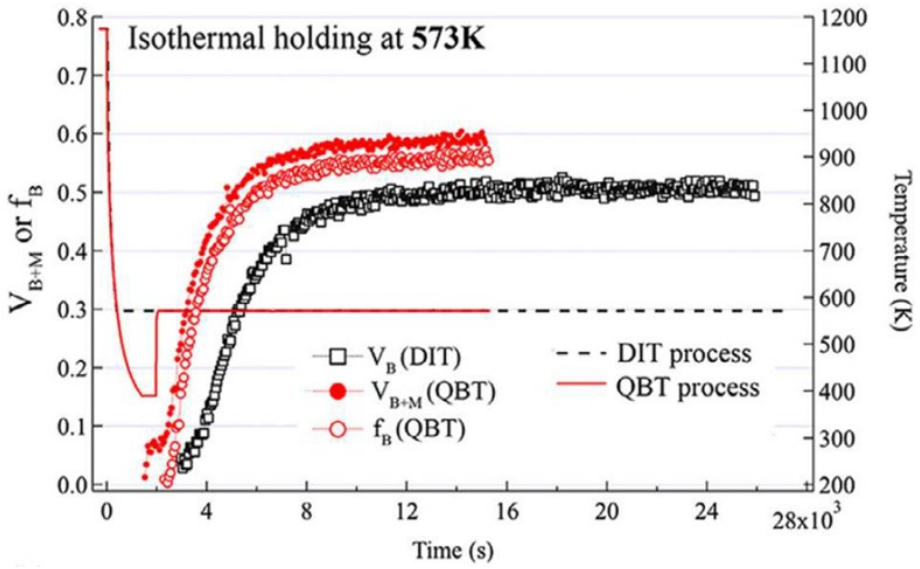

Figure 125. Bainite transformation kinetics of QBT and DIT at isothermal temperature of 300℃. [112]

The orientation of bainitic ferrite around martensite tends to be consistent with the martensite orientation, as shown in Figure 126, indicating that pre-existing martensite affects the variant selection of bainite. At the same time, the martensitic transformation causes the accumulation of dislocations around the original austenite interface which is beneficial to the nucleation of bainite. The scholars also found that the process also had a positive effect on the improvement of the strength and toughness of the structure while the bainite transformation was accelerated.

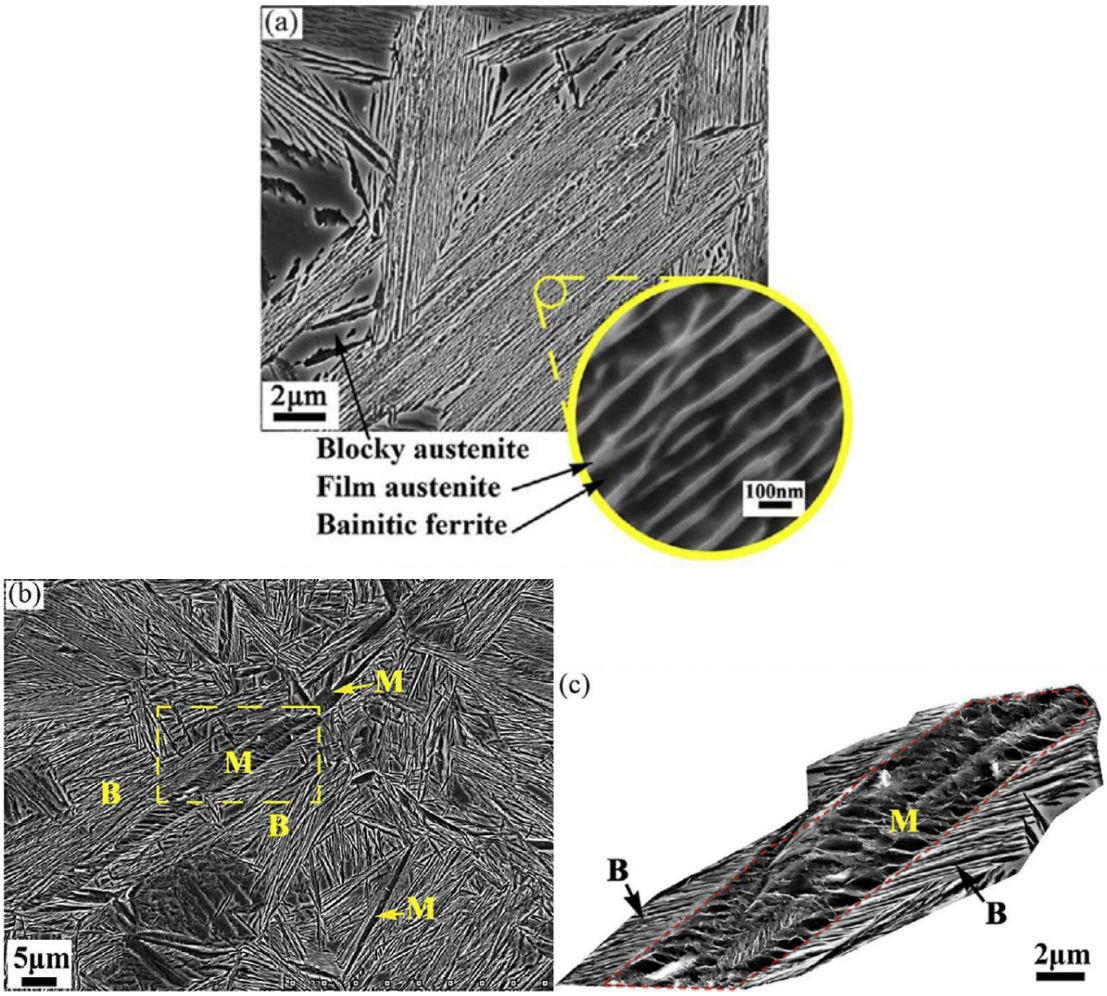

Figure 126. SEM micrographs of samples: (a) DIT, (b) QBT (low magnification) which shows martensite (M) and bainite (B) regions, and (c) QBT (the framed area in (b) viewed at high magnification). DIT: Direct isothermal bainite transformation. QBT: isothermal bainite transformation after partial quenching. [112]

Compared with some high carbon alloy steels, low carbon and low alloy steels have a higher martensitic transformation temperature and the first problem they face is how to form nanobainite. The researchers chose multi-step low temperature isothermal heat treatment for low carbon and low alloy steel to obtain a large amount of nanobainite, as shown in Figure 127. The phase transformation process is to control the carbon concentration in the retained austenite in stages so that the martensitic transformation temperature point of the local austenite gradually decreases. The temperature range of bainite transformation can be dynamically widened to obtain nanobainite by cooling isothermally for many times and accurately controlling the distribution of carbon elements.

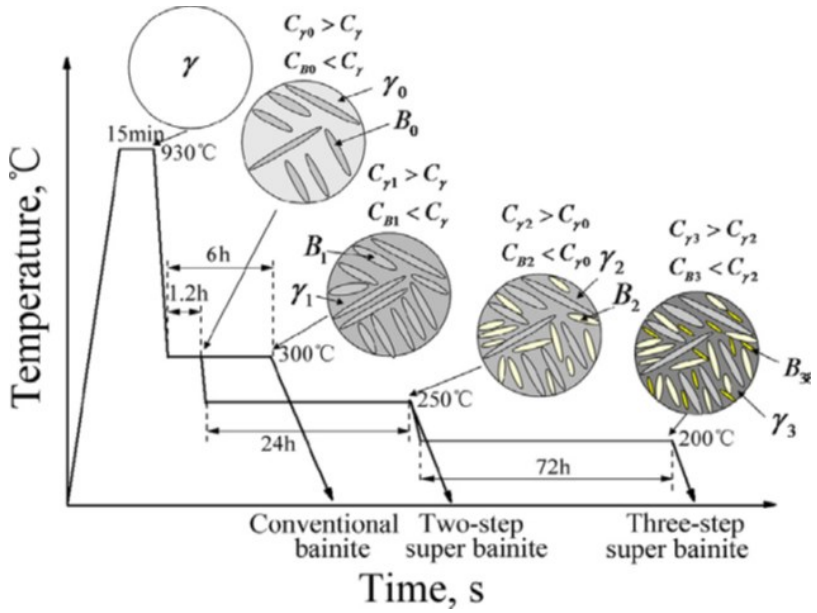

Figure 127. Schematic of muti-step isothermal bainitic transformation and the corresponding microstructural evolution. [113]

6.2.3. Other effecting factors:

In addition to adding alloys and changing the heat treatment regime, deforming the austenite before the bainite transformation occurs is also an effective means to accelerate the bainite transformation and improve the bainite morphology. The specific impact of this process can be subdivided into two situations: stress and strain. Studies have shown that the bainite transformation driving force can be increased and the bainite transformation rate can be accelerated by introducing stress below the yield strength into austenite. [114] At the same time, the introduction of stress may also change the bainite microstructure, but the influence of strain on the kinetics of nanobainite transformation is still controversial.

Similar to alloy composition, temperature, etc., magnetic field strength is also an important thermodynamic parameter. Since the magnetic susceptibility and dielectric constant of each phase of metal materials are different, adjusting the magnetic field intensity can change the phase transition behavior and microstructure of the material by changing the Gibbs free energy of the material. In the field of solid-state phase transformation of iron-based alloys, the introduction of a magnetic field has been found to promote the transformation process of part of the FCC phase to the BCC phase by changing the driving force of the phase transformation, [115] but the large-space strong magnetic field environment is currently only open for scientific research work, which is inconvenient to practical production of nanobainitic steels.

6.3. Mechanical properties of nanobainitic steels：

6.3.1. Strength vs. ductility：

The bainite structure obtained by low temperature transformation is harder than ever, with values in excess of 700 HV. Some strength and ductility data at room temperature are shown in Figure 128. Ultimate tensile strength (UTS) always exceeds 2000MPa and elongation could exceed 20%. The 0.6C grades (NB 9~12) do not exhibit significant difference in tensile properties as a function of composition. However, for the same transformation temperature, higher carbon grades (1~0.8C, NB 4~8) exhibit higher tensile strength (typically 2200 MPa) and lower elongation, with the exception of NB 7. Particularly surprising is that NB 7 alloy has an extraordinary combination of ductility and strength, that is a UTS of 2000MPa with a uniform elongation of 12%.

Most of the strength of nanobainitic steels originates from the unusually small bainitic ferrite platelets, which lead to a small mean free path for dislocation slip. The ductility is mainly controlled by retained austenite due to its softness, work hardening index and TRIP effect. Compared with bulk retained austenite, austempering at lower temperature decreases the lath thickness of bainitic ferrite and the volume fraction of retained austenite, but increases the content of thin-film retained austenite. This results in an increase in strength while retaining a great deal of ductility.

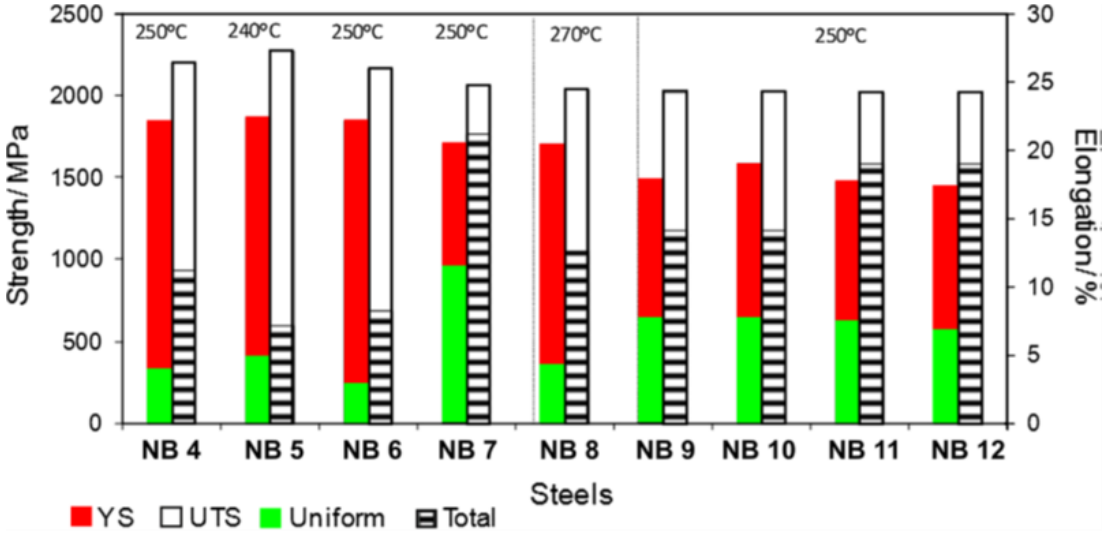

Figure 128. Relevant tensile properties of second generation of nanostructured bainitic steels at different isothermal temperatures. NB is short for NANAOBAIN. [103]

However, the bainitic ferrite or retained austenite content and lath thickness, which were selected as microstructural parameters do not provide any indication of the ductility. Similar parameters could result in significantly different ductility, with a clear difference in isothermal transformation temperature, as shown in Table 20. Even after heat treatment at 220°C and 250°C, NANOBEIN 7 exhibits the same retained austenite and bainite lath thickness, but its ductility is entirely different. The key to the ductility is the retained austenite mechanical stability.

Alloy	*T*, °C	YS, MPa	UTS, MPa	UE, %	TE, %	V_γ, %	*t*, nm
NANOBAIN 6	200	2019	2091	0.37	0.38	20	21
	250	1852	2164	2.86	8.29	22	32
NANOBAIN 7	220	1704	2287	7.37	7.37	36	32
	250	1698	2068	11.62	21.32	34	32
NANOBAIN 8	220	1931	2329	3.19	4.1	22	32
	270	1701	2036	4.44	12.64	24	36

t bainitic ferrite plate thickness, *T* isothermal transformation temperature, *TE* total elongation, *UE* uniform elongation, *UTS* ultimate tensile strength, V_γ austenite volume fraction, *YS* yield strength.

Table 20. Tensile test results on selected grades and conditions. [103]

6.3.2. Toughness:

In the study on improving the strength-toughness combination of nanostructured bainitic steels, [17] it was found that plane strain fracture toughness and impact toughness could be improved with increasing austempering temperature. This trend is attributed to the higher content of retained austenite, which absorbs a large amount of plastic work during crack propagation due to its higher ductility and higher energy consumption during its transformation to martensitic.

Impact energy is greatest at moderate austempering temperatures. The lower impact toughness at higher austempering temperature is related to the coarse morphology of retained austenite, while the decrease in toughness at the lowest temperature is attributed to insufficient volume fraction of ductile austenite phase. Therefore, higher retained austenite volume fraction can improve impact toughness when retained austenite is not bulky.

It has also been observed that refining the prior austenite grain size by adding V increases the density of bainite nucleation sites, thereby further refining the bainite sheaves. Smaller bainitic sheaves with different crystallographic orientations repeatedly change the crack propagation path, thereby improving the impact toughness of the steel.

C	Si	Mn	Mo	Cr	Al	Co	V/W/Ni/Cu/TiT/t		YS/UTS	TE/A	I	K	H
0.79	1.56	1.98	0.24	1.01	1.01	1.51	–	250/18	-/–1800	–13	-	–28	-
								300/5	-/–1600	–28	-	–52	-
								350/5	-/–1300	–5	-	–32	-
								350/5 + 250/18	-/–1500	–40	-	–63	-

Table 21. Chemical composition, transformation temperature (T) and time(t), mechanical properties, which include tensile strength, elongation and fracture toughness (K_{IC}/K_Q) in $MPam^{0.5}$. [116]

A two-steps isothermal transformation was performed on high carbon nanobainitic steels to reduce the bulk retained austenite and improve the fracture toughness of the steel. Compared with the conventional one-step isothermal transformation, the microstructure refinement, the reduction in the amount of massive retained austenite and the bimodal size distribution of the bainitic laths after the two-steps isothermal transformation are the main structural changes. Furthermore, the bulk retained austenite after the first-step transformation is geometrically divided by the formation of different crystallographic variants of the second-step bainite. Therefore, the two-steps transformation leads to the formation of a finer microstructure, higher bainitic ferrite content, more bainite variants and more stable retained austenite. Thus, ductility and fracture toughness are improved, as shown in Table 21. The fracture toughness values of nanostructured bainitic steels are in the range of 28~63 $MPam^{0.5}$.

6.3.3. Fatigue:

The perfect combination of strength and ductility makes nanobainitic steels potentially useful in the railway and automotive industries. In order to design safer components for extended service life, studies of fatigue crack initiation and propagation need to be focused. Some researchers

performed the high cycle fatigue tests on this type of steel. [117] The fatigue response of air-melted bainitic steels was found to be similar to other high strength steels of similar hardness. The fatigue limit was estimated to be 855 MPa based on the extrapolation of S-N data points obtained from tensile fatigue tests in the maximum applied stress range of 1200~1600 MPa. In high cycle 3-point bending fatigue tests on vacuum-melted nanostructured bainitic steels with tensile strengths in the range of 2080~2375 MPa, the fatigue limit without failure within 10^7cycles is determined to be 1033~1156 MPa. [118]

There are currently no studies on the high cycle fatigue response of nanobainitic steels. However, using bainitic quenching and partitioning steels with microstructural features larger than 100 nm, the combined effect of inclusion size and microstructure on ultra-high cycle fatigue behavior was observed. [119] Specimens with larger inclusions failed due to inclusion-induced crack initiation, whereas non-inclusion-induced crack initiation is facilitated by coarse bainite/ martensite blocks and bulk retained austenite observed only in specimens with coarser microstructures.

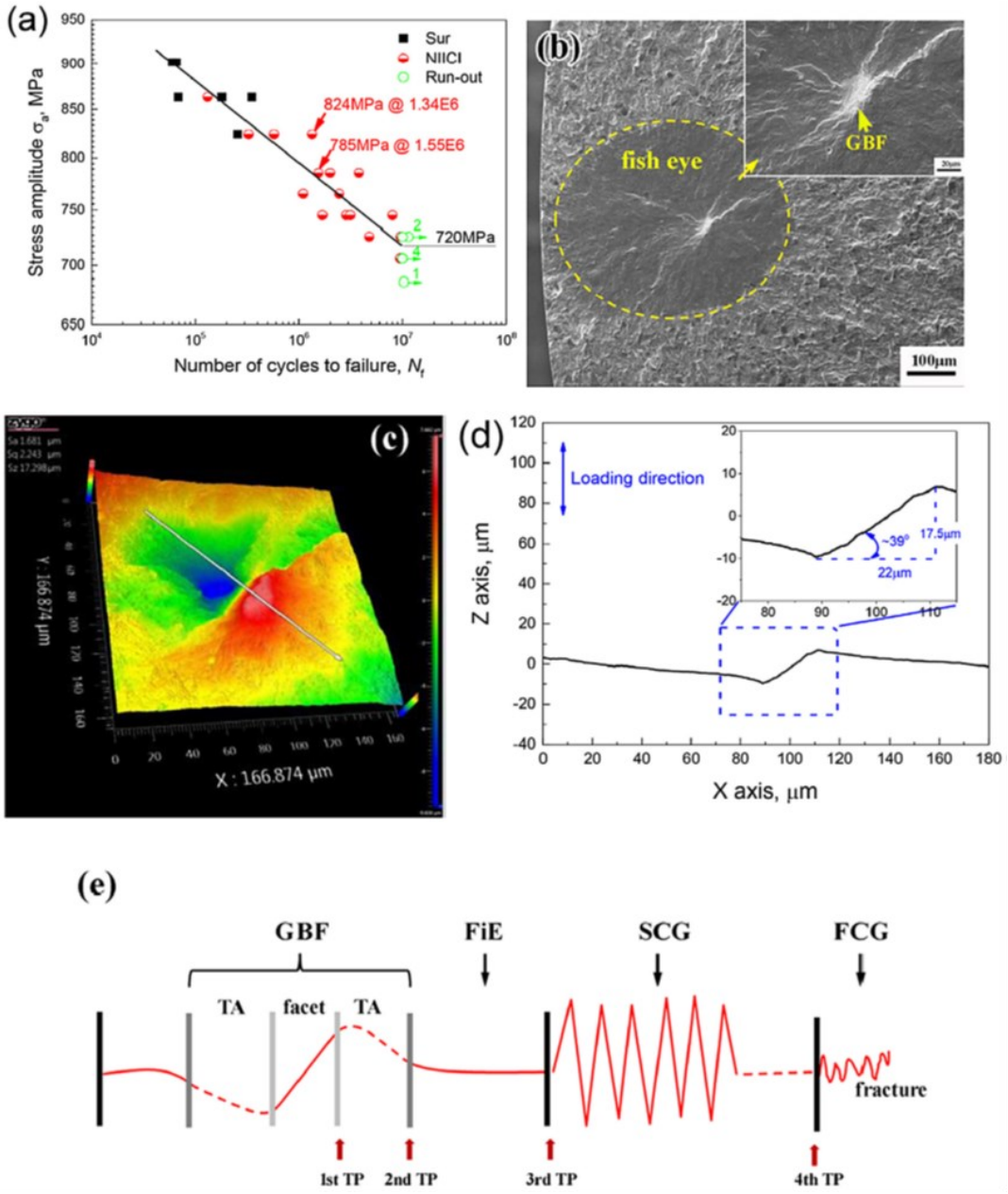

Figure 129. (a) S-N curve, Sur: fatigue crack initiation at surface, NIICI: non-inclusion-induced crack initiation at the interior microstructure. (b) SEM of a typical NIICI fracture surface. (c) 3D morphology image of GBF region in the inset of (b). (d) The sectional profile of the labelled line in (c). (e) The entire fatigue process from crack initiation to fracture, TA: transition area, TP: transition point, FiE: fish eye, SCG: slow crack growth region, FCG: fast crack growth region. [116]

In another study on clean medium carbon nanobainitic steels with retained austenite films in the 50~200 nm range, the average fatigue strength for 10^7 cycles is around 720 MPa. Figure 129 shows the S-N curve, fatigue fracture and other general characteristics of crack initiation and propagation until failure in high cycle fatigue tests. It was found that the transformation of film-type retained austenite to martensite (martensite is not brittle because of its film-type morphology) prevents the growth of small cracks, which is similar to the crack closure phenomenon for long cracks. On the other hand, the bulk retained austenite located at the prior austenite grain boundaries is not conducive to fatigue life. Since the austenite has more slip systems than bainitic ferrite, when the slip bands in the adjacent prior austenite grain collide with the prior austenite grain boundaries during cyclic loading, it is easy to activate slip on the preferred slip plane (such as {1 1 1}) in the bulk retained austenite. Therefore, the bulk retained austenite region is an effective site for the initiation of intergranular fatigue cracks. Figure 129(b) shows a typical non-inclusion-induced crack initiation (NIICI) point away from the specimen surface. A granular bright face surrounded by a "fish eye" labeled GBF was found to be the initiation point of the crack. The GBF consists of a microfacet and surrounding undulating areas. As shown in Figure 129(c) and (d), microfacets are generated due to the fracture of the first-stage short cracks formed in the plane where the shear stress is greatest. The undulations around the GBF are the transition area (TA) where the phase I short crack develops to the phase II crack. The complete fatigue phenomenon has been explained with the aid of the schematic diagram shown in Figure 129(e).

Since almost all engineering components contain areas of stress concentration in the form of fillets, holes, inclusions, etc., it is easy to initiate cracks where these stresses occur, or some kind of fatigue crack is already present in the component. Therefore, higher fatigue life could only be achieved by properly designing a microstructure that can hinder the growth of these small fatigue cracks to prevent them from reaching the critical length where microstructural barriers is no longer very important in blocking the cracks.

6.4. Discussion:

In recent decades, improving the strength and toughness of steels has been the pursuit of related research fields. Unlike the way of ultra-refinement of the structure by large deformation of the structure or the use of extreme heat treatment conditions, the successful development of nanobainite makes it possible to refine the structure at the nanoscale under conventional conditions. The related development of nanobainite has broad application prospects in engineering and industrial fields. In order to solve the practical problem of the long heat treatment time of nanobainite, relevant scholars have carried out a lot of exploration in the fields of alloy design, heat treatment, and pre-deformation.

In the future, the development of nanobainite will gradually face the field of medium and low

carbon steels and medium and high alloy steels. The phase transformation rate of nanobainite can be effectively improved by designing reasonable alloy composition, designing nano precipitation and rationally designing pre-transformation and pre-deformation. The specific scheme of accelerating the bainite transformation needs to combine with the thermodynamic conditions of the material, discuss the nucleation and growth of nanobainite in stages and design the corresponding composite transformation acceleration technology.

7. Cold drawn pearlitic wire

During the driving process of the car, the energy will be consumed by various resistances, of which about 20% of the gasoline is consumed by the rolling resistance of the tires. In addition to promoting the development of low rolling resistance tires, in terms of skeleton material, the use of ultra-high strength steel can ensure that the amount of steel in the cords and the tire weight can be reduced while meeting the tire strength. It reduces the rolling resistance of tires, saves fuel consumption and reduces carbon dioxide emissions.

Cold-drawn nano pearlite steel is a kind of lamellar autogenous composite material with excellent mechanical properties. Because of its high tensile strength and certain ductility, and the process conditions of large-scale industrial production, this kind of material is widely used in important engineering fields such as springs, steel cords for reinforced radial tires and suspension bridge cables. [120]

At the end of the last century, the strength of steel cords for tires has been increased from 2800 MPa to 4000 MPa. At present, in the laboratory, the ultimate tensile strength of cold-drawn nano-pearlite steel has reached 7000 MPa which is the highest strength mass-produced bulk material. [121]

Cold-drawn nano pearlite steel products generally use high carbon steel near the eutectoid point as the production raw material, and use lead bath isothermal quenching to obtain a pearlite structure with fine lamella spacing and good drawability, and then produced by cold drawing process.

The carbon content of cold-drawn pearlite steel wire is generally between 0.7 and 1.0 wt.%, and other additions are also very small, especially the additions of other metals are mostly too small to form considerable amounts of carbides. Table 22 shows, as examples, the composition of some pearlitic steel wires that were cold drawn to their respective true strain ε.

Fe	C		Si		Mn	Ni	Cr	ε
	wt%	at.%	wt%	at.%				
Bal.	0.82	3.71	0.2	0.4	0.5			
Bal.	0.82	3.71	0.2	0.4	0.5			5.00
Bal.	0.90	4.07	0.40	0.77	0.57			1.62
Bal.	0.85	3.85						1.8
Bal.	0.77	3.50	0.3	0.6	0.62	0.01		2.89
Bal.	0.86	3.89	0.84	1.61	0.75			1.57
Bal.	0.92	4.13	1.3	2.5	0.5		0.3	1.61
Bal.	0.92	4.13	0.22	0.42	0.48			4.61
Bal.	0.81	3.66	0.20	0.39	0.48			
Bal.	0.98	4.40	0.20	0.39	0.30		0.21	

Table 22. Composition of pearlitic steel wires examined in different studies. [122]

7.1. Processing of pearlitic wire:

Figure 130 is the production process flow chart of typical grade (SWRH82B) steel wire. First, hot rolling is carried out, the rolling temperature is 1120~1140°C, the final rolling temperature is 900~950°C and the spinning temperature is about 900°C. Then, the austenite is quenched to below the pearlite transformation temperature and the isothermal transformation is carried out to obtain a full pearlite structure. Generally, the pearlite lamella spacing should be controlled below 200nm. This step is called isothermal quenching. After hot rolling, it is coiled and then supplied to wire

drawing factories, so it is called wire rod. In general, by increasing the degree of undercooling, the interlamellar spacing of pearlite can be refined, thereby improving the mechanical properties of the wire rod. After purchasing the wire rod, the wire drawing factory first performs pickling and phosphating treatment, and prepares the steel wire by continuous multi-pass cold drawing, followed by hot-dip galvanizing in a zinc bath at about 450°C. In order to reduce creep, reduce stress relaxation rate and improve the stability of steel wire, stabilizing treatment should be carried out on steel wire after hot-dip galvanizing. Stabilization treatment is generally a tempering treatment process that applies a certain amount of tensile deformation to the steel wire or steel strand, and the temperature is generally lower than 400°C.

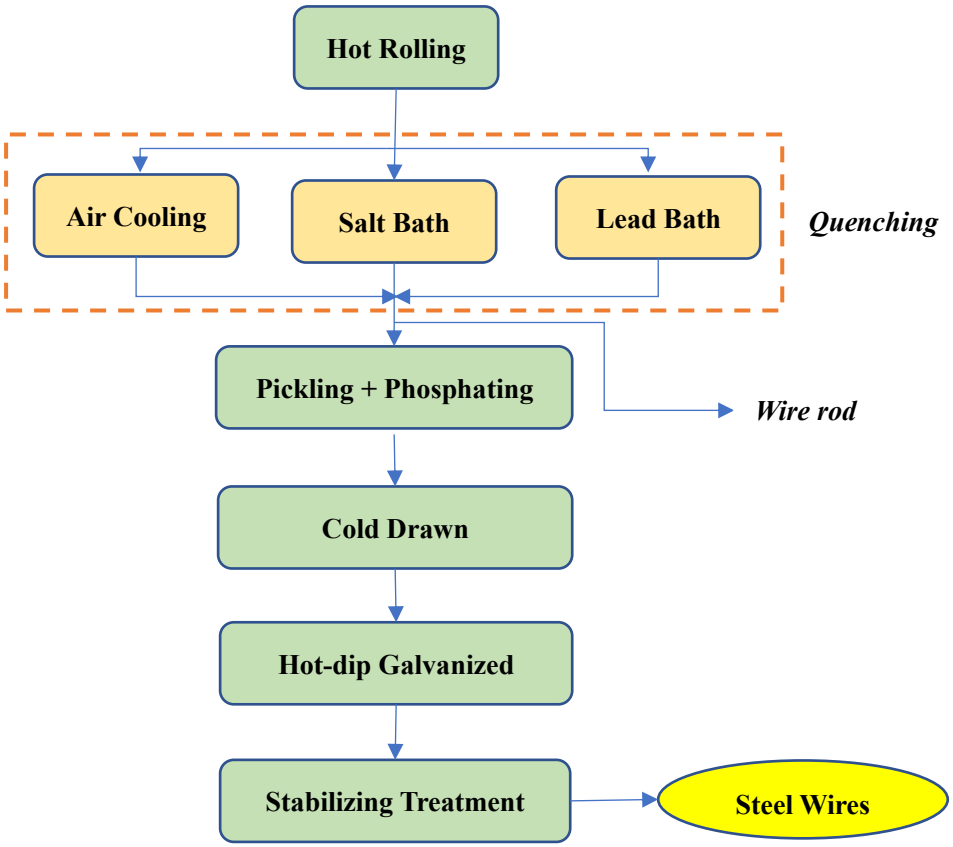

Figure 130. Flow chart of production technology of SWRH82B steel wires. [123]

7.1.1. Quenching process of wire rod:

In actual production, according to the different quenching process, isothermal quenching can be divided into two categories: on-line quenching (after-rolling quenching) and reheating quenching. Reheating and quenching mainly refers to lead bath quenching (lead patenting, LP). Due to the large footprint, large investment, high energy consumption, low productivity and high production cost of reheating and quenching, the reheating and quenching process is rarely used in actual production, but the on-line quenching is used. However, for certain steel wires with special requirements, such as steel cords, the reheating method is also used in some production plants.

The so-called on-line quenching refers to placing the equipment for quenching with residual heat after rolling at the end of the rolling line and quenching the wire rod at the final rolling

temperature. Compared with reheating and quenching, on-line quenching has the following advantages: (a) no need to build another quenching production line and intermediate warehouse and occupies a small area; (b) no need to build another heating equipment, low investment and low energy consumption; (c) high production efficiency and low production cost. At present, the online quenching methods of wire rod mainly include Stelmor control cooling process line (direct patenting, DP wire rod), water penetration cooling line after rolling, Schlomann control cooling process line and salt bath quenching control cooling process line (direct on-line patenting, DLP wire rod). Among them, the Stelmor control cooling line technology is the most mature and widely used. The DLP process is a unique patented technology in Japan, which is currently mainly used in Japan. The schematic diagrams of the cooling curves under the three production process conditions are shown in Figure 131:

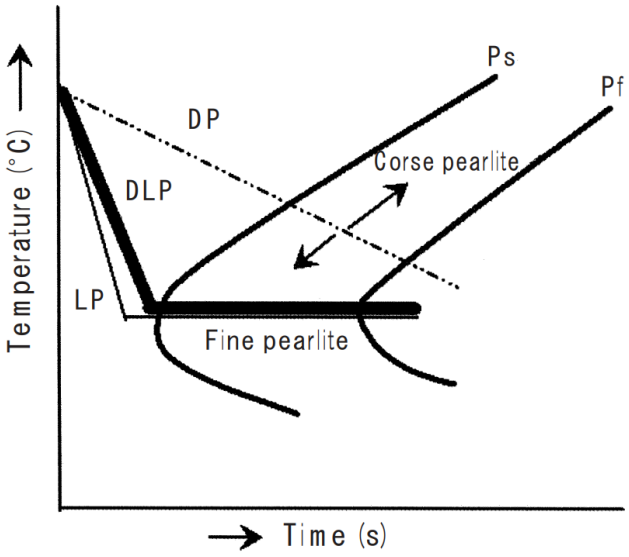

Figure 131. Scheme of cooling rate and pearlite transformation temperature. [124]

The Stelmor controlled cooling process is an on-line controlled cooling method for hot-rolled wire rods. It was jointly developed in 1964 by Canada's Stelco and American Morgan. As shown in Figure 132, this process is to cool the hot-rolled wire rod twice with two different cooling media at different cooling rates, that is, one water cooling and one air cooling [125~126]. After the wire comes out of the finishing mill, it is firstly cooled by water in the wire tube. The main purpose of water cooling is to control the size of the prior austenite grains. After water cooling, the spinning silk is scattered and rolled on the moving transport chain. The top of the transporter is open and the pearlite transformation (quenching) is done on the transport chain. Under the transport chain, the fan is forced to blow the wire upward through the nozzle for cooling. The cooling temperature and speed are controlled by changing the transport speed (that is, changing the overlapping density of the coils) and the air volume (the number of fans and the wind speed). For low carbon steel which the content of pre-eutectoid ferrite is high, generally set to slow cooling and the transformation temperature is relatively high. For high carbon steel, if you want to obtain fine pearlite, it needs to be set to fast cooling. The temperature is relatively low. Typically, when the wire reaches the Stelmor wire, the temperature is generally between 840°C and 940°C, while the pearlite transformation temperature is generally between 770°C and 600°C.

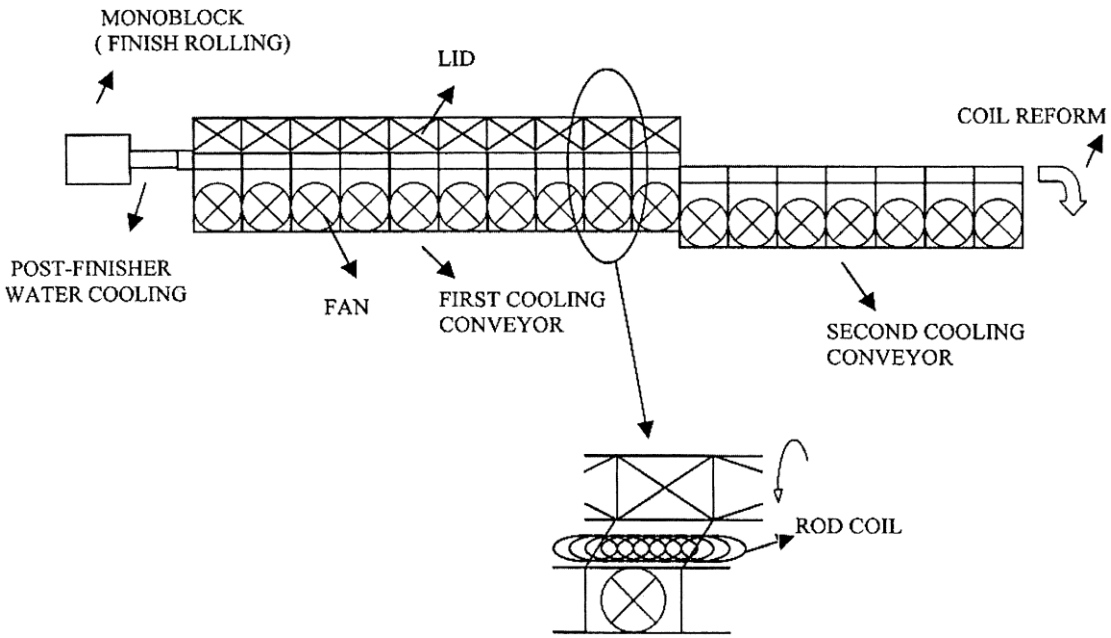

Figure 132. Schematic diagram of the Stelmor system. [126]

In 1985, the DLP production process was successfully used to produce pearlite wire rods. Since the DLP process uses salt to replace lead, the pollution to the environment is reduced and energy is saved. After more than 20 years of development, the DLP production process has gradually been popularized and applied in Japan. Initially, the advantages of the DLP industry are mainly two points: the use of on-line quenching saves a lot of energy; the use of salt instead of lead quenching reduces environmental pollution. As shown in Figure 133, the DLP equipment mainly contains two salt baths, namely, a cooling bath (No. 1 salt) and a constant temperature bath (No. 2 salt). The temperature of the cooling bath can be set to any temperature for special pretreatment of the wire rod, that is, by changing the temperature to control the grain size of the prior austenite. As the name implies, the temperature of the constant temperature bath is transformation temperature to obtain the sorbite structure.

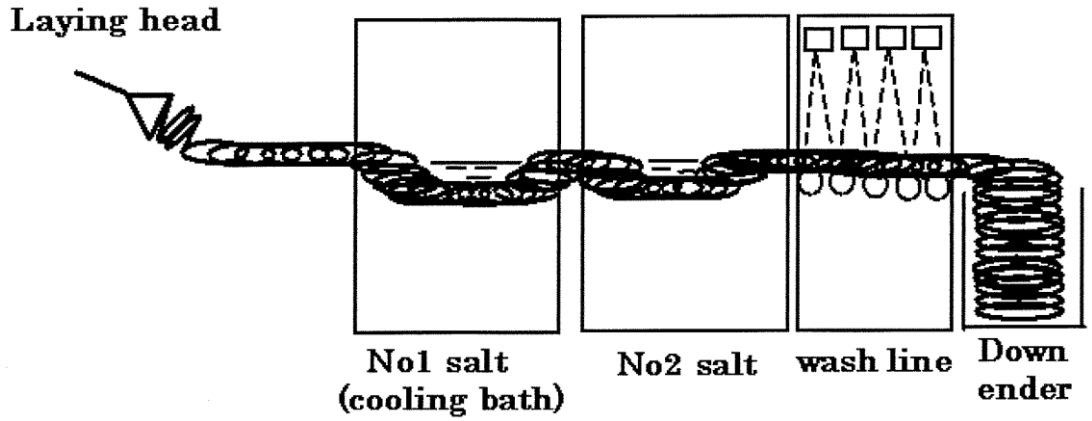

Figure 133. Outline of the DLP equipment. [124]

Stelmor air-cooling is the most widely used sorbite treatment process with fast production speed, low environmental damage and low cost. DLP process is a patented technology unique to

Japan. At present, DLP wire rods on the market are mainly produced by Nippon Steel, etc. The lead bath quenching process has great environmental pollution and is basically abandoned now. Since DLP wire rod has higher strength and toughness than DP wire rod of the same specification, its market price is also higher. The Stelmor cooling method is also slowly replaced by the DLP method due to the inhomogeneity of the tissue.

7.1.2. Cold drawing process of steel wire:

Cold drawing is one of the methods of metal pressure processing. Using the plastic deformation ability of metal wires, large-diameter wire rods are drawn to pre-designed smaller-diameter steel wires through special equipment. The wire drawing technology has a long history. After continuous technical improvement, the current drawing process is relatively mature. The surface condition of the wire rod, the lubricating medium, the drawing die, the heat dissipation capacity, the designation of the total compression ratio and the distribution of the partial compression ratio, the deformation rate, etc. are the key control points in the cold drawing of the steel wire.

There are generally two ways of drawing, namely wet drawing and dry drawing. Wet drawing is suitable for the drawing of smaller diameter wires, using liquid lubricating medium. For the large diameter of the steel wires, dry drawing is generally adopted and the lubricating medium is granular or powdery, commonly known as drawing lubricating powder.

The drawing tool is called a drawing die which is mainly composed of a die sleeve and a die core. The core is generally made of diamond, cemented carbide and other materials. Figure 134(a) is a schematic diagram of the structure of the wire drawing die and the drawing deformation of the wire. The drawing process of the steel wire is to first reach the entrance, enter the working area together with the lubricating powder through the lubricating area, plastically deform due to the pulling force in the drawing direction and the pressure generated by the wire drawing die and then stably deform through the sizing area, finally be removed from the exit. It can be seen that the deformation of the steel wire on the cross section is not uniform and the degree of plastic deformation changes from large to small from the outer layer of the steel wire to the center. The working cone half angle α of the wire drawing die is generally between 5 and 15°, the precision control of the cone angle has a great influence on the wire drawing. The selection of the compression ratio and the drawing speed of each pass will also affect the deformation of the steel wire and these are also difficult to control when the steel wire is drawn.

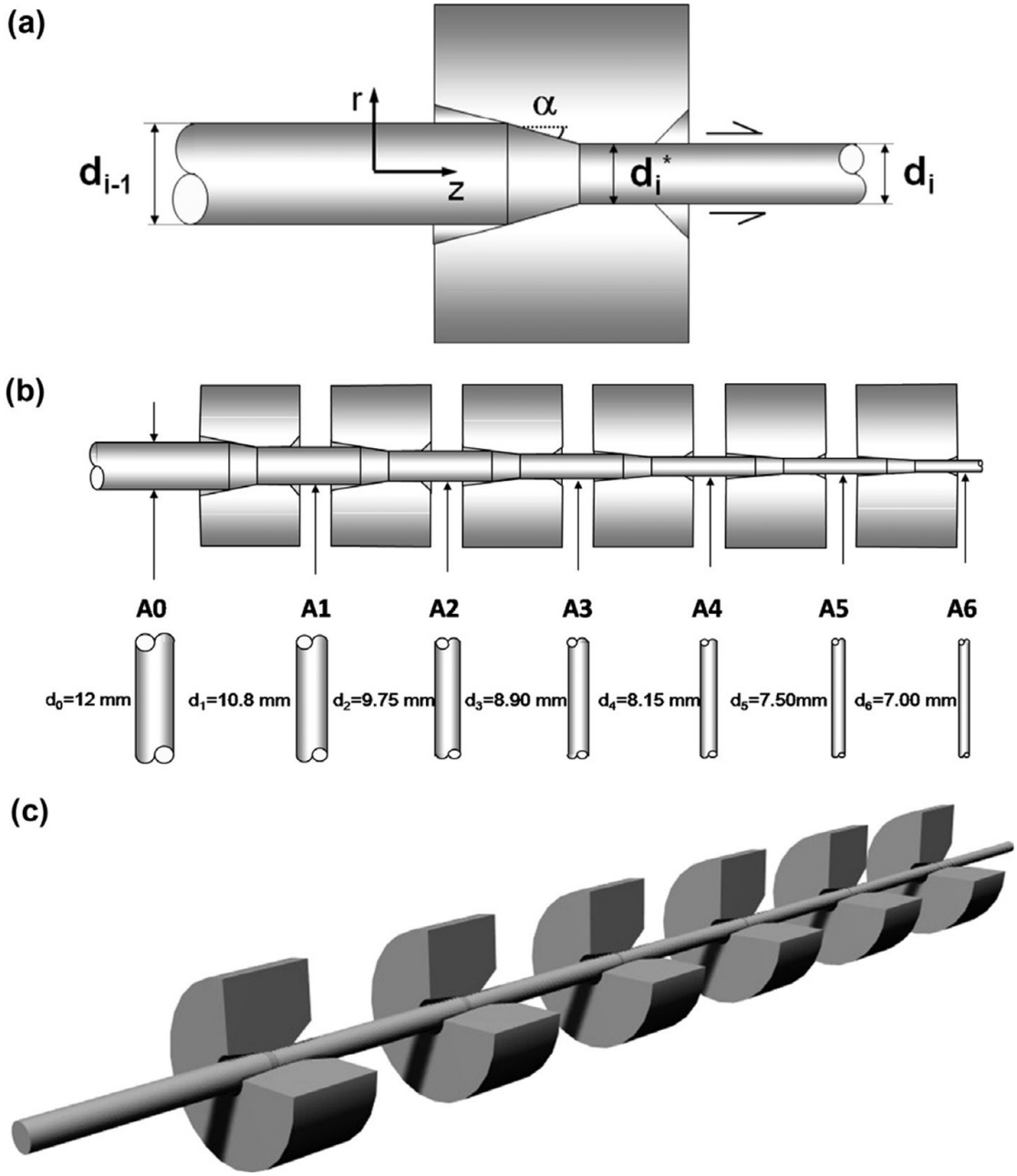

Figure 134. Scheme of the cold drawing process: (a) cold drawing in one pass of the steel through the die, (b) progressive cold drawing in six passes, (c) scheme of the whole chain of manufacturing. [122]

If the material was left in the heat-treated condition, the large crystals would lead to brittleness, but this effect is not found after several drawing passes: To avoid heat generation, the patented wire is heavily strained by wet wire drawing conducted at $3.3x10^2$m/s drawing speed with reduction area 20% per pass. Figures 134(b) and (c) show a drawing process scheme. The true strain ε obtained by continuous drawing is calculated by $\varepsilon = 2\ln(d_0/d)$, where d the wire diameter after continuous drawing and d_0 is the initial diameter. True strains as high as ε= 6.52 is reported to produce wires with strength as high as 7000 MPa.

7.2. Microstructure of cold drawn pearlitic wire:

Pearlite is the product of eutectoid decomposition of eutectoid austenite (about 0.80% C) after cooling to 550~720°C below the eutectoid line, through continuous cooling transformation or isothermal transformation. Pearlite is composed of two phases, ferrite (α-Fe) and cementite (Fe_3C). According to the different morphology of cementite, it can be divided into lamellar pearlite and spherical pearlite. The pearlite generated by eutectoid decomposition is generally lamellar pearlite (there may be a small amount of spherical pearlite in some areas). The difference in the transformation temperature of pearlite leads to the difference in the spacing between the pearlite lamellae. Therefore, according to the difference of lamellar spacing, it can be generally divided into pearlite (150~450nm, transformation temperature is A_1 ~650°C), sorbite (80~150nm, transformation temperature is 650~600°C) and troostite (< 150nm, the transformation temperature is 600~550°C). When the transformation temperature is lower, the diffusion rate of carbon atoms is smaller and the interlamellar spacing is smaller. For the convenience of description and discussion, both sorbite and troostite are collectively referred to as pearlite.

Lamellar pearlite is composed of alternating parallel ferrite and cementite lamellae. Figure 135 is a schematic diagram of lamellar pearlite. It can be seen that lamellar pearlite includes three microstructure parameters: pearlite nodule/grain, pearlite colony and pearlite interlamellar spacing (ILS). In pearlite, the structural units with the same crystal orientation of the ferrite matrix are defined as pearlite colonies/grains. The structural units with the same orientation of the cementite sheets are defined as pearlite colonies. Adjacent groups of ferrite sheets are defined as pearlite colonies. The thickness of the lamellae and cementite lamellae is defined as the pearlite lamellar spacing.

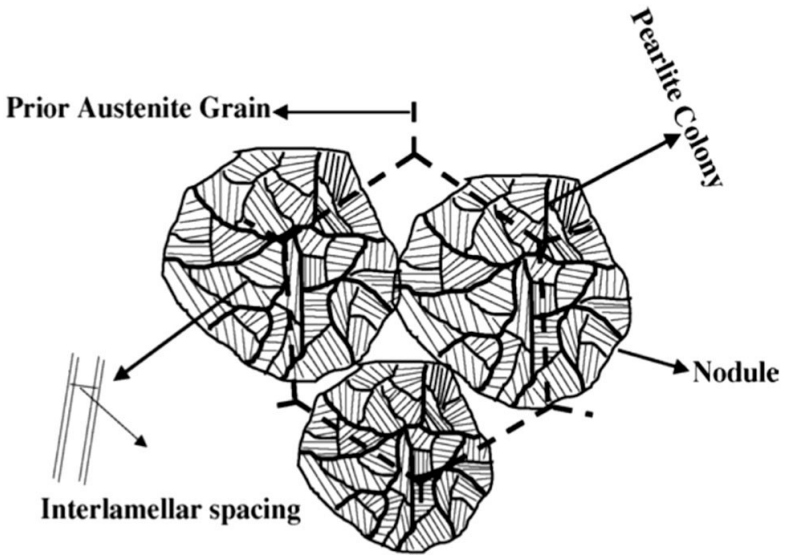

Figure 135. Schematic illustration of the various constituents of pearlite. [127]

Figure 136 is the microstructure photographs of the longitudinal section of the four kinds of steel wires with different strains along the drawing direction. When the amount of strain is 0, the structure presents a pearlite with relatively uniform lamellar spacing, in which the pearlite colonies are randomly arranged in all directions. When the strain amount is 0.54, under the drawing deformation, the pearlite colony gradually undergoes bending and torsional deformation and the

structure begins to appear directional, gradually turning and extending along the drawing direction. It was also found that a small amount of cementite sheet fractured perpendicular to the drawing direction. When the deformation amount is further increased to 1.58, the pearlite colonies have become inconspicuous, the lamellar spacing is further reduced. The degree of bending and twisting of the pearlite lamellae is more and more severe. The cementite with a certain angle to the drawing direction gradually turned to the drawing direction and the cementite lamella perpendicular to the drawing direction was significantly fragmented. When the strain amount reaches 2.29, the structure has been significantly elongated and the pearlite colony morphology and its microstructure details can no longer be observed in SEM. The cementite shows a good plastic deformation ability increase, and finally forms a fibrous structure parallel to the drawing direction.

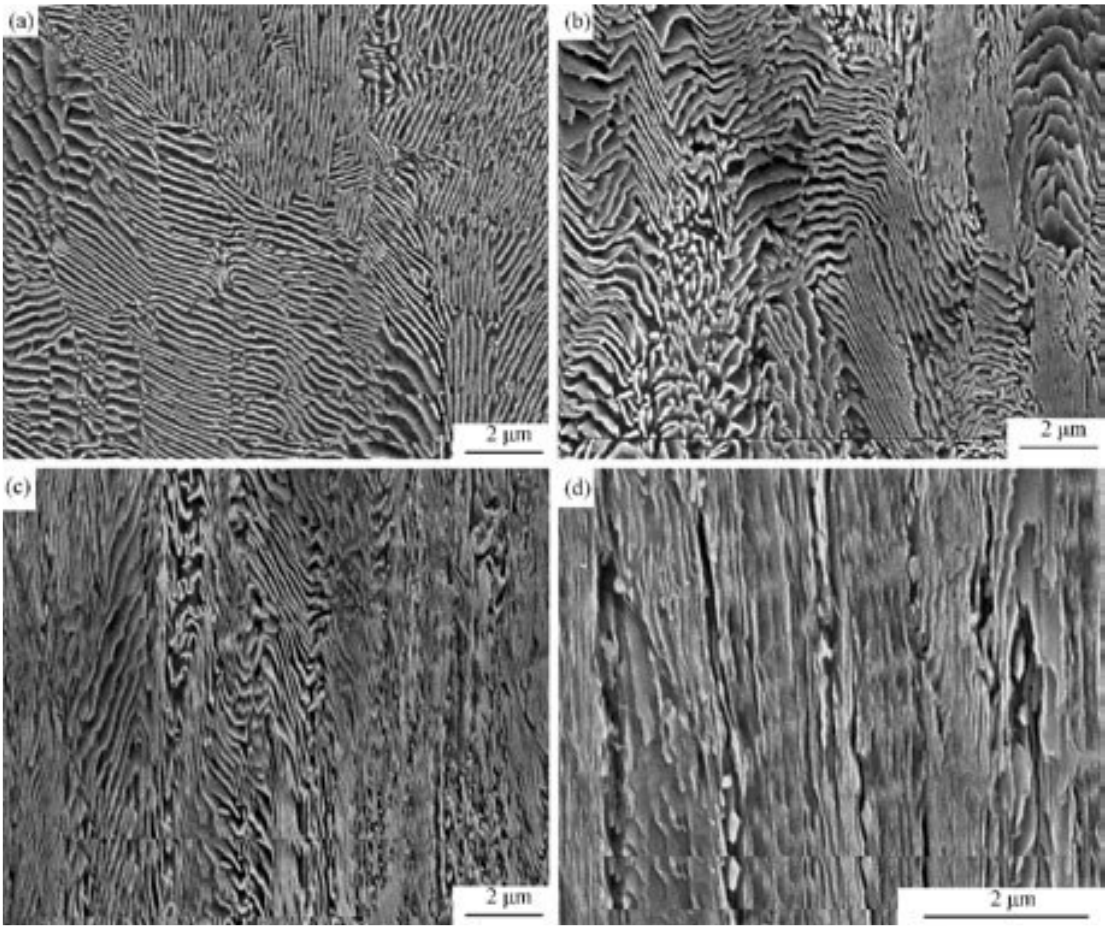

Figure 136. Microstructure of steel wires in the longitudinal section at different strain (a) ε =0, (b) ε =0. 54, (c) ε =1. 58, (d) ε =2. 29. [128]

Figure 137(a) is a TEM image of the original wire rod structure with 0 strain. It can be seen that in the initial structure, the cementite lamellae are continuous and relatively straight, almost no dislocation lines can be observed and the distance between the pearlite lamellae is about 100 nm. Cementite lamellae are more or less parallel in each individual nodule, while in different nodules they are randomly arranged relative to other nodules. Due to the slightly different patenting processes used for the different wires, the interlamellar spacing as well as the cementite lamella thickness will vary accordingly. Namely the interlamellar spacing is significantly influenced by the patenting temperature. Figure 137(b) is the TEM image of the microstructure of the longitudinal

section of the steel wire when the strain is 2.29. It can be seen that after strong deformation, a high density of dislocations is generated. The dislocation entanglement occurs and the lamellar spacing is reduced to about 40 nm.

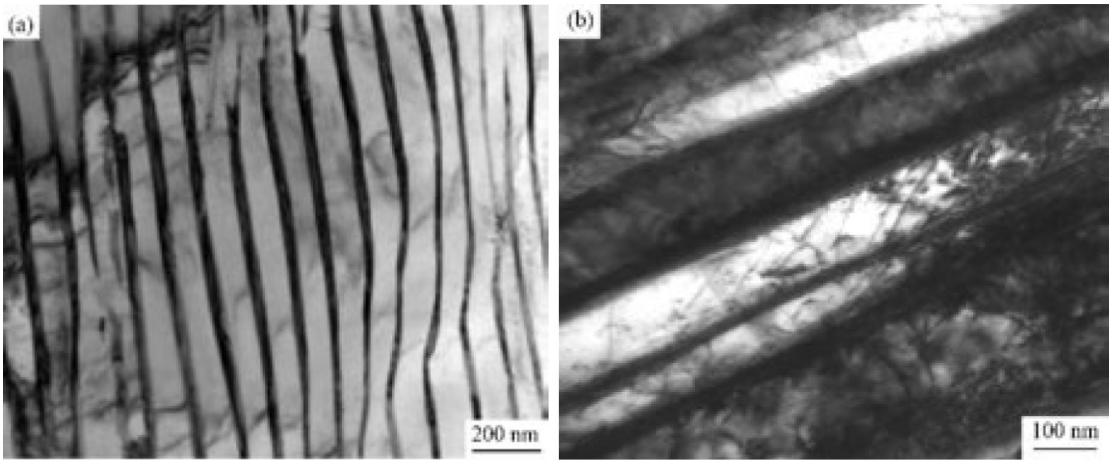

Figure 137. TEM microstructure of steel wires in the longitudinal section at different strain (a) ε = 0, (b) ε = 2. 29. [128]

The mechanical properties of deformed metals are dominated by dislocation storage, and the density of dislocations in ferrite lamella plays an important role in understanding strain hardening and its contribution to the flow stress of cold-drawn pearlite wire.

Figure 138(a) shows the dislocation configuration in the ferrite lamellae parallel to the drawing direction at a ε= 0.68. Most of the dislocations are distributed in ferrite lamellae, with the ends of the lines located at steps at the ferrite/cementite boundary. The calculated value of the dislocation density is $7x\ 10^{14}m^{-2}$. This is consistent with the results of crystallographic orientation measurement. Figure 138(b) shows a schematic diagram of the dislocation configuration in the ferrite lamellae at ε=2.67. Note that the distribution of dislocations in the ferrite lamellae is very regular with a spacing of 10~20 nm. The calculated value of the dislocation density is $8.8x10^{15}m^{-2}$. TEM and HREM studies of the wire at ε=3.68 showed a dislocation density of $2x10^{16}m^{-2}$.

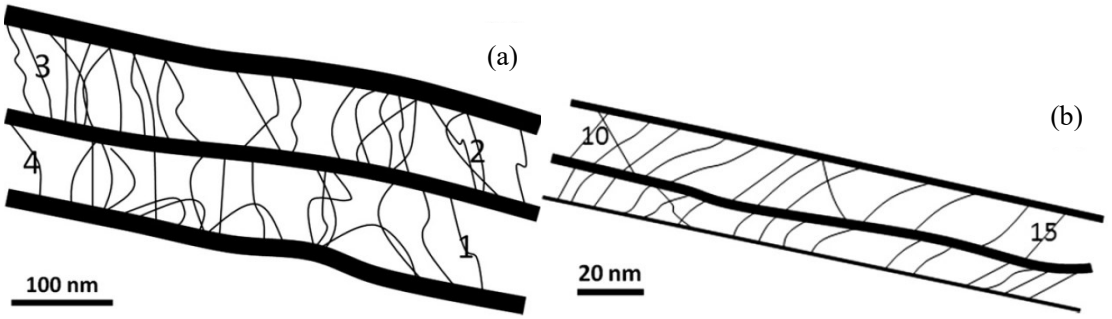

Figure 138. Schematic diagram of the dislocation in the ferrite lamellae. The dislocation density of a sample deformed (a) to a strain of 0.68 is $7x10^{14}m^{-2}$, (b) to a strain of 2.67 is $8.8x10^{15}m^{-2}$. [129]

Relevant studies show that the thickness of cementite lamella decreases gradually and the interlamellar spacing distance increases with the increase of the strain as shown in Figure 139. Figure 139(a) is a high-resolution transmission electron microscope (HRTEM) image of the initial sample with a strain of 0. In the figure, the atoms in the cementite lamellae are very regularly

arranged along the arrow direction and the overall lamellae are single crystals with an average thickness of 30 nm. In the sample with a strain of 2.29 (Figure 139(b)), the thickness of the cementite sheet is about 5 nm which shows that the cementite sheet has a good deformability. However, after strong deformation, although the cementite lamella still maintains the lamellar shape, the interior has been severely fragmented forming a large number of interfaces and dividing the cementite into fine grains. The atomic arrangement in different grains is not exactly the same. The cementite stripes are no longer arranged in only one direction indicating that the increase in the amount of strain makes the cementite far away from the equilibrium state and the atomic arrangement disorder in the cementite increases.

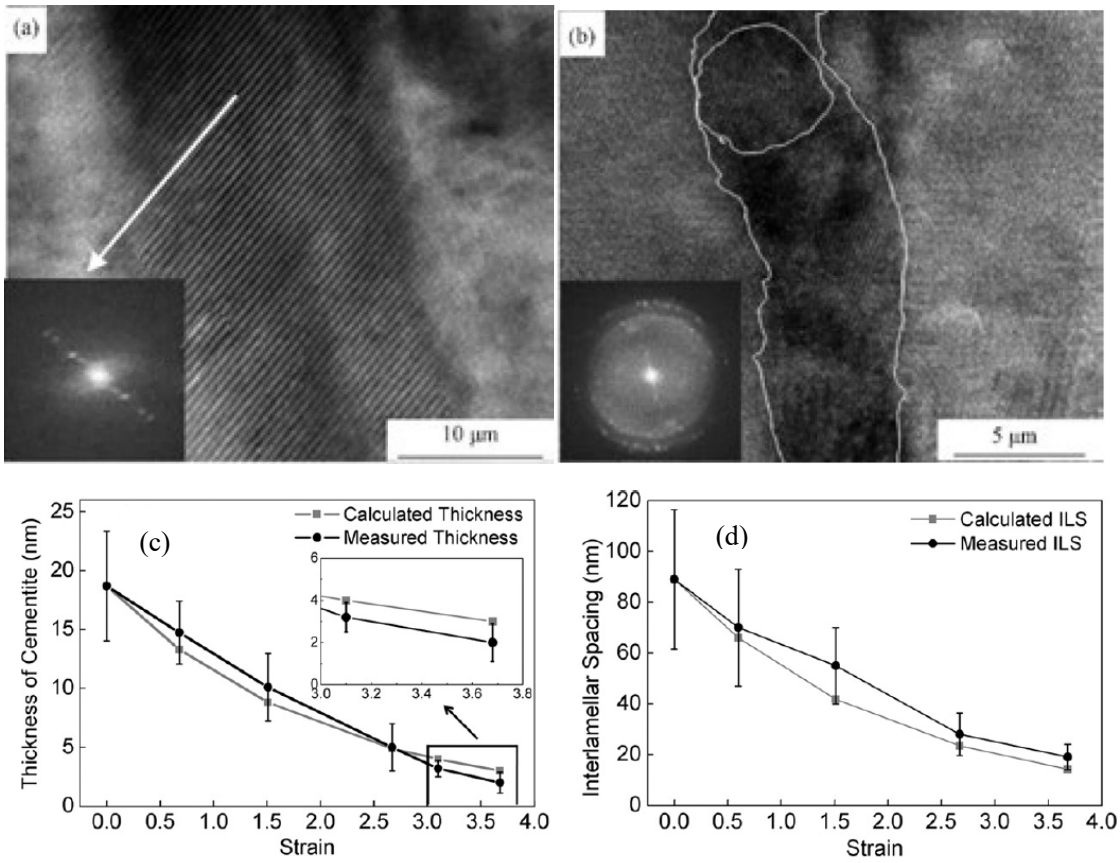

Figure 139. HRTEM microstructure of steel wires in the longitudinal section at different strain (a) ε = 0, (b) ε = 2. 29. (c) Thickness of the cementite lamellae and (d) ILS vs. drawing strain. [128~129]

As a strengthening phase in pearlitic steel, cementite is partially dissolved during cold drawing, however, the amount of cementite dissolved is an open question. In a fully pearlitic eutectoid steel with 0.8 wt.% carbon, there is only about 12 vol% cementite and this amount decreases during cold drawing. Higher amounts of dissolution were reported where the initial interlamellar spacing is smaller, the plastic deformation is higher and the temperatures reached during wire drawing are higher. Other scholars have revealed more generally that the dissociation degree of cementite is affected by alloying elements, which influence the binding between carbon atoms and dislocations. The cutting effect of dislocations on the cementite lamellae and the obvious thinning of the cementite lamellae also occur. It can be considered that the joint action of these two mechanisms leads to the dissolution of cementite. In contrast, recent atom probe tomography (APT) studies have

shown that dissolution of cementite reaches saturation values at true strains around 3.5 and does not proceed when drawn to higher strains. It implies that the dissolution of cementite depends entirely on the details of the wire's manufacture, perhaps also on the details of the composition.

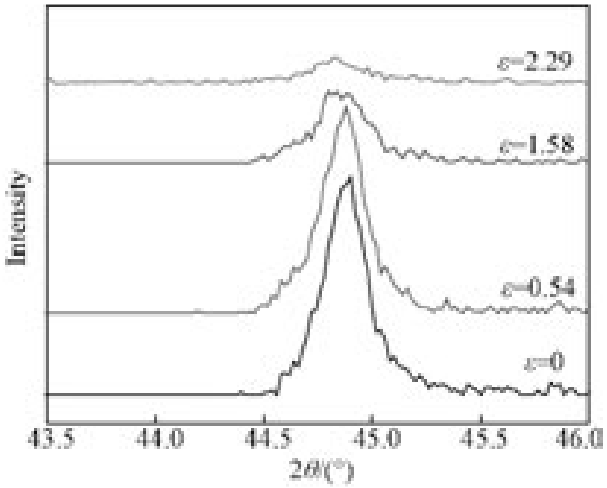

Figure 140. XRD patterns of the steel wire in the longitudinal section for the diffraction peak of (110) plane at different strain. [128]

Through the XRD analysis of α-ferrite peaks, it is found that the ferrite lattice constant becomes larger resulting in a slight left shift of the diffraction peak. The degree of distortion is also greater. This is because during the wire drawing process, the cementite dissolves and the generated carbon atoms enter the ferrite lattice. The physical disappearance of cementite is accompanied by chemical dissolution, i.e., the carbon concentration in the cementite lamellae decreases while the ferrite is rich in carbon. The resolution of cementite could also be attributed to the interaction of dislocations with carbon atoms during the drawing process, dragging them into the ferrite.

In addition to XRD analysis, study. The dissolution phenomenon of cementite could be visually characterized by HRTEM, Mössbauer spectroscopy, electron energy loss spectroscopy (EELS), APT and other analytical methods.

Analysis of the carbon concentration shown in Figure 141 by the results of APT found that the volume fraction of cementite decreased to about 6 vol% or less after continuous cold drawing. At the same time, the carbon content of cementite decreased from 6.7 wt.% to about 3.0 wt.% depending on the thickness of the cementite lamellae where thinner cementite lamellae contain less carbon.

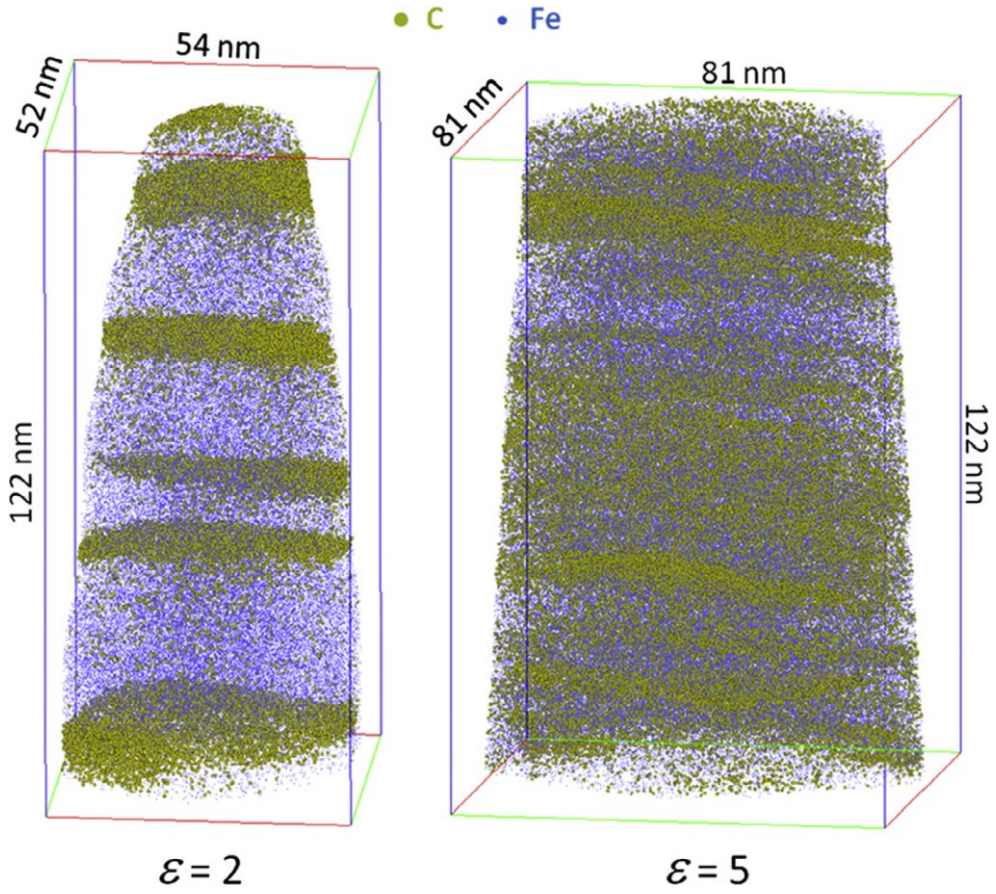

Figure 141. 3D atom maps of cold drawn wires for (a) ε = 2. (b) ε = 5. For clarity only 2% of the iron (blue) and 20% of the carbon (yellow) atoms are displayed. [122]

Due to the high hardening effect of carbon in solid solution, the carbon concentration in ferrite, C_α^ε, is also a first-order input parameter of the wire strength model. Since cementite gradually dissolves by losing its carbon, C_α^ε cannot be calculated considering that the carbon concentration C_θ^ε in the residual cementite is still equal to C_θ^0, which is 6.7 wt.%. Therefore, in addition to the changes in the volume fractions of ferrite and cementite during drawing, the strain-induced carbon partitioning between ferrite and cementite must also be considered.

The carbon distribution C (x, ε) in pearlite was calculated with the classical diffusion theory, then fitted to the experimental value of the maximum carbon concentration $\max(C_\theta^\varepsilon)$ in cementite obtained in the literature. C (x, ε) for different drawing strains is shown in Figure 142. [130] Obviously, with the increase of the drawing strain ε, the interlamellar spacing λ of pearlite gradually decreases, while the cementite dissolves and becomes thinner. The carbon content and volume fraction of cementite decrease. The initially discontinuous carbon crenel function gradually transforms into a bell-shaped curve as the cementite loses its carbon. The calculated cross profile is consistent with the experimental profile obtained by APT.

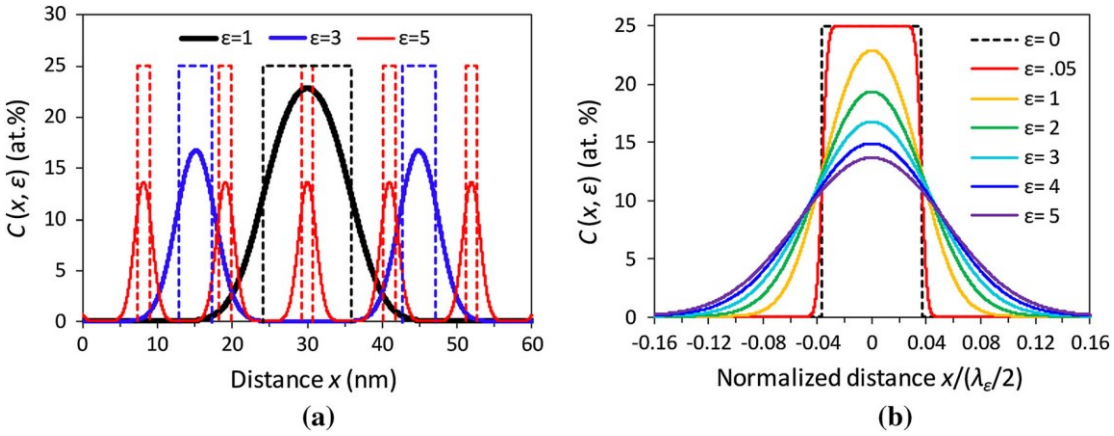

Figure 142. (a) Carbon cross profile in solid line C (x, ε) for different true strains, in pearlite with λ_0=100 nm. It would have been in dashed lines if cementite had not decomposed/dissolved. (b) Plot of carbon concentration against normalized distance showing spread of distribution as a function of strain. [130]

In addition, the addition of Cr or Mn elements will accelerate the dissolution of the cementite phase in the pearlite when drawing to a large strain, in which Cr has the greatest influence, but Si and Al elements do not significant effect.

This is because different alloying elements are enriched differently in the phases of ferrite/cementite as shown in Figure 143. The non-carbide-forming elements Al and Si are enriched in the ferrite phase, while the carbide-forming elements Mn and Cr are enriched in the cementite phase. Moreover, Mn and Cr are pushed to the cementite phase at the interface, while Al and Si are pushed to the ferrite phase at the interface.

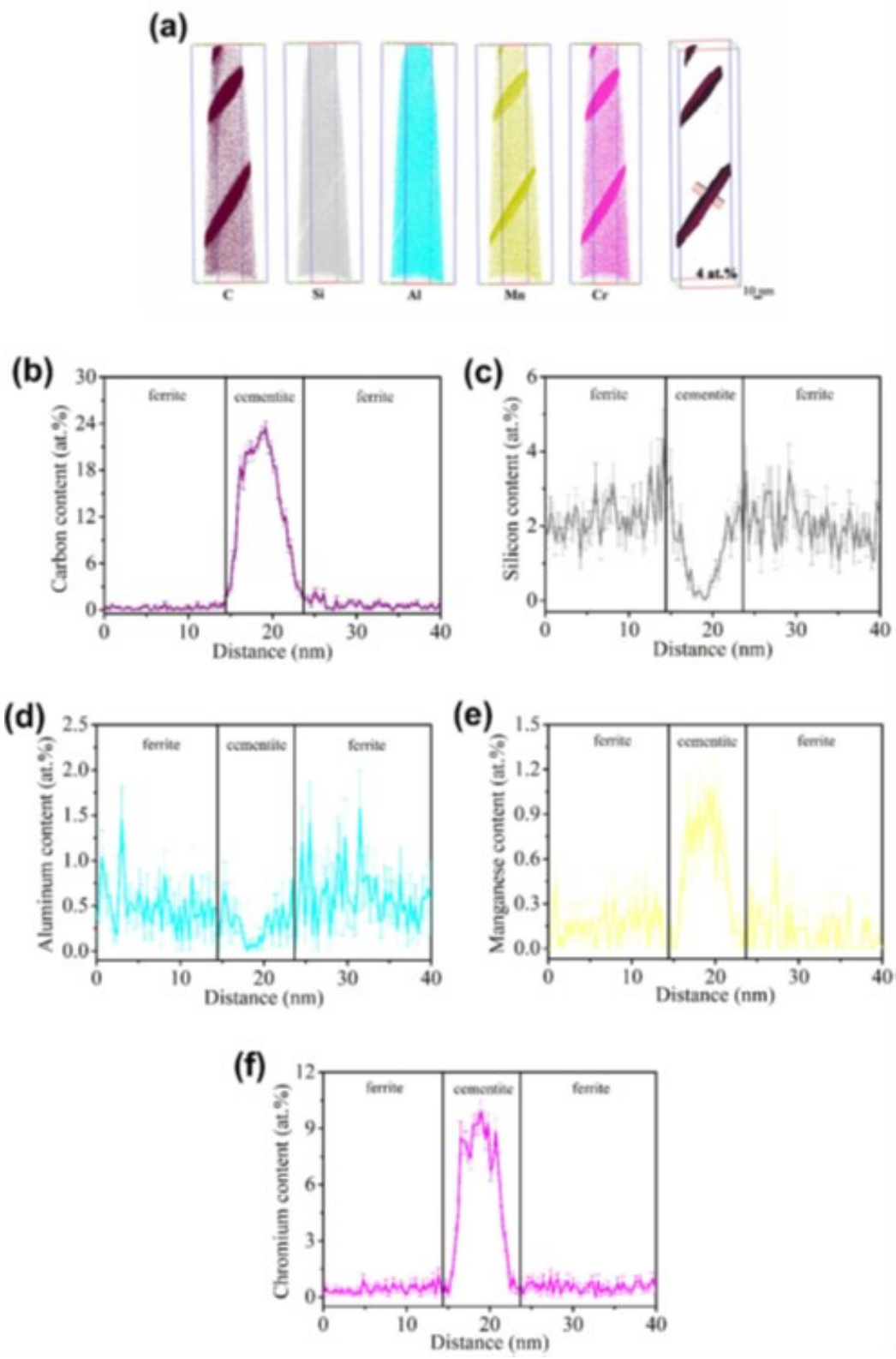

Figure 143. Determination of alloying element distribution between ferrite/cementite by APT. [131]

7.3. Mechanical properties of cold drawn pearlitic wire:

Cold drawing is commonly used to make pearlitic steel wires, which results in reduced interlamellar spacing, ferrite deformation with increased dislocation density and/or cementite decomposition, all of which would significantly increase the strength of the steel wires.

The elastic elongation of the wire, elongation at failure, ultimate tensile strength and yield strength subjected to the post-tension tensile test are shown in Figure 144. The yield strength and ultimate tensile strength continue to increase with the drawing strain, while elongation to failure decreases, but reaches a saturation value of about 2% for wire drawn to true strains ε=3 or higher. Therefore, with increasing strain and externally applied strain, the system counteracts the increase in strength through defect generation and carbon redistribution, i.e., the iron-carbon system reacts as required by Le Chatelier principle. On the contrary, the elastic elongation increases with increasing drawing strain and reaches a saturation value of about 1.6%.

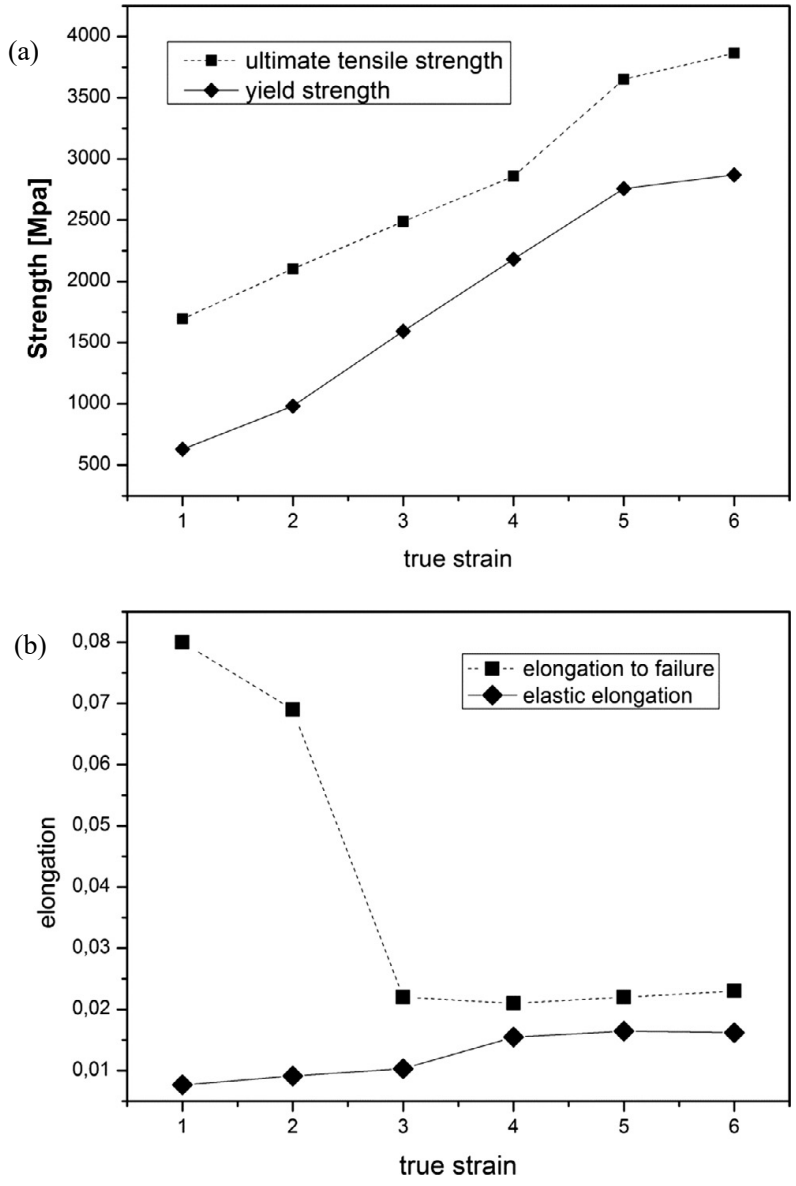

Figure 144. (a) Ultimate tensile strength, yield strength, (b) and elongation to failure, elastic elongation of wires subjected to post-drawing tensile tests. [122]

The strength increases due to cold drawing, measured by various researchers, are shown in Figure 145. As could be seen, the results fall on a common line with only slight deviations. In the patented state, the wire compositions are similar, but the tensile strength is different which is due to the slightly different patenting processes, resulting in different lamellar thickness and interlamellar spacings in the patented state.

The cementite lamellae thickness was found to be the primary determinant of the mechanical properties of pearlitic steels. The increase in tensile strength is very consistent, even though the actual stress-strain plots do not fall on a common line. However, there seem to be two regimes: the strength increases are lower at small strains $\varepsilon \leq 2 \sim 3$, while the strength increases are significantly higher at large strains. This might be as a result of the alignment of the cementite lamellae parallel to the drawing direction during the drawing process.

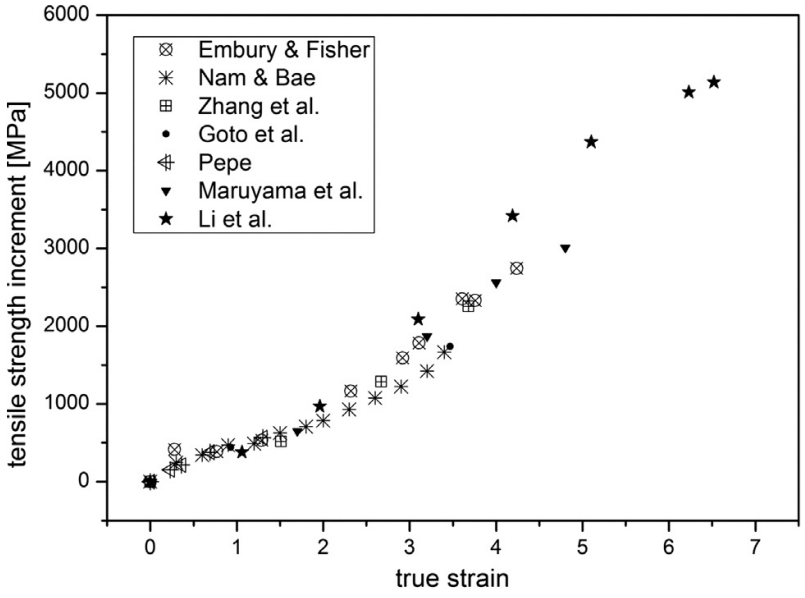

Figure 145. Strength increases due to cold drawing as measured by various researchers. [122]

Cold drawn pearlitic steel wires are sensitive to heat treatment. For example, cementite lamellae can take on a spherical shape when heated above 673K for a certain period of time. Therefore, the strength of heat-treated wire decreases with increasing ductility.

Figure 146 shows the tensile strength of pearlitic steel wire after cold drawing to true strain $\varepsilon = 5$ after annealing at different temperatures. No significant change in strength was observed when annealed at temperatures up to 523K, while the strength continued to decrease after annealing at higher temperatures.

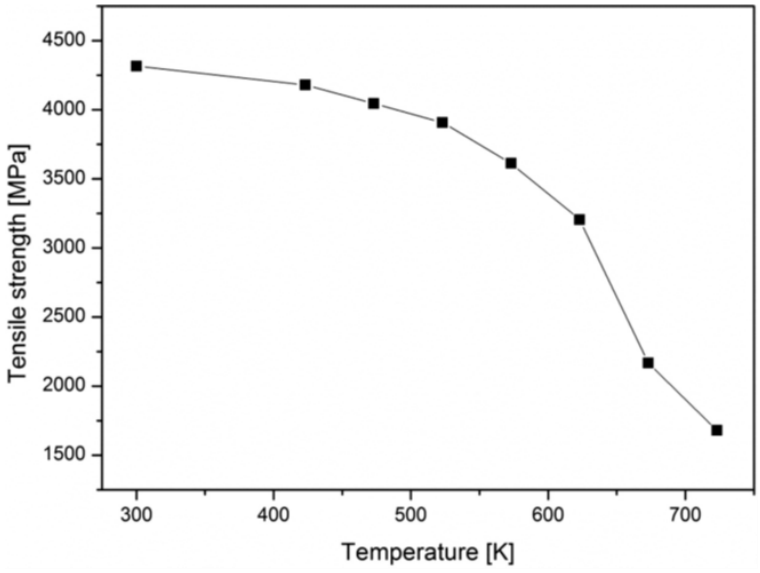

Figure 146. Tensile strength of a pearlitic steel wire cold-drawn to a true strain of ε= 5 annealing at different temperatures for 30 min. [122]

However, some authors [132] claim an increase in tensile strength after annealing at temperatures between RT and 523K, although the results shown in Figure 146 do not show an increase in tensile strength after annealing. In fact, the researchers' results are all within normal measurements within the accuracy range. One might speculate on a different composition. However, the biggest change is in the distribution of tensile strain. When annealing wire with high tensile strain, the rise in tensile strength is absent or within measurement uncertainty, the rise in tensile strength is evident when annealing wires with relatively low tensile strains.

This amount of dissolved carbon is increased in the ferrite phase due to the partial decomposition of cementite during annealing. Figure 147 shows a plot of carbon concentration in ferrite versus draw strain for drawn wire as measured by APT. The carbon concentration was increased until at ε=3, it reached a saturation value of about 0.6 at% (0.13 wt.%).

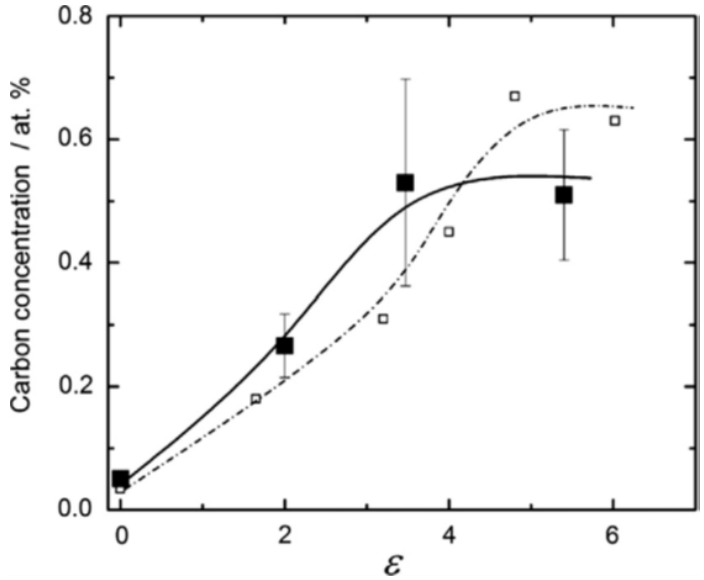

Figure 147. Carbon concentration in ferrite measured by APT plotted against the drawing strain. [122]

Carbon atoms from decomposed cementite segregated to dislocations in ferrite and/or at ferrite/cementite interfaces as heavily cold drawn pearlitic steel wires were annealed at lower temperatures (< 150 °C), which also increased the wire strength.

Figure 148 shows a SEM micrograph of the fracture surface of the wire after cold drawing to ε = 1~5. The sections exhibit clearly visible cup and conical sections for ε = 1~3. The failure of many ductile materials could be attributed to necked cup and cone fractures.

Ductile fracture of this form occurs at a stage after the onset of necking. First, small microvoids form inside the material. Next, the deformation continues and the microvoids expand to form cracks. The cracks continue to grow towards the edge of the specimen and laterally spread. Finally, the crack rapidly propagates along the surface at an angle of about 45 degrees to the axis of tensile stress. The new fracture surface appears irregular. The cup-cone section is so called because the final shearing of the specimen leads to one fracture being cupped and the adjacent connecting section being conical.

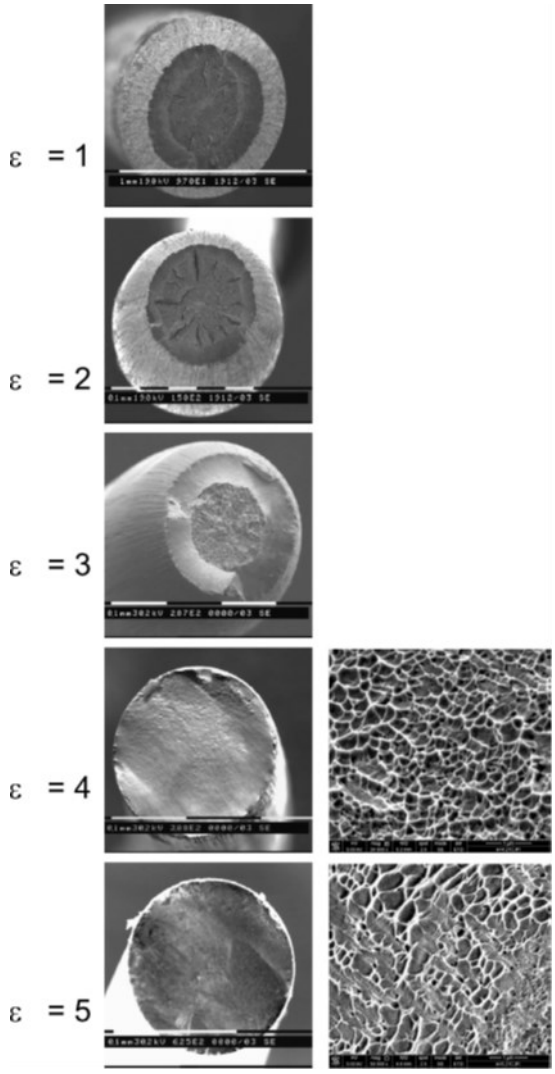

Figure 148. SEM micrographs of the fracture surfaces of the wires drawn to fracture after cold-drawing to ε= 1~5. [122]

In contrast, for wires cold drawn to ε = 4 and 5, the surface of fracture does not have obvious

necking, nor the appearance of cup and cone but a typical dimple structure, which implies the typical microvoids coalescence of ductile fractures, as shown in the close-up view of Figure 148. There appears to be a ductile fracture throughout, but a transition from necked to non-necked mode between $\varepsilon = 3$ and $\varepsilon = 4$. For $\varepsilon = 0.69$, necked cup and cone fracture was found and for $\varepsilon = 3.47$, a cup and cone fracture with necking was also found, indicating that the fracture mode of pearlitic steel wire cold-drawn to $\varepsilon \leq 5$ is generally consistent.

7.4. Strengthening Mechanism:

The main strengthening mechanisms in low alloy steel are mainly solid solution strengthening, precipitation strengthening, high angle grain boundary strengthening and dislocation strengthening. strengthening.

7.4.1. Solid solution strengthening:

Solid solution strengthening refers to the lattice distortion of the matrix caused by the atomic size effect, elastic modulus effect and solid solution ordering effect of other elements. The lattice distortion increases the resistance of dislocation movement and makes plastic deformation more difficult. The strength and hardness of the alloy solid solution increase. Solid solution strengthening can be further divided into interstitial solid solution strengthening and substitutional solid solution strengthening. The interstitial solid solution strengthening effect is remarkable, and the ductility decreases obviously. Cold-drawn pearlitic steel wire is a high carbon low alloy steel. The element that can play a role in interstitial strengthening in the steel is mainly C, all of which exist in the form of cementite, so the interstitial solid solution strengthening is very small. The elements that can play the role of substitutional solid solution strengthening mainly include Mn, Si, Cr and Ni, etc. The strengthening effect is much smaller than that of interstitial atoms, but has little effect on ductility and toughness. However, for the cold-drawn steel wire with large deformation, the cementite lamella is broken and dissolved, and C atoms are re-dissolved into the ferrite which distorts the ferrite lattice and even causes the matrix to transform from BCC structure to BCT structure. The solid solution strengthening effect is more significant at this time. Studies have shown that when the cold drawing strain amount reaches about 3.67, the solid solution strengthening caused by the re-entry of C atoms into the ferrite due to the dissolution of cementite is about 400MPa. [133]

7.4.2. Precipitation strengthening:

The precipitation strengthening is mainly attributed to the interaction between the second phase particles and the dislocation motion, which can be divided into bypass mechanism and cut-through mechanism according to their characteristics. Regardless of the bypass mechanism or the cut-through mechanism, the precipitation strengthening effect is related to the number density and size of the second-phase particles. When the volume fraction of the second phase particles is constant, the strengthening effect of the Orowan mechanism is roughly inversely proportional to the size of the second phase particles. The strengthening effect of the cut-through mechanism is proportional to the 1/2 power of the second phase particles. The yield strength of a material conforming to

precipitation strengthening is generally proportional to the square root of the true strain.

However, the precipitation strengthening model is only suitable for materials with dispersed distribution of second phase particles. For cold-drawn pearlite steel wire, cementite lamellae cannot simply be regarded as dispersed particles, and the yield strength of the wire is also not proportional to the square root of the true strain.

7.4.3. High angle grain boundary strengthening:

In the early days, some scholars used the fiber strengthening model to explain the strengthening mechanism of cold drawn pearlitic steel wire:

$$\Delta\sigma_w = v_a\sigma_a + (1 - v_a)\sigma_f$$

where σ_a and σ_f are the strengths of cementite and ferrite, respectively, and V_a is the volume percentage of cementite (6% after decomposition of half of the cementite). The fracture strength of σ_f is about 700Mpa, and the fracture strength of σ_a is about 6900Mpa. The yield strength (flow stress) of the steel wire calculated according to the model is only 1100Mpa, which is obviously lower than the measured value. The main reason for the large difference between the calculated strength of the composite strengthening model and the actual strength of the steel wire is that the premise of the composite strengthening model is that the fiber is infinitely long and is an independent variable, and the work hardening rate does not change with the increase of the cold drawing strain variable. Due to the different degrees of dislocation movement in the ferrite during the cold drawing process, the work hardening rate of the ferrite changes. Therefore, the composite strengthening model is not suitable for explaining the strengthening mechanism of cold-drawn steel wire.

High angle grain boundary strengthening is also called fine grain strengthening. The main reason is that the interface can hinder the movement of dislocations and thus produce strengthening. The most famous Hall-Petch formula directly reflects the strengthening effect of grain boundaries:

$$\Delta\sigma_{HP} = k\lambda^{-\frac{1}{2}}$$

where k is the so-called Hall-Petch constant and λ in most cases corresponds to the grain size, but it corresponds to the interlamellar spacing here. A value was found for the Hall-Petch constant of k = 0.422 MPam$^{1/2}$, yielding $\Delta\sigma_{HP}$=4220MPa for λ = 10 nm at ε=5. Embury and Fisher proposed a modified form of the Hall-Petch relationship, where true strain and lamella width after drawing are used: [134]

$$r_\epsilon = r_0 \exp(-\epsilon/2)$$

i.e., the relationship between the lamellar spacing after drawing to a true strain ε and original lamellar spacing:

$$\Delta\sigma_{HP} = k\lambda_0^{-\frac{1}{2}} \exp(\epsilon/4)$$

where λ_0 is the original interlamellar spacing, k is a constant and its size is related to the spacing between the pearlite lamellae of the initial wire rod. It can be seen from the formula that the yield strength of cold-drawn pearlite steel wire is proportional to exp(ε/4) and this relationship has been recognized by many researchers. It can be seen from the Figure 149 that the measured value of the yield strength of the steel wire has a good linear relationship with exp(ε/4).

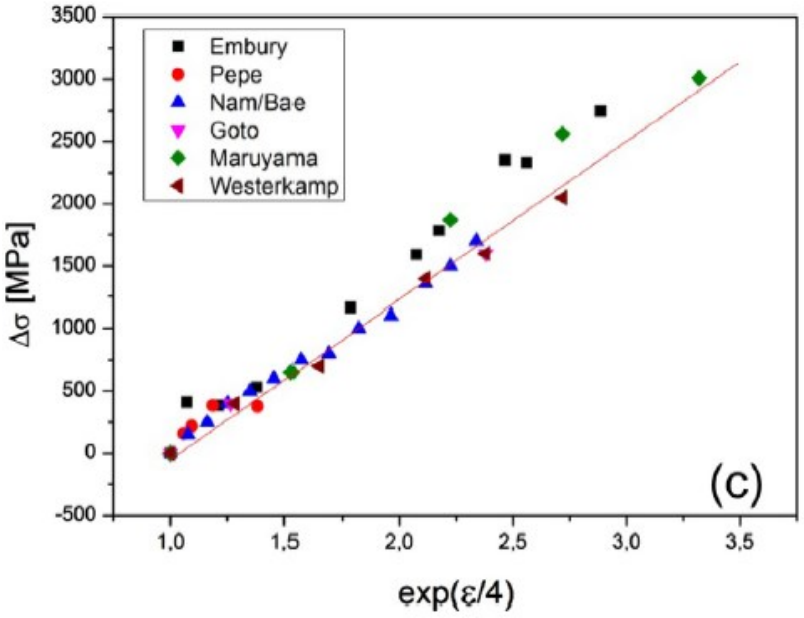

Figure 149. The relationship between yield stress of cold drawing pearlitic steel wires and exp(ε/4), ε means true strain. [122]

7.4.4. Dislocation strengthening:

It is believed that the dislocation density inside the ferrite sheet gradually increased during the drawing process, so the effect of dislocation strengthening should also be considered. Some researchers [129] pointed out that dislocation strengthening cannot be ignored. At the same time, the large strain is drawn, the cementite is dissolved and the supersaturation of C atoms is generated in the ferrite, resulting in solid solution strengthening. They proposed that there is interfacial strengthening, dislocation strengthening and solid solution strengthening simultaneously in cold-drawn large strain steel wire, and the relationship is shown in the following formula:

$$\Delta\sigma = \sigma_b + \sigma_\rho + \sigma_{ss}$$

where σ_b is the interface strengthening, σ_ρ is the dislocation strengthening, and σ_{ss} is the solid solution strengthening due to the dissolution of cementite. However, some scholars believe that once the lamellar cementite is broken into discontinuous or granular, or even dissolved, the preconditions for the establishment of interfacial strengthening also change (the cementite lamella does not have dynamic reply during the drawing process and no new slices are generated). Obviously, granular cementite and lamellar cementite have different hindering effects on ferrite dislocation slip. The strengthening mechanism of cold-drawn pearlite steel wire needs further research and discussion.

7.5. Discussion:

All in all, cold drawn pearlitic wire is an attractive material that can spark ongoing research activity. This topic will undoubtedly be revisited again and again in the future due to the ongoing development of experimental methods, particularly image generation techniques like TEM and APT.

8. Quenching and Partitioning steel

Over the years, advanced high-strength steel (AHSS) has attracted the research interest of many research institutions and personnel due to its high strength, good ductility and new steel grades. Focusing on the design of composition and heat treatment process, they regulated the microstructure and structural characteristics of steel. The development of AHSS has experienced the first-generation steel (such as dual-phase steels) based on ferrite and martensite. <DP>, multiphase steel <CP>, martensitic steel <MART>, transformation-induced plasticity steel <TRIP>, etc.) and second-generation steel based on austenite (such as twin-induced plasticity steel <TWIP> and austenitic stainless steel <AUST.SS>, etc.) as shown in Figure 150. Overall, the first-generation steel has more strength and slightly less ductility and toughness, while the second-generation steel has excellent ductility and toughness but high steel cost! At present, the third-generation steel -- quenching-partitioning steel <Q&P>, combines the characteristics of the first-generation and second-generation steels to a certain extent. It not only used dislocation strengthening, solid solution strengthening to increase the strength, but also make full use of multi-phase, multi-scale microstructure to improve ductility. In addition, it does not need to add a large amount of alloying elements thus the cost is low.

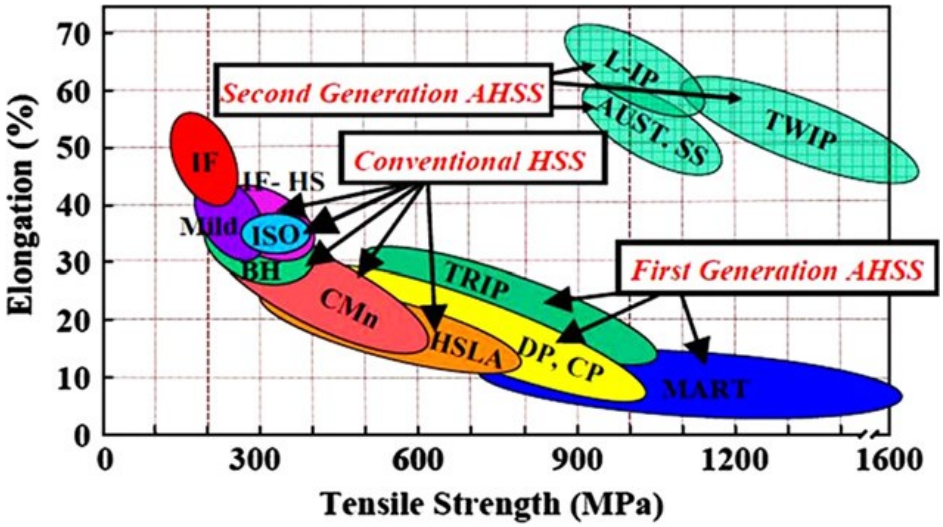

Figure 150. First and second generation AHSS. [135]

8.1. Q&P processing:

The traditional quenching and tempering heat treatment process of steel emphasizes obtaining a full martensitic structure through quenching and reducing the content of retained austenite to obtain high strength. In the tempering stage, the metastable retained austenite is decomposed. It is beneficial to improve the dimensional accuracy of the workpiece. Considering these practical properties, the role of retained austenite in steel (especially high-strength steel) has not been paid enough attention and research. In 2003, based on TRIP (transformation-induced plasticity) steel, American Speer et al. proposed a new process for heat treatment of steel—Quenching and Partitioning (Q&P). The core idea of the process is that the supersaturated carbon atoms in the

martensite are enriched in the retained austenite during the partitioning soaking process. The high carbon content stabilizes more austenite to room temperature which plays the role of improving ductility in high-strength steels. The quenching-partitioning (Q&P) process is shown in Figure 151. The steel is rapidly quenched to a certain temperature between the M_s point and the M_f point to obtain a certain amount of martensite and retained austenite which is more than room temperature. Then, isothermal treatment is performed at the quenching temperature (one-step method) or at a temperature above M_s (two-step method) to enrich the supersaturated carbon in the martensite to the retained austenite to achieve carbon partitioning. After that water quench to room temperature, a complex structure of martensite and retained austenite is obtained.

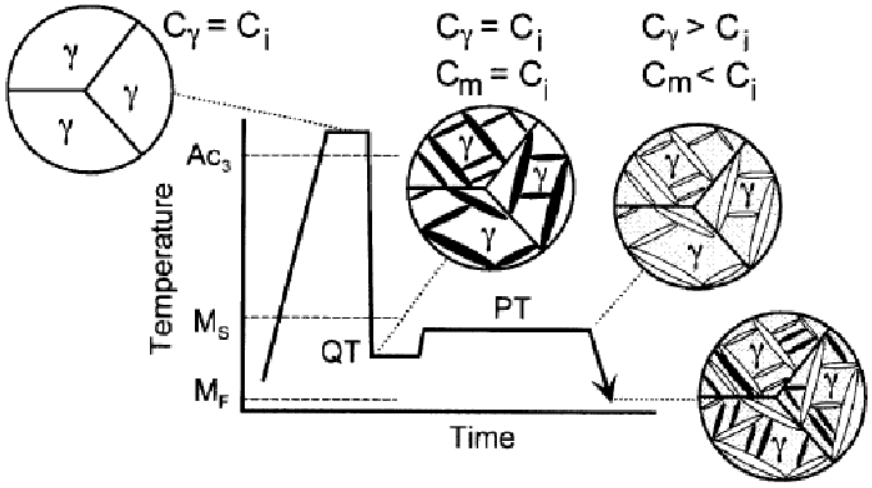

Figure 151. Scheme of the Q&P process, resulting in ferrite/austenite/martensite microstructures from homogeneous austenite. [136]

In the Figure 151, C_γ is the carbon concentration in the initial austenite, and C_i and C_m are the carbon content in the initial alloy and martensite, respectively. QT is the quenching temperature, and PT is the carbon partitioning temperature which is equal to or higher than the quenching temperature QT. For the thermodynamic process of carbon partitioning in the quenching-partitioning (Q&P) process, Speer et al. proposed a constrained carbon quasi-equilibrium CCE (Constrained Carbon Para-equilibrium) thermodynamic model and pointed out three conditions for calculation under this model: (1) The chemical potential difference of carbon between austenite and martensite is the driving force for the partition of carbon from martensite to austenite. When the chemical potential of carbon in the two phases is equal, the partition of carbon from martensite to austenite ends immediately; (2) During the whole process from the beginning to the completion of carbon partitioning, the phase interface of martensite/austenite does not move (that is, Fe atoms or solid solution atoms X on the two-phase interface do not undergo short-range diffusion); (3) During the whole carbon partitioning process, all carbon atoms are transferred to austenite to improve its carbon enrichment and chemical stability without the precipitation of carbides. Figures 152 shows two cases that fit the CCE model.

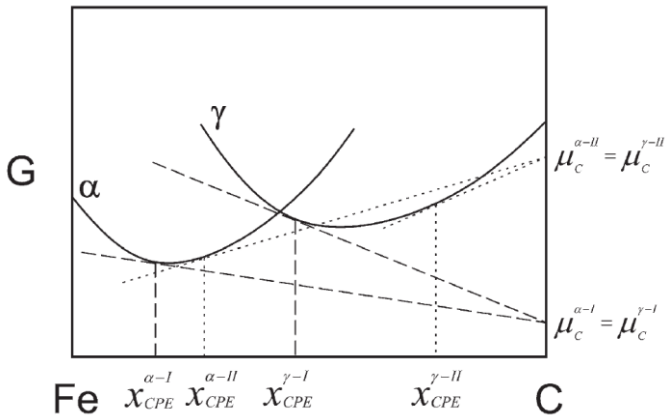

Figure 152. Gibbs free energy vs. composition diagram showing the common-tangent construction representing ortho-equilibrium between ferrite and austenite. [137]

The CCE conditions of Fe-C alloys can be calculated using the existing thermodynamic data and knowledge of the quenched structure, from the literature: [137]

$$RT \ln \frac{\Gamma_C^{\alpha}}{\Gamma_C^{\gamma}} = 76,789 - 43.8T - (169,105 - 120.4T) X_C^{\gamma} \tag{2}$$

where Γ_C^{α} and Γ_C^{γ} are the Henrian activity coefficients of C in martensite and austenite, respectively. R is the gas constant. When the CCE is satisfied, the carbon activities of the α phase and the γ phase are equal, so there is:

$$X_C^{\gamma} = X_C^{\alpha} e^{\frac{76,789 - 43.8T - (169,105 - 120.4T) X_C^{\gamma}}{RT}} \tag{3}$$

Among them, X_C^{γ} and X_C^{α} represent the mole fraction of carbon in martensite and austenite, respectively. Equation (3) gives the compositional relationship between the two phases at any temperature. Figure 153 shows the compositional relationship when the carbon activities in austenite and martensite are equal at 400 °C.

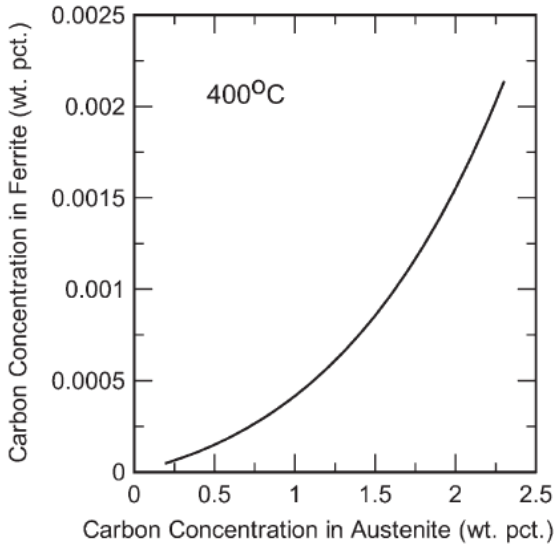

Figure 153. Calculated locus of ferrite and austenite compositions having equal carbon activities at 400 °C. [137]

In addition, according to the third condition of the CCE model, Fe atoms do not diffuse between the two-phase interface, so the Fe atoms in the alloy satisfy mass conservation before and after carbon partitioning, that is:

$$f_{CCE}^{\gamma}(1-X_{C_{CCE}}^{\gamma})=f_i^{\gamma}(1-X_C^{alloy}) \tag{4}$$

where f_i^{γ} is the mole fraction of austenite after quenching, f_{CCE}^{γ} and X_{CCE}^{γ} are the mole fraction and carbon content of austenite after completing carbon partitioning, and X_C^{alloy} is the carbon content in the original alloy. Although the CCE model requires that the martensite/austenite interface does not move, $f_i^{\gamma}\neq f_{CCE}^{\gamma}$ due to the long-range diffusion of carbon atoms leading to atomic adjustments in the two phases. Similarly, for the mass conservation of carbon atoms, we have:

$$f_{CCE}^{\alpha}X_{C_{CCE}}^{\alpha}+f_{CCE}^{\gamma}X_{C_{CCE}}^{\gamma}=X_C^{alloy} \tag{5}$$

and always have:

$$f_{CCE}^{\alpha}+f_{CCE}^{\gamma}=1 \tag{6}$$

Then the thermodynamic conditions of the CCE model are given by several equations (3) ~ (6). Although the above equations are derived from Fe-C binary alloys, they are also applicable to low alloy steels.

8.2. Chemical composition of Q&P steel:

Adding appropriate alloying elements to steel will not only affect the phase transformation process, but also control the formation of carbides, etc., which is the most commonly used method to control the properties of steel.

The alloy components of Q&P steel introduced by Speer and others mainly include C, Mn, Si (or Al) and the carbon content of Q&P steel is generally about 0.19~0.6 wt.%. Higher carbon content is often used to improve the stability of retained austenite. However, if the carbon content is too high, twin martensite with poor ductility and toughness will be formed which will affect the practical performance of the steel.

The manganese content of Q&P steel is generally high ranging from 1.2 to 2.0 wt.%. The core of Q&P process and the improvement of performance are mainly the effect of retained austenite. It is necessary to add more manganese to improve the decomposition resistance of retained austenite, so as to obtain a larger amount of retained austenite.

The silicon content of Q&P steel is generally not more than 2 wt.%, and 1.5~1.6 wt.% is mostly used. Both silicon and aluminum are non-carbide forming elements and are insoluble in carbides. During the carbon partition process of Q&P steel, it can effectively inhibit carburization so that carbon atoms are enriched in the retained austenite without the formation of carbides, thereby better improving the stability of the austenite.

In addition, Q&P steel does not add any micro-alloy carbide forming elements such as Nb, V, Ti, Mo, etc. in the composition design to avoid "consuming" carbon atoms when forming carbides.

8.3. Microstructure and properties of Q&P steel:

The microstructure of the third-generation advanced high-strength Q&P steel is relatively complex. It is usually composed of a multi-phase composite structure of martensite, ferrite and retained austenite. Generally, after quenching-partitioning (Q&P) treatment, martensite + retained austenite structure is obtained. Lath martensite is obtained when the carbon content is low, and twinned martensite is obtained when the carbon content is high, as shown in Figure 154.

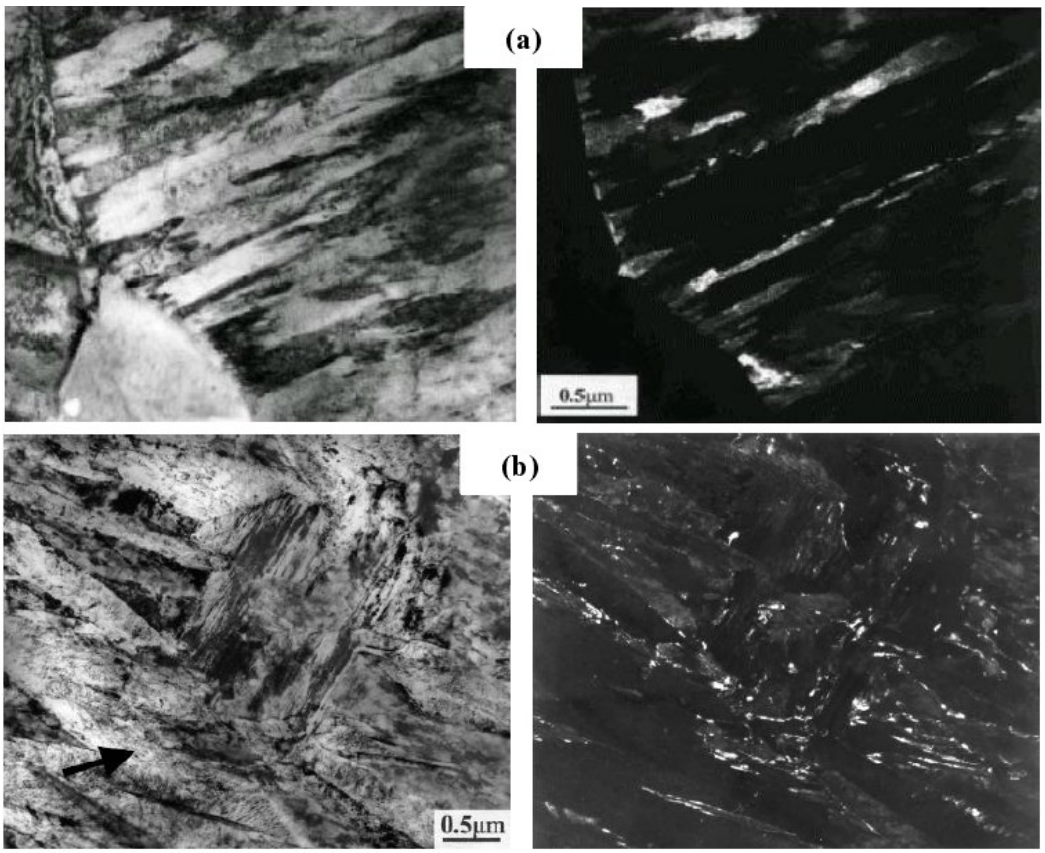

Figure 154. Typical microstructure of Q&P steel:(a) lath martensite + retained austenite; (b)twin martensite + retained austenite. [136, 138]

Similar to TRIP steel, Q&P steel can be partially austenitized in the two-phase region and then subjected to quenching-partition (Q&P) treatment, and the microstructure obtained at this time is bulk ferrite + martensite + retained austenite. The scholars reported related research, carefully observed and characterized the structure and pointed out that the partially austenitized TRIP steel in the two-phase region decomposes during the first quenching-partition (Q&P) treatment resulting in carbonization. Due to the long-range diffusion of carbon, epitaxial ferrite is observed. Figures 155 are schematic diagrams showing the changes in its structure and carbon concentration.

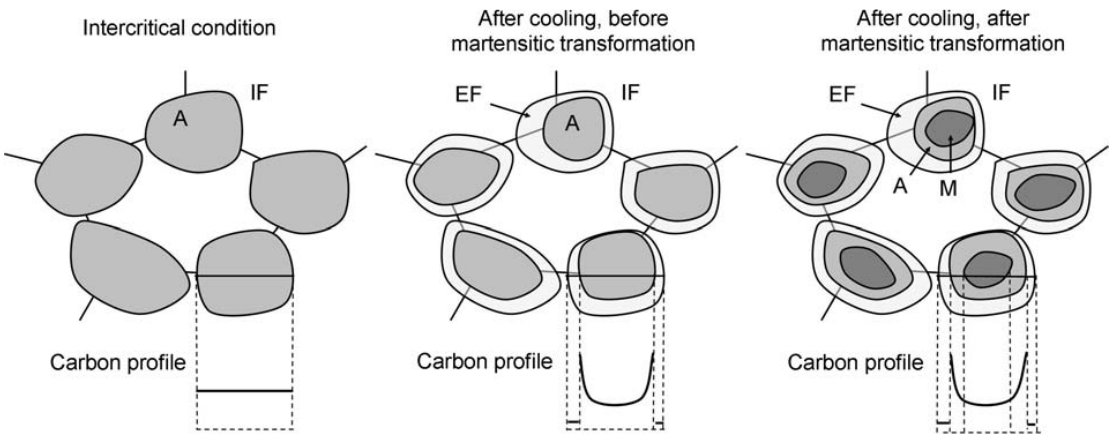

Figure 155. Schematic of morphology and carbon profiles during different stages of the Q&P process (A: austenite, IF: inter-critical ferrite, EF: epitaxial ferrite, M: martensite). [139]

The multi-phase and multi-scale structure of Q&P steel is coordinated with each other in the process of material deformation which lays the foundation for its excellent mechanical properties. It has the characteristics of high yield strength and tensile strength, significant work hardening and high elongation. The volume fraction of retained austenite and its stability are a major factor affecting the mechanical properties of Q&P steel. The morphology (bulk or film), chemical composition and restraint of retained austenite determine the mechanical and thermal stability. During the deformation process, the retained austenite in the Q&P steel undergoes martensitic transformation under the action of strain resulting in the TRIP effect, which increases the ductility of the material. At the same time, the film-like retained austenite which exists between the martensitic laths plays the role of absorbing dislocations and hindering crack propagation. It avoids fractures caused by the unstable crack propagation of high-strength martensite under the action of high dislocation density and high internal stress.

In general, the composition of Q&P steel is simple, and there is no need to add too many alloying elements, especially expensive metal materials such as Ni, Co, and V. After quenching-partitioning (Q&P) treatment, Q&P steel has high strength, good ductility, and comprehensive mechanical properties that can better meet engineering needs.

8.4. Q&P attempt in hot stamping steel:

After the hot-stamped steel obtains a high strength of 1500MPa, the ductility is seriously deteriorated and the elongation is only 6~8%, which greatly limits its impact energy absorption ability. The quenching-partitioning (Q&P) process can effectively improve the ductility of high-strength steels by introducing an appropriate amount of retained austenite into the martensite structure. Therefore, it can be considered to improve the ductility and toughness of the hot-stamped steel by combining the hot-stamping process and the quenching-partitioning (Q&P) process, thereby increasing the impact energy absorption effect of the hot-stamping steel as an automobile safety component and finally improving the safety performance of the car body.

The schematic diagram of the heat treatment process of the hot stamping process and the one step quenching-partitioning (Q&P) process is shown in Figure 156. The hot stamping process

requires that the sheet forming be completed before the martensitic transformation starts to reduce the forming resistance and ensure the dimensional accuracy. The one-step quenching-partition (Q&P) process is that after austenitizing, quenching to M_s. The temperature is kept warm to complete the carbon distribution. It can be seen that hot stamping and Q&P can be combined into a continuous heat treatment process, one before M_s temperature and the other after M_s temperature. Moreover, the design of the workpiece mold can be improved in the hot stamping process, so that it has functions such as heating and heat preservation or cooling rate control which is very beneficial to realize the quenching-partition (Q&P) treatment, as shown in Figure 156(c).

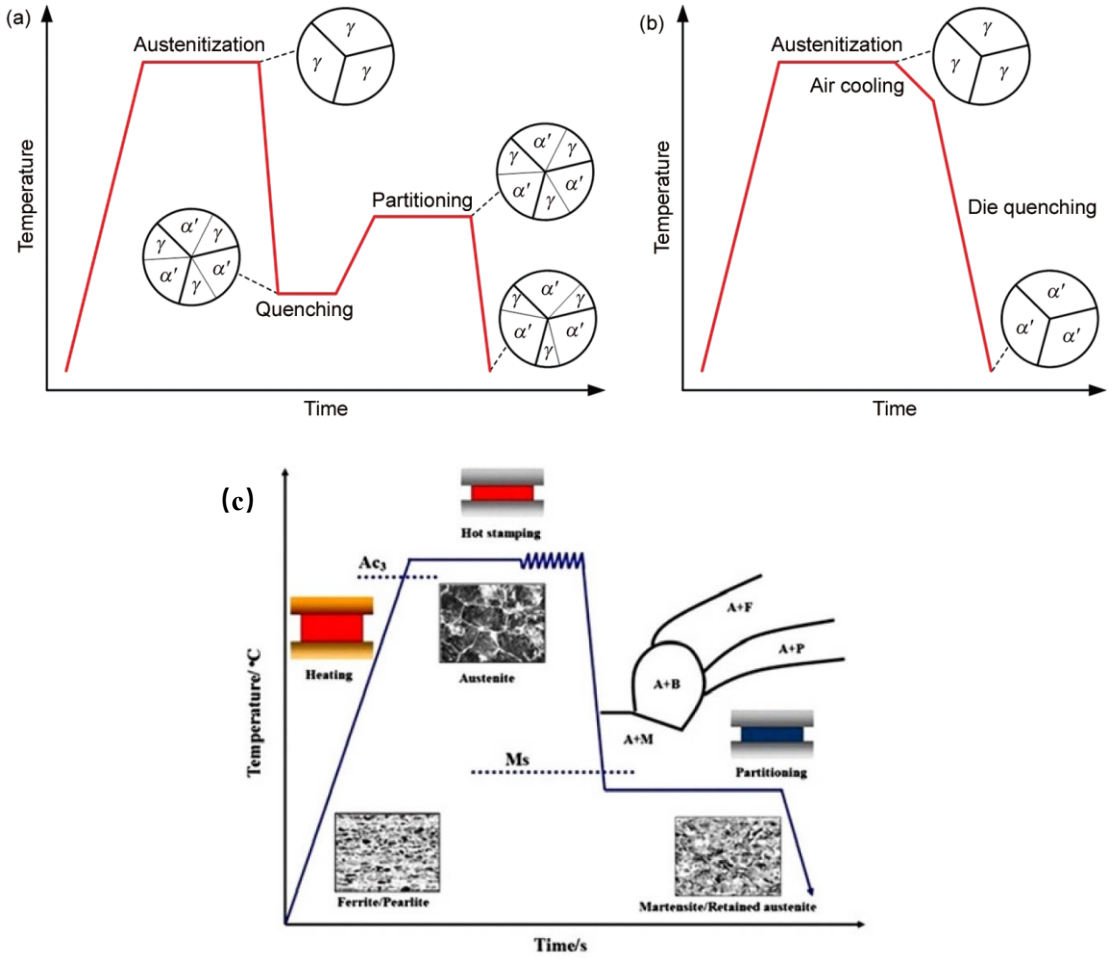

Figure 156. Schematic of heat treatment processes: (a)hot stamping process; (b)Q&P process; (c)continuous hot stamping + Q&P process. [79,140]

The composition of hot-stamped steel is mainly C, Si, Mn three alloying elements, containing a small amount of Ti to refine grains and a very small amount of B can improve the hardenability. Compared with the composition of Q&P steel, the Si in hot-stamped steel is relatively low, and Si is extremely important in the quenching-partitioning process. If carbides cannot be suppressed and a large amount of precipitation occurs, it will inevitably lead to insufficient carbon content in the retained austenite. The room temperature stable retained austenite required by the Q&P steel design cannot be obtained and the effect of the Q&P process cannot be fully utilized.

The research in recent years is mainly to make appropriate adjustments based on the original 22MnB5 steel composition to make the adjusted steel more suitable for Q&P treatment, that is, to

obtain enough retained austenite volume fraction of 5% to 20%. Whether the traditional 22MnB5 steel is suitable for Q&P treatment is of great significance.

Due to the low content of Si in the traditional 22MnB5 steel (about 0.22%), the researchers designed three new steel grades with different silicon content based on the composition of the 22MnB5 steel, containing 0.5%, 0.8% and 1.5 wt.% Si, respectively as shown in Table 23, using a one- and two-step Q&P process.

	C	Si	Mn	Cr	Al	B	Ti	N	P	S
Ref.	0.219	0.25	1.17	0.220	0.028	0.0029	0.029	0.0018	0.004	0.004
LSi	0.215	0.50	1.18	0.230	0.030	0.0031	0.031	0.0014	0.004	0.003
MSi	0.214	0.78	1.18	0.230	0.029	0.0028	0.029	0.0017	0.004	0.003
HSi	0.220	1.50	1.17	0.230	0.029	0.0028	0.031	0.0013	0.004	0.003

Table 23. Chemical composition of the Reference 22MnB5 and Si-added hot-stamped steels. [141]

It was found that retained austenite was obtained in the final microstructure only when the Si content was greater than 0.5%. Increasing the Si content to 0.5 to 1.5 wt.% in the 22MnB5 hot-stamped steel results in an increase in retained austenite (RA) after Q&P heat treatment. (The volume fraction is 2% to 8% as shown in Figure 157.)

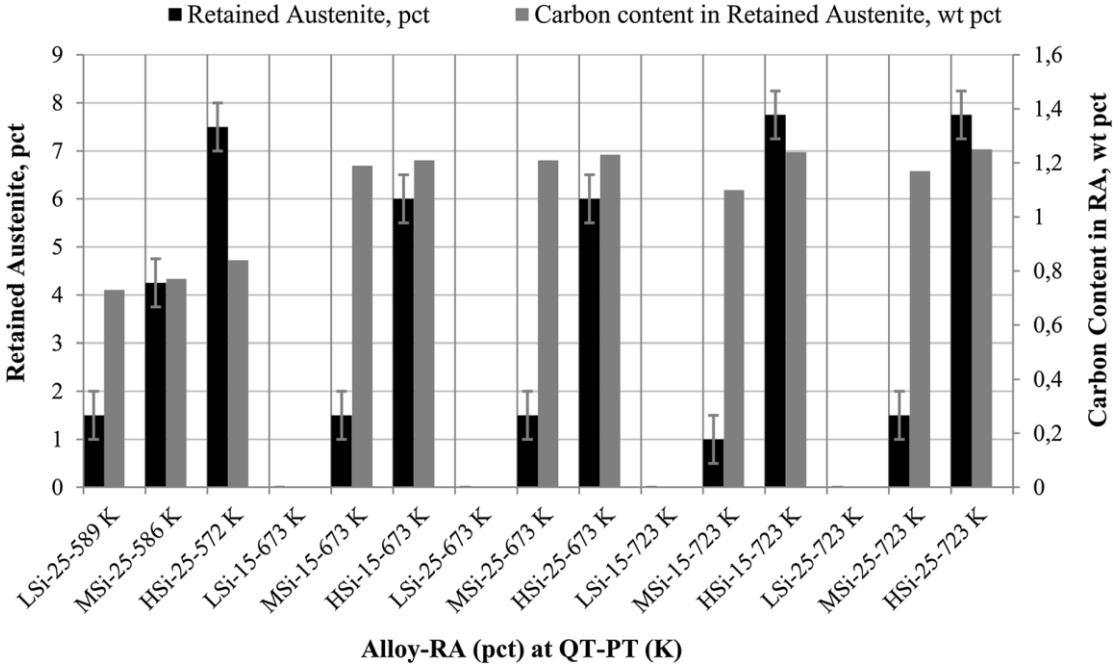

Figure 157. The RA content and C content in austenite in Si-added alloys were measured by XRD. No retained austenite was found after Q&P heat treatment. [141]

For all Si levels except 1.5 wt.%, the one-step process Q&P heat treatment produced most of the RA. While Si contents of 0.5 to 0.8 wt.% effectively hinder cementite precipitation within the martensitic lath, they do not appear to be sufficient to stabilize RA, especially at higher temperatures (two-steps method).

As shown in Figure 158, the elongation of the new design grade following Q&P treatment is greater than that of the typical 22MnB5 steel. RA appears to increase tensile elongation regardless of its stability, i.e., carbon content. This implies that the TRIP effect is at best secondary and other mechanisms might also be responsible for the increased ductility. Only the 1.5 wt.% Si level exhibits a significant increase both in elongation and tensile strength compared to 22MnB5 steel.

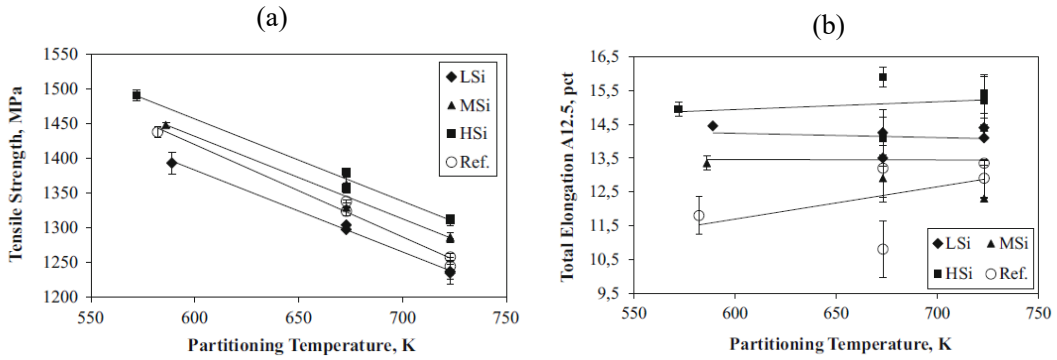

Figure 158. Effect of partitioning temperature on tensile properties after Q&P hot stamping: (a) tensile strength, (b) total elongation. In the two-steps process (PT = 673 K and 723 K), two different quenching temperatures were used, but exhibits no significant effect on the strength. [141]

However, RA does not help on bending. On the contrary, as shown in Figure 159, the bending angle decreases linearly with increasing RA content for carbon contents in RA of less than 1 wt.%. Stress-induced martensite formation which leads to a significant hardness difference to the surrounding matrix, might be a contributing factor.

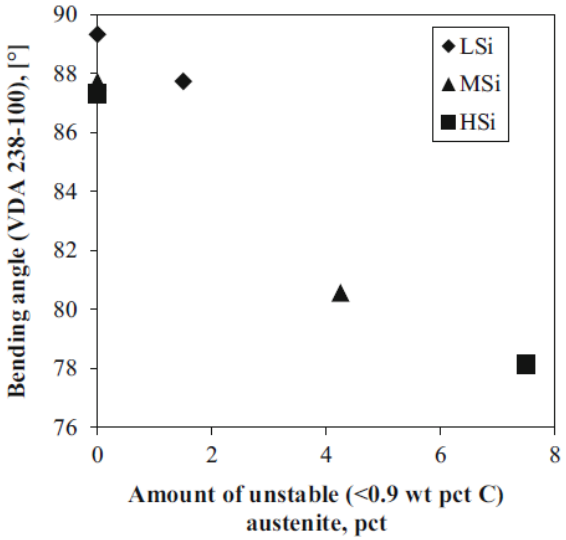

Figure 159. Correlation of the bending angle with the amount of unstable (<0.9 wt.% C) RA. [141]

Some researchers studied the feasibility of applying the Q&P process to a newly designed hot-stamped steel containing Si + Cr based on 22MnB5 steel. This grade contains 1.58% Si and 0.97% Cr as shown in Table 24. Compared to the conventionally processed 22MnB5 steel, the Q&P processed press hardening steel (PHS) improves ductility without losing strength.

	C	Mn	Si	Cr	Ti	N	B
Standard PHS	0.20 to 0.25	1.1 to 1.5	0.1 to 0.4	0.1 to 0.3	0.02 to 0.05	<0.01	0.001 to 0.005
Si-added PHS	0.27	1.50	1.61	0.001	0.027	0.0026	0.0025
Si + Cr-added PHS	0.28	1.46	1.58	0.970	0.023	0.0025	0.0023

Table 24. Chemical composition of the 22MnB5 PHS Grade and the two modified PHS. [142]

As shown in Figure 160, the microstructure of the Si-added and the Si + Cr added PHS have a tempered martensite matrix with islands of retained austenite and carbide-free bainite. The retained austenite could be found in the carbide-free bainite or at the lath borders of martensite. Due to the retained austenite's small grain size and significant C-enrichment in the range of 0.9 to 1.7 wt.%, its stability was extremely high. Partitioning and the bainite transition led to the C-enrichment of the austenite.

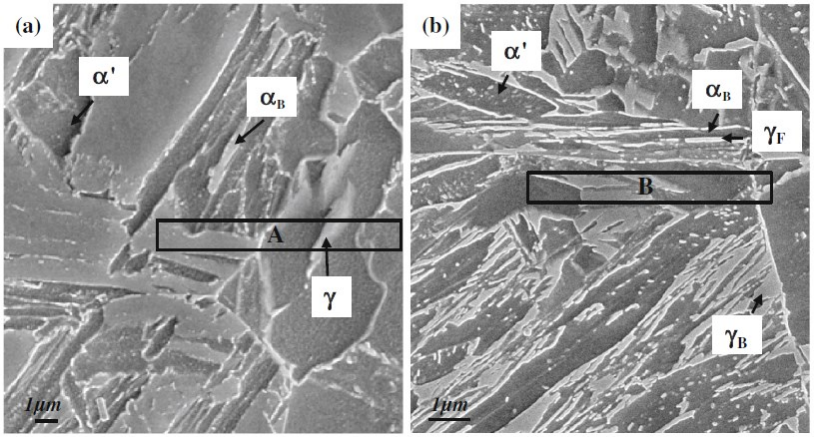

Figure 160. SEM micrographs of Q&P processed (a) Si-added PHS and (b) Si + Cr added PHS after quenching to 543 K and partitioning treated at 673 K for 10 min. α_B, γ_B, α and γ_F, represent carbide-free bainite, blocky-shape retained austenite, tempered martensite and film-shape retained austenite respectively. [142]

The additions of Si and Cr had a powerful synergetic effect. Si actively suppressed the formation of carbides, which led to the formation of carbide-free bainite. After Q&P processing, the addition of Cr increased the volume fraction of retained austenite. Therefore, the Q&P processed Si + Cr added PHS had better mechanical properties due to the retained austenite.

There are also some scholars [143], based on TRIP-assistted steel (Fe-0.23C-1.23Si-1.50Mn. mass fraction, %), using a three-dimensional atom probe (3DAPT) and other advanced characterization equipment to study the effect of hot stamping on the distribution of C atoms from martensite to austenite and the final microstructure and properties during Q&P treatment. The studied steels are similar to 22MnB5 steel except for the higher Si content. It was found that the deformation at the high temperature stage is beneficial to the Q&P process and can improve the stability of retained austenite.

The above Q&P treatment or Q&P treatment coupled with hot stamping are all carried out under some ideal conditions, but it should be noted that the Q&P process involves two crucial isothermal links, namely isothermal quenching and isothermal partitioning. The continuous quenching link in the hot stamping process cannot achieve precise control. Although the purpose of isothermal quenching and isothermal distribution can be achieved in the hot stamping process by heating the mold or using additional thermal insulation equipment, in the production cycle the production cost and energy consumption of hot stamping parts will increase accordingly. Because of this, the coupling of these two processes has obvious limitations in practical industrial applications.

8.5. Quenching and flash-partitioning (Q&FP):

In recent years, the concept of quenching and flashing (Q&FP) has been proposed based on carbon diffusion associated with martensitic transformation. For the Si-added steel with elevated M_S temperature, during the martensitic transformation, carbon can rapidly diffuse from the martensitic lath into its adjacent austenite in just a few seconds to replace carbides precipitation in Si-free steels by autotempering.

Increasing M_S in the alloy design based upon the Q&FP concept can stabilize the retained austenite during hot stamping. The gradual TRIP effect of retained austenite in Q&FP steels combined with conventional PHS which has higher tensile strength plays a significant role in improving ductility by about 50%, enabling the development of a combination of excellent mechanical properties without the need for additional processing and increased costs.

Based on the Q&FP concept, 1500 MPa and 1800 MPa hot-stamped steels have been designed and developed, referred to as QFP1500 and QFP1800 for short. Figure 161 shows the microstructures of QFP1500 and QFP1800 after hot-stamped treatment. About 7% retained austenite is obtained in the martensite of the two hot-stamped steel, and the retained austenite is distributed as a thin film between the martensitic laths. The average thickness of the martensite lath is about 200 nm, while the average thickness of the retained austenite is about 20 nm. The actual size of the retained austenite is very close to the calculated result of the diffusion distance of C in the austenite phase.

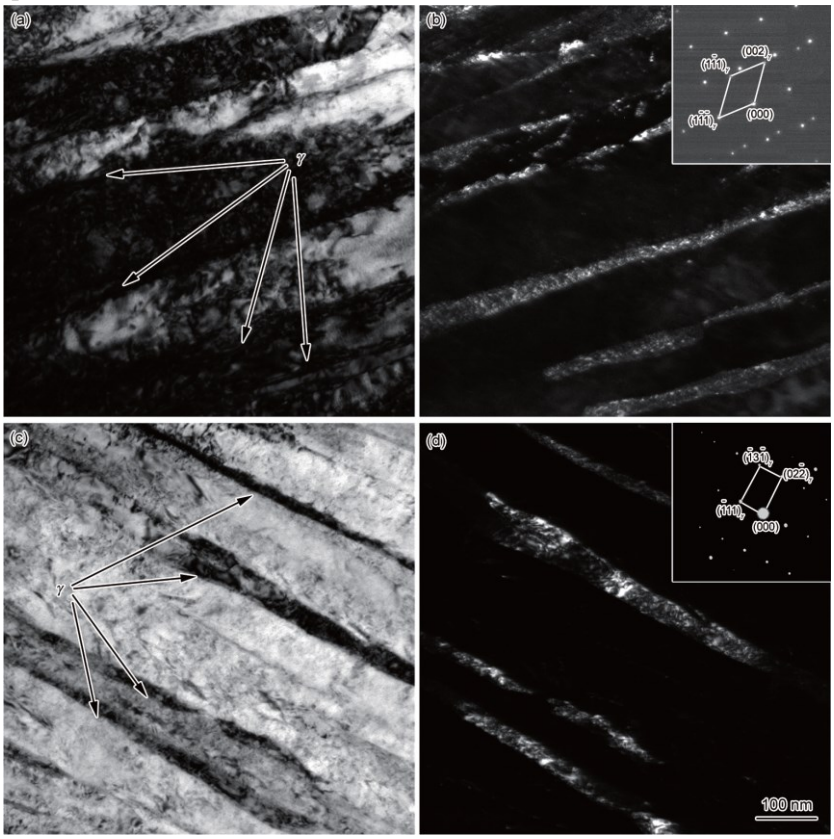

Figure 161. TEM images of QFP1500 (a) and (b) and QFP1800 (c) and (d) designed by Q&FP concept while (a) and (c) are bright-field and (b) and (d) are dark-field (γ represents retained austenite and the insets in (b) and (d) show the SAED patterns of γ). [144]

The microstructure of 22MnB5 steel after quenching is all martensite while the retained austenite in QFP1500 and QFP1800 exerts the TRIP effect in the process of plastic deformation. It increases the work hardening rate and delays the generation of necking which is the root cause of ductility improvement (as shown in Figure 162.) of QFP1500 and QFP1800.

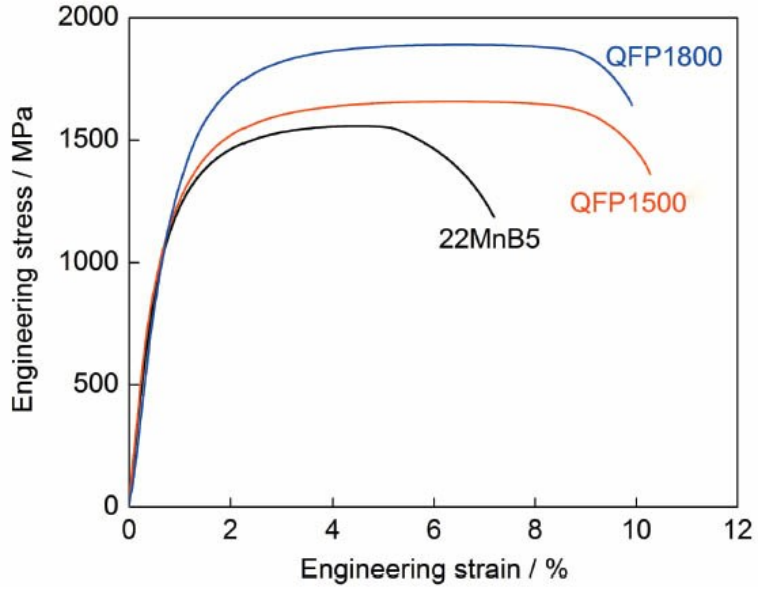

Figure 162. Engineering stress-strain curves of 22MnB5 steel and the PHS designed by Q&FP Concept. [79]

8.6. Discussion:

At present, the plasticizing and toughening of the Q&P process for hot-stamped steel is a research hotspot. Many teams have carried out systematic research on this, but further research on chemical composition and equipment is needed to be applied to production.

Both the Q&FP concept and the attempt of Q&P process in the hot stamping process can obtain steels with excellent properties, but the latter has limitations in practical industrial applications, while the former is based on the current industrial production conditions of hot-stamped parts which would not cause process and cost issues.

9.Conclusion

Making low alloy steels stronger than 2000MPa might have been a world-class problem 100 years ago, but that is no longer the case today, and today we hope to achieve a "huge improvement" in ductility of low alloy steels at ultimate tensile strengths above 2000MPa. For this reason, researchers in related fields have made endless explorations on the theoretical basis, alloy design and enhanced plasticization principles and methods. The steels studied in this paper are barely the tip of the iceberg.

These steels are usually used in the automotive, aerospace and defense industries. As one of the indispensable key components for equipment manufacturing in these fields, the R&D of bearing steel is not only the traditional fully hardened martensitic steel represented by 100Cr6 steel, but also many new low cost, environment friendly and higher performance steels.

The nanobainitic steels are definitely the one for manufacturing high-end bearings. Although the development time is still short, the nanotechnology has brought new vitality to the design of new ultra-high strength steels. In-depth, the database containing the service performance of nanobainitic bearings and laboratory data would be established and continuously improved, the proprietary standard of nanobainitic steels would also be established, that the deficiencies of nanobainitic steels will be overcome.

Compared with AISI 4340 steel, 300M steel and D6AC steel with similar microstructure will be more widely used in aviation, aerospace, warships, submarines and marine engineering. With the advancement of scientific materials and aviation technology, these existing steels might be used as a prototype steel in the future. Based on this, the fine evolution of the microstructure could be deeply studied and measures could be taken to improve fatigue and dynamic mechanical properties which are the development focus of low alloy engineering steels.

Hot-stamped steel, armor steel, wear resistant steel, Q&P steel and cold-drawn pearlitic steel wire came into being which have effectively promoted the development of automotive lightweight technology. The environmental damage and energy crisis has triggered mandatory requirements for energy conservation in the automotive industry. In addition, the requirements for automobile safety are increasing, while safety regulations are becoming more and more stringent. The development and application of a new generation of automotive lightweight steels requires the exploration of new ideas for organizational regulation and process control to realize the preparation and industrial application of ultra-high strength automotive steel.

Throughout the full paper, it can be found that the exploration of low alloy steel has moved from the traditional macro adjustment of composition to the ultimate control of microstructure, from the pursuit of a certain limit characteristic to the comprehensive consideration of performance and the actual control of cost and process. That’s the reason for great breakthroughs in strength and toughness.

However, when the alloy composition changes and the processing is complicated, it is difficult to integrate various factors and analyze the contribution of each flow to the performance. In the future, the combined application of advanced manufacturing methods, big data information calculation, numerical optimization simulation of heat treatment process and further exploration of the mechanism of strengthening and toughening will be an important solution.

This paper does not attempt and could not fully describe all about low alloy steels, but only

attempts to discuss and analyze some hot issues. Hope that it will be able to draw attention to the development of high-performance steel materials. The ever-changing steel materials have developed to now, just like a luxuriant tree, with wide varieties and still growing. To be sure, the steel of the future will be very different from the steel we see today.

Acknowledge

The years are fleeting, and there are many past events in my mind. Three years have passed in a flash. Looking back on the past, I sighed a lot. My degree thesis is about to come to an end, which means that my master's study career is coming to an end.

Turin does not have the prosperity of Rome, the romance of Venice, and the wildness of Naples. However, it has left an indelible trace in my student career. The ubiquitous cafes and exquisite afternoon tea, the wide boulevards lined with century-old Baroque buildings and, literally, the greatest football club. Even the streets you pass by inadvertently will make you miss the city. Every moment when I wandered around here was an unforgettable picture. It is fortunate to have spent the best seven years of my life which is almost all my youth here, with either pain or joy.

The work of this paper was completed under the careful guidance of my supervisor, Professor Paolo Matteis. Professor Matteis is a knowledgeable and kind gentleman. With his selfless help and patient guidance, my paper was successfully finished. Here, I would like to express my heartfelt thanks and blessings to Professor Matteis.

Sincere thanks to my parents for helping me grow and encouraging me to make progress in my years of study and life. It is precisely because of their selfless love and meticulous care that they have illuminated my path in studying. The pursuit of my life stems from the expectation of my mother when I was a child— “Be the pillar of your motherland and the pride of your parents”.

Special thanks to my dear friend He Xilong, who spent most of student career together with me. Most people never meet a true friend in their lifetime, but I am fortunate enough to get to know him. I wish him a successful study and a happy life in Italy. Also, thanks to all the friends who have helped me, your support is my huge motivation.

I would also like to thank Dr. Abbas Razavykia, the supervisor for my undergraduate paper. Thank you for your patient guidance 3 years ago. The words "You will have a bright and far future" you said is extremely important which has inspired me for a long time and supported me to insist on finishing my studies during the two-year covid pandemic.

“Long, long had been my road and far, far was the journey;
I would go up and down to seek my heart's desire.”

References

[1] Odenthal, Alken J, Kemminger A, Krause F, Vogl N, and Rühl S. Applied numerical simulation for safe and efficient process conditions of metallurgical plants. In 8th European Oxygen Steelmaking Conference (EOSC), Taranto (I), 2018.
[2] "World steel in figures 2021," World Steel Association, 2021.
https://www.worldsteel.org/.
[3] Bhadeshia H K D H. Steels for bearings. Progress in materials Science, 57, no. 2, (2012): 268-435.
[4] Heat-treated steels, alloy steels and free-cutting steels - Part 17: Ball and roller bearing steels (ISO 683-17:2014).
[5] Müştak, Ozan et al. Simulation of through-hardening of SAE 52100 steel bearings- Part 2: Validation at Industrial Scale. Materialwissenschaft und Werkstofft-echnik, 2015.
[6] Dai W. GCr15 Steel Spheroidizing Annealing Design. Journal of Wuhan University of Technology, 2002,26(1):138-140.
[7] Cao S-A et al. Forming and Improved Technology of Asymmetric Structure for Carbide Annealing of GCr15 Steel. Heat Treatment Process, 2005, 2:51-53.
[8] Mi Z-L et al. Effect of heat treatment process on microstructure and properties of a high carbon chromium bearing steel. TRANSACTIONS OF MATERIALS AND HEAT TREATMENT, 2015, 36(7):119-124.
[9] Daguier P, Roesch O, Trojahn W. New development in through hardened bearing steel grades for use in contaminated lubricants. J ASTM Int, 2007; 3: JAl14045.
[10] Zhao J, Wang T-S, Lv B, et al. Microstructures and mechanical properties of a modified high-C-Cr bearing steel with nano-scaled bainite. Materials Science and Engineering: A, 2015.
[11] Umbrello D, Jayal A.D, Caruso S, Dillon O.W, Jawahir I.S. Modeling of white and dark layer formation in hard machining of AISI 52100 bearing steel. Mach Sci Technol, 2010; 14:128–47.
[12] You S-J et al. Bainite quenching method at variable temperatures of high-carbon-chromium bearing steel. Application CN2011104475665A events, 2011.
[13] E V Zaretsky. Rolling bearing steels – a technical and historical perspective, Materials Science and Technology, 2012, 28(1):58-69.
[14] Eberhard Kerschera, Karl-Heinz Lang. Influence of thermal and thermomechanical treatments on the fatigue limit of a bainitic high-strength bearing steel. Procedia Engineering 2, 2010:1731-1739.
[15] Beswick J M. Fracture and fatigue crack propagation properties of hardened 52100 steel. Metall Mater Trans A, 1989, 20:1961–1973.
[16] Kar R J, Horn R M, Zackay V F. The effect of heat treatment on microstructure and mechanical properties in 52100 steel. Metall Trans A, 1979, 10:1711–1717.
[17] Alley E S, Neu R W. Microstructure-sensitive modeling of rolling contact fatigue. International Journal of Fatigue, 2010, 32(5):841.
[18] An X-L, Shi Z-Y, Xu H-F, Wang C-Y, Wang Y-H, Cao W-Q, Yu J-K. Quantitative Examination of the Inclusion and the Rotated Bending Fatigue Behavior of SAE52100. Metals, 2021, 11:1502.
[19] Zhang H-J, Yu F, Li S-X, He E-G. Fine granular area formation by damage induced shear strain localization in very-high-cycle fatigue. Fatigue and Fracture of Engineering Materials & Structures,

2021; 1–14.
[20] Chapetti M D, Tagawa T, Miyata T. Ultra-long cycle fatigue of high-strength carbon steels part I: review and analysis of the mechanism of failure. Materials Science and Engineering: A, 2003, 356(1-2): 227-235.
[21] Wang N-W. Improvement of heat treatment process for precise GCr15 bearings. SOUTHERN METALS, 2007,158:22-24.
[22] Cao Z-X et al. Effects of double quenching on fatigue properties of high carbon bearing steel with extra-high purity. International Journal of Fatigue, 2019, 128:105176.
[23] Cao Z-X et al. Carburization induced extra-long rolling contact fatigue life of high carbon bearing steel. International Journal of Fatigue, 2020, 131:105351.
[24] Standard Specification for Steel Bars, Carbon and Alloy, Hot-Wrought, General Requirements for[1]-A321: Specification for Steel Bars, Carbon, Quenched and Tempered (ASTM-A29A29M-2004).
[25] Lee E-W, Neu C-E, Kozol J. Al-Li alloys and ultrahigh-strength steels for U.S. Navy aircraft. Journal of the Minerals, 1990, 42(5): 11-15.
[26] Wang T-L, Lu Y, Ren F-Z, Wei S-Z, Tian B-H. Research progress of ultra-high strength low alloy steels. HEAT TREATMENT OF METALS, Vol. 40 No. 2, February 2015.
[27] Ozsoy N, Ozsoy M. Optimization of surface roughness in the turning process of AISI 4340 tempering steel. Emerging Materials Research, Volume 9 Issue 1, March 2020, pp. 104-109.
[28] S Roy, R Kumar, R K Das and A K Sahoo. A Comprehensive Review on Machinability Aspects in Hard Turning of AISI 4340 Steel. Materials Science and Engineering, (2018)012009
[29] ALL METALS & FORGE GROUP ISO 9001:2008 AND AS9100C manufacturer. https://steelforge.com/about-us/
[30] Clarke A, Miller M K, Field R, et al. Atomic and nanoscale chemical and structural changes in quenched and tempered 4340 steel. Acta Materialia, 2014,77:17-27.
[31] Woei-Shyan Lee, Tzay-Tian Su. Mechanical properties and microstructural features of AISI 4340 high-strength alloy steel under quenched and tempered conditions. Journal of Materials Processing Technology, 87 (1999): 198–206.
[32] Tomita Y, Okabayashi K. Effect of quench rate on microstructure and tensile properties of AISI 4320 and 4340 steels. Metallurgical and Materials Transactions A, 1987, 18(1): 115-121.
[33] Youngblood J L, Raghavan M. Correlation of microstructure with mechanical properties of 300M steel. Metallurgical and Materials Transactions A, 1977, 8(9): 1439-1448.
[34] Lai G-Y, Wood W E, Clark R A, et al. The effect of austenitizing temperature on the microstructure and mechanical properties of as-quenched 4340 steel. Metallurgical and Materials Transactions B, 1974, 5(7): 1663-1670.
[35] Khodamorad Abbaszadeh, Hassan Saghafian and Shahram Kheirandish. Effect of Bainite Morphology on Mechanical Properties of the Mixed Bainite-martensite Microstructure in D6AC Steel. J. Mater. Sci. Technol., 2012, 28(4), 336-42.
[36] Lu K, Lu L and Suresh S. Strengthening materials by engineering coherent internal boundaries at the nanoscale. Science, 2009, 324(5925): 349 − 352.
[37] Pan Q-W, Yan Ying, Li X-W, Wang B, Zhang P and Zhang Z-F. Effect of heat treatment on microstructure and tensile properties of double vacuum smelting AISI 4340 steel. TRANSACTIONS OF MATERIALS AND HEAT TREATMENT, 1009-6264(2021) 04-0087-09.
[38] Pang J-C, Li S-X, Wang Z-G and Zhang Z-F. General relation between tensile strength and

fatigue strength of metallic materials. Materials Science & Engineering, A564(2013)331–341.
[39] Zhang P, Li S-X and Zhang Z-F. General relationship between strength and hardness. Materials Science and Engineering, A529(2011)62–73.
[40] Cowley C, Jin M-Z. The latest progress in improving the mechanical properties of AISI4340 steel through control of the microstructure. Ordnance Material Science and Engineering, 1986(10): 65-72.
[41] Li H-F. Investigation on fracture toughness and crack growth mechanism of high-strength steels. Shenyang: Institute of Metal Research, Chinese Academy of Science, 2019.
[42] Sarikaya M, Jhingan A K and Thomas G. Retained austenite and tempered martensite embrittlement in medium carbon steels. Metallurgical and Materials Transactions A, 1983, 14(6): 1121-1133.
[43] Xia Z-X, Yang Z-Y, Su J, et al. Effect of type and morphology of inclusions on plastic properties of ultrahigh strength steel. Journal of Aeronautical Materials, 2008, 28(5): 17-21.
[44] Hickey C F, Anctil A A. Split heat mechanical property comparison of ESR and VAR 4340 steel. Journal of Heat Treating, 1985, 4(2): 177-183.
[45] Lee S, Lee D-Y and Asaro R J. Correlation of microstructure and tempered martensite embrittlement in two 4340 steels. Metallurgical Transactions A, 1989, 20(6): 1089 − 1103.
[46] Li J-Y, Gao H-L, Tang Z-H, et al. Effect of inclusions on toughness of ultra-high strength steels. Ordnance Material Science and Engineering, 1990(11): 12-19.
[47] Duan Q-Q, Pang J-C, Zhang P, Li S-X and Zhang Z-F. Quantitative Relations between S-N Curve Parameters and Tensile Strength for Two Steels: AISI 4340 and SCM 435. Research & Reviews: Journal of Material Science, 10.4172/2321-6212.1000207.
[48] Zhirafar S, Rezaeian A and Pugha M. Effect of cryogenic treatment on the mechanical properties of 4340 steel. Journal of Materials Processing Technology 186 (2007) 298-303.
[49] Tomita Y, Okabayashi K. Mechanical properties of 0.40 pct C-Ni-Cr-Mo high strength steel having a mixed structure of martensite and bainite. Metallurgical and Materials Transactions A, 1985, 16(1): 73-82.
[50] John M. Tartaglia and Kathy L. Hayrynen. A Comparison of Fatigue Properties of Austempered Versus Quenched and Tempered 4340 Steel. ASM International, 10.1007/s11665-011-9951-y.
[51] Tomita Y, Okawa T. Effect of microstructure on mechanical properties of isothermally bainite-transformed 300M steel. Materials Science and Engineering: A, 1993, 172(1/2): 145-151.
[52] Li Keqiang. The development trend of automobile technology and China's countermeasures. Automotive Engineering, 2009(11): 1005-1016.
[53] Norrbottens Jaernverk A B. Manufacturing a hardened steel article, 1977-11-02.
[54] Ma N. Research on hot forming of high strength steel. Dalian University of Technology, 2011.
[55] Steinbeiss H, So H, Michelitsch T and Hoffmann H. Method for optimizing the cooling design of hot stamping tools. Production Engineering volume 1, pages: 149–155 (2007).
[56] Shi C, Daun K-J, Wells M-A. Evolution of the spectral emissivity and phase transformations of the Al-Si coating on Usibor® 1500P steel during austenitization. Metall. Trans., 2016, 47B: 3301.
[57] Liang J-T. Strengthen-toughening mechanism and application technology of 2000 MPa grade hot stamping steel. University of Science and Technology Beijing, 2019.
[58] Hu P, Ying L, He B. Hot Stamping Advanced Manufacturing Technology of Lightweight Car Body. Singapore: Springer Singapore,2017:45.
[59] ArcelorMittal. Steels for hot stamping -Usibor®[EB/OL].

http://automotive.arcelormittal.com/saturnus/sheets/E_EN.pdf.
[60] ThyssenKrupp. Manganese-boron steel for hot form curing [EB/OL].
https://www.thyssenkrupp-steel-europe.com/en/products/sheetcoated-products/manganese-boron-steel-for-hot-form-curing/manganese-boron- steel-for-hot-form-curing.html.
[61] Rana R, Singh S B. Automotive Steels: Design, Metallurgy, Processing and Applications. Cambridge: Woodhead Publishing, 2017:387.
[62] Jin X-J, Gong Y, Han X-H, et al., A review of current state and prospect of the manufacturing and application of advanced hot stamping automobile steels. ACTA METALLURGICA SINICA, Vol.56 No.4, Apr. 2020.
[63] Karbasian H, Tekkaya A E. A review on hot stamping. Journal of Materials Processing Technology, 2010, 210(15): 2103-2118.
[64] Wang H, Yang H-L, He Y-L and Li L. Effect of annealing process o the performance and microstructure of 22MnB5 steel. SHANGHAI METALS, Vol.37, No.6 2015.11.
[65] T. Taylor, A. Clough (2018): Critical review of automotive hot-stamped sheet steel from an industrial perspective, Materials Science and Technology.
[66] Daniarta, Kolasinski S and Rogosz P B. Waste Heat Recovery in Automotive Paint Shop via Organic Rankine Cycle and Thermal Energy Storage System—Selected Thermodynamic Issues. Energies, 2022, 15, 2239.
[67] Li Y, Ying L, Hu P, Shi D-Y, Zhao X, and Dai M-H. Coupled numerical simulation of hot stamping process and experimental verification. AIP Conference Proceedings, 1532, 471 (2013).
[68] ArcelorMittal. Steels for hot stamping -Usibor®[EB/OL].
https://automotive.arcelormittal.com/products/flat/PHS/usibor_ductibor.
[69] Turetta A, Bruschi S and Ghiotti A. Investigation of 22MnB5 formability in hot stamping operations. JOURNAL OF MATERIALS PROCESSING TECHNOLOGY, 2006, 177(1-3SI):396-400.
[70] Geiger M, Merklein M, Hoff C. Basic investigations on the hot stamping steel 22MnB5. Advanced Materials Research Vols 6-8 (2005) pp 795-804.
[71] HIDALGO J, SANTOFIMIA M J. Effect of Prior Austenite Grain Size Refinement by Thermal Cycling on the Microstructural Features of As-Quenched Lath Martensite. Springerlink.com. 2016.
[72] Zhou J, Wang B-Y, Huang M-D, and Cui D. Effect of hot stamping parameters on the mechanical properties and microstructure of cold-rolled 22MnB5 steel strips. International Journal of Minerals, Metallurgy and Materials, Volume 21, Number 6, June 2014, Page 544.
[73] Wang S-M, Hu Z-H, Wang Z-Y, Luan D-C, Wang N and Chen Ji. Effect of tempering temperature on microstructure and properties of 22MnB5 steel for automobile. HEAT TREATMENT OF METALS, Vol. 45 No. 7 July 2020.
[74] Xu D-C, Zhao H-F, Li X-T, Fan H-M, Teng H-X and CUI Y. Effect of tempering temperature on microstructure and mechanical properties of 22MnB5 hot stamping steel after quenching. TRANSACTIONS OF MATER IALS AND HEAT TREATMENT, Vol. 39 No. 8, August 2018..
[75] Akisue O, Usuda M. New types of steel sheets for automobile weight reduction. Nippon Steel Tech. Rep., 1993, 57: 11.
[76] Kim H-G, Lee H-J, Park S-H, Park S-J and Yoon J-H. Effect of laser patterning on the material behaviour of 22MnB5 steel with induced local strengthening. The International Journal of Advanced Manufacturing Technology, Received: 27 November 2019 /Accepted: 22 April 2020.
[77] Ying L, Chang Y, Hu P, Shen G-Z, Liu L-Z and Li X-D. Influence of Low Tempering

Temperature on Fracture Toughness of Ultra High Strength Boron Steel for Hot Forming. Advanced Materials Research, Vols. 146-147 (2011) pp 160-165.
[78] Fei W-J, Xu Z-H, Li H-G, Li X and Wang Z-Z. Effect of Quenching Temperature on Microstructure and Properties of 22MnB5 Ultra High Strength Steel. Hot Working Technology, 2019, Vol. 48, No.4.
[79] Yi H-L, Chang Z-Y, Cai H-L, Du P-J and Yang D-P. Strength, Ductility and Fracture Strain of Press-Hardening Steels. ACTA METALLURGICA SINICA, Vol.56 No.4, Apr. 2020.
[80] Naderi M. Hot stamping of ultra high strength steels [D]. Aachen: University of Aachen, 2007.
[81] Yi H-L, Liu H-L, Chang Z-Y, et al. Steel for hot stamping forming, hot stamping forming process and hot-stamping formed component. Chin Pat, 10535069.3, 2016.
[82] Bhadeshia H, Honeycombe R. Steels: Microstructure and Properties. Oxford: Butterworth-Heinemann, 2017: 111.
[83] Liu A-M, Feng Y, Zhao Y, et al. Effect of niobium and vanadium microalloying on microstructure and property of 22MnB5 hot press forming steel. Mech. Eng.Mater.,2019,43(05): 34 37, 53.
[84] Takahashi J, Kawakami K, Kobayashi Y. Origin of hydrogen trapping site in vanadium carbide precipitation strengthening steel. Ac ta Mater, 2018, 153: 193 204.
[85] Li X-T. Study on cracks propagation mechanism and control technology of Zn-coated press hardened steel. Central Iron & Steel Research Institute, 2018.
[86] SSAB. Armox steel. https://www.ssab.com/en/brands-and-products/armox/armor-ballistic-steel
[87] Showalter D D, Gooch W A, and Burkins M S. Ballistic Testing of SSAB Ultra-High-Hardness Steel for Armor Applications. Weapons and Materials Research Directorate, ARL, ARL-TR-4632: October 2008.
[88] Barenyi I, Hires O and Liptak P. Changes in Mechanical Properties of Armoured UHSLA Steel ARMOX 500 After Over Tempering. PROBLEMS OF MECHATRONICS. ARMAMENT, AVIATION, SAFETY ENGINEERING, 4, 4 (14), 2013, 7-14.
[89] Crouch I G. Metallic armour - from cast aluminium alloys to high-strength steels. Materials Forum,1988,12:31-37.
[90] SSAB. Armox steel. The steel you want between you and risk.
https://www.ssab.com/en/brands-and-products/armox/download
[91] IAN G C. The Science of Armor Materials. United Kingdom: Woodhead Publishing, 2017.
[92] SSAB. Armox steel. WORKSHOP RECOMMENDATIONS.
https://www.ssab.com/en/brands-and-products/armox/download
[93] Gooch W， Burkins M et al. Ballistic Testing of Swedish Steel Armox Plate for U.S. Armor Applications. 21st International Symposium on Ballistics, Adelaide, South Australia, [S. l.]: [s. n.], 2004.
[94] Garbarz B, Burian W, Marcisz J and Wisniewski A. The Nano-Duplex NANOS-BA Steel for Application in Construction of Armours. PROBLEMS OF MECHATRONICS. ARMAMENT, AVIATION, SAFETY ENGINEERING, 4 (10), 2012, 7-22.
[95] SSAB. Hardox. Steel. https://www.ssab.com/en/products/brands/hardox
[96] Białobrzeska B, Jasi ´ nski R, Konat Ł and Szczepa´ nski Ł. Analysis of the Properties of Hardox Extreme Steel and Possibilities of Its Applications in Machinery. Metals, 2021, 11, 162.
[97] Abrasion Resistant Steel Plates of JFE Steel. JFE 技報, 2007,(18): 72-74.

[98] SSAB. Hardox. Steel. The beast. https://www.ssab.com/en/products/brands/hardox/hardox-download
[99] SSAB. Hardox. Steel. Your one stop wear shop. https://www.ssab.com/en/products/brands/hardox/hardox-download
[100] Caballero F G, Bhadeshia H K D H. Very strong bainite. Current Opinion in Solid State and Materials Science, 2004, 8(3): 251.
[101] Bhadeshia H K D H. Bainite in steels. Third edition. UK: Maney Publishing, 2015.
[102] Efremenko V G, Hesse O, Friedrich T, et al. Two-body abrasion resistance of high-carbon high-silicon steel: Metastable austenite vs nanostructured bainite. Wear, 2019, 418: 24.
[103] Caballero F G, Garcia-Mateo C, Miller M K. Design of Novel Bainitic Steels: Moving from UltraFine to Nanoscale Structures. The Minerals, Metals & Materials Society, JOM, Vol. 66, No. 5, 2014.
[104] Bhadeshia H K D H. Thermodynamic analysis of isothermal transformation diagrams. Metal Science, 1982, 16(3): 159.
[105] Zhu K, Mager C, Huang M. Effect of substitution of Si by Al on the microstructure and mechanical properties of bainitic transformation induced plasticity steels. Journal of Materials Science & Technology, 2017, 33(12): 1475.
[106] Hu H, Xu G, Wang L, et al. The effects of Nb and Mo addition on transformation and properties in low carbon bainitic steels. Materials & Design, 2015, 84: 95.
[107] Sun D, Liu C, Long X, et al. Effect of introduced vanadium carbide at the bay region on bainite transformation, microstructure and mechanical properties of high-carbon and high-silicon steel. Materials Science and Engineering: A, 2021, 811.
[108] Singh K, Kumar A, Singh A. Effect of Prior Austenite Grain Size on the Morphology of Nano-Bainitic Steels. Metallurgical and Materials Transactions A, 2018, 49(4): 1348.
[109] Jiang T, Liu H, Sun J, et al. Effect of austenite grain size on transformation of nanobainite and its mechanical properties. Materials Science and Engineering: A, 2016, 666: 207.
[110] Yang J-R, Huang C-Y, Hsieh W-H, et al. Mechanical Stabilization of Austenite against Bainitic Reaction in Fe–Mn–Si–C Bainitic Steel. Materials Transactions, JIM. 1996, 37(4): 579.
[111] Yang Z, Chu C, Jiang F, et al. Accelerating nano-bainite transformation based on a new constructed microstructural predicting model. Materials Science and Engineering: A, 2019, 748: 16.
[112] Gong W, Tomota Y, Harjo S, et al. Effect of prior martensite on bainite transformation in nanobainite steel. Acta Materialia, 2015, 85: 243.
[113] Wang X-L, Wu K-M, Hu F, et al. Multi-step isothermal bainitic transformation in medium-carbon steel. Scripta Materialia, 2014, 74: 56.
[114] Hase K, Garcia-Mateo C, Bhadeshia H K D H. Bainite formation influenced by large stress. Materials Science and Technology, 2013, 20(12): 1499.
[115] Shimozono T, Kohno Y, Konishi H, et al. Effects of pre-strain, heat treatments and magnetic fields on α′ martensite formation in Fe-25.5%Ni-3-5%Cr alloys, Materials Science and Engineering: A, 1999, 273-275(15): 337.
[116] Kumar A, Singh A. Mechanical properties of nanostructured bainitic steels. Materialia, 15 (2021), 101034.
[117] Peet M J, Hill P, Rawson M, Wood S, Bhadeshia H K D H. Fatigue of extremely fine bainite. Mater. Sci. Technol, 27 (2011), 119:123.
[118] Yang J, Wang T-S, Zhang B, Zhang F-C. High-cycle bending fatigue be- haviour of

nanostructured bainitic steel. Scr. Mater, 66 (2012) 363:366.
[119] Gao G, Xu Q, Guo H, Gui X, Zhang B, Bai B. Effect of inclusion and microstructure on the very high cycle fatigue behaviors of high strength bainite/martensite multiphase steels. Mater. Sci. Eng, A. 739 (2019) 404:414.
[120] Languillaume J, Kapelski G, Baudelet B. Evolution of the tensile strength in heavily cold drawn and annealed pearlitic steel wires. Materials Letters, 33, (1997), 24l-245.
[121] Li Y-J, Choi P, Goto S, Borchers C, Raabe D, Kirchheim R. Evolution of strength and microstructure during annealing of heavily cold-drawn 6.3 GPa hypereutectoid pearlitic steel wire. Acta Materialia, 60, (2012), 4005–4016.
[122] Borchers C, Kirchheim R. Cold-drawn pearlitic steel wires. Progress in Materials Science, 82, (2016), 405–444.
[123] Guo N. A study on microstructural characterization and mechanical properties of cold drawing pearlitic steel wires for bridge cable. Chongqing University, 5, (2012): 84-86.
[124] Ohba H, Nishida S, Tarui T, Yoshimua K, Sugimoto M, Matsuoka K, Hikita N and Toda M., 2007. High-performance wire rods produced with DLP. Nippon steel technical report, 96, no.6, (2007): 50-56.
[125] Campbell P C, Hawbolt E B, and Brimacombe J K. Microstructural engineering applied to the controlled cooling of steel wire rod: Part I. Experimental design and heat transfer. Metallurgical Transactions A, 22, no.11, (1991): 2769-2778.
[126] Kazeminezhad M, and Karimi Taheri A. The effect of controlled cooling after hot rolling on the mechanical properties of a commercial high carbon steel wire rod. Materials & design, 24, no.6, (2003): 415-421.
[127] Torkamani H., Raygan Sh, Garcia-Mateo C, Rassizadehghani J, Palizdar Y and San-Martin D. Evolution of pearlite microstructure in low-carbon cast microalloyed steel due to the addition of La and Ce. Metallurgical and materials transactions A, 49, no.10 (2018): 4495-4508.
[128] Liu X, Ni Z-F, Yao L-L, Xue F, Yan M-X, Di H-F. Microstructure evolution of hypereutectoid steel wire in cold deformation. TRANSACTIONS OF MATERIALS AND HEAT TREATMENT, Vol.36, No.8, August 2015.
[129] Zhang X, Godfrey A, Huang X, Hansen N and Liu Q. Microstructure and strengthening mechanisms in cold-drawn pearlitic steel wire. Acta Materialia 59, no. 9 (2011): 3422-3430.
[130] Guelton N and François M. Microstructure–Property Relationship in Cold-Drawn Pearlitic Steel Wires. Metallurgical and Materials Transactions A 51, no. 4 (2020): 1543-1566.
[131] Liu S, Zhang F, Yang Z, Wang M and Zheng C. Effects of Al and Mn on the formation and properties of nanostructured pearlite in high-carbon steels. Materials & Design, 93, (2016), 73–80.
[132] Wei D, Li L, Min X, Fang F, Xie Z and Jiang J. Microstructure and mechanical properties of heavily cold drawn pearlitic steel wires: Effects of low temperature annealing. Materials Characterization, 153, (2019): 108-114.
[133] Li Y-J, Choi P, Borchers C, Westerkamp S, Goto S, Raabe D and Kirchheim R. Atomic-scale mechanisms of deformation-induced cementite decomposition in pearlite. Acta Materialia, 59, no. 10, (2011): 3965-3977.
[134] Embury J D and Fisher R M. The structure and properties of drawn pearlite. Acta Metallurgica, 14, no.2 (1966): 147-159.
[135] Aydin H, Essadiqi E, Jung I-H and Yue S. Development of 3rd generation AHSS with medium Mn content alloying compositions. Materials Science & Engineering, A564 (2013) 501–508.

[136] Edmondsa D.V, Hea K, Rizzo F.C, De Coomanc B.C, Matlock D.K. and Speer J.G. Quenching and partitioning martensite—A novel steel heat treatment. Materials Science and Engineering, A 438–440 (2006) 25–34.
[137] Speer J G, Matlock D K, De Cooman B C, et al. Carbon Partitioning into Austenite after Martensite Transformation, Acta Materialia, 2003, 51(9): 2611-2622.
[138] Clarke A, Speer J.G, Matlock D.K, Rizzo F.C, Edmonds D.V. and He K. Microstructure and carbon partitioning in a 0.19%C-1.59%Mn-1.63%Si trip sheet steel subjected to quenching and partitioning (Q&P). International Conference on Solid-Solid Phase Transformations in Inorganic Materials, Vol. 2, Page. 99 - 108 (2005).
[139] Santofimia M J, Zhao L, Sietsma J, Microstructural evolution of a low-carbon steel during application of Quenching and Partitioning heat treatments after partial austenitization. Metallurgical and Materials Transactions A, 2009, 40(1): 46-57.
[140] Liu H-P, Lu X-W, Jin X-J, Dong H and Shi J. Enhanced mechanical properties of a hot stamped advanced high-strength steel treated by quenching and partitioning process. Scripta Materialia, 64 (2011) 749–752.
[141] Linke B M, Gerber T, Hatscher A, et al. Impact of Si on microstructure and mechanical properties of 22MnB5 hot stamping steel treated by quenching & partitioning(Q&P). Metall.Trans., 2018,49A:54.
[142] Seo E-J, Cho L, Cooman B C D. Application of Quenching and Partitioning(Q&P) Processing to Press Hardening Steel. Metall.Trans, A,45(9):4022-4037.
[143] Ariza E A, Poplawsky J, Guo W, et al. Evaluation of carbon partitioning in new generation of quench and partitioning (Q&P) steels. Metall. Trans., 2018, 49: 4809.
[144] Cai H-L, Chen P, Oh J-K, et al. Quenching and flash-partitioning enables austenite stabilization during press-hardening processing. Scr. Mater., 2020, 178: 77.